Dental Ecometrics as a Proxy of Paleoenvironment Reconstruction in the Miocene of South America

by

Jackson Ples Spradley

Department of Evolutionary Anthropology
Duke University

Date:_____

Approved:

_____
Richard F. Kay, Supervisor

_____
Blythe A. Williams

_____
James D. Pampush

_____
V. Louise Roth

_____
Doug M. Boyer

Dissertation submitted in partial fulfillment of
the requirements for the degree of Doctor of Philosophy
in the Department of
Evolutionary Anthropology in the Graduate School
of Duke University

2017

ABSTRACT

Dental Ecometrics as a Proxy of Paleoenvironment Reconstruction in the Miocene of South America

by

Jackson Ples Spradley

Department of Evolutionary Anthropology
Duke University

Date:_____

Approved:

_____
Richard F. Kay, Supervisor

_____
Blythe A. Williams

_____
James D. Pampush

_____
V. Louise Roth

_____
Doug M. Boyer

An abstract of a dissertation submitted in partial fulfillment of the requirements for the degree of Doctor of Philosophy in the Department of Evolutionary Anthropology in the Graduate School of Duke University

2017

Abstract

In this dissertation I compile modern mammalian faunal lists, as well as ecomorphological measurements on living marsupials and rodents, to relate the diversity of small mammals, specifically the distributions of their dental topographies, to the climates in which they are found. The emphasis of this dissertation is to demonstrate the potential of distributions of dental topography metrics as proxies for the reconstruction of paleoenvironments in the Miocene of South America.

In Chapter 2, I compile complete, non-volant mammalian species lists for 85 localities across South America as well as 17 localities across Australia and New Guinea. Climatic and habitat variables were also recorded at each locality using GIS spatial data. Additionally, basic ecological data was collected for each species, including: diet, body size, and mode of locomotion. Niche indices that describe the relative numbers of different ecologies were calculated for each locality. These indices then served as the predictor values in a handful of regression models, including regression trees, random forests, and Gaussian process regression. The Australian/New Guinean localities were used as a geographically and phylogenetically independent for the purposes of testing the models derived from South America.

As for the dental ecomorphological analysis, I use three separate measures of dental topography, each of which measures a different component of dental topography; relief (the Relief Index, or RFI), complexity (orientation patch count rotated, OPCR), and

sharpness (Dirichlet normal energy, DNE). Together, these metrics quantify the shape of the tooth surface without regard for tooth size. They also do not depend on homologous features on the tooth surface for comparative analysis, allowing a broad taxonomic sample as I present here. After a methodological study of DNE in Chapter 3, I present correlative studies of dental topography and dietary ecology in marsupials and rodents in Chapters 4 and 5, respectively. Finally, using the same localities from Chapter 2, I analyze the distributions of dental topography metrics as they relate to climate and habitat.

Results suggest that sharpness and relief are positively correlated with a higher amount of tough foods—such as leaves or insects—in the diet of marsupials, and that relief is positively correlated with grass-eating in rodents. The distributions of all three metrics show some utility when used as a proxy for climatic variables, though the distributions of RFI in marsupials and OPCR in rodents demonstrate the best correlations.

Overall, this dissertation suggests that dental topography can be used to discriminate dietary categories in a wide variety of mammalian groups, and that the distributions of dental ecometrics can be used as proxies for paleoenvironment reconstruction. This may eliminate the need to reconstruct behavior in individual taxa in order to construct ecological indices for fossil mammalian communities, thus offering a more direct avenue to reconstructing past environments.

Dedication

"Nature never did betray the heart that loved her."

-William Wordsworth

To my mother and father, Patti and Ples Spradley, for their passing on to me the joy of understanding, and encouraging in me a love and appreciation of the Natural World.

"You give but little when you give of your possessions. It is when you give of yourself that you truly give."

-Khalil Gibran

To my wife, Sara, for her unceasing love, support, and companionship during this journey of intellectual and personal growth.

Table of Contents

List of Tables

List of Figures

Acknowledgements

First and foremost I would like to thank my Ph.D. advisor, Dr. Richard Kay, for his guidance and mentorship. I cannot imagine going through this process with anyone else. The passion and good humor that he brings to his work every single day is inspiring, and he has served as a role model for my career and in my personal life. From conducting research to teaching Human Body, it has truly been a pleasure.

I would also like to thank my committee members, beginning with Dr. Blythe Williams. Without a doubt, Dr. Williams has been akin to my co-advisor, not just because of her proximity to my own office, but because she is always there for a conversation or for a quick piece of advice. I have had the pleasure to get to know her very well over these past five years and it is no stretch to say that she is among my favorite people.

Thank you as well to Dr. JD Pampush, without whom this dissertation would not have happened. In the brief amount of time we spent together I have become a better researcher and a better professional, and so much of that is because of his willingness to lend his assistance with any part of any project.

To Dr. Doug Boyer, who has lent me so much of his time and his lab space so that I could complete this dissertation. He is also one of the most thoughtful researchers I know and his attention to detail has made this dissertation all the better.

And to Dr. Louise Roth, with whom I have had a number of insightful conversations, and whose mammalogy course was a big inspiration behind the fixation I now have with wanting to include more and more mammalian species in my research.

An enormous thank you to my good friend, Bryan Glazer, for his assistance with the modeling approaches used in the second chapter of this dissertation. This became a lynchpin of my entire project and this dissertation would not have been possible without him.

I would also like to thank the museum curators that allowed me access to the specimens I used in Chapters 4 and 5, including: Jake Esselstyn (LSUMZ), Robert Voss (AMNH), Sandy Ingleby (Australian Museum), and Darrin Lunde (USNM).

Finally, I would like to acknowledge funding support from the National Science Foundation (NSF Grant 1349741 to RF Kay).

1. Introduction

In this dissertation, I examine the relationships between niche distributions of South American mammalian communities and six bioclimatic variables, including precipitation, temperature, seasonality (in terms of temperature and precipitation), primary productivity, and canopy height. Since previous analyses have primarily used traditional linear regression, I also use this opportunity to test a number of different regression techniques that have become popular in the ecological literature since the early 2000s. Using training data and a randomly selected test data set, estimations from all techniques are compared for accuracy—that is, the degree to which they are correlated with and can serve as proxies for the climate variables. Having demonstrated a relationship between mammal species richness and climate variables, I then move on to establishing a relationship between morphology and ecology in two groups of small mammals (marsupials and rodents). This is followed by a use of the morphometric distributions as proxies for environment using the same regression techniques—multivariate linear regression, regression trees, Random Forests, and Gaussian process regression—introduced in Chapter 2. The value of this approach is that the potential source of error in paleoenvironment reconstruction introduced by the accuracy of behavioral reconstructions of individual fossil taxa, and instead distributions of quantitative measurements themselves can be used.

1.1 Historical Context

The relationship of organisms' form and the nature of their behavior and preferred habitat has been one of the cornerstones of naturalism for millennia, long before even the contributions of Darwin's *Origin*. In his text *History of Animals,* published in the fourth century BCE, Aristotle recorded the distinguishing features of animals, while also noting that groups of animals with similar features tended to behave in similar ways, and that certain features indicated the kinds of habitats those organisms preferred. Such qualitative observations laid the foundation of zoology, and his *scala naturae* provided the primary way of thinking of the relationship between organisms for almost two thousand years after his death. While the naturalists of the 18th and 19th centuries eventually freed zoology from some of its anthropocentric underpinnings, the idea that an organism's form is indicative of its environment, at least indirectly, was retained.

1.2 Modern Methods

The field of paleoecology is generally synthetic in its approach, and at its broadest scale includes information from disciplines such as paleobotany, sedimentology, geochemistry, taphonomy, and paleontology, to name a few (Gingerich, 1989; Lowe and Walker, 1984). This study, however, will focus primarily on creating models based on modern mammalian communities and then ground-truthing them for application to the fossil record. Modern mammalian communities serve as valuable

study tools for understanding the ecology of extinct faunas due to the principle of convergence. Animals that play the same ecological role (Hutchinson 1965) tend to have similar adaptive responses, an observation that has been made since even the earliest naturalists (Huston, 1994). If we assume that animals in the past faced similar challenges as today, then it stands to reason that we can reconstruct their ecological roles (Sepkoski and Ruse, 2009).

The potential for inferring paleoecological information from fossilized mammal teeth is particularly high for several reasons: 1) mammals represent the dominant class of tetrapods in the Cenozoic (thus are readily available), thereby giving us a chance to study evolutionary trends in the most recent and abundant fossil records (Vrba, 1992); 2) their bones are relatively dense as compared to other types of organisms (e.g., birds) and are more likely to be preserved in the fossil record (Janis, 1993); 3) the most frequently preserved skeletal element (the dentition) is also the most taxonomically diagnostic and strongly ecologically correlated in terms of size and diet; and 4) analysis of mammalian species richness, community structure, and ecomorphology have been demonstrated to be highly correlated with habitat types and climate (Andrews et al., 1979; Fleming, 1973; Janis, 1993; Kay and Madden, 1997; Kay et al., 1997; Kay et al., 2012a; Louys et al., 2015; Vrba, 1992). From the paleontology literature, these studies are often discussed in the context of finding faunal proxies of climate that can be easily recovered from the fossil

record. These proxies include species richness (Kay and Madden, 1997; Kay et al., 1997) and niche metrics (Andrews et al., 1979; Gingerich, 1989; Kay and Madden, 1997).

That mammal species occupying similar habitats have convergent adaptations is one of the foundational blocks of Darwin's work (Darwin, 1859), and this serves as the theoretical basis for the use of niche metrics as a method of paleoecology (Hutchinson 1965). This premise is validated by the strong correlation between aspects of phenotype and environment as documented by countless studies designed to test it (Anthony and Kay, 1993; Boyer, 2008; Boyer et al., 2013; Crompton and Lumsden, 1970; Ross and Kirk, 2007). While this implies an adaptive link between form and function (Kay and Cartmill 1977), it is not dismissive or at odds with the reservations of Gould and Lewontin (1979)—who suggested that not all morphology is adaptive—since such research is extremely circumscribed in how it defines morphological candidates for adaptation (e.g., Kay and Cartmill 1977, Kay et al. 2004; Boyer et al. 2013). While there have been a multitude of paleoecological methods that incorporate ecomorphology (Reed, 2013), this study will focus on two of the broadest and most popular; community structure and ecometrics.

While it was Harrison (1962) and Fleming (1973) who established that mammalian communities vary predictably with latitude, Andrews *et al.* (1979) demonstrated that even when latitude was held constant, mammalian community structure is significantly correlated with habitat type. When both latitude and habitat

type are similar, mammalian niche structure is "remarkably constant" (Andrews et al. 1979). In this context, community structure is the number and types of niches (ecological roles) that are available and filled in any given habitat. Previous studies of community structure and paleoecology, (e.g. Andrews et al. 1979, Kay and Madden 1997, and Vizcaino et al. 2010), have observed the relative abundance of arboreal vs. terrestrial species, frugivores vs. folivores, herbivores vs. carninvores, and the distribution of large and small body sizes in modern communities. These observations are the variables used to create indices (both separate and composite) to search for consistent relationships with habitat type. These indices are also considered to be taxon-free (Damuth et al., 1992; Reed, 2013) because they describe what the species is doing, i.e. the niche, and thus can be used to compare communities of extinct species irrespective of phylogenetic relationships. This claim is not without controversy, however. For instance, the concepts of 'niche conservatism' (Wiens and Graham, 2005) or 'phylogenetic inertia' (Blomberg and Garland, 2002)—i.e. the tendency of taxa to retain ancestral ecological traits—would suggest that no ecological analysis would be free of phylogeny. Andrews and Hixson (2014) have argued that no paleoecological method has been completely successful in being taxon-free since every regression and comparison is made within taxonomic groupings, though they assert that community level analysis is the most resistant to effects of phylogeny. Another potential confounding factor is the effect of processes that affect large-scale differences in

community structure (Whittaker, 1972). For example, because of a climatic or geographic barrier, if only a few mammalian families ever make it to a particular geographic region where they would be ecologically suited, then the community structure will reflect the phylogenetic constraints of those families (Ricklefs 2004).

While analysis of community structure is concerned primarily with relative proportions of various ecologies (Andrews and Hixson 2014), the ecometric approach takes quantitative measurements of ecologically relevant morphological traits (Eronen et al., 2010a). This ecometric approach is therefore related to the previously discussed analysis but contributes quantitative data that can be measured in individuals, populations, species, communities or metacommunities (Eronen et al. 2010a). This has the added benefit of being able to record morphological variation in climate change across multiple taxonomic levels—e.g. the niche structure of rodents, primates, or marsupials—in individual localities, even when the difference in overall community structure between localities is negligible (Reed 2013). So far, such ecometric studies of mammals have been limited to comparisons of body size distribution in relation to climate (Ashton et al. 2000; Blackburn et al. 1999; Secord et al. 2012) tooth structure and precipitation (Eronen et al., 2010b; Fortelius et al., 2002; Liu et al., 2012) as well as calcaneal morphology, "gear ratios" and climate (Polly 2010). The results from these studies suggest that there is utility in using quantitative methods for reconstructing paleoclimate and environment.

An example of the ecometric approach is seen in the evolution of high crowned cheek teeth (i.e. "hypsodonty"). Trends towards hypsodonty are regarded an adaptive response to abrasive and/or fibrous foods (Janis and Fortelius 1988; Jernvall and Fortelius 2002; MacFadden 2000; Williams and Kay, 2001; Van Valen 1960) and are considered ecologically informative because these abrasive/tough foods are found in abundance in open, dry (or seasonal) environments (Damuth and Janis, 2011; Eronen et al. 2010b; Janis and Fortelius 1988; Jernvall and Fortelius 2002). These studies have generally used large-bodied ungulates as their subjects of study (though Williams and Kay [2001] also included rodents in their analysis), and for this reason are unable to discern finer scale differences in environments, particularly within the same latitudinal zones (Eronen et al. 2010a; Liu et al. 2012).

An apparent issue with using body size in any paleontological context is the problem of body mass prediction in fossil organisms. Complete skeletons are exceedingly rare in the fossil record, and therefore body mass prediction equations (BMPE) are often focused on specific skeletal elements. The most commonly used element has been teeth (Beard et al., 1996; Conroy, 1987; Gingerich, 1977; Gingerich et al., 1982; Kay and Simons, 1980). However, other studies have used other skeletal elements such as: craniofacial elements (Martin 1981; Cartelle and Hartwig, 1996; Steudel, 1980), the femur (Cartelle and Hartwig, 1996), and the ankle bones (Dagosto and Terranova 1992; Yapuncich et al., 2015). The potential pitfalls of body mass

prediction in fossils are numerous. First, BMPE's are only appropriate when the fossil for which mass is to be estimated is of a known phylogenetic affiliation (Smith, 2002). For example, even within one order (Primates), using a cercopithecoid-derived BMPE to estimate the mass of a fossil ape could produce an estimate that is more representative of monkeys than it is of apes, because of the phylogenetic specificity of the scaling relationship of the proxy used. The unresolved phylogenetic affiliation of many fossils can present uncertainty as to which taxon-specific model to use. Moreover, the small sample size of fossils introduces another problem. The sample mean is only an estimate of the species mean, and with very small sample sizes (as is often the case in the fossil record) the confidence interval for that estimate can be large (Smith, 2002).

1.3 Dental Topography Metrics

To overcome the problem of body size reconstruction, I use dental topography metrics that have been shown to be independent of size. Quantification of whole tooth surfaces has taken a number of forms in the past two decades (Reed, 1997; Jernvall and Selanne, 1999; Ungar and M'Kirera, 2003; Dennis et al., 2004); of these I include three recent methods: orientation patch count rotated (OPCR) (Evans et al., 2007; Evans and Jernvall, 2009), relief index (RFI) (M'Kirera and Ungar, 2003; Boyer, 2008), and Dirichlet normal energy (DNE) (Bunn et al., 2011; Winchester et al., 2014). Each of these metrics takes advantage of tooth surface scans that can be translated into 3D meshes that comprise polygonal—in the case of my study, triangular—faces. These meshes can be

standardized across different species—even in broad taxonomic samples such as I use here—by maintaining equivalent relative resolution between scans and by making the absolute number of faces used to reconstruct the 3D surfaces equivalent across all scans. These surfaces can then be modified to remove any defects or noise introduced by the scanning process—a potential source of error that I explore in the context of DNE in Chapter 3 (Spradley et al., 2017)—resulting in a 3D reconstructions of tooth surfaces that can be quantified using these established metrics.

The dental metrics are described in greater detail in the following chapters, but I will provide a brief of explanation of each here. Introduced by Evans et al. (2007), orientation patch count (OPC) seeks to quantify the complexity of a surface by counting the number of "patches" on that surface. If the surface is reconstructed using triangular faces, each patch is a group of at least three adjacent faces that all lie in the same plane of slope orientation, typically defined within 45° vectors around the central vertical axis of the tooth (analogous to the four cardinal and four intercardinal directions found on a compass). The seams between patches are then assumed to be analogous to "breakage sites" or cutting crests (Lucas, 2004; Evans et al., 2007), which aid the tooth in the breakdown of food. Thus, the number of patches is correlated with the number of seams between patches, which are assumed to be cutting edges on the tooth surface. A derivation of OPC, OPCR (Evans and Jernvall, 2009), was later developed that helped solve the issue associated with the arbitrary orientation of the tooth or tooth row during

analysis, which affects the measurement of patches. Evans and Jernvall (2009) demonstrated that OPCR is positively correlated with herbivory in rodents and carnivorans, suggesting its broad taxonomic potential, though results from OPCR in rodents (Evans and Jernvall, 2009) and primates (Ledogar et al., 2013; Winchester et al., 2014) are weaker, suggesting further separation of herbivorous diets may be problematic.

M'Kirera and Ungar (2003) demonstrated in African hominoids that a relief index (RFI)—a ratio of the surface area of the 3D occlusal surface to the 2D planometric area created by the "footprint" of that tooth—is related to the diet of species. Specifically, they showed that the tall crown and high crests and/or cusps of the folivorous *Gorilla gorilla* distinguished it from the more frugivorous *Pan troglogdytes*. Boyer (2008) modified the approach of M'Kirera and Ungar (2003) and expanded his analysis to include 19 different genera from across Euarchonta, and his results indicated that this pattern was generalizable to this broader taxonomic sample as well. Among the benefits of RFI include; 1) it is an easy to understand and easy to illustrate metric; 2) it has a demonstrated relationship with tooth wear (Pampush et al., 2016b); and 3) it is relatively resistant to noise on the surface introduced by the process of scanning (Boyer, 2008). Additionally, RFI is a good proxy for hypsodonty, an important adaptation in mammalian tooth morphology that is discussed further below.

The most recently developed of the three metrics, DNE is best described as a measure of the curvature of a surface (Winchester et al., 2014; Spradley et al., 2017). DNE begins with the calculation of an "energy value" for each face (i.e. each triangle) on the surface, and this energy value is associated with normal vectors assigned to each vertex (Bunn et al., 2011). At each vertex we can find a normal vector emanating from that point. The direction of each 'vertex normal' is the average of the normal from each face affixed to the vertex, and if we follow these normal vectors emanating from vertices out a specified distance, we can then draw another triangle from the ends of these vectors, and measure the area of this resultant triangle. The difference in size between the projected triangle's area, and surface polygon triangle's area results in the Dirichlet energy density (DED) of the face. Large differences (in either direction) between the projected triangle and the surface polygon triangle result in high DED. Faces on a curvy surface will produce a greater difference between resultant triangles, and in turn contribute to the overall measure of DNE (see Pampush et al., 2016a for detailed figures illustrating these concepts). Ledogar et al. (2013) and Winchester et al. (2014) demonstrated that DNE is a good discriminator of dietary ecology in platyrrhine primates (Ledogar et al., 2011; Winchester et al., 2014) and strepsirrhine primates (Winchester et al., 2014). DNE may also reflect changes in dental topography that allow the tooth to maintain functional efficiency and prolong the functional life of the tooth as it wears (Pampush et al. 2016b). All of these previously published studies of DNE point

to its promise as a metric with broad-scale utility for discriminating tooth complexity in relation to diet.

1.4 Ecometrics of Small Mammal Cheek Teeth

As might be ascertained above, the vast majority of previous ecometric studies have focused on large mammals. This discrepancy is likely due to two reasons: 1) the sampling bias of large mammals in the fossil record; and 2) the abundance of large mammalian taxa in the savannahs of East Africa, an area of intense study in hominin evolution. While these taxa have been useful for studies of hominin paleoecology, they do not present much utility for discerning differences in the forested habitats that likely played an essential role in the evolution of early primates, and indeed other forest-dwelling primate clades. Additionally, such studies may be extended to other mammalian clades have evolved in association with changing environments, in ways that are both similar and dissimilar to primates.

For this purpose, small mammals intuitively serve as a more viable option. Small arborealists are dependent on the productivity and/or complexity of the vegetation, which are themselves dependent on various aspects of the climate (Kay and Madden, 1997). Terrestrial forms are in turn dependent on the types and complexity of ground cover, which is often dependent on climate (Louys et al., 2011). Additionally, unlike the large herbivores of the savannah, small mammals have relatively small geographic ranges, making them ideal candidates for proxies in response to localized

changes in climate and environment (Montuire et al., 2006; van Dam, 2006). Small body sizes also typically translate to high metabolic rates, resulting in higher rates of heat and water loss, making them more susceptible to small-scale changes in climate and environment (Pearson 1947; Churchfield, 1990). Finally, non-volant small mammals do not migrate, and must adapt to any seasonal changes in their environment; thus we would expect to see differences in niche structure related to seasonality.

A significant obstacle to using small mammals in this way is that their preservation in the fossil record is relatively poor when compared to large mammals, as evidenced by taphonomic studies of faunal composition and bone preservation (Behrensmeyer et al., 1992; Kidwell and Flessa, 1996). However, due to their high hardness relative to other parts of the skeleton (Newbrun and Pigman, 1960; Lucas et al., 2013), teeth are differentially preserved in the fossil record, especially those of small mammals. In fact, many small mammalian genera are known only from their dentitions. This implies that any study interested in reconstructing broad-scale community ecologies in these small mammals should focus on teeth first, as this would be the most broadly applicable. Fortunately, teeth are also highly informative as to diet. Despite their phylogenetic signal (Crompton, 1971; Fox, 1975; Read, 1975; Luo et al., 2001; Woodburne et al., 2003), teeth are, in a sense, where the "rubber meets the road," a focal point of the interaction between an organism and its environment. It is of no surprise then, that tooth morphology is intimately related to the types of foods and food materials consumed by

the organism (Crompton and Lumsden, 1970; Kay, 1975; Evans and Sanson, 2003). This close relationship allows paleontologists to reconstruct dietary ecology in extinct mammal species based on relationships established in modern mammalian samples, and forms the backbone for a great deal of paleoecological studies. In addition, the ubiquity of small mammal teeth in the Cenozoic fossil record (particularly rodents after the Eocene) creates a great potential for their use in reconstructing climate on a continental or even global scale (Montuire et al., 2006; van Dam, 2006).

1.5 Vagaries of the Fossil Record

Any attempt of a faunal-level analysis in the fossil record is necessarily fraught with a number of assumptions inherent in the fossil record including: temporal resolution (time-averaging), spatial resolution, and taphonomy will affect the composition of a faunal list. The degree to which these have an effect on such an analysis is dependent on the quality (both taphonomic and stratigraphic) of the fossil record and the research question.

A problem that has been discussed frequently in the literature, is that of time-averaging. Briefly, time-averaging is "the process by which organic remains from different time-intervals come to be preserved together" (Kidwell and Behrensmeyer, 1993, p.4). While every geological record is time-averaged at some scale, it is typically only discussed in relation to its effect on paleoecological analyses. Time-averaging can affect faunal lists in two very distinct ways: overcompleteness and incompleteness

(Flessa et al., 1993; Kidwell and Flessa, 1996). Overcompleteness is generally a result of stratigraphic mixing, wherein the resolution of the geologic record is coarser than the turnover of the fauna (Kidwell and Flessa, 1996). This lends itself to the compilation of species lists that represent two or more temporally distinct faunas that may be from distinctly different environments, and thus an overestimate of the richness of the fauna. In the context of this study, this would confuse the interpretation of results in a fairly predictable way; namely, that higher richness would make the reconstruction of the environment seem wetter, warmer, and more productive than it was, since in South America richness is positively correlated with precipitation and temperature (Kay and Madden, 1997; Kay et al., 1997).

The degree to which time-averaging affects any specific fossil fauna is difficult to quantify (see Croft [2013] for a critique of the definition of the Santa Cruz formation fauna), though there are methods by which previous studies have sought to control for the effect of potential 'incompleteness'. One common method is rarefaction analysis, in which species richness is assessed as a function of the number of samples from the fauna (Hurlbert, 1971; Heck et al., 1975; Stucky, 1990). This leads to a rarefaction curve (Stucky, 1990) that gives a confidence interval for the "true" species richness (or other features of the community, such as morphological diversity) of the community and an asymptote by which an estimate for a level of sampling that is likely to give a stable estimate of the richness (Foote, 1992). This method has been employed for a number of fossil faunas,

including the Miocene fauna of the Santa Cruz formation (Croft, 2013) and the Eocene fauna of the Willwood formation (Chew, 2009)

A field biologist recording the species present at a particular site is able, however precisely, to control the area sampled. This allows for other factors regarding the environment to be controlled, or at least included in an ecological analysis; including habitat heterogeneity, elevation, and potentially even high-resolution data for the environment like plant diversity, soil pH, and canopy height. In the fossil record, however, this sort of precision is impossible. Animals that die in or near bodies of water can be subject to post-mortem transport, eventually depositing downstream. Once discovered, this process can lead to faunal lists that overestimate the richness of the community. While this can be hard to quantify, research on bone assemblages in modern mammalian communities can give an indication as to the likelihood of transport. From field experiments with purposefully placed bones, it is deemed unlikely that downstream transport affects the composition of bone assemblages—and therefore fossil assemblages (Behrensmeyer, 1982; Behrensmeyer et al., 1992; Kidwell and Flessa, 1996).

Ultimately, this dissertation is meant to be a "proof of concept" for the potential of using dental ecometric distributions as proxies of environment. To avoid many of the potential pitfalls described above, I will apply the above-mentioned models derived from extant assemblages to two fossil faunae that are heavily sampled and temporally narrowly constrained: the Monkey Beds stratigraphic interval of La Venta, Colombia

and Faunal Levels (FL) 1-7 of the Santa Cruz Formation in southern Argentina. Both fossil localities represent especially rich deposits of mammalian fossils, and complete faunal lists have been published for each (the Monkey Beds: Kay and Madden, 1997; Santa Cruz FL 1-7: Kay et al., 2012b). The paleogeography of these two sites is described in further detail in Chapter 2, but both of these deposits are from the Early and Middle Miocene of South America. As such, there are three clades of relatively smaller bodied mammals that predominate in these faunas; Primates, Rodentia, and Marsupialia (Patterson and Pascual, 1968; Kay and Madden, 1997; Kay et al., 2012b). In the context of dental ecomorphology, the latter two are much less well understood than the first, and thus are the primary focus of this dissertation.

1.6 Outline of Chapters

With the discussion in the previous sections in mind, the guiding question of this dissertation is as follows: can the distributions of dental ecometrics in small mammals be used to reconstruct climate and habitat in the Miocene fossil record of South America? To answer this question, I approach it in three successive steps. To begin, I attempt to establish the relationship between the distribution of ecologies within mammalian communities and six bioclimatic variables, including precipitation, temperature, seasonality (in both temperature and precipitation), primary productivity, and canopy height. Since previous analyses have primarily used traditional linear regression, I also use this opportunity to test a number of additional regression techniques that have

gained currency in the ecological literature since the early 2000s. Using training data and a randomly selected test dataset, models are produced from each regression technique with accompanying error metrics to assess the performance of these models. I end this chapter by applying these models to the above-mentioned Miocene fossil localities in South America. Estimations from all techniques are compared with one another and previous paleoecological reconstructions for these sites (Kay and Madden, 1997; Kay et al., 2012b).

Having demonstrated a relationship between the diversity/richness and climate, I then move on to establishing a relationship between dental topography and ecology in two small mammal taxa—marsupials and rodents—that are important to the faunal diversity of the Miocene in South America. In this study I will focus on three metrics of dental topography: DNE, RFI, and OPCR. DNE being the most novel of the three and the least standardized, I use Chapter 3 to establish a protocol that justifies decisions made regarding the downsampling and smoothing—together termed as "retriangulation"—of 3D meshes representing scanned tooth surfaces.

In Chapter 4, I examine how dental topography in marsupial species relates to their dietary ecology. As mentioned above, marsupials are very diverse in the Miocene of South America; however, the diversity of extant marsupials in South America is more limited, so in order to capture the diversity that we find in the South American fossil record, I include data from extant Australian diprotodontids, paramelids, and dasyurids

in my study. Starting with CT scans of tooth surfaces, I measure the three dental topography metrics and use phylogenetically-corrected one-way ANOVAs to test for the effect of diet on these metrics. Post-hoc tests are also used to identify significantly different means of dietary groups. I conclude this chapter by combining the dental topography metrics for all marsupial species (or at least all species sampled in this study) found at a number of modern mammalian localities from across Australia and New Guinea. The distributions of these dental ecometrics—namely statistics associated with distributions including the means, ranges, coefficients of variation, and skewness—are correlated with the same six bioclimatic variables in Chapter 2. This analysis is intended to show the utility of the distributions of dental ecometrics as proxies of climate and habitat.

Chapter 5 includes a similar analysis to Chapter 4, except with the other mammalian group of interest, the rodents. South America represents the ideal continent for broad-scale analyses of rodent morphological diversity, as this continent has the most ecologically diverse community of rodents in the world (Kay and Hoekstra, 2008). In a sample including caviomorph, sigmodontine, and sciurid rodents, I once again correlate dental topography metrics with dietary ecology using phylogenetically-corrected methods. Additionally, I use the distributions of these metrics across the South American localities included in Chapter 2 to study how rodent dental topography can be used as a proxy of climate and habitat. Using this large collection of localities also allows

me to apply the same regression techniques used in Chapter 2 to directly compare the use of distributions of quantitative measurements in a single taxon to qualitative indices of entire faunas as potential proxies of environment. In combination with Chapter 4, this analysis is intended to demonstrate that the distributions of ecometrics can be used as climatic proxies in place of qualitative indices. This circumvents the need to reconstruct behavior in the fossil record—a potential source of error—and instead provides a proxy that relies on measurements that can be taken directly from the fossil themselves.

I conclude this dissertation with a brief summary of my results as well as a discussion as to how well the question above was answered. I also outline future directions for related projects and how these studies may help us to better understand mammalian evolution in the context of changing environments in the Miocene of South America.

2. Past Life Regression: Mammalian Faunas, Ecological Indices, and Machine-Learning Regression for the Purpose of Paleoenvironment Reconstruction in the Miocene of South America

Reconstructing paleoenvironments has long been considered a vital component of understanding the biology of extinct organisms, as well as the patterns that guide the evolutionary pathways of species and higher-level taxa. However, the ability for researchers to reconstruct past environments is necessarily limited by the available lines of evidence; including geochemical indicators of the environment (Wilson, 1974; Hayes et al., 1990; Kohn, 2010; Cerling et al., 2011), the adaptations of the organisms present in a fossil assemblage (Andrews and Van Couvering, 1975), and the ecological diversity of the assemblage (Fleming, 1973; Andrews et al., 1979; Kay and Madden, 1997; Kay et al., 2012a). For the purposes of this study, I focus on this latter form of evidence, ecological diversity. That is, the number and types of ecological niches (Hutchinson, 1957) filled within any given faunal community. This study proposes a novel approach for paleoecology reconstruction in utilizing two machine-learning algorithms—the random forest (RF) and Gaussian process regression (GPR)—which are applied to faunal diversity and climate data from several extant Central and South American localities to produce a paleoecology prediction model. In order to gauge the predictive power of the generated models, the models were used to estimate climate parameters at several extant Australian and New Guinean sites based on their faunal assemblages.

Australia/New Guinea serves as an ideal test for my data for two primary reasons: 1) due to the relative geographic isolation of the Australian continent and New Guinea, the mammalian fauna there is phylogenetically distinct from that of South America, and thus similar ecologies and morphologies between the two faunas are almost certainly due to convergence rather than shared descent; and 2) Australia, with the addition of New Guinea, is a large continent with a great diversity of climates and habitats, much like South America.

Having demonstrated the accuracy of my model for estimating modern climate parameters in phylogenetically distinct faunas, I use the model to reconstruct paleoclimatic variables in two well-sampled Miocene faunas from South America, the Santa Cruz fauna from Argentina and the La Venta fauna from Colombia. The former is an unusually well sampled (from the perspective of species richness and fossil completeness) Early Miocene fauna from the far southern tip of South America. The latter is the only Middle Miocene neotropical locality for which I have a relatively complete sample of well-preserved mammal taxa. For both formations, I am restricting my analysis to specific complete levels that have previously been identified as approximating a contemporary fauna, faunal levels 1-7 (FL1-7) of the Santa Cruz formation (Kay et al., 2012b) and the Monkey Beds of the Honda Group in La Venta (Kay and Madden, 1997). These retrodictions are compared to those from more

traditional linear regression and regression tree models, as applied to the modern and extinct faunas.

2.1 Background

That mammal species occupying similar habitats have convergent adaptations is one of the foundational blocks of natural philosophy, including Cuvier (Gould, 1982) and Darwin (Darwin, 1859), and serves as the theoretical basis for the use of ecological diversity as an avenue for understanding and reconstructing paleoecology. Referred to by CS Elton in 1927 as ecological "vicars", Darwin, Elton, and others envisioned species as filling roles (or niches) within an ecosystem, roles that would be present and filled in similar environments regardless of the taxonomic affiliation of the species that are actually present; just as the duties of a village vicar would be performed regardless of what individual actually assumed the role. While the metaphor can only go so far, when describing the niche structure of a community it nevertheless becomes useful to describe species not by name but rather by what they do (e.g. how large are they, what do they eat, what part of the environment they inhabit, etc.). This premise is validated by the strong correlation between aspects of phenotype and environment as documented by countless studies designed to test this relationship (e.g., Anthony and Kay, 1993; Boyer, 2008; Boyer et al., 2013; Crompton and Lumsden, 1970; Ross and Kirk, 2007). While this implies an adaptive link between form and function (Kay and Cartmill, 1977), it is not dismissive or at odds with the reservations of Gould and Lewontin (1979) who

suggested that not all morphology is adaptive, since such research is extremely circumscribed in how it defines aspects of morphology that can be candidates for adaptive processes (e.g., Kay and Cartmill 1977, Kay et al. 2004; Seiffert et al. 2009; Boyer et al. 2013).

The link between form and function allowed for studies such as the seminal work of Andrews et al. (1979) that sought to identify patterns in the distributions and frequencies of various niches within mammalian communities, particularly as they relate to the general structure of the environments they inhabit. While it was Harrison (1962) and Fleming (1973) who established that mammalian communities vary predictably with latitude, Andrews et al. (1979) demonstrated that even when latitude was held constant, mammalian community structure is significantly correlated with habitat type. And when both latitude and habitat type are similar, mammalian niche structure is "remarkably constant" (Andrews et al. 1979). Other studies have gone on to show that niche structure covaries predictably with precipitation (Kay et al., 1997). The former approach of Andrews et al. (1979), for reconstructing the habitat type reveals a potential flaw of the approach of Kay et al. (1997); namely, focusing on a specific climate variable fails to consider that a climate variable (such as precipitation) is related to community structure only in that it is also correlated with a certain habitat type. In other words, by using community structure to reconstruct a single climate variable like rainfall, I am potentially losing track of the important matter of describing the habitat in

which these animals lived. On the other hand, using quantitative variables eliminates the need to subjectively characterize a habitat into one category or another. To reconcile these two approaches, I include a number of different climatic variables (temperature, precipitation, and seasonality) as well as two quantitative variables directly associated with the habitat (canopy height and net primary productivity). Combined, these variables can give a suitable description of the habitat without relying on somewhat subjective qualitative descriptions of habitat.

In the context of paleoclimate reconstruction, it is thus advocated that the distribution of niches within a mammalian fauna can serve as a proxy for habitat structure or climate, as has been done in a number of previous studies (e.g., Andrews et al., 1979; Gingerich, 1989; Vizcaino et al., 2010; Kay et al., 2012a; 2012b). Such studies are limited by a multitude of factors, specifically related to the difficulties inherent to sampling, both in living faunas and in the fossil record. In relation to living faunas, an incomplete sampling effort can lead to the exclusion of rare species from a faunal list. It can also be difficult to give an accurate estimation of the general climate or habitat, depending on the length of the observation. Therefore, I include only data from long-term field studies from biological field stations. Such stations collect data on the fauna present as well as track various climatic variables (e.g., precipitation, temperature, etc.) over decades, providing an approximation for the ecosystem that is robust to aberrant seasons or years.

Similar issues arise when defining a fossil fauna in both space and time. When recording the species in a modern mammalian community, one can control the size of the area sampled, and be confident that all species are contemporaneous, i.e., not time averaged. With a fossil fauna, however, assumptions must be made as to the fidelity of the fossil assemblage as compared to the prehistoric life assemblage. Taphonomic studies in mammals suggest a bias against recovery of small mammals in bone assemblages (Behrensmeyer and Dechant-Boaz, 1980; Damuth, 1982; Sept, 1994). As an illustrative example, Behrensmeyer and Dechant-Boaz (1980) found that only 60% and 21% of small (<1kg) herbivores and carnivores, respectively, that were recorded in a six-year study of a mammalian community were also recorded in the bone assemblage. That is compared to large mammals (>15kg), of which 95-100% were also recorded in the bone assemblage.

A second commonly mentioned obstacle to assessing fossil community structure—time averaging—may be the solution to the first. Time averaging is the process by which distinct events appear to be synchronous in the geological record in part because the processes associated with burial are generally slower than population turnover (Walker and Bambach, 1971). Time averaging potentially creates over-completeness—i.e. oversampling of a fauna that results in an over-estimation of the total number of species—in an assemblage instead of under-completeness (Kowaleski, 1996). While the ways in which time-averaging can affect a fossil assemblage are varied and

distinct (Kidwell and Flessa, 1996), in the context of this study the biggest concern is that a single fossil assemblage, by being a sampling of extinct species from an interval of time (versus a single time slice, as in a modern fauna) might encompass an interval of environmental change, thereby blunting the environmental signal of the data. However, such extreme cases are rare (Kidwell and Flessa, 1996) and are typically recognized by incongruences within a geological context (e.g., unconformities). When temporal resolution is constrained, time-averaging allows for even rare species within a fossil assemblage to be recorded, thus providing a presumably complete inventory of the fossil community.

Finally, Croft (2013) warned that in the context of paleoecological analyses, the area sampled whilst compiling faunal lists for extant communities must be considered in relation to the presumed area of the fossil locality. This is based on the reasoning that ecological diversity within a community will have a positive correlation with the area sampled. While this is certainly true, as Croft (2013) himself notes, this is an inherently difficult task and the degree to which it affects the results of such analyses is a relative unknown. In addition, estimates for the area sampled are frequently excluded from published faunal lists. Therefore, I exclude this variable from my analyses, and can only conjecture as to its influence on my results.

2.1.1 Regression Methods of Paleoecological Reconstruction

While the long history of paleoecology necessarily makes it impossible to review all available methods, I focus here on several techniques that take advantage of regression statistics for prediction—or more appropriately, retrodiction. Until recently, studies seeking to reconstruct past habitat and climate from the mammalian fossil record have used linear regression models and Principal Components analyses using variables drawn from those regression analyses (Andrews et al., 1979; Kay and Madden, 1997; Kay et al., 2012a, 2012b). This study tests the applicability and accuracy of newer, more computationally complex regression techniques that have been used in the ecology literature. These techniques include regression tree analysis, random forests, and Gaussian process regression.

Beginning with a dataset of modern South American mammalian localities, I test each of the methods described below for their accuracy and predictive power, as applied to test samples from South America and Australia/New Guinea. My objective is to assess the potential of machine-learning algorithms for paleoecological reconstruction, and compare their performance to previously published regression techniques.

2.1.1.1 Multivariate Linear Regression

Kay and Madden (1997) and Kay et al. (2012b) use a multivariate linear regression… (to do what?). First performing a PCA of the ecological variables included in their study, they then use the first principal component axis (PC1) as an independent

variable in a simple bivariate correlation. A linear regression performed on this correlation then provides a simple linear model for reconstruction (in the case of Kay et al. [2012b], the Santa Cruz faunal levels 1-7). While I do not include all the ecological indices Kay and Madden (1997) and Kay et al. (2012b) employed, I include this multivariate approach in my study for comparison, and generally refer to it as "linear regression".

2.1.1.2 Regression Tree Analysis

While traditional regression techniques assume some specified relationship between the predictor variable(s) and the response variable (e.g. a straight line, quadratic, etc.), regression tree analysis (RTA) builds a series of rules for partitioning the data into homogenous subsets based on values of the predictor variables. This series is best illustrated as nodes, branches, and leaves—hence the "tree." At each node, the best predictor variable is chosen from all other predictor variables to split the data into its largest homogenous groups, these groups are then further split—i.e. "recursive partitioning"—using other predictor variables until the data can no longer be split. Each leaf then is a cell that carries all data points that have the same partitioning course. The resultant tree can then be used to predict new values in an efficient, easy to understand (and illustrate) manner (see Figure 1 for an illustrative example using hypothetical data).

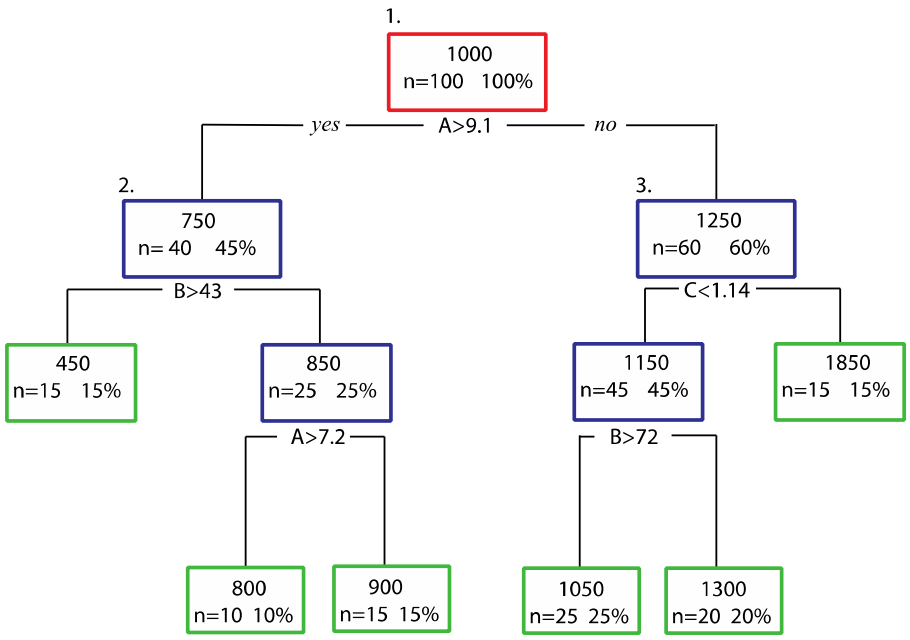

Figure 1: I Illustrative regression tree constructed using hypothetical data. In each box there are three numbers. The first number, n=## indicates the total number of individual data points represented in the subset at that node. For instance, in the first node (colored red), there are 100 data points represented at this node. The number to the right of the N value indicates the percentage of the total dataset represented at that node. In the case of the first node, this would be the complete dataset, 100%. The number above these two is the average value of the response variable (the variable that I am trying to predict) of that subset. Below this box, we also see "A>9.1". This represents the predictor value that best subdivides the data into homogenous groups. In this hypothetical data, any data point that has a value of "A" greater than 9.1 is now represented in node 2. As the algorithm proceeds through the nodes—colored in blue—eventually it comes upon subsets of data that effectively cannot be further subdivided into homogenous groups. These are the "leaves" of a regression tree, and are colored in green here.

The advantages that RTA carries over classical regression are immediately clear. First and foremost among these is the ability to incorporate non-linear relationships between a response and a predictor variable, a trait that is particularly useful in biology

wherein complicated, non-linear relationships are common (Moore et al., 1991; Kay and Madden, 1997). In addition, the simplistic output of the tree allows for the relative importance of the various predictors on the distribution of the data to be clearly shown, providing insight into the spatial influence of the predictors (Iverson and Prasad, 1998; De'ath and Farbricius, 2000).

However, RTA is not without its disadvantages, even when compared to conventional regression. First, any linear functions that happen to be included in the analysis are only approximated, and because of the nature of RTA these linear functions tend to be binned in a manner that oversimplifies the linear relationship, leading to a "coarseness" of the RTA output. Those values that lie close to the boundary of two bins are more likely to be misidentified. Additionally, results from RTA are highly dependent on the input data, can be unstable with small changes to the input data producing highly divergent trees. While this can be overcome with an appropriately large dataset, particularly one in which the variables are normally distributed, such a dataset is frequently hard to obtain in ecology.

2.1.1.3 Random Forests

Introduced by Breimann (2001), RF is a machine-learning approach based heavily on RTA. RF analysis works in the following steps (Liaw and Wiener, 2002):

1. The original data is bootstrapped into a specified number of re-sampled data sets.

2. Regression trees are produced for each bootstrapped sample with an alteration to the node partitioning. Node partitioning is performed on a random sampled subset of the resampled predictor variables, and the best predictor is chosen among that subset.
3. New predictions are made through aggregating and averaging all the trees of the bootstrapped samples. Data is predicted by averaging the predictions of all the trees of the bootstrapped samples.

While the result from any given tree may differ dramatically from that of another tree, the high number of trees that are typically grown in RF—≥1000, hence the "forest"—allows it to effectively construct the best fit of the data irrespective of minor perturbations within and amongst individual trees. This is further illustrated in Figures 2 and 3.

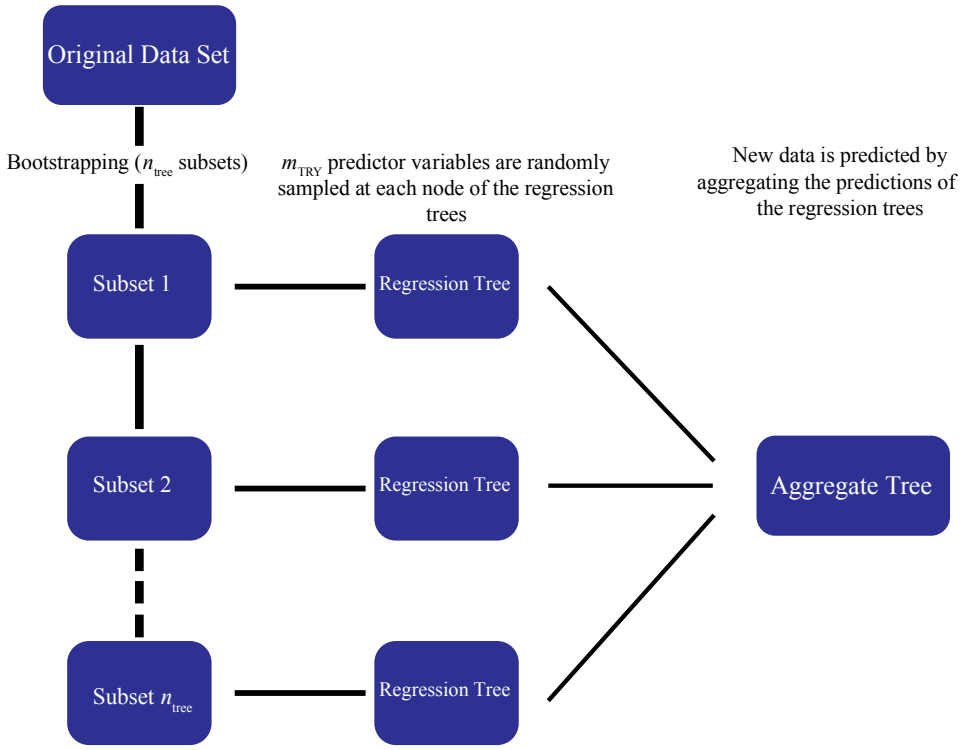

Figure 2: Overview of the procession of the random forest algorithm from the original data set to predicting new data.

One of the complaints frequently leveled at RF is its apparent lack of interpretability, that it is a "black box" (Cutler et al., 2007). This criticism stems from the fact that RF lacks the illustrative efficiency of more traditional regression techniques. Instead of producing one tree, RF predicts "out-of-bag" observations by calculating the average of hundreds (or even thousands) of fully-grown, bootstrapped trees, meaning that the relationship between variables is impossible to demonstrate. This is also true for

error estimates as, unlike traditional regression, RF is incapable of providing confidence intervals for new values of y.

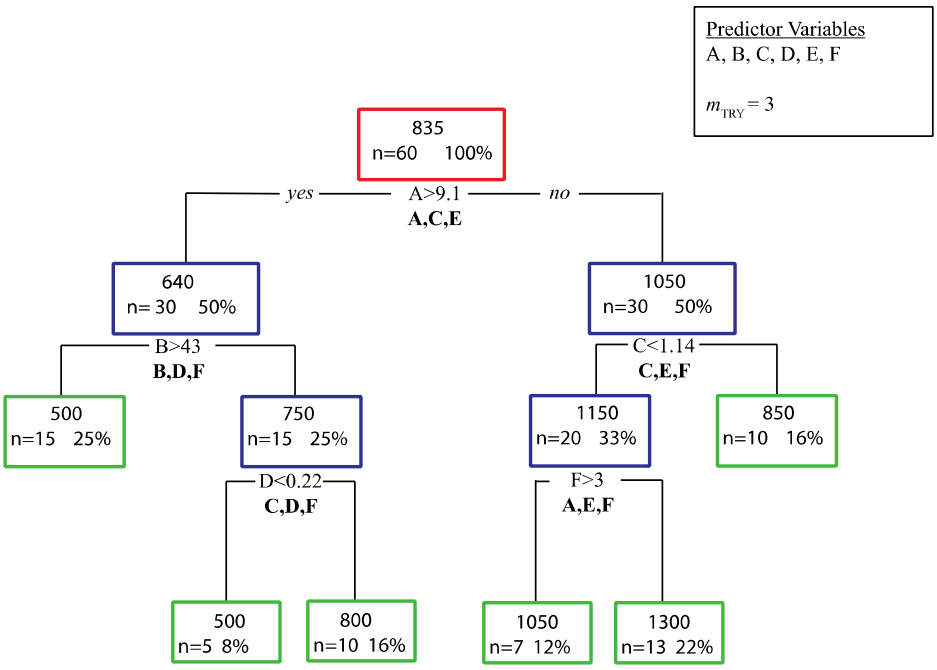

Figure 3: Example of a single tree from a random forest analysis. In this example, at each node three (m_{try}) of the six predictor variables are randomly chosen and the variable that best splits the data into homogenous groups is chosen.

However, RF carries many advantages over traditional methods. Chief among these is that instead of having to select one or two predictor variables from a set of highly correlated predictors, RF can include all variables and even determine the relative importance of each variable (Cutler et al., 2007). Additionally, because a large number of trees are grown, the potential of the training data error to be radically different from the underlying model error for a given population is small, minimizing the potential of overfitting (Prasad et al. 2006). Furthermore, while RF does not require an *a priori* model selection, there are parameters that must be chosen, namely the number of predictor variables randomly chosen per node (m_{try}), and

the number of trees (n_{tree}). Though the chosen values of these parameters can influence the results (i.e. the predictive accuracy of the RF model), this effect has been shown to be relatively negligible (Briemann, 2001; Liaw and Wiener, 2002; Cutler et al. 2007).

2.1.1.4 Gaussian Process Regression

GPR can be differentiated from standard linear regression in that rather than producing a model (typically a straight line) that seeks to capture the relationship and variance of the dataset as a whole—and thus provide a simple equation that describes the general relationship between the independent variable(s) and the dependent variable—it instead can model the covariance of a vector between only two points (Rasmussen, 2006). It is, in essence, a model of interpolation; wherein the estimation of a new data point that lies in between two observed data points has a smaller confidence interval (that is, it can be estimated with greater confidence and lower error) than would a new data point that lies between two observances that are more distant to one another. This is done through the formation of a Gaussian, or normal, distribution for the potential function that connects two known data points. If the observed data clusters in close proximity, then the distribution that represents the likely feature-space of a function that connects those two points will be narrower.

In other words, in simple linear regression, the uncertainty is standardized for all new estimations. In GPR the uncertainty of predictions is dynamic, changing depending on the richness and proximity of observed data. GPR has been demonstrated to be an

effective predictive model for non-linear relationships between continuous variables, including in species distribution mapping (Weir and Pettit, 2000; Verrelst et al., 2012).

The mathematics of GPR is explained in further detail in Appendix B, which represents a collaborative document created in conjunction with Bryan Glazer, whose knowledge and expertise in this modeling technique contributed greatly to its application in this study.

2.1.2 Paleoecological Reconstruction

While the above methods have been used previously in ecological literature (e.g., Okubo & Levin, 1980; Dunning et al., 1995; Monestiez et al., 2005; Rigby et al., 2010; Verrelst et al., 2012) they have yet to be applied to the fossil record for the purposes of environmental/climatic reconstruction. Heretofore, linear regression has been the favored method due to its simplicity of output, application, and interpretation (Andrews et al., 1979; Kay and Madden, 1997; Kay et al., 2012b). Here, I test these other regression methods along with the more conventional linear regression in order to explore their potential in paleoenvironmental reconstruction. Additionally, I apply these methods to two well-sampled fossil localities in South America, the La Venta and Santa Cruz Miocene faunas. The reconstructions derived from the different methods are subsequently compared among one another and—where possible—to previously

published reconstructions (e.g., papers with the older reconstructions). Brief descriptions of each of these fossil localities are presented below.

2.1.2.1 La Venta Paleogeography

The La Venta faunal list used in this study comes from the Monkey Beds of the Honda Group in the Magdalena river valley in Colombia. The Honda Group, at about 5°N latitude, attains a thickness of 1150m (Guerrero, 1996) and is constrained by radiometric and paleomagnetic evidence to a period beginning at approximately 13.5ma and ending at approximately 11.8m (Flynn et al., 1996; Guerrero, 1996; Madden et al., 1996). The Monkey Beds comprise a richly fossiliferous layer of the Honda Group with a thickness of approximately 14.8m (Guerrero, 1996; Kay and Madden, 1997). Magnetostratigraphic evidence limits the time interval of the Monkey Beds to ~15,000 years from between 13-12.85ma (Flynn et al., 1996; Kay and Madden, 1997).

In the mid-Miocene, the La Venta region was situated within 5 degrees of the equator on a peninsula in northern South America, bordered to the west by the Pacific Ocean and to the north and east by the Caribbean Sea (Whitmore and Stewart, 1965; Duque-Caro, 1990; Hoorn et al., 1995; Kay and Madden, 1997). Fossil vertebrate evidence from amphibians and reptiles, suggests low elevation (<100m) in the middle Miocene La Venta. This conclusion stands in contrast to the region today, which is largely dominated by the Colombian Andes—though the actual fossil locality lies in the

Magdalena river valley (approximately 500m in elevation) between the Central and Eastern Cordilleras (Kay and Madden, 1997).

Previous paleoecological reconstructions at La Venta (Kay and Madden, 1996; Kay and Madden, 1997) have suggested a forested environment within a complex system of meandering rivers, with a mean average rainfall of between 1500-2000 mm/year. Seasonality was estimated to be an insignificant component of the middle Miocene at La Venta (Guerrero, 1996; Kay and Madden, 1997).

The mammalian fauna from La Venta, Colombia remains the only well-sampled Tertiary tropical paleofauna known from South America. As such it offers a rare window into the understanding of the evolution of South American tropical communities. Kay and Madden (1997) reconstructed the rainfall at La Venta to be between 1500-2000 mm/year, and posited that the habitat was marked by heterogeneity in both ground cover and the distribution of river systems. Croft (2001) came to a similar conclusion using cenogram analysis. The conclusions of Kay and Madden (1997) were drawn from least squares and polynomial regressions involving ecological indices obtained from 18 extant mammalian communities (all of which are included in this study, as well).

2.1.2.2 Santa Cruz Paleogeography

The Santa Cruz Formation (SCF) in southern Argentina is an exposure of early Miocene deposits stretching from the Atlantic coast of Patagonia in east to the Andes in

the west, and is found between 50.3° and 51.6°S latitude. The SCF lies in approximately the same latitude today as it did in the early Miocene.

The fauna that I analyze here is found in the southern part of the SCF on and near the Atlantic coast near Monte León. Tauber (1994) identified several fossil layers (FL) 1-7 in this region, concluding that levels were successively younger from north to south. Tephrostratigraphic correlations reported by Perkins et al. (2012) established that these levels are very close in age, spanning a period of about 100,000 years (~17.5-17.4 ma). Based on this information, Kay et al. (2012b) chose to treat FL 1-7 as a single paleofauna, as I do here.

Previous paleoecological analyses of the FL 1-7 of the SCF indicate a mosaic environment of open grasslands and patches of forests, with a high degree of temperature seasonality, rainfall of approximately 1000-1500 mm/year, and mean annual temperatures >14°C (Vizcaino et al., 2012). This reconstruction was based on a variety of different sources and techniques, including paleosol records indicating fluvial deposits (Matheos and Raigemborn, 2012), paleofloral records (Brea et al., 2012), the presence of both terrestrial and arboreal ecologies in the mammalian fauna (Degrange et al., 2012; Prevosti et al., 2012; Bargo et al., 2012; Candela et al., 2012), the presence of a species of frog (Fernicola and Albino, 2012), the presence of a single primate species (Kay et al., 2012c), and community level analyses similar to what I present in this study (Kay et al., 2012b).

The faunal levels 1-7 of the SCF—considered by Kay et al. (2012a; 2012b) to be essentially a contemporaneous fauna—represent another of the most well sampled fossil mammalian localities in South America. Unlike La Venta however, the SCF is of a much higher latitude and thus presents us with a chance to compare results between two localities that *should* have significantly different estimates for climate. Additionally, work by Vizcaino et al. (2010) and Kay et al. (2012a; 2012b) uses many of the same techniques and ecological indices as this dissertation. The primary differences between this paper and those previous studies is threefold: 1) Kay et al. (2012b) uses 25 modern localities to create their regression models; 2) Regression techniques are limited to linear regression; and 3) Climate variables were limited to just temperature and rainfall, no habitat variables were incorporated. Thus, I compare my results from GPR, RF, and RTA to these previous estimates and interpret those differences in the context of the paleoenvironment of the SCF.

2.2 Materials and Methods

Faunal lists for a total of 85 localities across Central and South America (Figure 2.4), as well as 14 localities from across Australia (Figure 2.11) , were compiled from the literature (see supplemental documents for references) as well as the Information Center for the Environment (ICE) Biological Inventories of the World's Protected Areas (*http://www.ice.ucdavis.edu/bioinventory/bioinventory. html*). ICE is an online archive of the world's national parks, and features mammalian faunal lists for each of the archived

parks. Because this study is concerned with community structure and depends on the listed community being more or less complete, only faunal lists that were recorded by ICE as being either "complete" or "essentially complete" were included in this study. While it is likely that a few species go unrecorded in these lists, this procedure provides a more reliable representation of any given fauna at a locality than does the use of distribution maps (Spradley et al., 2015).

Figure 4: Map of South American illustrating the faunal localities used in this study.

For each locality, the presence or absence of 617 species of non-volant mammals was recorded. In addition, basic ecological information for each species was compiled from the literature (see supplemental documents for references). This information includes average body size, primary diet, and preferred locomotion. The identification

of any of these variables in the fossil record is problematic and is not as precise as their identification in living species. Thus, I follow Kay and Madden (1997) and Kay et al. (2012) for the categorization of ecological variables. These are summarized in Table 1. In addition, I include a predator/prey ratio, calculated as the number of faunivores divided by primary consumers with a body mass between 500g-500kg.

Table 1: Definitions of the ecological categories used in this study. Each species was assigned a number from each variable.

Body Mass Category	Definition	Locomotor Category	Definition
1	10-100g	1	Large terrestrial (>1kg)
2	100g-1kg	2	Small terrestrial (<1kg)
3	1-10kg	3	Arboreal (including gliding)
4	10-100kg	4	Arboreal/Terrestrial (Scansorial)
5	100-500kg	5	Semi-aquatic
6	>500kg	6	Fossorial (including semi-fossorial)
Dietary Category	Definition		
1	Vertebrate Prey		
2	Ants and termites		
3	Insects (with some fruit)		

4	Fruit (with some animals)
5	Small seeds of grasses (and other plants or insects)
6	Fruit with leaves
7	Leaves (browse)
8	Stems and leaves of grasses (graze)
9	Tree gums (with fruit/insects)

After assigning every species an appropriate category, a series of indices were used to describe the relative abundance of a specific ecology (or ecologies) within each mammalian community (Kay and Madden, 1997). These indices include the Arboreality Index (AI: the relative number of arboreal and scansorial species to the total number of species in a fauna), the Frugivore Index (FI), the Grazing Index (GI), and the Browsing Index (BI). These indices serve as my primary variables of interest in relation to climatic variables (see below). Faunal lists, along with ecological information for each species, are presented in the supplementary documents.

Spatial maps for six bioclimatic variables were downloaded from *WorldClim.org*. These spatial maps are produced from data collected at weather stations across the continent and represent averages of 20-50 years. Areas between weather stations are filled in with interpolated data. In addition, spatial maps for net primary productivity

(NPP) and canopy height were downloaded from the Numerical Terradynamic Simulation Group (NTSG; http://www.ntsg.umt.edu/project/mod17) and the NASA Spatial Data Access Tool (SDAT: http://webmap.ornl.gov/wcsdown/wcsdown.jsp?dg_id=10023_1), respectively. These spatial maps were then uploaded into QGIS® (Open Source Geospatial Foundation, 2007) and the values for each variable were recorded for each locality at their associated GPS coordinates using the "point sampling" plugin in QGIS. Bioclimatic variables for each locality are presented in a supplementary table.

Following Kay and Madden (1997) and Kay et al. (2012b), the localities' first Principal Component (PC1) scores from a Principal Components Analysis (PCA) comprising the ecological indices included in this study, as well as latitude and elevation were used in a linear regression. The PC1 scores were plotted against each climatic variable. A least-squares regression was fit to each plot and the subsequent linear equation was obtained, which in turn was used to predict climatic variables for the other localities in the test dataset (including the fossil localities). Spatial autocorrelation in both the species predictor variables and the environmental target variables was calculated and visualized using a Mantel correlogram (Legendre, 2011).

While choosing the values for the pertinent parameters for the two machine learning algorithms included in this study—RF and GPR—the recommendations of previous literature were followed when available (Liaw and Wiener, 2002; Stitson et al.,

1999). For RF, m_{try} was set to 4, representative of $p/3$, where p is the number of predictor variables (Liaw and Wiener, 2002), and n_{tree} was set to 1000, the default for RF.

To compare regression techniques, I obtained two metrics that measure the average error between predicted and observed values in predictive modeling; root mean squared error (RMSE) and mean absolute error (MAE). MAE is simply the average difference between the estimate and the observed value for a given data point. RMSE is a similar measurement, but instead squares the difference between an estimate and the observed value, and then takes the square root. These differences are then averaged across all estimations. Compared to MAE, RMSE is more sensitive to outliers—i.e. predictions that are extremely different than the observed value. While MAE is more commonly used in other studies incorporating predictive models given its simplicity, RMSE is preferred by others for its sensitivity (Chai and Draxler, 2014).

All statistical analyses were performed in the open-source statistical software, R. The "rpart" package (Therneau et al, 2015) was utilized for RTA and the "randomForest" package (Liaw and Wiener, 2002) utilized for RF. The "gGPRlot2" and "forestFloor" (Welling et al., 2016) packages were used to visualize the results from these analyses.

2.3 Results

2.3.1 Spatial Autocorrelation

No statistically significant autocorrelation among the climatic variables across the South American localities was found using Mantel's r_M statistic. This indicates general independence between my localities, but as a conservative measure any potential spatial autocorrelation between closely associated localities in my dataset was accounted for in the models by including latitude and longitude as predictor variables.

2.3.2 South American extant faunas

Results from the models obtained from the training data as applied to the test data are presented in Table 2. For the multivariate linear regression, the first principal component (PC1) explained 46.2% of the variance. Plotting the PC1 scores against the climatic variables resulted in strong correlations with temperature (R^2= 0.68), precipitation (R^2= 0.50), and temperature seasonality (R^2= 0.59). These correlation coefficients are weaker for net primary productivity (R^2= 0.36) and canopy height (R^2= 0.32), though still statistically significant ($p < 0.001$). The relationship of PC1 scores and precipitation seasonality was not statistically significant ($p = 0.54$).

To quantify the error from these predictions, both root mean squared error (RMSE) and mean absolute error (MAE) are presented. Generally, linear regression (LR) outperforms regression trees, but is surpassed in predictive performance by both random forests (RF) and Gaussian process regression (GPR). RF has significantly lower

error terms for both mean annual precipitation (MAP) and precipitation seasonality. GPR has significantly lower error terms for both net primary productivity (NPP) and temperature seasonality. GPR and RF are roughly equivalent in their predictive performance in respect to both mean annual temperature (MAT) and canopy height, though GPR has slightly lower error in both cases. Figures 5-10 illustrate predicted values vs. actual values derived from the test data for all six bioclimatic variables.

Table 2: Root mean squared error (RMSE) and mean absolute error (MAE) for each of the bioclimatic variables across the South American localities, using each of the regression techniques, included in this study. These error metrics indicate the average amount of error between the predicted values of bioclimatic variables and the actual recorded values.

	Mean Annual Temperature	
Method	**MAE**	**RMSE**
Baseline Average	66.04	80.33
Linear Regression	36.03	42.60
Regression Tree (RTA)	41.69	57.55
Random Forests (RF)	25.86	32.92
Gaussian Process Regression (GPR)	27.52	36.78
	Temperature Seasonality	
Baseline Average	1600.21	1840.17
Linear Regression	850.82	1106.17
Regression Tree (RTA)	644.67	909.99
Random Forests (RF)	673.70	857.65
Gaussian Process Regression (GPR)	525.76	674.62
	Mean Annual Precipitation	
Baseline Average	802.46	944.28
Linear Regression	410.48	512.29

Regression Tree (RTA)	536.19	647.26
Random Forests (RF)	377.71	439.09
Gaussian Process Regression (GPR)	491.02	618.48
	Precipitation Seasonality	
Baseline Average	25.54	38.17
Linear Regression	25.07	38.11
Regression Tree (RTA)	22.30	30.92
Random Forests (RF)	20.76	31.12
Gaussian Process Regression (GPR)	21.40	31.20
	Net Primary Productivity	
Baseline Average	3722.19	5115.32
Linear Regression	3194.49	4115.02
Regression Tree (RTA)	3461.80	4494.48
Random Forests (RF)	2686.40	3597.34
Gaussian Process Regression (GPR)	2918.79	4054.40
	Canopy Height	
Baseline Average	8.04	9.29
Linear Regression	6.07	7.61
Regression Tree (RTA)	7.76	9.99
Random Forests (RF)	5.41	6.87
Gaussian Process Regression (GPR)	4.72	6.54

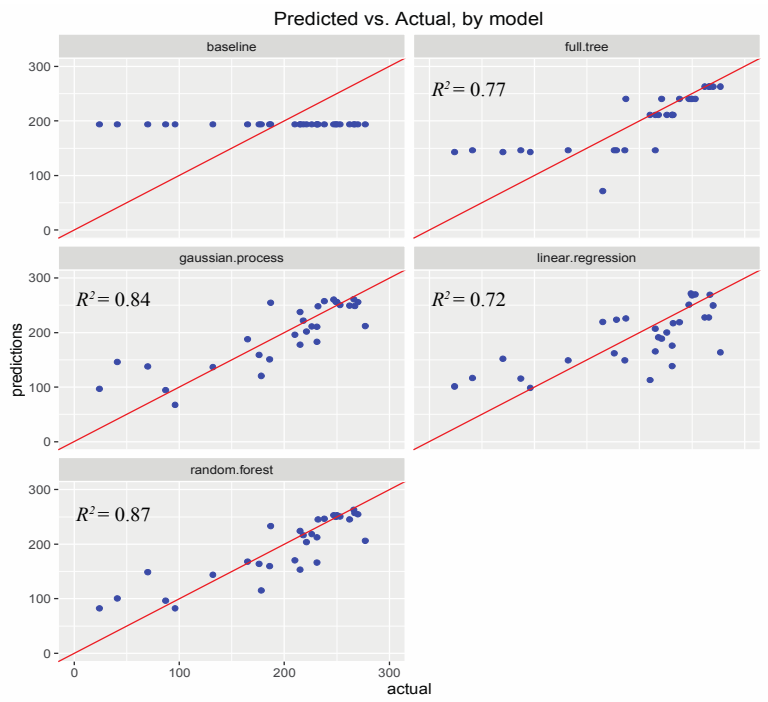

Figure 5: Actual MAT (x-axis) and predicted MAT (y-axis) values for the test dataset. MAT values are presented as °C x 10. The plots represent the five different regression techniques—and also a baseline mean (top left corner) that represents the average value for MAT across all localities—included in this study. The red line represents a hypothetical 1:1 relationship between predicted and actual values, and would suggest a perfect fit for the values predicted by the models and the observed values.

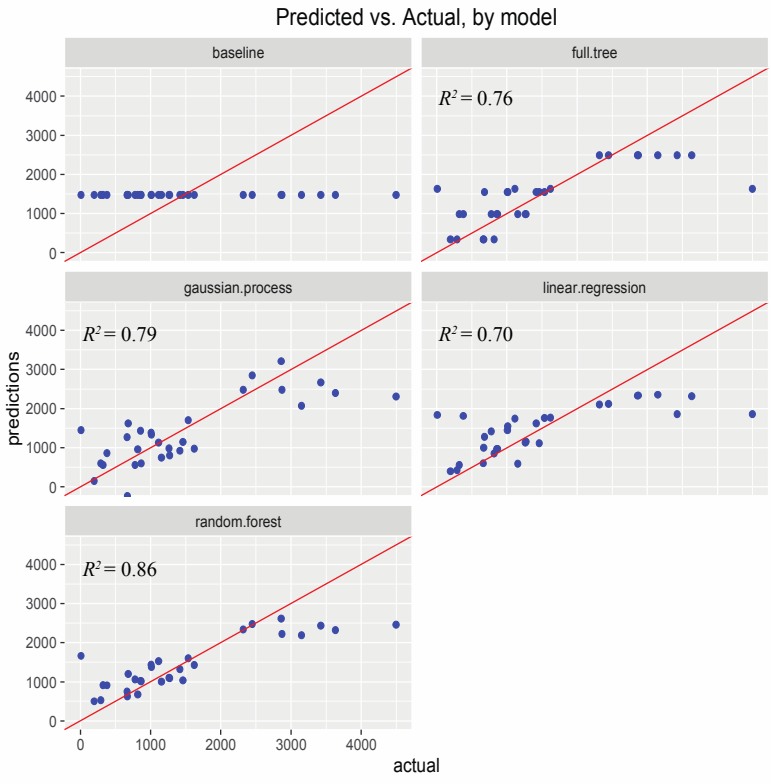

Figure 6: Actual MAP (x-axis) and predicted MAP (y-axis) values for the test dataset. MAP values are presented as mm/year.

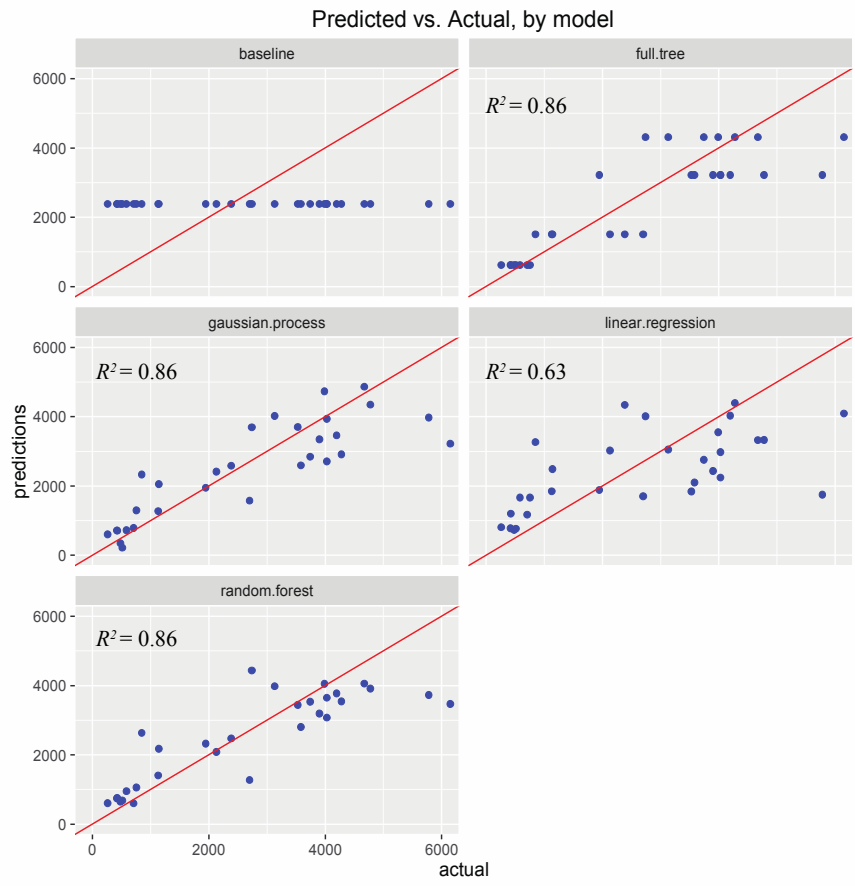

Figure 7: Actual temperature seasonality (x-axis) and predicted temperature seasonality (y-axis) values for the test dataset. Temperature seasonality is presented as the standard deviation of the MAT multiplied by 100.

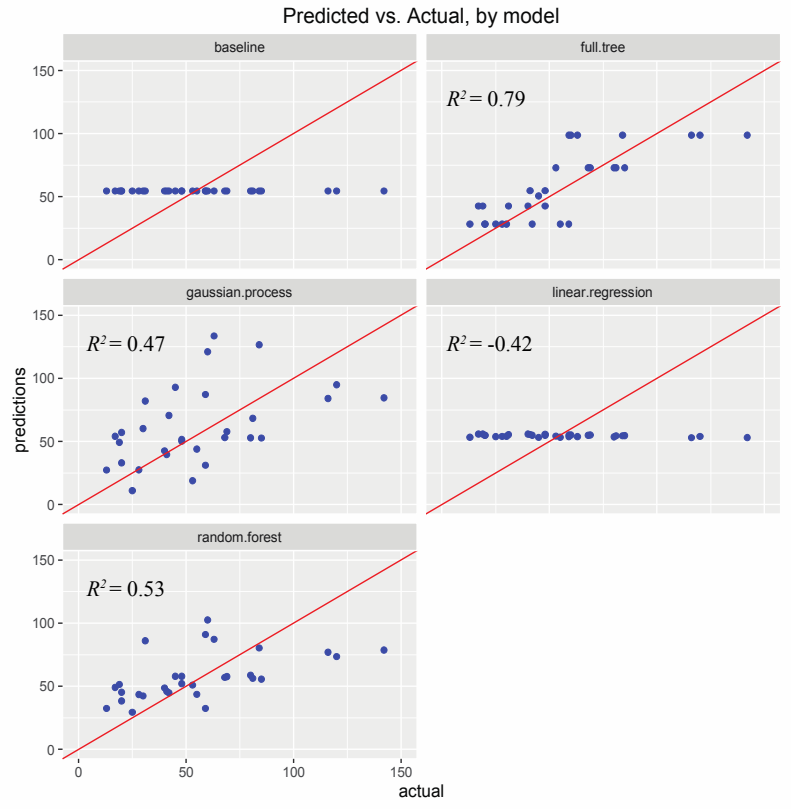

Figure 8: Actual precipitation seasonality (x-axis) and predicted precipitation seasonality (y-axis) values for the test dataset. Precipitation seasonality is presented as the coefficient of variation of the MAP.

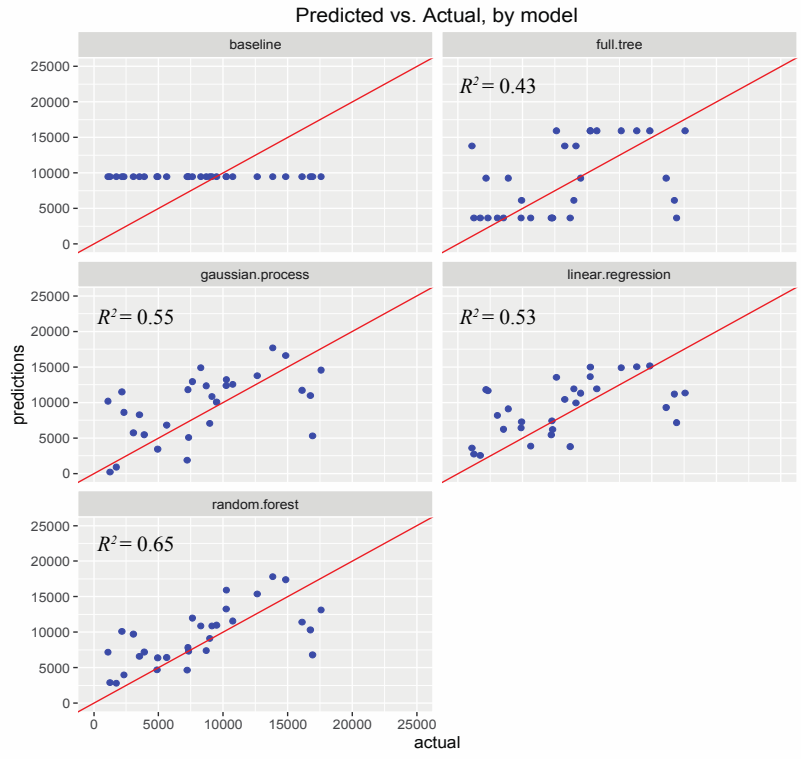

Figure 9: Actual NPP (x-axis) and predicted NPP (y-axis) values for the test dataset. NPP as a metric is discussed in the text.

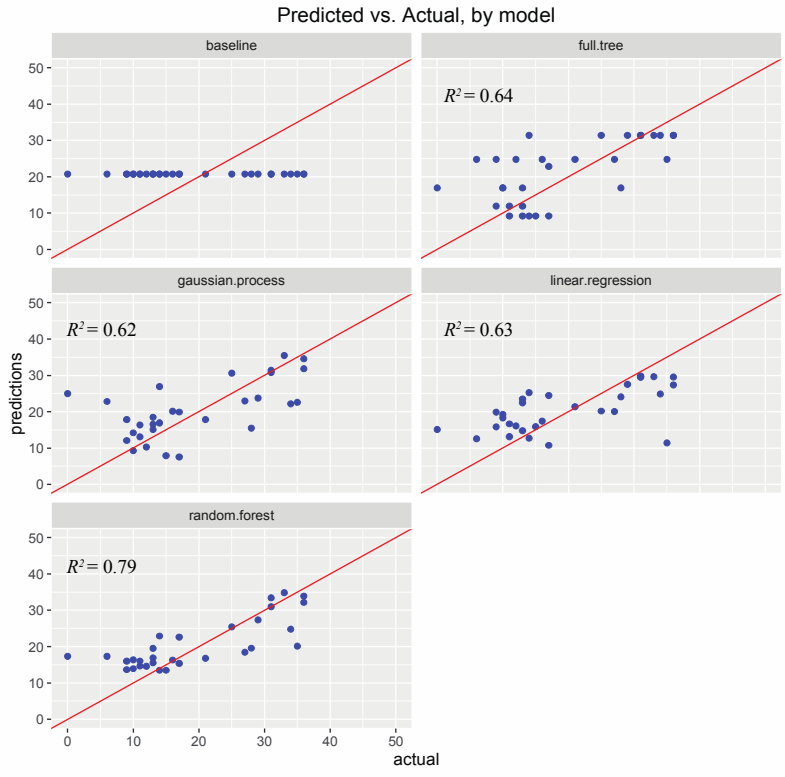

Figure 10: Actual canopy height (x-axis) and predicted canopy (y-axis) values for the test dataset. Canopy height is presented here in meters.

2.3.3 Australian extant faunas

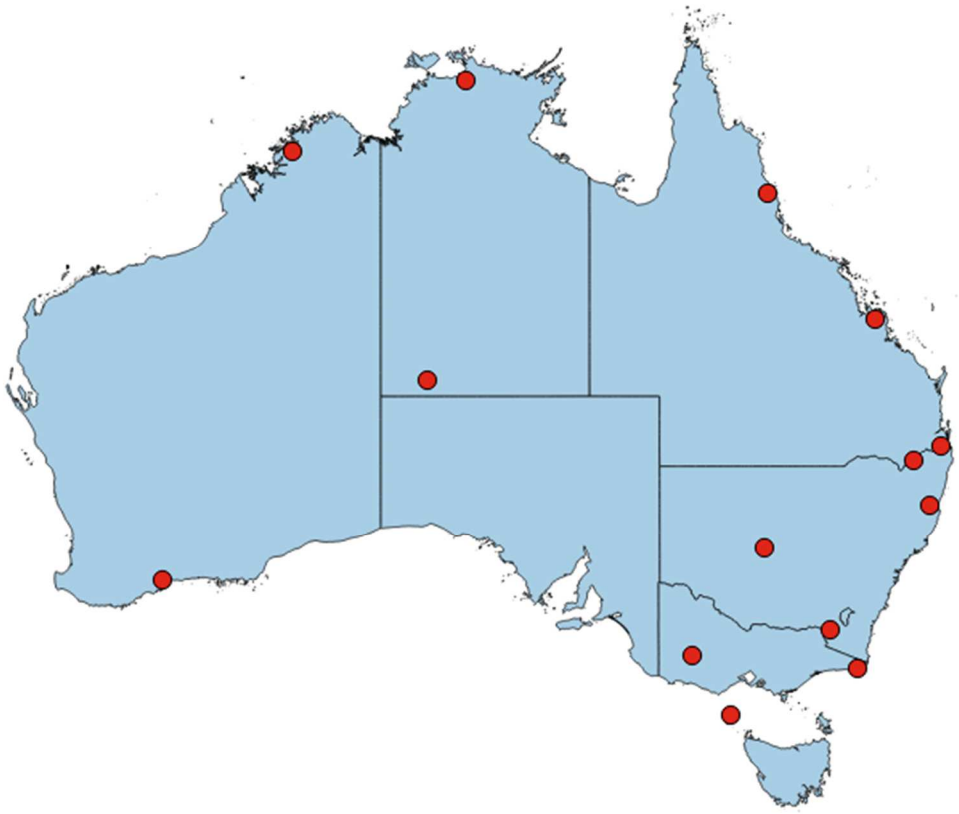

Figure 11: Map of Australian faunal localities used as a test data set in this study.

Results from the models obtained from the South American training data as applied to the Australian data are presented in Table 3. In general, the error of predicted values for Australian localities is slightly worse than that from the values of South American localities (Table 2). For instance, the root mean squared error for MAT using RF and GPR in South America is 3.3°C and 3.7°C, respectively, but is 5.5°C and 5.0°C in Australia. However, this is not true for MAP, for which the RTA, RF, and GPR all have lower error terms than what is seen in the South American test sample (Table 3, Fig. 13).

For example, RF has a RMSE of 439.9 mm/year for the South American test sample, but only 245.99 mm/year in the Australian sample. For all climatic variables except MAP, a pruned RTA outperforms—that is, demonstrates the lowest mean error—all other modeling techniques, likely due to the small number of faunas sampled in the Australian dataset (discussed further below). My results do suggest that the model derived from South America is broadly applicable to geographically and phylogenetically distinct fauna.

Table 3: Root mean squared error (RMSE) and mean absolute error (MAE) for each of the climatic variables across the Australian localities, using each of the regression techniques, included in this study.

	Mean Annual Temperature	
Method	**MAE**	**RMSE**
Baseline Average	42.58	54.03
Linear Regression	81.14	95.22
Regression Tree (RTA)	49.34	61.26
Random Forests (RF)	48.00	55.03
Gaussian Process Regression (GPR)	43.06	49.92
	Temperature Seasonality	
Baseline Average	1025.22	1258.04
Linear Regression	1797.61	2184.02
Regression Tree (RTA)	780.29	1020.65
Random Forests (RF)	569.36	956.86
Gaussian Process Regression (GPR)	590.28	973.86
	Mean Annual Precipitation	
Baseline Average	443.71	525.31
Linear Regression	641.77	765.67
Regression Tree (RTA)	230.00	315.25
Random Forests (RF)	183.15	245.99
Gaussian Process Regression (GPR)	207.60	269.19

	Precipitation Seasonality	
Baseline Average	23.82	30.19
Linear Regression	24.95	29.45
Regression Tree (RTA)	11.78	15.22
Random Forests (RF)	17.78	21.21
Gaussian Process Regression (GPR)	27.34	33.43
	Net Primary Productivity	
Baseline Average	5249.90	5856.94
Linear Regression	4783.83	5552.42
Regression Tree (RTA)	5401.68	6891.30
Random Forests (RF)	4400.88	5933.50
Gaussian Process Regression (GPR)	3533.06	5129.98
	Canopy Height	
Baseline Average	7.29	9.16
Linear Regression	6.91	8.66
Regression Tree (RTA)	7.29	8.96
Random Forests (RF)	5.92	8.27
Gaussian Process Regression (GPR)	7.15	8.36

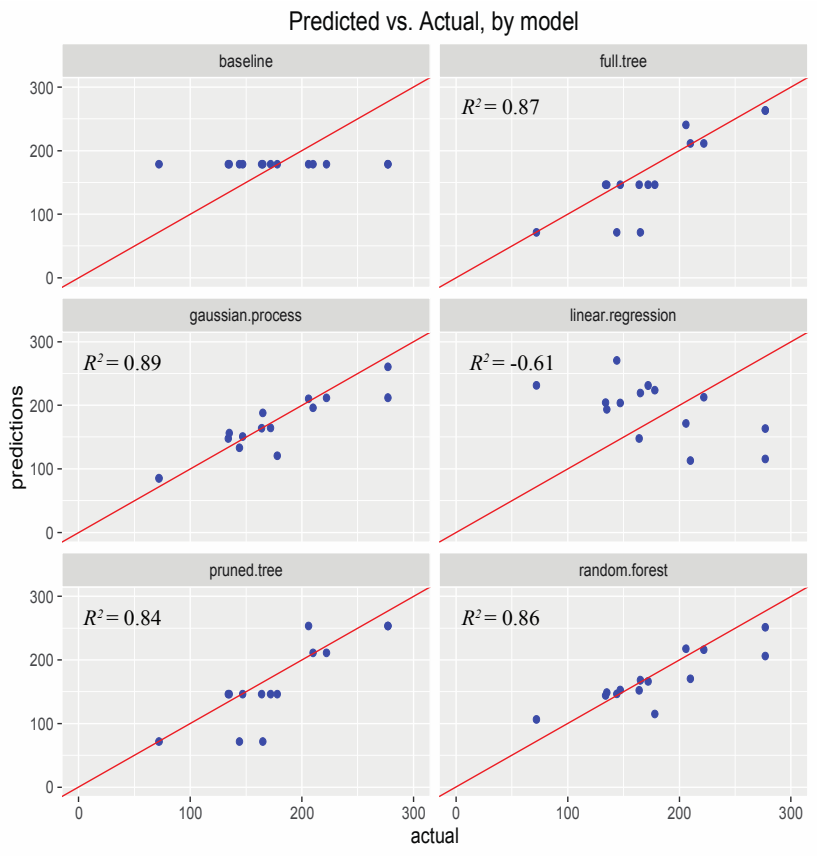

Figure 12: Actual MAT (x-axis) and predicted MAT (y-axis) values for the Australian dataset. MAT values are presented as °C x 10.

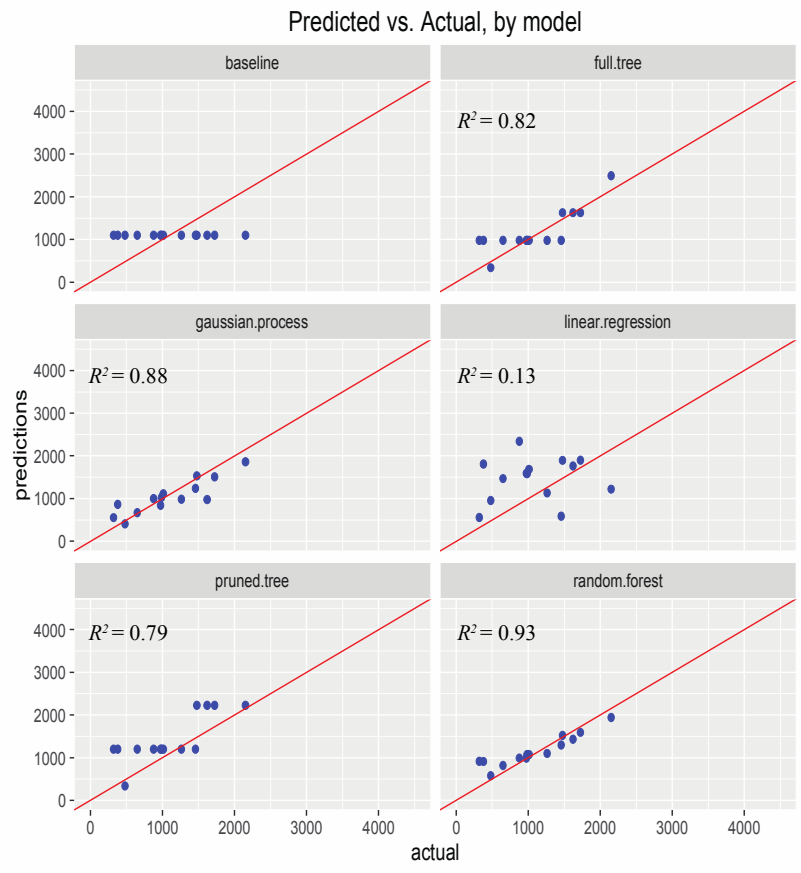

Figure 13: Actual MAP (x-axis) and predicted MAP (y-axis) values for the Australian dataset. MAP values are presented as mm/year.

2.3.3 Paleoclimatic Reconstructions

2.3.3.1 The Monkey Beds of La Venta

Table 4 summarizes the estimations of climate and habitat from each of my models for the Monkey Beds. All models suggest rainfall between 1500-2000 mm/year, though the two machine-learning algorithm models suggest slightly higher predictions, in the vicinity of 2000 mm/year. With the exception of the multivariate linear regression

model which has a much lower estimates of ~21°C, estimations of MAT are between 25-26°C. There is disagreement between the models for the other bioclimatic variables. GPR and RTA both predict much lower values of temperature seasonality relative to linear regression and RF. RTA estimates both the precipitation seasonality and NPP at the Monkey Beds as much higher than the other models. RTA also predicts that the canopy height is considerably lower (~17m) than the other models. On the other hand, GPR reconstructs the canopy height as significantly higher (~30m) than the linear regression or RF (between 22-23m).

Table 4: Estimations of climatic variables in the Miocene of La Venta using the regression methods included in this study.

Model	MAP	MAT	Temp. Seasonality	Precip. Seasonality	NPP	Canopy Height
Linear Regression	1914.9	22.0	1700.3	54.7	10411.2	23.1
Regression Tree	2287.5	25.8	613.4	81.4	7334.7	22.8
Random Forest	2361.5	25.2	1069.4	55.7	9894.6	24.5
Gaussian Processes	2956.6	25.3	648.5	58.6	13468	29.9

2.3.3.2 Santa Cruz Faunal Levels 1-7

Estimates of climate variables for the Miocene of Santa Cruz FL1-7 are summarized in Table 5. The most obvious differences between the estimations of the different models are the estimations of MAP and NPP as produced by the regression tree model. Both of these estimations (~500 mm/year and 2191.7 mg of carbon/m^2/day,

respectively) are considerably lower than the other models, which predict that rainfall was between ~1050 mm/year and 1690 mm/year, and NPP was between ~6000 and 8600 mg of carbon/m^2/day. Temperature seasonality is also reconstructed as much higher in the regression tree model. In other words, the regression tree model is reconstructing the climate in the Miocene of Santa Cruz FL 1-7 to be much drier, seasonal, and less productive than the reconstructions from the other models. Otherwise, there is general agreement between the models, and results suggest that the climate was considerably drier, cooler, and more seasonal than that of the Monkey Beds of La Venta, as well as the habitat having lower productivity and a shorter canopy height.

Table 5: Estimations of climatic variables in the Miocene of Santa Cruz using the regression methods included in this study, exclusively with the South American data set.

Model	MAP	MAT	Temp. Seasonality	Precip. Seasonality	NPP	Canopy Height
Linear Regression	1056.5	14.9	3226.4	57.2	6264.4	16.2
Regression Tree	499.0	17.4	4118.5	34.3	2191.7	22.5
Random Forest	1268.8	16.6	3166.1	42.9	6598.9	21.04
Gaussian Processes	1689.9	15.1	3641.4	16.9	8681.3	24

2.4 Discussion

The relationship between the community structure of a mammalian fauna and environment is undoubtedly complex, and it is impossible to take every potential confounding variable into consideration. Previous studies of paleoenvironment

reconstruction have acknowledged this complexity, but have otherwise sought to establish linear relationships that can provide simple, easy to interpret estimations from the fossil record. However, advances in computational power has allowed incorporation of many more variables with more complex, non-linear relationships unlike least-squares regression. Given the importance of applying all available evidence to reconstruct paleoclimates and paleoenvironments, I seek to test the efficacy of sophisticated regression techniques on the estimation of climate variables. These methods allow researchers to include several uncertainty parameters (discussed in the introduction) and allow for narrower error ranges for any given, novel data point. This is partly due to the fact that simplifying assumptions inherent to techniques like linear regression are not necessary in these approaches.

2.4.1 Performance of regression techniques in South American data

My results show a consistent improvement in accuracy for the two machine-learning algorithms, random forests (RF) and Gaussian process regression (GPR), over all other included methods. These two methods clearly benefit from the ability to apply data learning to the model, and thus account for the variation of the data. This is opposed to linear regression, which only fits a best-fit line to the data. A posterior distribution allows GPR to more accurately account for non-linear relationships between predictor variables and the response variable (Williams, 1997; Cutler et al., 2007), while random bagging allows RF to test a large number of potential tree-like models before

deciding upon which produces the best fit. There are, however, important *a priori* decisions in each technique before running the analyses, each of which will have significant effects on the results. These can be summarized as follows:

1. The percentage split of data randomly chosen for either the training or testing dataset.
2. The covariance function used in the GPR model and its free parameters.
3. The number of response variables chosen in each bagging attempt (RF).

Ultimately the first decision is arbitrarily chosen, though intuitively one would be best served by choosing a majority of the data for the training set. The compromise lies in choosing enough of the data to have a meaningful effect on the trained model so that it essentially captures the variation of the entire dataset, but also having enough of the data set aside for testing so that interpretations from the results are meaningful. In general, previous studies have chosen a threshold of 70-80% for the training dataset (Cutler et al., 2007), and my choice of 70% is thus in keeping with previous studies. The second decision on the other hand is again chosen *a priori* on the basis of the structure of the data. Given that I am working with multidimensional regression, the recommended kernel function is the ANOVA function (Hoffman et al., 2008).

Finally in regards to the number of response variables (m_{try}) randomly chosen at each node during RF modeling, setting m_{try} too high results in overfitting the data—discussed further in relation to regression trees below—while setting m_{try} too low also

results in a significant decrease in performance. The current standard, used here, is to take the square root of the total number of predictor variables (Briemann, 2001: Liaw and Wiener, 2002).

Interestingly, regression trees do not perform as well as least-squares regression in the majority of the response variables included in this study. This is likely due to the fact that the output of the regression tree is binning the data too broadly, resulting in estimations that fit into a limited number of bins. Each bin has its own mean, so the result is that the estimations are themselves limited to just a handful of means equivalent to the number of bins. The relatively few number of bins may be related to the relatively small number of localities in this study (<100), which is significantly less than other similar studies (>300) that have used regression tree analysis in relation to communities and environment (De'ath and Fabricius, 2000; De'ath, 2002). While a larger tree could potentially fix this problem, the standard protocol for determining tree size in previous studies is to choose the tree that has the smallest mean square error (De'ath, 2002), in a process known as "pruning".

2.4.2 Results from modern localities

2.4.2.1 Mean annual precipitation (MAP)

An interesting aspect of my results is that the localities with particularly high MAP (>2500mm/year) are consistently underestimated, regardless of which regression model is used. This suggests two things: 1) the various ecological indices used do not

have a linear relationship with MAP, particularly at higher values, as has been suggested by previous studies (Kay et al., 1997; Spradley et al., 2015); and 2) the amount of data available for localities of such high MAP is limited, such that even the machine-learning based models only have a few data points with which to extrapolate (or interpolate). This difficulty is acknowledged by previous studies of mammalian community structure (e.g., Andrews et al., 1979; Kay and Madden, 1997; Kay et al., 1997). In the context of the fossil record, it makes environments with extreme amounts of rainfall difficult to identify, and it is likely only through indicator species (such as aquatic forms) that such an environment can be identified (Kay et al., 1997). It is also worth noting that in predicting MAP, the linear regression technique of Kay et al. (2012b) performed better than any other technique. This was the only climatic variable in which the linear regression outperformed either of the machine-learning approaches.

2.4.2.2 Mean annual temperature (MAT)

In general, MAT is estimated with high accuracy in modern South American faunal localities, particularly by GPR and RF. In fact, in my results GPR and RF display a low amount of error for almost all MAT values for the entire test dataset. The only exceptions are two localities, the Ulla Ulla National Reserve in Bolivia and the Lauca National Park in Chile, which happen to correspond to the two localities with the highest elevation in my study, at ~5000m and ~4500m respectively. 89.4% of the localities in this study are found at altitudes *below* 1500m, so the inability of the models to

accurately estimate the climate variables at high altitudes should come as no surprise, as high altitudes produce much different physiological demands on the organisms (Lenfant, 1973; Monge and León-Velarde, 1991). In general, my results suggest that mammalian community ecological indices are closely related to temperature. This bears close resemblance to plant communities, amongst which diversity and richness have also been shown to have a positive correlation with temperature (see Pausas and Austin, 2001 for review of studies of plant species richness), and is also in agreement with the energy-water hypothesis of species richness of Hawkins et al. (2003).

2.4.2.3 Temperature seasonality

Discarding the pruned regression tree, the regression models, and GPR in particular, predict temperature seasonality very accurately. This result is consistent with similar studies that found temperature seasonality to be a good predictor of animal species richness (Danell et al., 1996; Andrews and O'Brien, 2000; Hawkins et al., 2003; Hurlbert and Haskell, 2003). Temperature seasonality has a particularly strong relationship with latitude relative to the other climatic variables, and thus may be a key driver of the latitudinal gradient of species richness. In a review of species richness and climate, Hawkins et al. (2003) noted that lower temperatures not only drive plant productivity down by limiting energy for photosynthesis, but they also create higher metabolic demands on the fauna. Both factors are likely limiting the ecological richness of the mammalian fauna in these localities. Kay et al. (2012b) previously suggested that

many ecological niches in these highly seasonal environments might be filled by migrant avian species that can disperse during seasons of low plant productivity. This hypothesis is supported by the findings of Aizen and Ezcurra (1998), who noted that seed dispersal in temperate forests is accounted for by just a few bird species, many of them migratory. Therefore, a seasonally productive environment may not carry a strong mammalian faunal signal. Regardless, my results suggest that temperature seasonality can be accurately predicted using ecological indices, with the best performing variables being the Frugivore Index, the Arboreality Index, and the Grazing Index.

2.4.2.4 Precipitation seasonality

Seasonality in precipitation displays a much more complex relationship with mammalian faunas. This is illustrated by the fact that RF performs only slightly better than the baseline (the average precipitation seasonality value from across all 85 localities), and GPR even performs slightly worse. Unlike temperature seasonality, precipitation seasonality does not have a consistent relationship with any other climatic variable included in this study. This suggests that it might be more dependent on local geography than temperature, or reflective of short-term climatic events, which occurred during the decades of the BioClim data collection. That this result stands in contrast with that from temperature seasonality may suggest that precipitation seasonality in and of itself is not as limiting to plant productivity (and thus faunal richness) as is temperature seasonality. While these potential causes of this poor relationship are purely speculative,

the fact remains that based on my results, precipitation seasonality would be difficult—if not impossible—to predict accurately based purely on mammalian niche structure.

2.4.2.5 Net primary productivity (NPP)

As it is the most direct measure of the potential amount of resources available to herbivores, NPP should have a strong correlative relationship with many of my ecological indices. However, results from my models suggest that it is nevertheless a difficult variable to predict using those same indices. This is perhaps best illustrated by a simple bivariate plot of NPP and the Frugivore Index (Figure 14), showing that the relationship between these two variables is extremely poor (R^2=.04).

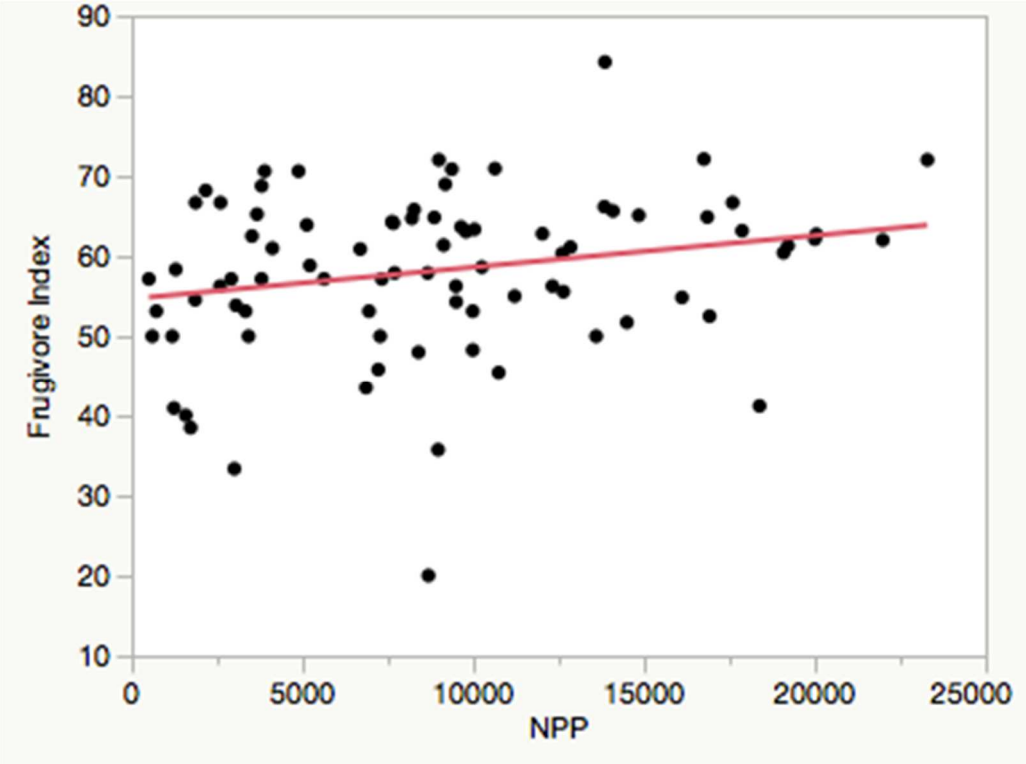

Figure 14: NPP versus Frugivore Index for the South American dataset. Solid red line represents least-squares regression (R^2=.049).

This is a surprising result considering that NPP is supposedly an indirect measure of the metabolism of plants as they absorb carbon dioxide during the production of sugars and starches during photosynthesis (specifically, NPP is the difference between CO_2 taken in during photosynthesis and CO_2 released during respiration and is measured in grams of carbon per square meter per day). Higher NPP values would suggest that plants are converting more and more carbon dioxide into energy; energy that would presumably be available to the mammalian fauna for consumption (Kay et al., 1997). We might expect, then, that primary consumers in the community should be particularly species rich in an environment with high NPP. That we do not find such a relationship may be indicative of three things: 1) NPP is a poor predictor of plant species richness, such that NPP is being driven by a relatively small number of plant species with high abundance (and thus ecological diversity in the mammalian fauna is similarly low); 2) methods used to measure NPP (NASA's Moderate Resolution Imaging Spectroradiometer, or MODIS) are inexact for the level of resolution that is present in the other variables included in this study; or 3) mammalian species richness is not inherently linked to NPP. Once again, regardless of the cause, NPP would appear to be a difficult variable to predict accurately from the mammalian fauna alone.

2.4.2.6 Canopy height

Results from my regression models suggest that both GPR and RF are capable of predicting canopy height accurately to within less than five meters. This, unsurprisingly, is being driven by the arboreality index and the browsing index, two indices that directly (or at least indirectly) measure the richness of arboreal species in the community. This is in accordance with Louys et al. (2015), which found that tree cover (likely related to canopy height) had a positive correlation with similar ecological indices. That these variables may be able to be reconstructed in the fossil record suggests the potential to reconstruct fine scale differences in paleoenvironments, and in combination with geochemical traces in the fossil record (Cerling et al., 2011) can allow paleontologists to study the effects of such differences on the evolution of different arboreal clades.

2.4.2.7 Australian comparison

In order to compare my results from South America to another continent, I also include data on a number of environmentally diverse localities from across Australia and New Guinea. One interesting result from this dataset is that the regression tree, and particularly the pruned regression tree performs well, especially regarding the mixed results from these same models in the South American dataset. This is likely because of the small number of localities from Australia and the binning effect that limited the regression trees' accuracy in South America are actually manifested as a positive effect

on the accuracy in Australia. I would suggest that including a greater number of localities from Australia-New Guinea might decrease the accuracy of the regression tree and would be more comparable to the results from South America.

In general, however, my results do suggest that models derived from the South American data can be used to predict the climate variables in Australian localities. This in turn suggests that the patterns we see in South America are generalizable to other continents, and are not just a regional phenomenon of the South American continent, and also increases my confidence in extrapolating my findings to the SA fossil record.

2.4.2 Paleoenvironment reconstructions

Finally, I applied these models to two well-sampled Miocene faunas from the South American fossil record. One from the Santa Cruz Formation of southern Argentina, and the other from the Monkey Beds of the Honda Group in La Venta, Colombia. In addition to being well sampled, the two faunas are different from one another in apparent diversity and ecological makeup (see: Kay and Madden, 1997; Kay et al., 2012) making them an ideal test of my modeling techniques.

2.4.3.1 The Monkey Beds of La Venta

My own estimates of rainfall for La Venta exceed those of Kay and Madden (1997) and suggest rainfall in the range of 2000-2500 mm/year, with the lowest estimate suggesting rainfall in the range of 1800-2000 mm/year. In general, the reconstructed climatic variables suggest an environment that is much more likely to be characterized

as a tropical rainforest, with high average temperatures (>25°C), high NPP, and a relatively tall canopy (>23m). These estimates most closely resemble other lowland Amazon sites in my dataset, such as those in Brazil, Peru, or Venezuela. This reconstruction differs substantially from Kay and Madden (1997), and suggests an environment much more like the modern environments from a similar geography. This is also in accordance with other modern localities that have a similarly high number of primates (Spradley et al., 2015), which tend to have high canopies and uninterrupted ground cover (i.e. heavily forested with very few breaks in the canopy).

However, my estimations for temperature seasonality for La Venta are substantially higher than most modern tropical lowland localities in the Amazon (the same can be said of precipitation seasonality, though as mentioned above, the difficulty I had in accurately predicting precipitation seasonality with my models gives us pause in claiming anything definitive about this variable in the fossil record). This high seasonality may help to explain the conclusions of Kay and Madden (1997) and Croft (2001) that the La Venta fauna seems to have inhabited a significantly different environment compared to modern tropical environments at similar latitudes and geography, and may still suggest a habitat unlike that of the modern Orinoco and Amazon Basin. This may be related to the uplift of the Eastern Cordillera of the Colombian Andes, which has been dated to approximately the same period as the La Venta fauna (Barke and Lamb, 2006) or even earlier (Horton et al., 2010), and has been

suggested as a major driver of environmental change in the Miocene of this region (Hoorn et al., 1995). On the other hand, other studies have suggested that this uplift is considerably younger than the La Venta fauna (Guerrero, 1996).

2.4.3.2 Santa Cruz Faunal Levels 1-7

Kay et al. (2012b) summarizes the climate of the SCF as a markedly seasonal environment with rainfall >1000 mm/year and a MAT of >14°C. Unsurprisingly, given the considerable overlap in my methods with those of Kay et al. (2012b), their estimates are generally in line my results derived from GPR, RF, and linear regression of PC1, providing further evidence for these paleoclimatic reconstructions. There is considerable difference, however, with the results from RTA, which has a significantly lower estimate for MAP and NPP. Given the difficulties I encountered with RTA in the extant dataset, however, I believe that it is safe to dismiss these particularly low estimates from RTA as spurious.

2.5 Summary and Conclusions

My results suggest that ecological information from the mammalian fauna can be successfully used to predict (or reconstruct) several bioclimatic variables in the Miocene of South America beyond precipitation as has been previously demonstrated (Kay and Madden, 1997; Kay et al., 2012b). Among the six bioclimatic variables included in this study, MAT, MAP, temperature seasonality, and canopy height were the most accurately predicted by my regression models. Precipitation seasonality and NPP are

more difficult to reconstruct accurately, presumably because both of these variables have considerably more complex relationships with the local geography and/or other historical factors.

Additionally, of the regression models that I include in this study, I demonstrate that two machine-learning approaches—random forests and Gaussian process regression—consistently show high levels of accuracy in predicting my bioclimatic variables in a test dataset. The tradeoff that comes with this accuracy is the lack of interpretability and clarity of the model(s). Unlike a least-squares linear regression or a regression tree, neither RF nor GPR have an illustrative output of the structure of the model, be it a figure or even an equation. This presents a problem for the utility of these methods for future studies, particularly when combined with the fact that these machine-learning approaches work best with larger datasets. Given that faunal lists derived from species distribution maps are, at best, unreliable (Spradley et al., 2015), this requires a great deal of data compilation on the part of the researcher. As a way of accommodating these issues with the fact that machine-learning methods do seem to be more accurate, I suggest including a more conventional approach along with RF or GPR. This can allow readers to appreciate the general pattern/direction of the relationships in the data, while also presenting results from RF or GPR.

As a manner of testing the general applicability of my results, I used my South American-based models to predict bioclimatic variables in localities from Australia/New

Guinea. The patterns that we see in South American faunas are also found in the geographically and phylogenetically distinct faunas of Australia, providing support for application of my models to the fossil record.

The reconstructions of two Miocene mammalian faunal localities in South America from my results suggest that the La Venta locality had more annual precipitation than previously estimated (Kay and Madden, 1997), as well as a warm climate and tall forest canopy. This generally conforms to the kinds of environments that are common in tropical forests of similar latitudes today, though I also reconstruct the temperature seasonality to be much greater in the Miocene at La Venta than those same modern tropical localities. This may explain the somewhat strange composition of the La Venta fauna as noted by Kay and Madden (1997), who noted that there is an "extraordinarily high number of browsing species…compared with modern faunas…" (p. 179). Regarding the Santa Cruz formation, my results generally conform to those of Kay et al. (2012b), suggesting a highly seasonal environment with rainfall of approximately 1000-1500 mm/year. My results also suggest a considerably tall canopy height (>20m), which would help to explain the high number of arboreal species present in this fauna.

3. Smooth Operator: The effects of different 3D mesh retriangulation protocols on the computation of Dirichlet normal energy

Disclaimer: This chapter was published before submission of this dissertation, and represents a collaborative effort between my co-authors and me. The citation for this article is as follows:

Spradley JP, Pampush JD, Morse PE, and Kay RF. 2017. Smooth Operator: The effects of different 3D mesh retriangulation protocols on the computation of Dirichlet normal energy. American Journal of Physical Anthropology 163(1): 94-109.

Developments in 3D scanning and image processing technologies over the past 15 years have enabled the digital reconstruction of tooth surface topography (Ungar and Williamson, 2000; Ungar and M'Kirera, 2003; Boyer, 2008; Ungar and Bunn, 2009; Winchester et al., 2014; Allen et al., 2015). When combined with new software tools for the analysis of surface topography and surface complexity, these approaches add a novel quantitative component to the study of occlusal surfaces. Prevalent among these new surface scan-based measures are Orientation Patch Count Rotated (OPCR, Evans et al., 2007; Evans and Jernvall, 2009), Relief Index (RFI; Boyer, 2008), and Dirichlet Normal Energy (DNE; Bunn et al., 2011).

The application of these metrics has been primarily restricted to lower molar occlusal surfaces, and has an advantage over previous approaches that require measurements between biologically corresponding landmarks. Freedom from the constraints of identifying these landmarks allows more flexibility in contrasting tooth

morphologies amongst disparate taxa. As with landmark-based datasets, these new measures likely contain functional information about the masticatory performance of teeth, as evidenced by the systematic variation among species with different dietary habits, irrespective of taxonomic propinquity (Evans et al., 2007; Boyer, 2008; Bunn et al., 2011; Winchester et al., 2014; Allen et al., 2015). Implementation of these new measures relies on segmented 3D meshes of tooth crown surfaces, which—thanks in large part to online digital archives like *MorphoSource* (Boyer et al., in press) are becoming more widely available (see also: Skinner et al., 2013; Copes et al., 2016). Before these analytical tools are applied to digital 3D surfaces, 3D models are typically simplified and smoothed to improve data consistency, to remove potential artifacts produced during scanning, and to reduce data size, with the goal of retaining an accurate and biologically meaningful representation of surface morphology.

DNE is an integral measure of the collective 'sharpness' of a surface (Winchester, 2016; Pampush et al., 2016a). As such, it has the advantage of being unaffected by differences in the size of a structure, or its orientation (unlike RFI, which relies on a ratio of two area measurements and will differ depending on the orientation of the tooth relative to a somewhat arbitrary defined occlusal plane; or OPCR, whose aggregate 'face-count' is also dependent on specimen orientation). But DNE is also more sensitive to jagged artifacts produced in surface reconstruction and processing than are RFI and OPCR. Previous work has addressed methodological issues surrounding the impacts of

mesh preparation (and tooth orientation) on the latter two metrics (Boyer, 2008; Evans and Janis, 2014), but no published work addresses these issues in regards to DNE. Up until now, there have been two outstanding issues with DNE's implementation, both likely arising from confusion regarding mesh preparation. First, published DNE analysis has only been performed by a narrow set of researchers connected to a small number of research groups including: Boyer & Winchester (e.g., Bunn et al., 2011; Ledogar et al., 2013; Winchester et al., 2014; Prufrock et al., 2016; Winchester, 2016) and Pampush & Kay (e.g., Pampush et al., 2016a,b; this study) suggesting that the method has remained somewhat inaccessible. Second, every study utilizing DNE has used a slightly different protocol to produce and analyze 3D meshes, raising concerns about the comparability and repeatability of results (Pampush et al. 2016b). Development of a generalized protocol to prepare 3D meshes for DNE analysis is an essential process that allows for greater methodological transparency and improved clarity of results and their interpretations. The goal of this work is twofold: [1] to make the process of DNE estimation on dental surfaces less opaque and therefore more accessible to researchers; and [2] to inform mesh preparation and processing decisions. For readers unfamiliar with the calculation of DNE or the acquisition and manipulation of scan data to produce 3D surfaces, we present a background section that outlines the various steps in this process. Those familiar with the process may find it convenient to skip to the section entitled "*The Utility of a Hemisphere*," wherein we present a justification for using a

simple geometric shape as a control, in better understanding the effects of protocol alteration on the topographic metric DNE.

3.1 Background

First used in morphological studies of teeth by Bunn et al. (2011), Dirichlet Normal Energy (DNE) is an application of differential calculus to surface geometry. DNE is the integral of the squared normal of a gradient—or the measure of variability—of a function. In the context of morphology, Bunn et al. (2011: p. 249) put it simply: "DNE measures the deviation of a surface from being planar." The DNE of a flat plane is zero, and DNE increases as a function of surface irregularity, with particularly large increases in value associated with sharp crests or steep crevices. DNE has been used as a measure of molar surface topography in extant primates with interspecific variation found to correspond with primate dietary categories (Bunn et al., 2011; Winchester et al., 2014). As with OPCR and RFI, one of the benefits of applying DNE in studies of homologous organs (such as a lower first molar) is that it is not reliant on establishing inter-specimen landmark correspondence, allowing researchers to draw comparisons among species with vastly different molar structures. Moreover, as noted above, because DNE simply measures the relative curvature of a surface, it has the benefit of being unaffected by surface size and orientation. This provides researchers with a more complete quantitative metric of the entire tooth surface, adding a new dimension to, and potentially building upon, previous studies of tooth morphology.

Prior studies have focused primarily on demonstrating the utility of DNE through showing differences in average DNE values of unworn molars among Euarchonta (Dermoptera, Scandentia, and Euprimates) with different diets (Bunn et al., 2011; Winchester et al., 2014). The typical workflow for measuring DNE and other surface topography metrics from these studies is summarized in Figure 15 along with some terminological clarification. To date, studies that have relied on surfaces generated from a set of polygons connecting points in a 3D point cloud—hereafter referred to as a *mesh*—for dental topographic analyses have used technical terms inconsistently when describing mesh preparation. Therefore, we offer some operational definitions aimed at distinguishing and clarifying the description of the steps involved in creating digital surfaces from physical specimens. We identify four fundamental phases in the process of generating measurements of surface topography for a physical specimen (1. *Scanning and reconstruction*, 2. *Segmentation*, 3. *Retriangulation*, and 4. *Analysis* [Fig. 1]) which are described in detail below.

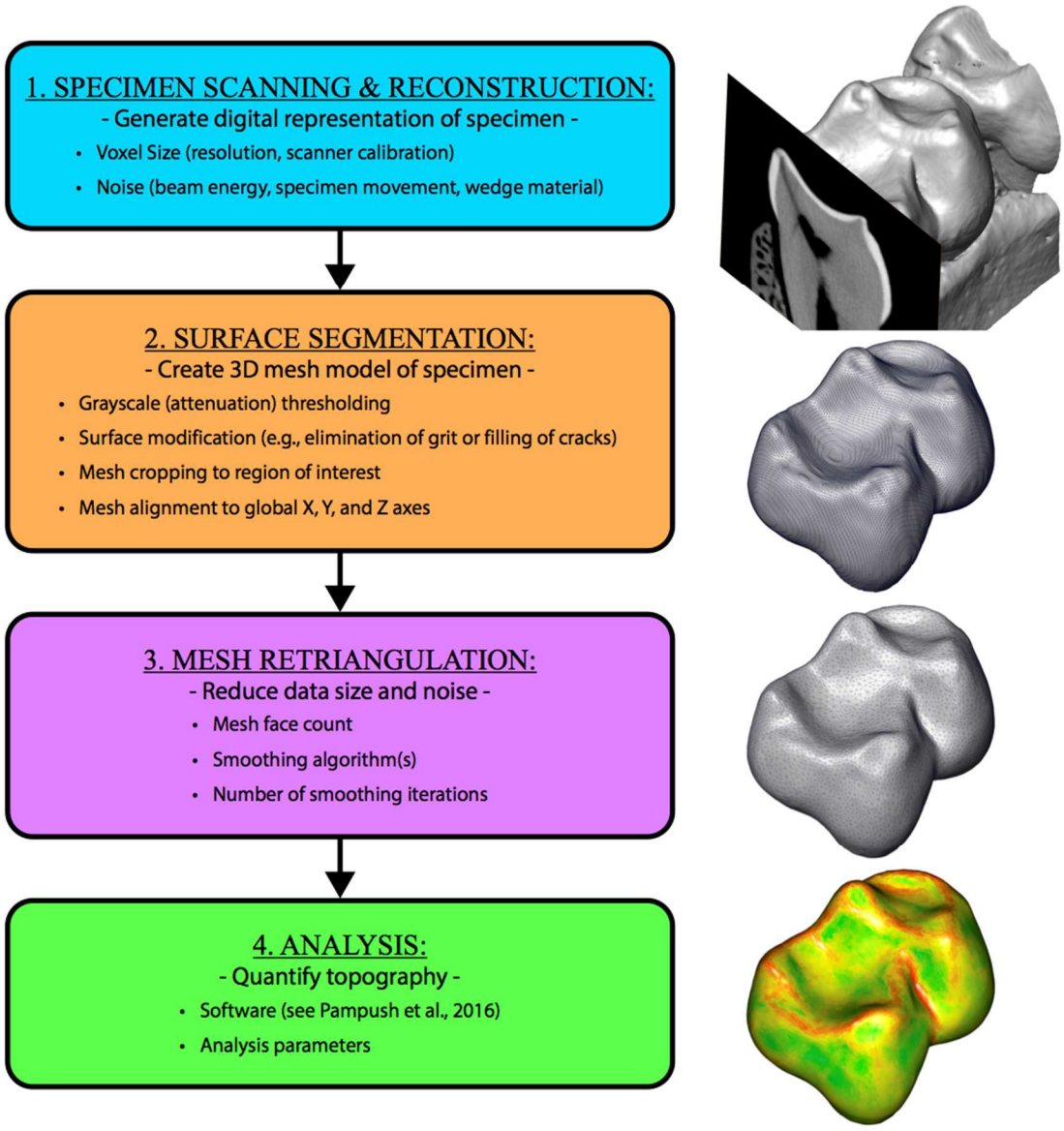

Figure 15: Workflow for quantifying surface topography of a dental specimen. Bulleted list within each step highlights points where differences in protocol among researchers could alter results. This paper is primarily concerned with issues of mesh rendering (step 3).

3.1.1 Scanning and reconstruction

The process of creating a mesh suitable for measurement of DNE begins with *scanning* the physical surface of interest using a μCT or a laser scanner. A μCT scanner

operates by generating X-rays that are transmitted through a rotating sample to a detector on the opposite side in order to acquire a series of projection images. These images capture the relative attenuation of the X-rays passing through the studied sample (Elliot and Dover, 1982; Feldkamp et al., 1984). Generating lower energy X-rays, or passing them through a sample of high density, means much of the X-ray energy will be absorbed before it reaches the detector (high attenuation). Conversely, increasing the X-ray energy or using a less dense sample will result in more of the X-rays reaching the detector (lower attenuation). When maintained at a constant energy level and passed through a rotating sample, a μCT generates a series of projection images that indicate the amount of X-ray energy that was not absorbed or deflected by the sample at each orientation. A laser scanner on the other hand creates a cloud of points by reflecting a targeted laser off of a surface, recording evenly spaced positional data (Ungar and Williamson, 2000). *Reconstruction* is the process of taking the original scanner projections and creating a series of images or volume that can then be loaded as a group into a reconstruction and visualization software program such as *Avizo*/*Amira* 8.1 (FEI Visualization Sciences Group, Berlin, Germany) or VG Studio Max. There are conventional algorithms for reconstruction, with the convolution/back-projection formula summarized by Feldkamp et al. (1984) being the most commonly used in cone-beam scanners. Reconstruction is unique to CT scanning, and is typically not needed when using a laser scanner. Thus researchers using a laser scanner will skip this step

The precision of this process is expressed in voxel size (voxels are 'volumetric elements,' a 3D analogy to the 2D pixels that comprise a computer screen) and is governed by scanner design, the size of the sample, the distance of the sample from the energy source and detector, and other instrument specific settings during the scan. Noise and artifacts are introduced to the scan data through a variety of sources, including specimen movement, beam scattering, energy filtering of the beam by the sample, beam energy artifacts, and geometric indistinctness.

3.1.2 Segmentation

The process of creating a 3D mesh from the reconstructed image stack or volume is referred to as *segmentation*. Performed in *Avizo* and similar programs, segmentation seeks to differentiate the specimen/surface of interest from the other components of the scanned sample (for instance the air, matrix or other material surrounding it during scanning). Tools exist in *Avizo* that limit the range of pixel grayscale values—an expression of the material attenuation from the sample—that are viewable during analysis, aiding researchers in isolating the desired material. However, the potential for human error or misinterpretation of the data at hand can add uncertainty to this process. This is true of fossil specimens in particular, when the attenuation from the specimen can be close to the attenuation from the matrix in which it was preserved. However, Boyer (2008) reports that visual assessment of appropriate grayscale threshold values is likely sufficient.

3.1.3 Retriangulation

After segmentation, surface data for quantitative topographic analysis is saved in a polygon file format, or "PLY" file. PLY files allow for three-dimensional data to be saved as an object made of simple, planar polygons by incorporating two matrices: one describing the x-y-z coordinates of the points that compose the mesh, and the other describing the links between those points to form faces. It is worth noting that though PLY files are used in DNE analysis, there are many other commonly used file formats that are capable of representing the same type of 3D data, (e.g., STL, OBJ, OFF). However, the currently available software programs capable of analyzing DNE (*MorphoTester* and molaR, see below) specifically require triangular PLY files as input, as the underlying algorithm is reliant on the triangular structure of the faces.

Retriangulation refers to further processing of these files (e.g., smoothing, simplifying, and cropping, discussed in greater detail below). Retriangulation is a necessary step meant to offset surface noise captured during scanning and segmentation. There are already established protocols for minimizing error introduced during initial scanning, reconstruction, and segmentation (Boyer, 2008; Winchester et al., 2014; Pampush et al., 2016a). However, issues related to the effects of mesh retriangulation remain under-described.

Studies making use of 3D data must employ retriangulation protocols with the goal of faithfully retaining the geometry of features considered biologically relevant

while simultaneously reducing file size and eliminating localized variation arising from noise during scanning, segmentation, and reconstruction (Schumaker, 1993; Desbrun et al., 1999; Dyn et al., 2000). Surface smoothing is the primary way this is achieved. *Avizo* has an internal smoothing function that reduces mesh surface irregularity by averaging the position of mesh vertices with those of their neighbors (with the exception of points on the mesh boundary, which are only averaged to neighboring boundary vertices). This function has been employed—to a varying extent—in all previously published studies measuring DNE (Bunn et al., 2011; Winchester et al., 2014; Prufrock et al., 2016; Pampush et al. 2016a). Additional downstream smoothing of *Avizo*-smoothed surfaces has been employed inconsistently in different projects (see Fig. 2), including the varying use of 'Laplacian smoothing' (Prufrock et al., 2016) and 'implicit fairing smoothing' (Bunn et al., 2011; Winchester et al., 2014; Prufrock et al., 2016).

Another critical retriangulation step that must balance manageable file size with surface detail representation is the simplification of a surface to a target face count. On one hand, too few faces may result in the loss of relevant surface detail,[1] particularly after smoothing; on the other hand, too many faces can result in unmanageable files sizes and significantly slower computational speed, potentially without the reward of greater resolution. Unlike simple geometric shapes (such as a hemisphere), a

[1] The exact definition of what constitutes "relevant surface detail" may change depending on the hypothesis or research question being examined.

mammalian cheek-tooth does not have an *a priori* theoretical limit for DNE. Instead, the scale-dependent complexity of biological surfaces potentially allows for a scan of sufficiently high resolution to capture a nearly indefinite number of surface features revealed through higher and higher surface magnifications, limited only by the scanner's upper limit of resolution. In the context of DNE, this is likely to result in higher and higher values as the fine scale complexity of the surface is revealed, plateauing as the scanner resolution limit is approached. There is also a plateau for the number of *faces* that can be used to represent a surface topography, beyond which the adding of more faces will not capture any additional features (and will not contribute to DNE). This is also related to scanning resolution (see above) though it is a distinctly separate issue, and one that we briefly address in this paper. In the case of scanner resolution and DNE, we do not tackle this relationship, but rather control for resolution by using scans with approximately the same resolution (voxel size, measured in microns).

Finally, retriangulation includes the user-directed cropping of surface meshes to some consistent boundary. In the case of dental surfaces, the cemento-enamel junction has frequently been employed as the boundary to which surfaces are cropped by hand in software like *Avizo* (Bunn et al., 2011; Winchester et al., 2014, Prufrock et al., 2016). These boundaries can be erroneously interpreted during DNE analysis as sharp edges. DNE calculation therefore includes a "boundary exclusion" criterion that mitigates the

effects of boundary faces by excluding them from the analysis result (see Pampush et al., 2016b). There are two options for boundary exclusion in molaR: 1) excluding just the triangular faces that have two vertices, and therefore a triangle leg (i.e., an edge), on the mesh boundary; or 2) excluding *any* faces that have even one vertex on the mesh boundary. This second, more conservative option excludes a larger number of faces from the total mesh DNE, potentially controlling for meaninglessly high DNE estimations resulting from the behavior of vertices on the mesh boundary.

3.1.4 Analysis

Analysis is the final quantification of surface topography from a retriangulated 3D mesh saved as a PLY file. Several different software platforms currently exist for calculating DNE on a surface mesh: *MorphoTester*, a Python-based, open-source application (Winchester, 2016), *Teether* a MATLAB code available from Yaron Lipman (Bunn et al., 2011), and an open-source *R* package "molaR" (Pampush et al., 2016b), though only *MorphoTester* and molaR are hosted online for public download.

In this study, we focus on retriangulation procedures that have been employed in previous studies using DNE with the goal of quantifying and describing their effects on the estimation of DNE. We investigate each of the following: 1) choice of smoothing algorithm(s), and number of iterations for which each is implemented; 2) the number of faces comprising the 3D mesh after simplifying; and 3) the boundary exclusion criterion

used during the DNE calculation. To do so we analyze digital surfaces of simple hemispheres (discussed below) and occlusal surfaces of howling monkey molar teeth.

3.1.5 The Utility of a Hemisphere

Here we compare the effects of different surface retriangulation treatments on a simple shape (a hemisphere) that has a theoretical DNE value that can be easily calculated, and use this as a guide for understanding the effects of mesh processing on occlusal surfaces. The theoretical DNE value for a perfectly smooth hemisphere is:

Equation 1

$$\mathrm{DNE} = \frac{2}{r^2} \times 2\pi r^2$$

Therefore a hemisphere has a DNE value of 12.566 (rounded).[2] For a more thorough explanation of the DNE calculation on a hemisphere, see Pampush et al. (2016b).

Our use of a hemisphere as a simple model unintentionally raises an important question as to the nature and value of shape descriptors as metrics: namely, how is a metric (such as DNE) best calibrated? One goal of metrics like DNE, RFI, and OPCR is to provide a new means of capturing tooth morphology differences among species. Although—as noted above—signal noise is a potentially important source of error with scanned surfaces, and retriangulation is required to limit the amount of noise that can

[2] As can be appreciated from inspection of Eq. (5), all hemispheres will have a DNE value of ~12.566 (4π) regardless of the length of the radius.

affect the measurement. Therefore, one means of arriving on DNE calibration is to choose a retriangulation procedure which most accentuates the DNE disparity among dental morphologies associated with differing diets. Such an approach may have practicality when the primary goal is to use DNE as a pattern recognition tool in the fossil record. However, if the goal is to better understand dietary adaptations of occlusal surfaces, then aiming to maximize DNE disparity among dentitions of pre-assigned diet categories is fraught with tautological issues. We believe that the more conservative approach to calibration—and one which allows for the use of DNE as a new tool in examining dietary adaptation—is to study a surface devoid of a presumed functional role, and one which can be calculated *a priori*, which is not the case for tooth crown surfaces.

The approach taken here to calibrating the retriangulation protocol is to evaluate how accurately the DNE of the resultant surface matches the mathematically expected DNE, without any concern to interpretation of its meaning. By this philosophy, the only surface retriangulation needed is that which will remove any "noise" that impedes an accurate, stable measurement of the surface's DNE. Stability, in this sense, is defined as an asymptote in the relationship between DNE and any given step within a retriangulation protocol. If the functional groups we choose to define (i.e., dietary groups) are reflected in the surface topography of teeth, then they should naturally segregate from appropriately calculated DNE values. If they do not, then the *functional*

interpretation that can be gleaned from DNE is minimal, or potentially invalid. In this study, we have chosen to take the conservative approach outlined above, focusing on the stability of the measurement rather than its ability to discriminate predetermined groups. Therefore, we have elected to use a simple geometric shape (a hemisphere) as a model to study the effects of retriangulation protocols.

While any tooth surface is appreciably more complex than a hemisphere, a hemisphere has a simple DNE value that can be calculated (Eq. 1), and any alterations to its surface should have predictable effects on its total DNE. We analyzed a hemisphere of a scanned rubber ball, complete with its surface irregularities, to examine how retriangulation influences the contributions of surface features of different magnitudes to surface DNE. We believe this analysis provides an important discussion of mesh preparation protocols that is unbiased by functional considerations.

3.2 Materials and Methods

3.2.1 Production of Virtual Hemispheres

Two methods were used to produce hypothetical DNE values for a hemisphere to serve as a baseline for comparing the effects of different retriangulation protocols. First, an 'ideal' DNE value of ~12.566 was calculated using the formula for DNE of a hemisphere (Eq. 5) to measure against DNE values calculated on 3D mesh surfaces. Second, a virtual hemisphere was created in *Avizo* as follows: A sphere was generated using the 'Create Object' function and choosing the sphere option from the list under

'Surfaces and Grids.' The maximum number of points per unit squared was set to 20, with a minimum edge length of 0.01, and a radius of 1. This resulted in a sphere with roughly 290,000 faces. This 'parent' sphere was saved to serve as the template for generating a series of 'daughter' spheres to be simplified to different face counts. To produce a daughter sphere, the face count of the parent sphere was reduced with *Avizo*'s 'remesh surface' function, with the option for interpolation checked for 'smoothly'. This resulted in a series of daughter spheres with the following approximate face counts: 1k, 2k, 10k, 20k, 40k, 60k, 80k, 100k, 130k, 150k, and 175k. Each daughter sphere was exported into R, where the 'Morpho' package (Schlager, 2015) was used to cut them in half with the 'cutMeshPlane' function. The resulting hemispheres were then retriangulated and analyzed in *Avizo* and R, respectively. These hemispheres were used to explore the effect of face count on the measurement of DNE. The 20k sphere (and corresponding 10k hemisphere) were used as exceptionally smooth virtual objects to which scanned hemisphere surfaces of equivalent face count could be compared.

3.2.2 Scanning and Segmenting of Physical Hemisphere

To compare the effects of *Avizo*'s smoothing function on an actual hemispherical surface scan against our idealized DNE measures, a small-diameter rubber ball was scanned using the μCT scanner housed at the Shared Materials Instrumentation Facility (SMIF) at Duke University. Scanner settings were approximately 140 kv and 135 μA, with a resolution of ~26 microns. The TIFF image sequence was cropped in ImageJ to

represent a single hemisphere (half of the original ball). This cropped image stack was uploaded into *Avizo*.

Segmentation of 3D surface files in *Avizo* is done with the "Edit New Label Field" dialog. Through using the histogram of greyscale values in the image stack provided by *Avizo*, the portion of the range of gray shades corresponding to the material attenuation of the rubber ball was selected using the "magic wand" tool. The threshold was refined so that only the surface of interest was selected, and extraneous material (air and packing material) was excluded. Once the selection appeared to accurately represent the object, it was added to a material and the "Generate Surface" module was applied with "No smoothing" selected. The resulting surface was an unsmoothed and un-simplified (beyond the parameters of the initial scan) digital model of half of the rubber ball.

3.2.3 Test of Different Retriangulation Protocols

Using the *Avizo* "Smooth Surface" module, the raw surface representing a hemisphere of the scanned rubber ball was iteratively smoothed to differing degrees to produce variably smoothed surfaces. The smoothing function was performed in intervals of twenty on the raw surface mesh, evenly spaced from 20-200 iterations to generate ten new surfaces meshes. The lambda parameter—associated with "lambda-connectedness," a parameter that helps the smoothing algorithm decide a threshold for connecting two points (Chen and Adjei, 2009)—of each operation was kept at the default

value of 0.6. Each smoothed surface mesh was saved as a Stanford PLY file for analysis in molaR.

Some studies that calculated DNE have employed other forms of smoothing after smoothing in *Avizo*, including 'implicit mesh fairing' (Bunn et al., 2011; Winchester et al., 2014; Prufrock et al., 2016) and MeshLab's Laplacian smoothing algorithm (Prufrock et al., 2016). These additional smoothing methods are both theoretically founded on the Laplace operator, a differential operator that captures the rate of change across a spatial gradient, which in 3D surface analysis is approximated using the eigenvectors of the surface mesh (Taubin, 1995). Approximating the Laplace operator describes the mesh as a series of changing spherical radii, and these smoothing algorithms seek to reduce the amount of local radial change while maintaining large-scale topography, with the effect of producing a more even and consistent local curvature (a method very distinct from *Avizo*'s smoothing method, see above). The protocol of Prufrock et al. (2016) calls for one such smoothing step performed in MeshLab with the "Laplacian Smoothing" function. To assess the effect of Laplacian smoothing on the measure of DNE we performed different levels of Laplacian smoothing (from 1-200 iterations) on the scanned rubber ball hemisphere, resulting in 13 new surface meshes. An alternative approach to fairing smoothing—'implicit fairing' (Desbrun et al., 1999)—was employed by the original studies involving DNE, which utilized the now-unsupported MATLAB application *Teether* (Bunn et al., 2011; Winchester et al., 2014). Other studies using older versions of

the *MorphoTester* software (e.g., Prufrock et al., 2016) also include this implicit fairing step, as it was formerly integrated by default into all *MorphoTester* DNE analyses (see Pampush et al., 2016b; Winchester 2016). As a means to assess differences in topographic measures produced by the addition of an implicit fairing smoothing step, we used *MorphoTester* version 1.1.2 to output implicit faired PLY meshes with three smoothing iterations and a step size of 0.1 (consistent with published studies). The PLY files were imported into R for topographic analysis in molaR (Pampush et al., 2016b). DNE was calculated for each 3D mesh using molaR's batch function. These values were plotted against the number of smoothing iterations to illustrate their relationships.

To observe the effect of changing face count, the 11 hemispheres resulting from bisecting the virtual 'daughter' spheres (described above) were analyzed. These hemispheres had face counts ranging from approximately 500 to 100,000 faces. Each simplified hemisphere was smoothed identically using *Avizo*'s "Smooth Surface" function with a lambda of 0.6. DNE was calculated on the full set of simplified hemispheres three times: after each surface had been smoothed with 1, 25, and 100 iterations. Since the number of faces located on the mesh boundary is directly related to the total number of faces of the mesh, the same hemispheres were analyzed and compared using both DNE boundary exclusion criteria.

3.2.4 Primate Molar Occlusal Surfaces

To test the applicability of our results with the hemispheres to primate dental surfaces, we analyzed 3D meshes representing the occlusal surfaces of first upper and lower molars of the Costa Rican mantled howling monkey (*Alouatta palliata*) from the Glander collection at Duke University (Glander, 1975). Individual M_1s were segmented from whole skulls, scanned at ~195 kv and 215 μA, with a scanning resolution of approximately 60 microns. These specimens represent seven different individuals at different wear stages and were subjected to the same series of sampling, smoothing, and statistical treatments as the rubber ball hemisphere (described above).

3.2.5 Comparison of Published Methods

Finally, we compared the retriangulation protocols of previously published research that calculated DNE, specifically those of Bunn et al. (2011), Winchester et al. (2014), Prufrock et al. (2016), and Pampush et al. (2016a). The un-smoothed, segmented meshes of both the rubber ball and a single, unworn tooth (specimen DU-LP-33) included in the other analyses (see above) were processed according to the protocols of each of the four studies (Fig. 2), as well as a fifth treatment that included only 100 iterations of smoothing in *Avizo*. DNE was then calculated on each mesh in molaR using the default boundary exclusion criterion.

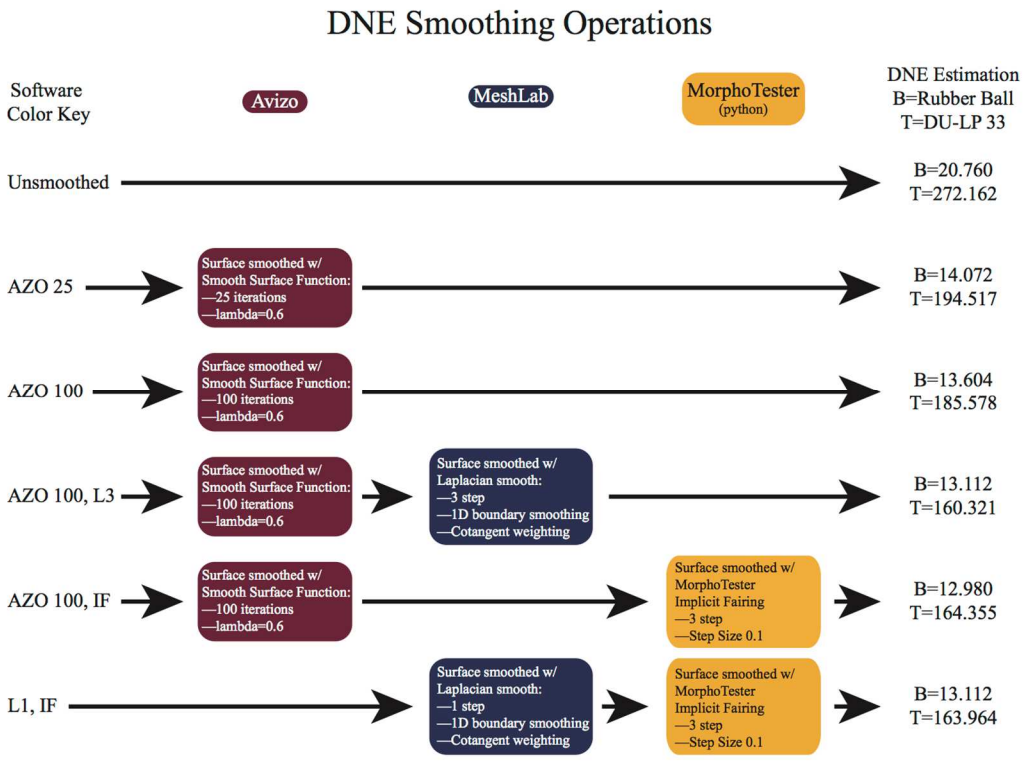

Figure 16: Workflows for previously published retriangulation protocols used to generate tooth surfaces. Resultant DNE values for both the ball and a tooth surface (DU-LP-33) are also included.

3.3 Results

3.3.1 The Virtual Hemisphere

The DNE value of the virtual hemisphere comprised of 10,000 triangular faces created in *Avizo* and measured in molaR using default settings is 12.254 (rounded). In combination with the "ideal" DNE value of a hemisphere as calculated by the DNE formula (12.566, see above), these results serve as benchmarks in assessing the DNE of the scanned rubber ball hemisphere that was subjected to various smoothing treatments. The DNE value of the virtual hemisphere is lower than the *a priori* hemisphere

calculation for two reasons: [1] The virtual hemisphere calculation includes boundary exclusion that was not accounted for in the ideal calculation of hemisphere DNE (Eq. 5). This causes the surface to be slightly 'flatter' via trimming a ring of faces off the bottom edge. [2] The ~10,000 PLY-face count slightly simplifies the curvature of the surface, wherein a larger number of faces would capture more of the subtle curvature of the hemisphere.

3.3.1.1 Avizo Smoothing

Table 6: Changing values of DNE on a rubber ball versus the number of smoothing iterations performed in Avizo to which the surface mesh is subjected.

# Iterations	**0**	**20**	**40**	**60**	**80**	**100**
DNE	22.987	14.275	14.547	14.433	14.384	14.368
# Iterations	**120**	**140**	**160**	**180**	**200**	
DNE	14.371	14.386	14.409	14.438	14.472	

Results from the scanned ball show that the DNE value approaches those of the theoretical and 10,000-face virtual hemispheres after ~20 *Avizo* smoothing iterations (Table 6, Fig. 17). The apparent discrepancy between the values of the scanned surface and those of the virtual hemispheres is likely the result of real surface features and is elaborated upon below.

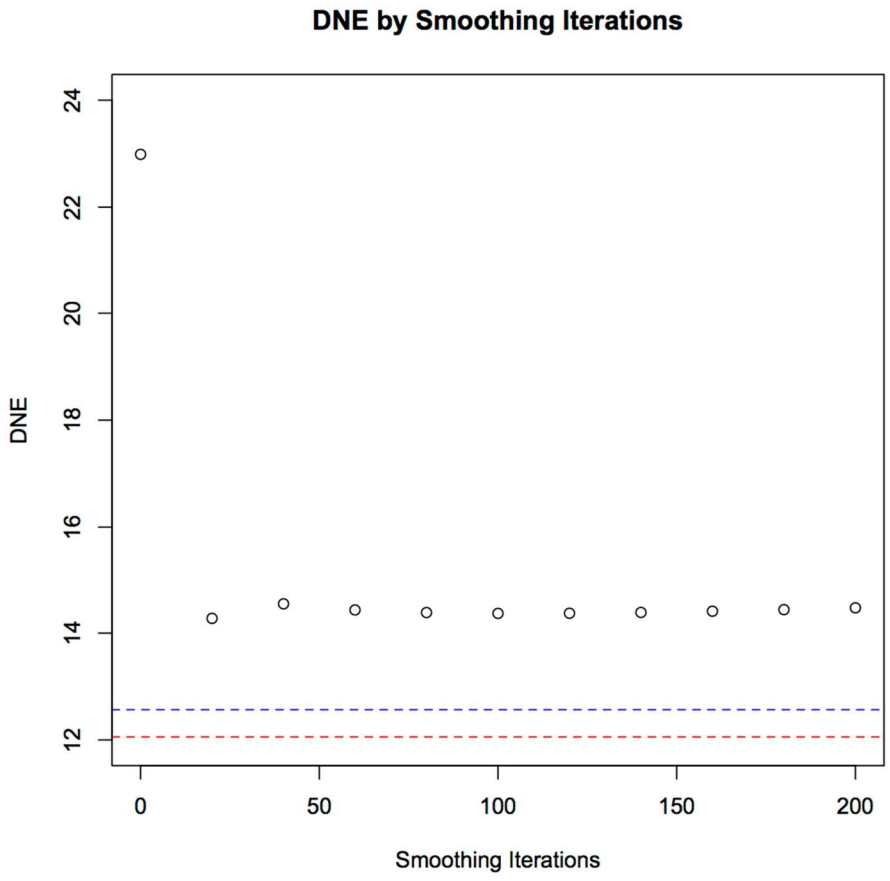

Figure 17: Bivariate plot of DNE as a function of the number of smoothing iterations in Avizo. The blue dashed line represents the theoretical value as predicted by the formula for DNE. The red dashed line represents the value obtained from the virtual hemisphere created in R.

3.3.1.2 Laplacian Smoothing

Table 7: DNE on a rubber ball versus the number of Laplacian smoothing steps performed in MeshLab to which the surface mesh is subjected.

No. Laplacian Smoothing Steps	**0**	**1**	**2**	**3**	**4**	**5**	**10**
DNE	20.75992	14.77942	13.73844	13.29082	13.02916	12.85918	12.46307

No. of Laplacian Smoothing Steps	**15**	**20**	**25**	**50**	**100**	**150**	**200**
DNE	12.28782	12.17280	12.08384	11.77686	11.38361	11.09786	10.87233

Beginning with the unsmoothed hemisphere created through scanning a rubber ball, Laplacian smoothing considerably decreased DNE values. This effect was particularly dramatic after several steps of smoothing (Table 7, Fig. 18), and resulted in the DNE value falling *below* both the theoretical value for a perfectly smooth unit hemisphere, and the value calculated from the virtually created hemisphere, contrary to expectations for a surface containing obvious and fairly large irregularities.

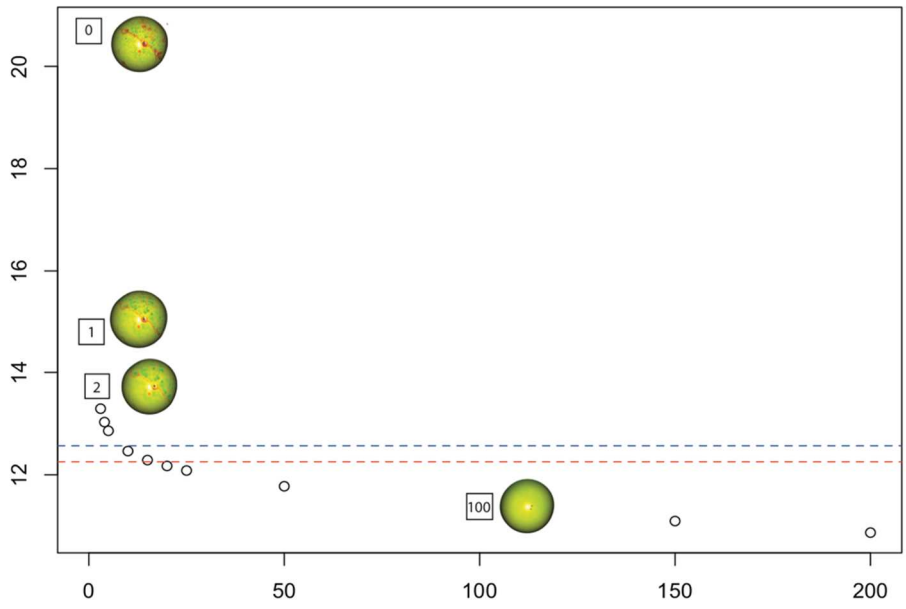

Figure 18: Bivariate plot of DNE as a function of the number of Laplacian smoothing steps as performed in MeshLab. The blue dashed line represents the theoretical value as predicted by the formula for each measurement. The red dashed line represents the value obtained from the virtual hemisphere created in R. Inset

figures (corresponding data points labeled with numbers) are 3D figures created in molaR that illustrate the effect of Laplacian smoothing in eliminating surface features. Hotter colors refer to regions of greater surface DNE.

3.3.1.3 Implicit Fairing

The results of three iterations of implicit fairing in *MorphoTester* bear a close resemblance to those of the Laplacian smoothing performed in MeshLab, consistent with the underlying algorithmic similarity of these two smoothing functions. DNE values obtained after performing these methods are presented in Table 9 (labeled as 'IF').

3.3.1.4 Face Count and Boundary Exclusion

DNE results from virtual hemispheres of varied number of faces (generated from the original 'parent' sphere in *Avizo* and subsequently bisected in R), as well as the two mesh boundary exclusion criteria, are presented in Figure 19 and Appendix A. The degree to which face count affects DNE is influenced by the number of smoothing iterations performed in *Avizo*. Varying the number of faces on surface meshes smoothed more than once (Fig. 19B,C) has a greater effect on DNE values than does varying face count on a surface mesh that has been smoothed only minimally (Fig. 19A). In addition, DNE values for meshes that were analyzed with the boundary exclusion criterion to include faces which have at least one vertex on the boundary (i.e., the BoundaryDiscard="vertex" argument in molaR, Fig. 19, blue circles) are consistently lower and track the expected DNE value of a hemisphere more closely than those with

the boundary exclusion criterion excluding only faces with two vertices and an edge on the boundary (i.e., the BoundaryDiscard="leg" argument in molaR, Fig. 19, red circles).

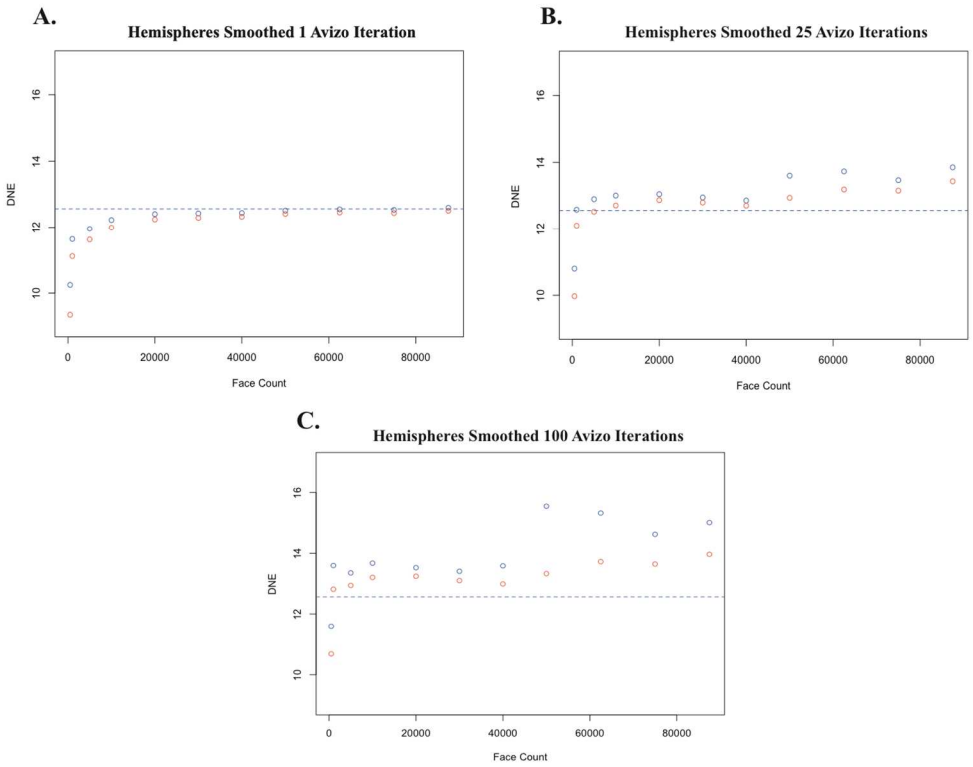

Figure 19: Bivariate plot of DNE as a function of the number of faces in a virtual hemisphere created in R. The blue dashed line represents the DNE value for a unit hemisphere as predicted by the DNE formula (see Introduction section of this paper).

3.3.2 Analysis of Occlusal Surfaces

Table 8: Percent change in DNE from the original unsmoothed surface with increasing number of smoothing steps performed in Avizo (first column). The top row summarizes the scanned specimens included in this study, a rubber ball plus seven dental surfaces of *Alouatta palliata* from the Glanders Collection at Duke University.

Smoothing Iterations	Ball	DU-LP-03 Right M_1	DU-LP-06 Left M^1	DU-LP-09 Right M_1	DU-LP-12 Left M^1	DU-LP-20 Right M^1	DU-LP-25 Right M_1	DU-LP-41 Left M_1
0	100	100	100	100	100	100	100	100
20	62.10	88.07	85.96	91.66	80.33	79.79	76.86	84.93
40	63.29	87.36	84.30	92.29	76.99	77.72	74.53	86.32
60	62.79	87.18	83.34	92.71	75.25	76.22	73.68	87.57
80	62.58	87.39	82.77	93.15	74.81	75.09	73.37	88.89
100	62.51	87.66	82.47	93.56	74.43	74.94	73.39	90.25
120	62.52	88.08	82.38	94.07	74.29	74.71	73.67	91.64
140	62.59	88.66	82.50	94.58	74.42	74.67	73.95	93.07
160	62.69	89.25	82.64	95.27	74.71	74.76	74.40	94.50
180	62.81	89.92	83.03	96.11	75.14	75.00	75.01	95.94

Results from the analyses of the first upper and lower molars of *Alouatta palliata* specimens are presented in Table 18, Figure 20. Visual inspection of the plots reveals a similar relationship between the number of smoothing iterations and DNE value as

those observed for the scanned rubber ball, particularly in the immediate drop in DNE after the first 20 iterations of smoothing. A notable exception is DU-LP-41 (Fig. 20, purple circles), which shows a considerable and unexpected *increase* in DNE after ~20 iterations of smoothing. The likely cause and implications of this result are discussed below.

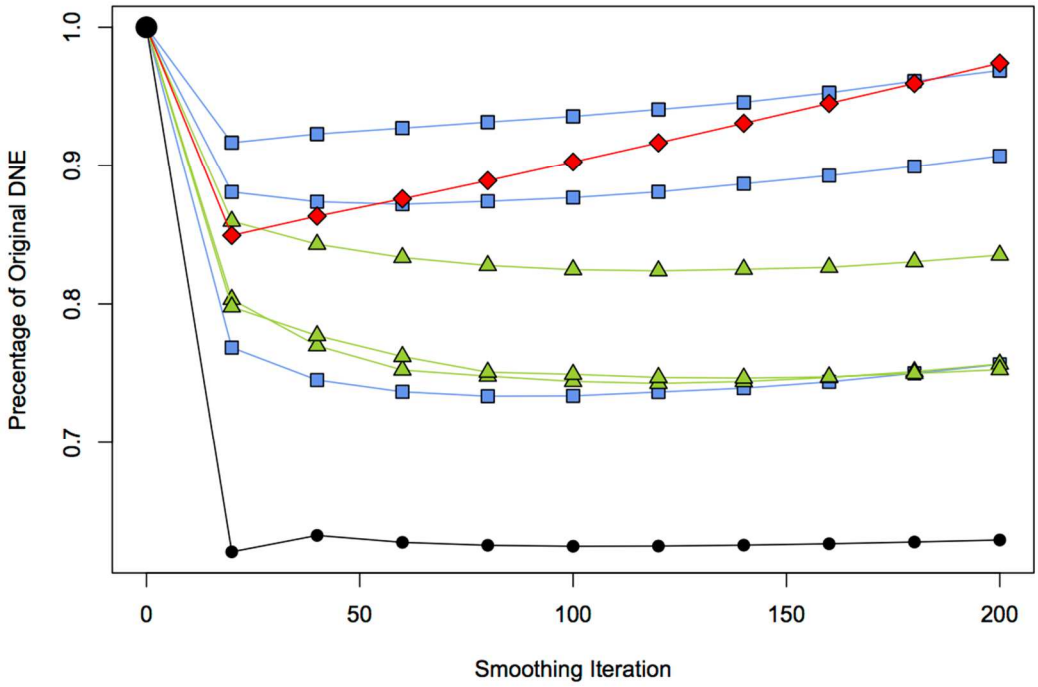

Figure 20: Bivariate plot of the percent change in DNE values from the original surface mesh after undergoing the number of smoothing iterations as indicated on the abscissa. Blue symbols represent upper molars of *Alouatta palliata,* and red symbols represent lower molars. Black circles represent the scanned rubber ball hemisphere. Purple circles represent a lower molar of *A. palliata* that shows a notably different relationship with smoothing. This result is discussed further in the text.

3.3.2.1 Comparison of Published Methods

Table 9: DNE values for both the scanned rubber ball hemisphere and a surface mesh of an *Alouatta* lower first molar after undergoing various retriangulation protocols used in previous studies incorporating measurement of DNE.

Retriangulation Treatment	DNE
Ball: Unsmoothed	20.75991775
Ball: Smoothed 25 iterations	14.0719258
Ball: Smoothed 100 iterations	13.6034746
Ball: Smoothed 100 iterations, L3	13.11185255
Ball: Smoothed 100 iterations, IF	12.97989092
Ball: L1, IF	13.11185256
Tooth: Unsmoothed	272.1616309
Tooth: Smoothed 25 iterations	194.5174572
Tooth: Smoothed 100 iterations	185.5780956
Tooth: Smoothed 100 Iterations, L3	160.3209809
Tooth: Smoothed 100 iterations, IF	164.3547692
Tooth: L1, IF	163.9636

Values of DNE measured on the scanned rubber ball processed using five different previously published protocols (as well as the original, unsmoothed surface) are presented in Table 9 and illustrated in Figure 21A. All methods show a similar decrease in DNE from the unsmoothed surface, though there is variation in the degree of DNE deflation among the retriangulation protocols. A consistent pattern emerges in the DNE values calculated for the *Alouatta* tooth surface (DU-LP-33; Fig. 21B) following each retriangulation protocol.

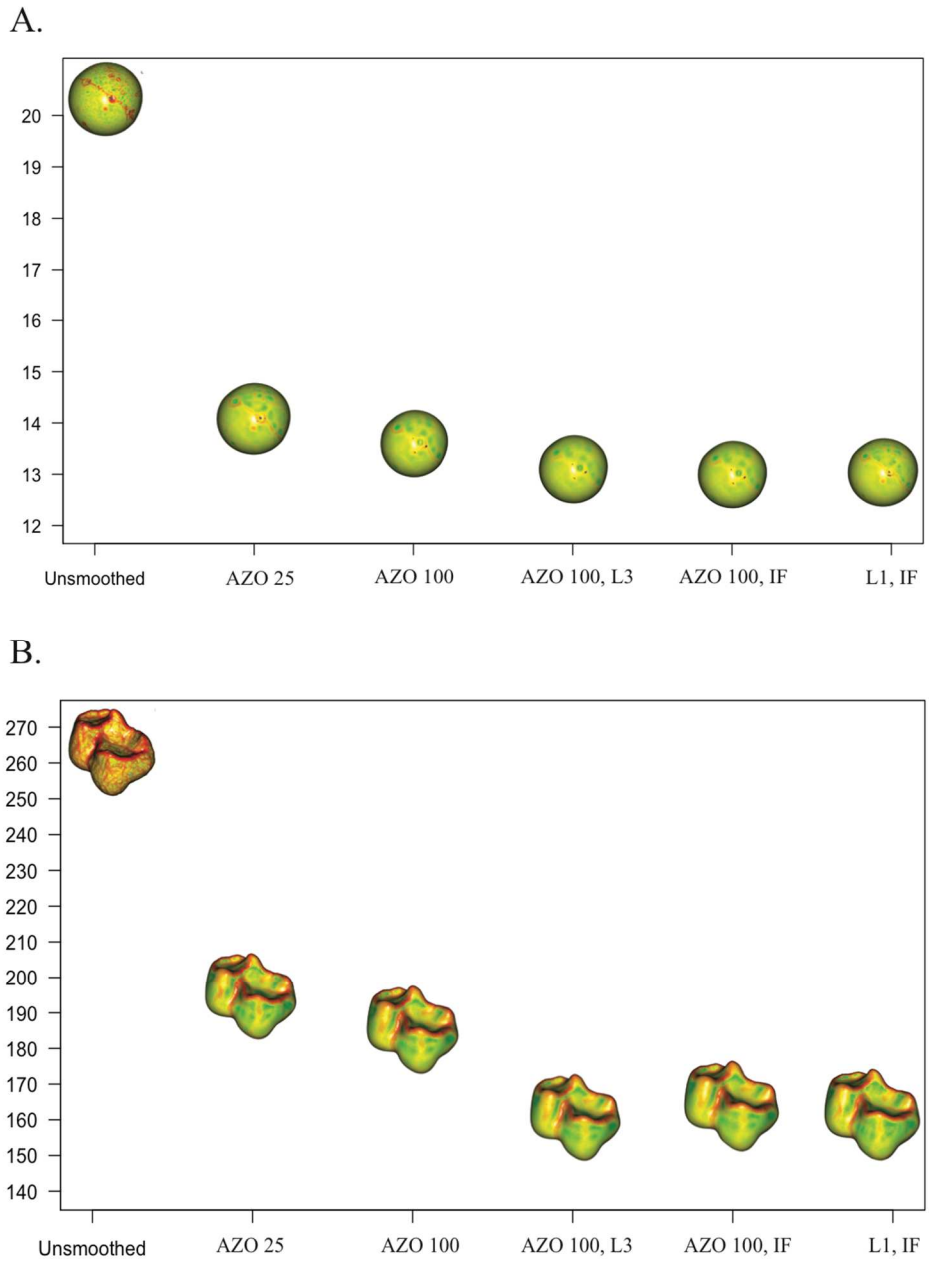

Figure 21: A) One-way- plot of DNE as a function of the type of smoothing method employed on an unsmoothed surface scan of a rubber ball. Each 3D image was created using the DNE3d() function in molaR. B) One-way plot of DNE as a function of the smoothing method on an unsmoothed surface scan of an *Alouatta palliata* lower first molar. Hotter colors refer to regions of greater surface DNE.

3.4 Discussion

Given the number of different protocols for retriangulation and analyzing 3D meshes of tooth crowns, we seek here to make protocols associated with retriangulation less opaque by presenting the effects of various retriangulation decisions on DNE.

3.4.1 Effects of Different Smoothing Protocols

The smoothing method employed in *Avizo* (and similar programs) treats local topography as a scalar field, generates a set of distances between neighboring vertices, and then seeks to minimize these distances. Collectively this typically has the effect of flattening small irregularities on the surface. After approximately 20 iterations of smoothing in *Avizo*, DNE values remain generally consistent regardless of continued smoothing performed in *Avizo*. There is a consistent discrepancy between the DNE calculated for the rubber ball surface and the DNE of both the hand-calculated ideal hemisphere and the molaR estimate of DNE from a virtual hemisphere of 10k faces created in *Avizo*. This discrepancy is explained by surface irregularities from scarring, and a dimple produced during the manufacturing process. That the process of scanning, segmenting and retriangulation captured the dimple feature suggests that such a protocol faithfully captures fine details on the surface. Further smoothing, particularly with implicit fairing, tends to eliminate the effect of these features on the total DNE of the surface. In other words, over-zealous smoothing has the potential to obliterate real surface features. It is difficult to speculate as to the potential importance of this

phenomenon in regards to morphological studies, as the size of 'relevant' features is intrinsically related to the question being asked by the researcher.

As a demonstration of the analytical process needed to arrive at an appropriate protocol, we present results from tooth surfaces and provide an informed framework for designing a smoothing and simplifying protocol. Similar to the protocol of Pampush et al. (2016a), we approached our sample with the objective of capturing the essential surface geometry of the tooth, so as to make broad-scale comparisons of tooth shape, regardless of tooth size or orientation. The results from *Avizo* smoothing trials on meshes derived from tooth surfaces generally resemble those from the rubber ball. A notable exception to this pattern is specimen DU-LP-41. Unexpectedly, as the number of smoothing iterations performed in *Avizo* increases, the DNE value of this specimen increases, even approaching the value of the original, unsmoothed mesh (Fig. 20, purple circles). Visual inspection of the 3D mesh produced from DU-LP-41 reveals that as the number of smoothing iterations increases, a few small "horns" form and are accentuated on the surface (Figure 22). Given the high angularity of these "horns", it is probable that they alone are responsible for the increase in DNE calculated for this specimen. Though this specimen was the only one from this sample to respond to smoothing this way (i.e., 1 out of 7), we do not know how common an occurrence this 'horn-growing' is in a larger sample. Based on our results with this irregular specimen, and the finding that DNE remains roughly consistent despite increased *Avizo* smoothing iterations in the

other specimens, we recommend applying only ~20-30 *Avizo* smoothing iterations. Such a threshold should provide sufficient noise reduction while also limiting the growth of these horns and their influence on the DNE value of a surface mesh. Researchers employing a larger number of *Avizo* smoothing iterations should check occlusal meshes for such artifacts to ensure the integrity of their sample.

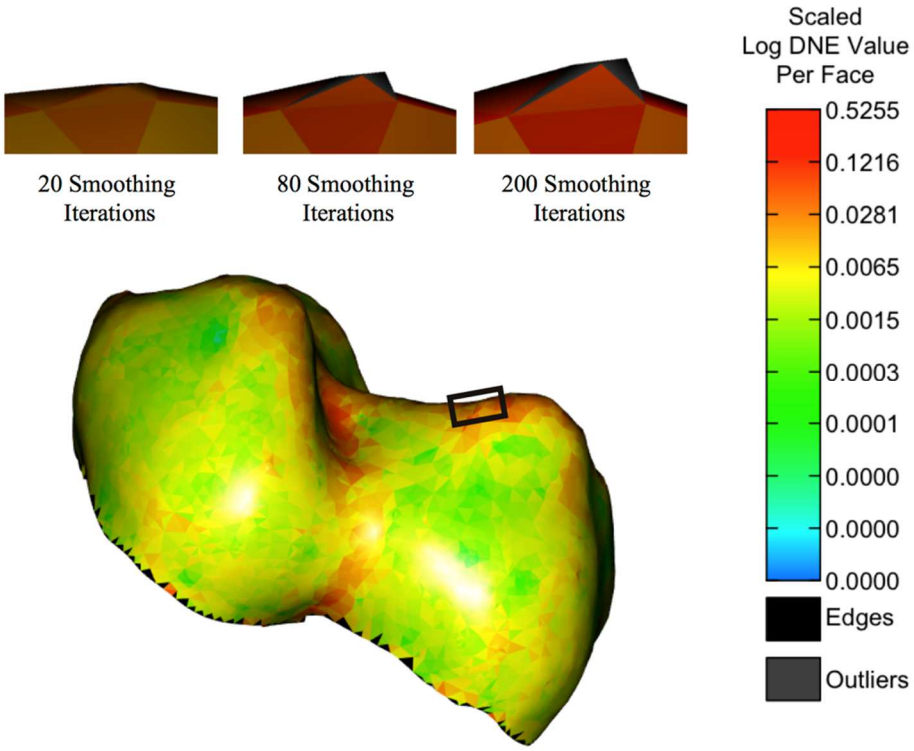

Figure 22: Illustration of the creation of artifacts on the surface reconstruction of DU-LP-41. As the number of smoothing iterations increases from left to right, the artifacts (circled) increase in prominence, increasing the total DNE value of the surface. Surface reconstruction created with molaR.

MeshLab's Laplacian smoothing and *MorphoTester's* implicit fairing on the scanned rubber ball hemisphere are much more aggressive smoothing algorithms; in

fact there exists a point at which a 3D mesh can have much of its topographic resolution obliterated. Implicit fairing may result in the loss of biologically relevant surface detail. We find that as the number of mesh fairing smoothing steps (Laplacian or implicit) increases, the DNE value for the rubber ball eventually falls below the theoretical value of a unit hemisphere—a result not observed with *Avizo* smoothing. This suggests a high potential for distortion of the mesh when a smoothing protocol includes Laplacian or implicit fairing smoothing. Indeed, if one regards the difference between the theoretical DNE value of an ideal hemisphere (blue line, Fig. 18) and the molaR DNE estimate of a nearly smooth virtual hemisphere of 10k faces created in *Avizo* (red line, Fig. 18) as an acceptable (and perhaps inevitable) amount of error incurred during analysis, then it should be noted that even a single step of either Laplacian or implicit fairing smoothing—applied to a surface *already* smoothed with *Avizo*—reduces the DNE value of the rubber ball surface by an amount larger than this analytical error (i.e., the differences between the molaR DNE estimate, and the theoretical DNE value of a hemisphere). This observation underscores the aggressive nature of these smoothing algorithms.

In comparing the effects of the smoothing protocol on the hemisphere vs. the tooth surface, there were differences in relative magnitude of DNE decrease, but not in the pattern of decrease. That is to say, the hemisphere demonstrated a greater percent decrease in DNE than did the tooth surface, but both showed an initial precipitous

decrease in DNE followed by little change in DNE with increased smoothing iterations in *Avizo*. By comparing these dramatically different surfaces that produced such similar patterns, it can be inferred that DNE change with smoothing is consistent regardless of the surface. Our results indicate that more complex surfaces are likely to show relatively smaller decreases with smoothing. This is likely to reflect the relationship of noise from the scan as it relates to the magnitude of the features on the surface. Given identical scan parameters, noise should be approximately consistent from scan to scan. Therefore, the relative size of the features—in the case of this study, either a small dimple on a hemisphere or the crests and cusps of a tooth—is going to either enhance or diminish the effect noise has on the overall DNE of the surface. This concept likely explains why in our results, the hemisphere—for which noise is contributing a greater relative proportion of the DNE prior to smoothing—shows a relatively larger decrease in DNE with smoothing than does the tooth surface. Stepping back, the comparison of these smoothing analyses highlights the importance of the tradeoff inherent during smoothing, namely between the elimination of noise and the distortion of important surface features. These effects are particularly important to consider when measuring DNE, because it is sensitive to small changes in curvature on a surface.

3.4.2 Effects of Different Face Counts and Boundary Exclusion on DNE

Another potential source of variation when retriangulating meshes to calculate DNE or other topographic measures is alterations made to the number of triangular

faces that compose the mesh. This is of particular concern with regard to teeth with relatively small but functionally significant features, which may lose meaningful resolution with too small a face count. As Figure 19 illustrates, the number of faces does indeed affect the values of DNE, and it is also apparent that too few faces can distort the surface (in this case, away from the value of an ideal hemisphere predicted by the DNE formula). As illustrated in Figure 23, too few faces can result in a tooth surface mesh that is only a rudimentary representation of the original surface (Fig. 23A), while too many faces can capture features in the mesh that may be on the original surface, but may be extraneous to the essential surface geometry of a tooth, such as microfeatures on the occlusal surface (Fig. 23C, D). This is relevant, as small but jagged surface features—whether they are artifacts or actual surface features—can have a much more significant contribution to the overall DNE of a surface than large areas free from jaggedness. It should be noted that the relevance of these features is wholly dependent on the research question, but no published studies using DNE so far have prioritized the contribution of surficial microfeatures to overall tooth crown DNE. The amount of smoothing performed in *Avizo* also affects DNE in meshes of different face counts (Fig. 19), underscoring the importance of establishing a consistent protocol of both mesh smoothing and simplification if DNE results are to be combined among broad taxonomic groups, and/or across studies. A conservative approach to smoothing as advocated here is more likely to be appropriate for a greater range of tooth

morphologies than a more intense smoothing protocol. A second consideration is the tradeoff between processing speed and data richness. Figure 19 shows that the theoretical value of DNE can be attained on a simple hemispherical mesh comprised of between 10,000 and 15,000 faces. A similar plateau is not seen in the results from the tooth surface, which is a consequence of the scale-dependent complexity of the tooth surface (discussed in the Background) and the upper limit in our computer processing ability. Provided the processing ability is available, it is likely that DNE would consistently increase with face count on a given tooth scan until it meets the limit imposed on it by the initial scanning resolution. That said, DNE processing speed in molaR and *MorphoTester* is greatly slowed by the number of faces, and system memory limits tend to prevent DNE calculation on meshes with more than 125,000 faces (unless there is access to a cluster for processing). While there may be specific questions or interest in DNE best addressed using meshes with a large number of faces, for the purposes of gross dietary differentiation among extant primate taxa, simplifying meshes to 10,000 faces—as has been done in past studies—appears to be a reasonable and appropriate threshold. This approach seems to capture biologically meaningful signal, without over-burdening the analysis tools.

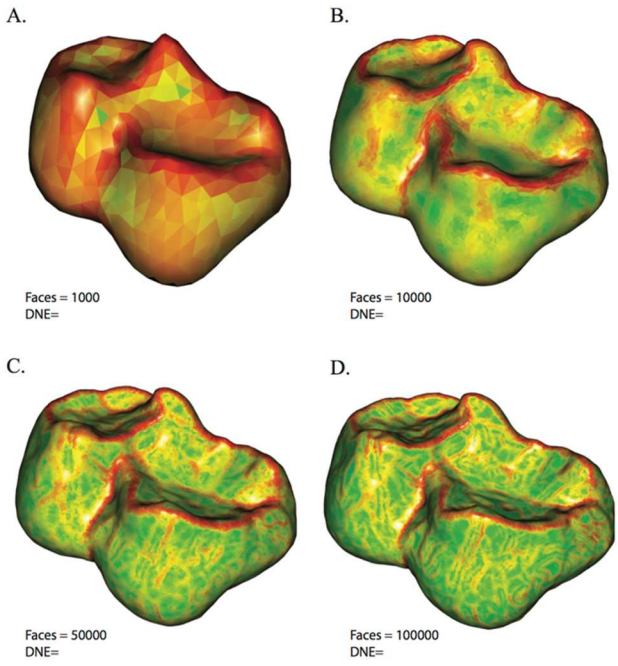

Figure 23: Illustration of the effect of increasing the number of faces on the surface reconstruction of a howling monkey (*Alouatta palliata*) lower first molar. The number of faces for each surface is as follows: A) 1000; B) 10,000; C) 50,000; D) 100,000.

The boundary exclusion criterion chosen during analysis also has a significant effect on DNE values. Unsurprisingly, when faces that have at least one vertex on the boundary are excluded, DNE values are lower than when boundary exclusion is limited to only those faces that have an entire leg (i.e., two vertices) on the boundary. The motivation for boundary exclusion during DNE calculation is that faces on the boundary are much more likely to possess erratically oriented vertex normals (which are fundamental to the mechanics of the DNE estimation in both *MorphoTester* and molaR), owing to the lack of adjacent faces (Pampush et al., 2016b). If the boundary faces are included, this can result in a DNE estimation where portions of the boundary are

erroneously interpreted as a sharp ridge. A higher number of faces and greater *Avizo* smoothing iterations appears to result in more erratic vertex normals along the mesh boundary, contributing to higher DNE values (Fig. 19). This effect is best countered by a boundary exclusion criterion that removes all faces from the calculation that have at least one vertex on the boundary, ensuring that the DNE calculation does not treat the boundary as a sharp ridge. However, while this effect is clear on the simple surface of a hemisphere, it is not obvious that complex occlusal surfaces with a larger number of faces subjected to higher amounts of smoothing suffer from these boundary issues. This is likely because the raw level of complexity on these surfaces swamps the DNE contribution from a few faces possessing extreme vertex normals. Regardless, a more exclusive approach to the mesh boundary is more likely to remove these problem faces.

3.4.3 Comparing Results from Previously Published Protocols

Despite the methodological challenges associated with smoothing and the measurement of DNE, the metric has enormous potential as a tool in the study of the ecomorphology of mammalian dentitions. This potential has already been demonstrated in primates (Bunn et al., 2011; Winchester et al., 2014; Pampush et al., 2016a) and rodents (Prufrock et al., 2016). In this context, it is important to note that a tooth surface, unlike a hemisphere, does not have an *a priori* value of DNE that we can expect to approach with an optimal retriangulation protocol (i.e., a calibration guide). That these studies used different protocols does not take away from the validity of their findings—particularly

for how DNE relates to other factors/metrics—for as we have argued here, the most important aspect of any study that requires image processing of CT scans is internal consistency. Still, our results from the comparative analysis of the smoothing methods used in previously published studies of DNE suggest that DNE values should not be combined from studies using differing retriangulation protocols. Table 10 presents the differences in DNE among five different tooth surfaces retriangulated using different previously published protocols. The average DNE difference between a protocol that includes only smoothing in *Avizo* and one that includes Laplacian smoothing or implicit fairing is roughly 18 to 25 (or approximately 10-15%), depending on the comparison. Comparing this disparity with the results from Winchester et al. (2014), in which the mean difference between frugivores and folivores amongst their platyrrhine sample was 25.77, it is clear that any researcher looking to compile DNE measurements across studies (and particularly across research groups) must take care to ensure that all surfaces were given the same retriangulation treatment. The easiest way to rapidly account for discrepancies between retriangulation protocols is for researchers to publish their raw segmented surface meshes (pre-retriangulation) in online repositories such as *MorphoSource* (Boyer et al., in press) for reanalysis, as has been done already by some researchers (e.g., Boyer, 2008; Bunn et al., 2011; Winchester et al., 2014; Prufrock et al., 2016; Pampush et al., 2016a). Posting mesh surface data (or even better, the

reconstructed CT scans or surface scans themselves) will promote transparency, validation of results, and general research quality for studies using DNE.

Table 10: The absolute value difference of DNE between previously published protocols on five different tooth surfaces. Each column represents the difference in DNE between the given protocol and the most conservative approach in our study (i.e. AZO 25). "AZO ##" stands for number of smoothing iterations performed in Avizo. "L#" stands for number of Laplacian smoothing steps performed in MeshLab. "IF#" stands for number of implicit fairing smoothing steps performed in MorphoTester.

Tooth	AZO 25 and AZO 100[1]	AZO 25 and AZO 100, L3[2]	AZO 25 and AZO 100, IF3[3]	AZO 25 and L1, IF3[4]
DU-LP-03	0.822994	19.074693	25.723668	23.724235
DU-LP-09	2.311034	11.474234	20.94698	17.297139
DU-LP-25	6.153555	25.164651	29.281715	20.340152
DU-LP-41	9.039472	1.345679	16.828984	18.060112
DU-LP-33	8.939361	34.196476	30.162688	48.016274
AVERAGE	5.4532832	18.2511466	24.588807	25.4875824

[1]Pampush et al., 2016a
[2]Pampush et al., 2016b
[3]Winchester et al., 2014
[4]Prufrock et al., 2016

3.4.4 Considerations When Designing a Retriangulation Protocol for Tooth Surfaces

The combined information from our results suggests that a conservative approach to smoothing generally limits the complications and irregularities associated with mesh retriangulation. For our sample hemisphere and teeth, 25 iterations of smoothing in *Avizo* performed on a mesh simplified to 10,000 faces reduces the likelihood of irregularities in the 3D mesh that became especially apparent in our results with ~40 or greater iterations. Similar 'horn' artifacts to those produced with *Avizo* through over-smoothing are observed on tooth DU-LP-41 after only a few iterations (5 or more) of Laplace operator-based smoothing algorithms. The error introduced by these artifacts can have a significant effect on the estimation of DNE. Additionally, more aggressive smoothing algorithms (including "Laplacian smoothing" in MeshLab, or "implicit fairing smoothing" in *MorphoTester*) may eliminate real topographic information or potentially contribute to the formation of false topography. We also demonstrate that excluding all faces with any vertices on the mesh boundary (boundary exclusion criterion in molaR set to "vertex") improves the consistency of DNE results.

Though we caution against use of mesh fairing smoothing algorithms, we do not challenge the findings of previous studies incorporating such techniques. This stance is informed by the fact that there is no easily calculable "true" value of DNE for a tooth, as there is for a hemisphere. Yet, our analysis of different published protocols performed

on the same surface produced a range of DNE values greater than the differences that separate morphological or dietary groupings among primates (Bunn et al., 2011; Winchester et al., 2014). We suggest that because of this potential pitfall, researchers take great care in only combining results from prior studies that have equivalent retriangulation protocols, as combining results from studies with different protocols may lead to erroneous conclusions.

3.5 Conclusions

Dirichlet Normal Energy (DNE) was calculated for PLY files of an ideal hemisphere, a bisected scanned rubber ball, and dental occlusal surfaces of *Alouatta palliata* (as an example of a medium-sized primate) and subjected to a variety of retriangulation protocols, including different smoothing algorithms, different amounts of smoothing, and different face counts. The simple geometry of the hemisphere provides a well-understood "ideal" benchmark to compare with results of the effects of variation in retriangulation steps in a way that a complex surface like a tooth crown cannot. The secondary, informed examination of dental occlusal surfaces allows us to extrapolate these results further. Based on our results, for future 3D surface retriangulation with the aim of calculating DNE, we recommend:

- Avoiding Laplace operator-based smoothing algorithms, or excessive smoothing iterations

- A boundary exclusion criterion that excludes all mesh faces on the surface boundary from the final surface DNE (the BoundaryDiscard="vertex" argument in molaR).
- Consistency with retriangulation protocol across all surface meshes included in a study.
- Avoiding the combination of results from prior studies using different retriangulation protocols.

We also demonstrate here a framework for decision-making in regards to retriangulation protocol that can be applied to most research questions. A conservative approach to smoothing such as we demonstrate in this paper (i.e. a minimal number of smoothing iterations and the use of less aggressive smoothing algorithms) is more likely to eliminate scanning noise, while capturing the essential surface geometry of the tooth surface and retaining the fine scale features, without causing many of the potential pitfalls associated with retriangulation. Higher face counts are able to capture the complexity of the tooth surface in greater detail, but do so at the expense of computational power. Finally, we strongly advocate that researchers publish un-processed, segmented PLY files in online archives in addition to the retriangulated PLY meshes used for analyses.

4. Dental Topography in Marsupials: Proxies for Dietary Ecology and Environmental Reconstruction

4.1 Introduction

Having diverged from placental mammals well over 100 million years ago, the metatheria clade is extremely diverse, and are represented in a set of ecologies that spans almost the entire range of placental diversity (major exceptions being the lack of marine and flying forms) (Szalay, 2006; Ungar, 2010). Metatherians constitute a major component of the fauna for the entire Cenozoic in South America, Australia (as they still do today), and Antarctica (Simpson, 1950; 1961; Keast, 1977; Chornogubsky et al., 2009). For this reason, there is a great amount of potential for their use as an environmental proxy on these continents. However, such an approach requires a foundational dataset of ecometrics—measurements from ecologically relevant morphological features—from a broad taxonomic and ecologically diverse sample. If the ecologies of mammals can be reconstructed reliably, then there is evidence that the distribution of ecologies within any given fauna may be used to reconstruct the environment or climate that that fauna inhabits (Andrews et al., 1979; Kay and Madden, 1997; Kay et al. 2012). Given the abundance of teeth in the mammalian fossil record, deciphering how dentitions relate to dietary ecology has been a major focus of the mammalian paleoecological literature (Owen, 1871; Simpson, 1933; Kay, 1975; Walker et al., 1978; Anthony and Kay, 1992; MacFadden, 2000; Williams and Kay, 2001; Boyer, 2008; Lucas et al., 2008; Damuth and Janis, 2011).

Broad-scale ecomorphological studies of marsupials are scarce for several reasons, chief among them is that the methods that have been used for placental groups cannot be easily applied to a clade as evolutionarily distinct as the marsupials. Ecomorphological studies typically rely on homologous structures that can be identified and measured in all the included taxa—such as specific tooth crests (e.g., Kay and Covert, 1984)—and thus marsupials are typically excluded from such studies. However, a number of homology-free metrics of tooth surfaces have opened the door for analyzing and comparing taxa with greater morphological disparity. I present here a study of three dental topography metrics—Relief Index (RFI), Orientation Patch Count Rotated (OPCR), and Dirichlet Normal Energy (DNE)—as they relate to the dietary ecology of marsupials. I demonstrate that these metrics do indeed relate to diet in marsupials and can be used to reliably infer dietary ecology. I also demonstrate the potential for the metatherian community niche structure to serve as a proxy for reconstructing past climates and environments.

4.1.1 Measuring Tooth Shape

In a general sense, dental topography metrics allow for the treatment of the tooth surface as a geometric surface, quantitatively assessing the features of that surface. This gives these metrics a couple notable advantages over landmark-based metrics: 1) As suggested above, comparisons of highly divergent dentitions often lack obviously homologous features that can be juxtaposed in a biologically meaningful manner; and 2)

Researcher subjectivity in deciding the exact definition of certain landmarks—or qualitative trait scores—is reduced, thereby reducing inter-observer error. However, the precise attributes of the surface that the metrics evaluate differ significantly, potentially resulting in drastically different interpretations. Before proceeding, I provide a brief description of each topographic metric included in this study.

4.1.1.1 Relief Index (RFI)

Introduced conceptually by Ungar and M'kirera (2003) and further refined into the utilized metric in this study by Boyer (2008), relief index (RFI) is most simply described as a ratio of the 3D surface area of the tooth crown to its 2D-projected planometric footprint (illustrated in Figure 24). In Figure 24, we see that the 2D planometric area is representative of the silhouette of the tooth if a light were to be shown downward perpendicularly to the occlusal surface. Boyer (2008) demonstrated the usefulness of RFI in distinguishing dietary categories amongst prosimian primates as well as other euarchontan taxa (Scandentia and Dermoptera). RFI also has been demonstrated to be relatively robust to minor changes in tooth morphology that occur naturally as the teeth wear (Boyer, 2008), giving it greater potential utility in the fossil record, for which worn teeth constitute a significant component. Though studies incorporating RFI have mostly concentrated on primates, the inclusion of a few euarchontan taxa, *Cynocephalus* and *Tupaia*, in Boyer (2008), suggests that it is capable of distinguishing diets in non-primate taxa as well.

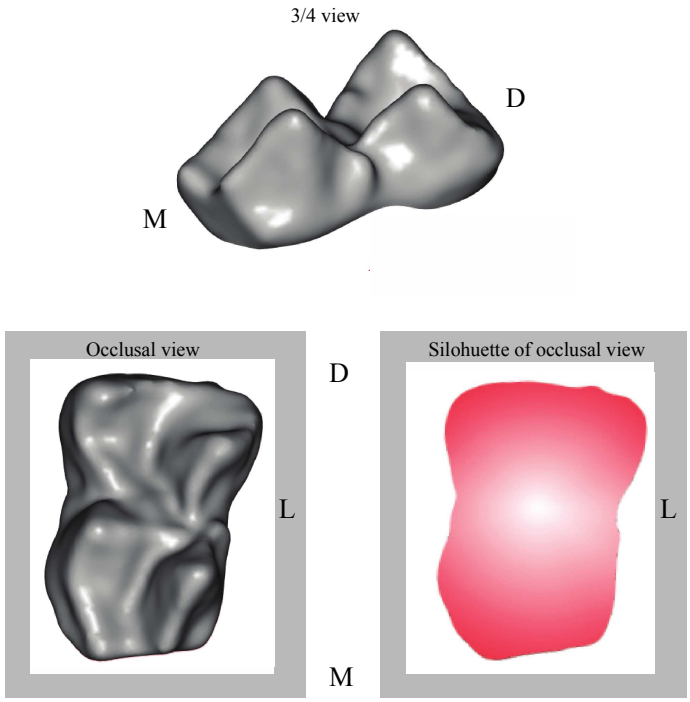

Figure 24: Illustration of the 3D surface area (top) and 2D planometric area (bottom right) that compose the ratio of RFI. Image derived from Boyer (2008).

4.1.1.2 Orientation Patch Count Rotated (OPCR)

Introduced by Evans and Jernvall (2009), orientation patch count rotated (OPCR) is founded on the concept that the complexity of the tooth surface is related to the required degree of mechanical processing brought on by the demands of the diet. To measure surface complexity, OPCR sums the total number of "patches", or groups of adjacent faces that have the same orientation (as defined by one of eight cardinal and intercardinal directions). A simple way to understand how surface complexity and OPCR are related is to picture the different constructions of a pyramid (Figure 25). As we increase the number of triangles used to form the pyramid, the number of different

planes that make up that pyramid increases, and thus the complexity of the pyramid increases. OPCR is simply the sum of differently oriented planes that make up a 3D surface.

A modification of the original orientation patch count (OPC) (Evans et al., 2007), OPCR is a means to compensate for a problem associated with OPC in which the number of patches is sensitive to the orientation of the tooth. This is done by rotating the tooth surface eight times—each time by 5.625° for a total of 45°--and OPC is measured for each orientation. The average of these eight different OPC values is then the recorded OPCR value. OPCR has demonstrated an ability to distinguish faunivorous from herbivorous taxa (Evans et al., 2007; Evans and Jernvall, 2009), and has been used to infer changes in diet in horse evolution (Evans and Janis, 2014). It has also been suggested to reflect the 'toughness' of primate dietary items (Bunn et al., 2011; Ledogar et al., 2013), the most commonly accepted definition of which is generally the amount of energy needed to propagate a crack (Ashby, 1992; Lucas, 2004; Williams et al., 2005; Berthaume, 2017).

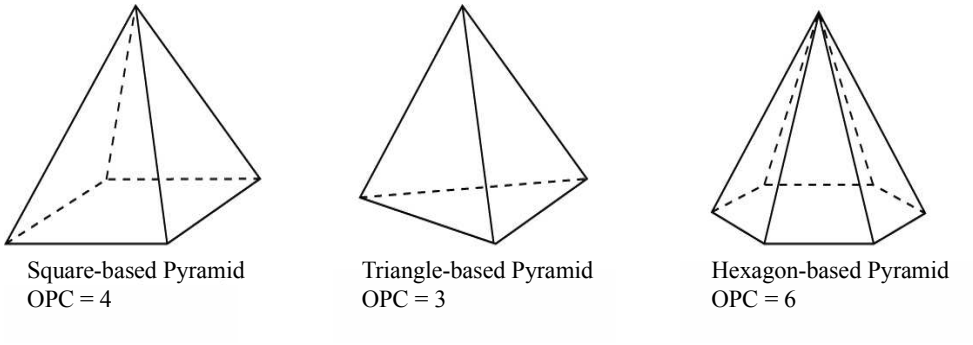

Figure 25: Pyramids of different face counts reflecting the effect of face count on the measurement of OPCR. Geometric images are courtesy of Kullabs (http://www.kullabs.com/).

The calculation of OPCR on a surface can be affected by a number of different decisions made by the researcher, including the face count of the 3D reconstruction and minimum size of the patch. The influence of face count is obvious, as illustrated in Figure 25. The standard for minimum patch size is 3 (Evans and Sanson, 2014; Pampush et al., 2016a), though it is easy to imagine that allowing a single face to be considered a patch would greatly increase the OPCR value, and likewise setting the minimum patch size especially high would greatly decrease the OPCR value. Here, I use the standard minimum patch size.

4.1.1.3 Dirichlet Normal Energy (DNE)

Bunn et al. (2011) initially proposed the use of Dirichlet normal energy (DNE) as a measure of dental topography, and its utility in distinguishing dietary categories within primates has since been well demonstrated (Winchester et al., 2014). Because

DNE is discussed in great detail in Chapter 3, I will provide only a brief summary here. In essence, DNE provides a measure of the sum curvature of the surface, with sharper features contributing more DNE than more rounded features. Winchester et al. (2014) noted the strong positive correlation between DNE and the Shearing Quotient (Kay and Covert, 1984), and indeed DNE can be thought of as an inclusive, automated way of measuring shearing on a tooth surface. Primarily, DNE has been used in the study of primate teeth, though recent work by Prufrock et al. (2016) has included primitive rodents and preliminary studies suggest its utility to distinguish dietary categories in marsupials (Spradley and Kay, 2016).

4.1.2 Predictions

Given that tooth shape is generally constrained by the functional requirements of food properties (Kay, 1975; Evans and Sanson, 2003), I expect my results to generally mirror those from a similarly ecologically-broad clade like Primates. Indeed, Kay and Hylander (1978) found that, within in a limited sample of phalangeriform marsupials, dental shearing correlated with diet in a manner similar to the patterns observed in primates. Thus, I predict folivorous and insectivorous marsupials to have the highest values of RFI, OPCR, and DNE, as these two diets have been suggested to have the highest degree of tough food items. Kay (1975) suggested that folivores and insectivores are not easily distinguished except by body (and tooth) size. Since these metrics do not include any measure of tooth size, I do not expect to see significantly different values of

any metric between these two dietary categories. Additionally, frugivorous marsupials should have significantly lower values for all three metrics, as has been demonstrated in primates (Winchester et al., 2014).

True faunivory is rare in primates—limited to a few genera, including *Tarsius, Arctocebus*, and *Loris*—and in fact there are no large vertebrate prey specialists as I find amongst the marsupials (e.g. *Sarcophilus, Thylacinus,* etc.). It is thus hard to predict how DNE will behave or even if it will be useful. Nevertheless, given the high protoconid and/or paraconid cusp(s) of the carnassial teeth of marsupial carnivores, we might expect that faunivores will have higher DNE and RFI values than frugivores.

Evans et al. (2007) and Evans and Jervnall (2009) explored faunivory using the OPCR metric. They report that carnivorous species have significantly lower OPCR values, and suggest that the relatively easily digested proteins and fats within meat did not require the same tooth surface complexity as the more difficult to digest fibrous dietary components of herbivorous species. Thus, I predict that the faunivorous species in my sample will demonstrate similarly lower OPCR values.

Ultimately, dental topography should have a strong relationship with food material properties. Though a more in-depth exploration of this interaction is beyond the scope of this study, I expect gross differences in food material properties across taxa to generally align with traditionally used heuristic dietary categories, enabling the use of diet categories as a stand-in for the more difficult to measure material properties. With

this caveat in mind, the employed dental topography metrics are expected to be predictive of diet category within the marsupials studied here.

4.2 Materials and Methods

4.2.1 Sample Preparation

To investigate the relationship between dental topography and dietary ecology, I scanned and segmented the lower second molars of 135 individual specimens representing 43 genera, and 59 species of marsupials (Table 1). To capture the wide ecological variety of marsupials present in the fossil record of South America, it was necessary to sample both South American and Australian/New Guinean extant marsupials. Specimens were obtained from the American Museum of Natural History, the National Museum of Natural History, and the Australian Museum in Sydney, and include both skeletal material and epoxy casts poured from molds of teeth. Cast fidelity was examined by comparing scans of casted and original dentitions for a subset of specimens. The complete sample of species, along with a phylogenetic tree topology, is depicted in Figure 26. Primary dietary categories were assigned to each species according to MammalDIET, an online archive of dietary information (Kissling et al., 2014). This resource was supplemented and cross-referenced with sources from the primary literature, including taxonomic and ecological reference volumes (Gardner, 2008; Flannery, 1995). The sources for these characterizations are summarized in

Appendix C. These dietary categories are necessarily broad owing to the often imprecise nature of the dietary information.

Table 11: Dental topography metrics and dietary category for each species included in this study. All values represent means for multiple individuals (when available).

Family	Species	Diet	DNE	RFI	OPCR	M_2 Area
Acrobatidae	*Acrobates pygmaeus*	Frugivore	205.54	0.38	72.5	0.69
Potoridae	*Aepyprymnus rufescens*	Browsing	249.19	0.43	92.6	29.43
Dasyuridae	*Antechinus minimus*	Insectivore	308.93	0.62	79.4	3.66
Potoridae	*Bettongia gaimardi*	Browsing	187.88	0.49	67.5	21.16
Caenolestidae	*Caenolestes fuliginosus*	Insectivore	326.01	0.58	77.1	2.59
Didelphidae	*Caluromys derbianus*	Frugivore	212.98	0.52	67.6	2.67
Didelphidae	*Caluromys lanatus*	Frugivore	161.42	0.57	51.6	4.60
Burramyidae	*Cercartetus caudatus*	Frugivore	190.97	0.48	62.2	1.58
Didelphidae	*Chironectes minimus*	Faunivore	240.37	0.62	69.5	14.09
Petauridae	*Dactylopsila palpator*	Insectivore	137.74	0.43	53.6	7.16
Petauridae	*Dactylopsila trivirgata*	Insectivore	182.30	0.45	78.4	7.73
Dasyuridae	*Dasykaluta rosamondae*	Insectivore	283.68	0.61	67.2	9.65
Dasyuridae	*Dasyurus hallucatus*	Insectivore	213.91	0.58	62.6	10.81
Macropodidae	*Dendrolagus lumholtzi*	Folivore	182.65	0.56	64.2	28.80
Didelphidae	*Didelphis albiventris*	Frugivore	162.69	0.50	50.5	14.32
Macropodidae	*Dorcopsis hageni*	Browsing	230.37	0.63	65.9	24.94

Macropodidae	*Dorcopsis luctuosa*	Browsing	203.02	0.59	48.6	23.04
Macropodidae	*Dorcopsulus macleayi*	Browsing	183.76	0.48	60.0	26.34
Microbiotheriidae	*Dromiciops gliroides*	Insectivore	199.76	0.56	59.3	1.43
Pseudocheiridae	*Hemibelideus lemuroides*	Folivore	224.98	0.48	78.4	10.71
Hypsiprymnodontidae	*Hypsiprymnodon moschatus*	Frugivore	166.73	0.46	75.5	8.01
Peramelidae	*Isoodon obesulus*	Insectivore	200.74	0.48	60.0	8.86
Thylacomyidae	*Macrotis lagotis*	Omnivore	175.89	0.56	58.8	22.44
Didelphidae	*Marmosa mexicana*	Insectivore	221.07	0.60	65.4	1.69
Didelphidae	*Marmosa murina*	Insectivore	272.33	0.61	70.5	1.95
Didelphidae	*Metachirus nudicaudatus*	Insectivore	302.80	0.66	67.9	5.85
Didelphidae	*Monodelphis domestica*	Insectivore	284.26	0.68	63.7	3.41
Peroryctidae	*Peroryctes raffrayana*	Insectivore	315.67	0.62	73.3	8.42
Pseudocheiridae	*Petauroides volans*	Folivore	306.05	0.52	85.5	8.81
Petauridae	*Petaurus australis*	Frugivore	150.87	0.46	70.9	3.37
Petauridae	*Petaurus breviceps*	Frugivore	146.69	0.46	50.4	3.08
Pseudocheiridae	*Petropseudes dahli*	Folivore	292.20	0.55	76.5	13.89
Phalangeridae	*Phalanger gymnotis*	Frugivore	157.75	0.40	63.3	22.75
Phalangeridae	*Phalanger mimicus*	Frugivore	183.70	0.43	57.3	17.25
Phalangeridae	*Phalanger orientalis*	Frugivore	196.67	0.46	72.1	18.04
Phascolarctidae	*Phascolarctos cinereus*	Folivore	210.95	0.42	81.4	38.89
Potoridae	*Potorous tridactylus*	Folivore	251.32	0.54	87.4	15.99
Pseudocheiridae	*Pseudocheirus peregrinus*	Folivore	216.40	0.50	68.4	8.26
Pseudocheiridae	*Pseudochirops archeri*	Folivore	264.58	0.47	88.5	14.36
Pseudocheiridae	*Pseudochirulus larvatus*	Folivore	245.01	0.42	88.3	6.56

Dasyuridae	*Sarcophilus harrisii*	Faunivore	172.59	0.55	39.8	78.27
Macropodidae	*Setonix brachyurus*	Browsing	202.09	0.58	61.8	20.74
Dasyuridae	*Sminthopsis crassicaudata*	Insectivore	325.78	0.71	63.8	1.40
Phalangeridae	*Spilocuscus maculatus*	Frugivore	186.81	0.41	64.5	38.74
Phalangeridae	*Strigocuscus pelengensis*	Frugivore	178.95	0.42	60.3	13.89
Didelphidae	*Thylamys elegans*	Insectivore	271.67	0.67	57.4	1.88
Macropodidae	*Thylogale stigmatica*	Folivore	277.30	0.63	58.9	24.15
Phalangeridae	*Trichosurus vulpecula*	Frugivore	188.09	0.44	62.1	20.42
Vombatidae	*Vombatus ursinus*	Browsing	247.21	0.59	79.5	56.57
Macropodidae	*Wallabia bicolor*	Browsing	252.61	0.52	61.0	67.52
Phalangeridae	*Wyulda squamicaudata*	Folivore	175.61	0.35	86.5	20.80

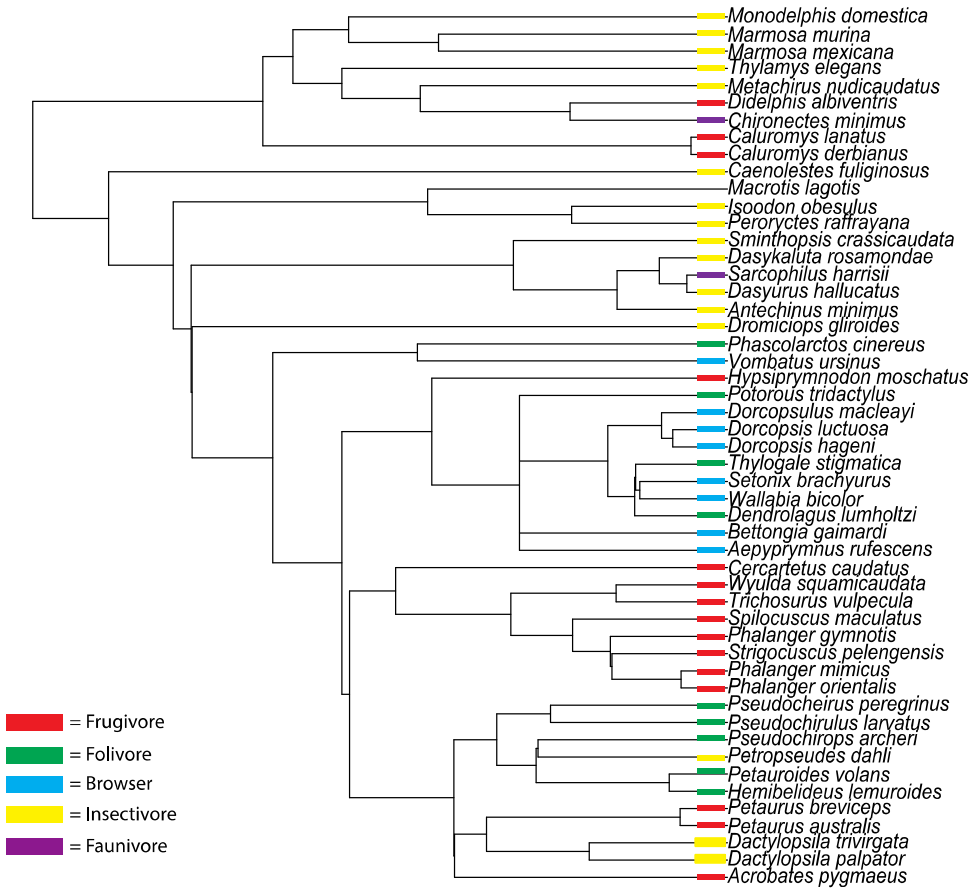

Figure 26: Phylogenetic tree of all marsupial species included in this study. Colors on tips represent dietary categories assigned to each species. Tree topology modified from Bininda-Emmons et al. (2008).

After scanning and segmentation (see introduction of Chapter 3 for brief review of these processes and terms), we have a 3D representation of a tooth surface that is comprised of thousands of triangular faces (specifically in a PLY format). It is then necessary to perform retriangulation on the surface to eliminate any possible artifacts that may influence the measurement of dental topography. This was done in accordance with Spradley et al. (2017), wherein we outline a rationale for retriangulation decisions.

Ultimately, I chose to downsample all PLY files to 10,000 faces and smooth the 3D mesh via 25 smoothing iterations performed in Avizo® (FEI Visualization Sciences Group, Berlin, Germany). This fairly conservative retriangulation protocol ensures that the effect of smoothing artifacts is minimized whilst maintaining the essential geometry of the tooth surface, which is a concern when more aggressive smoothing algorithms are employed (Spradley et al., 2017). Nevertheless, artifacts were identified on a limited number of surfaces in my sample, and to eliminate these they were deleted and the resultant 'holes' were filled using Geomagic® (3D Systems, Inc., Rock Hill, SC). After all PLY files were retriangulated, the resultant files were uploaded to the open-source statistical software R via the package "molaR" (Pampush et al., 2016a). The boundary exclusion criterion of molaR was set to "vertex", and DNE, RFI, and OPCR were calculated for each tooth surface. Linear measurements of the maximum mesiodistal length and buccolingual width were also taken for each tooth, and this was used as an approximation of the molar area. Because molar area was not normally distributed, the area of each molar was natural-log transformed.

4.2.2 Statistical Analyses

With the exception of phylogenetically informed analyses, all statistical tests were performed with an alpha level of 0.05, and a modified Bonferroni correction, using the open-source statistical software R. My Bonferroni correction follows that of Cheverud (2001), which controls for covariation in the data and is more rigorous than

simply accounting for the number of tests being performed. In order to discern how these different metrics might relate to one another, a Principal Components Analysis (PCA) was performed using all three metrics. To account for effects of phylogenetic relatedness among species, mean species values were compiled and a phylogenetic ANOVA was performed using the R package 'phytools'. Pairwise comparison tests were then undertaken using a phylogenetically-corrected Tukey's Honestly Significant Difference (HSD) test using the R package 'caper'. Finally, a discriminant function analysis (DFA) was performed to test the ability of these metrics to successfully reconstruct diet with a given dental topography.

4.2.3 Distributions of Ecometrics as Climatic Proxies

Having established that these metrics are ecologically informative in my marsupial sample, I seek to demonstrate that the distributions of these ecometrics (ecologically relevant metrics; see Eronen et al., 2010) within communities of marsupials can be used as proxies for variables of climate and habitat. The six variables of interest presented here are the same six from Chapter 2: MAT, MAP, temperature seasonality, precipitation seasonality, NPP, and canopy height. Faunal lists were compiled using the UC-Davis ICE "Biological Inventories of the World's Protected Areas" (http://www.ice.ucdavis.edu/bioinventory/bioinventory.html) and supplemented with primary sources of published faunal lists (Bulmer and Menzies, 1972; Helgen, 2007; Mamu, 2008). Species means for DNE, RFI, and OPCR were recorded for each species in

this study and the distributions of those means were recorded at each locality. For some genera with multiple species for which not all species were sampled in this study, the mean of the species sampled was used as a stand-in value for missing species. Genera for which no species were sampled were not included.

Figure 27: Map of mammalian localities used in this study of distribution of ecometrics and environment.

Since this is an exploratory analysis, I used three basic statistical measures of distributions—mean, coefficient of variation, and skewness—and these were calculated for the distribution of each metric at every locality. These statistical measures will serve as the proxies for environment at my marsupial faunal localities (note: these are the same Australian localities presented in Chapter 2). By using these statistics, I seek to

explore the potential of distributions of ecometrics to be used in place of distributions of known ecologies—as in Chapter 2 of this dissertation. Because the reconstruction of behavior in the fossil record is problematic, this method would skip this step and instead rely only on quantitative measurements that can be directly taken from fossil teeth.

4.2.3.1 Exclusion of Range

I decided to exclude the use of range. This decision was made after analysis of all variables suggested that ranges do not have significant relationships with my bioclimatic variables. Before moving forward, it is important that I first explain these results in the context of my dataset. First of all, the ranges of these ecometrics are not were overly broad, and not informative. A majority of localities having high ranges of DNE, OPCR, and RFI. Exploring the data, this is likely because most localities have at least one insectivore (typically high values of DNE, OPCR, and RFI) and at least one frugivore (typically low values of each). Thus, the ranges are fairly consistent from one locality to the next regardless of the actual shape of the distribution.

4.3 Results

4.3.1 Dental Topography and Dietary Ecology

4.3.1.1 Correlations Among Topographic Variables

Summary statistics for correlation analyses between dental topography metrics are presented in Table 12. Least-squares regressions between each pair of variables are

presented in Figures 28-30. One-way ANOVA tests reveal that after a modified Bonferroni correction to reset the alpha to 0.019, RFI and OPCR are not significantly correlated ($p = 0.13$). DNE on the other hand is significantly correlated with both RFI and OPCR ($p < 0.019$), though the correlation coefficient between DNE and RFI ($R^2 = 0.38$) is higher than it is between DNE and OPCR ($R^2 = 0.18$).

In order to observe the combination of these metrics in morphospace, I performed a principal components analysis (PCA). My PCA plot (Figure 31) illustrates that DNE has the greatest ability to distinguish among species with similar diets, as it forms the primary driver behind the first principal component, which itself explains 42.5% of the variance.

Table 12: Results from ANOVA tests for comparisons between dental topography metrics. R^2 values are from the least-squares regressions illustrated in Figures 28-30.

Comparison	*F*	*p*-value	R^2
DNE-RFI	45.441	< 0.0001	0.380
DNE-OPCR	10.928	0.002	0.182
RFI-OPCR	2.390	0.129	0.045

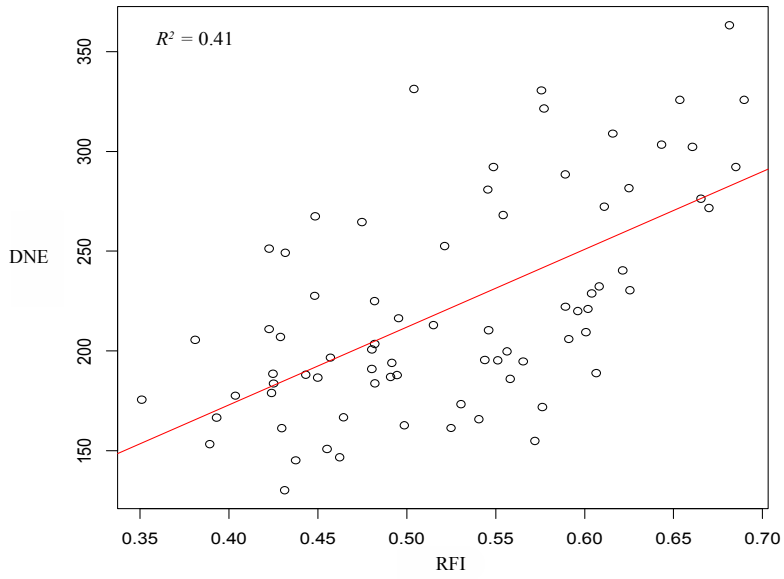

Figure 28: Bivariate plot of DNE as a function of RFI. Red line represents least squares regression, with associated correlation coefficient presented in upper left-hand corner of plot.

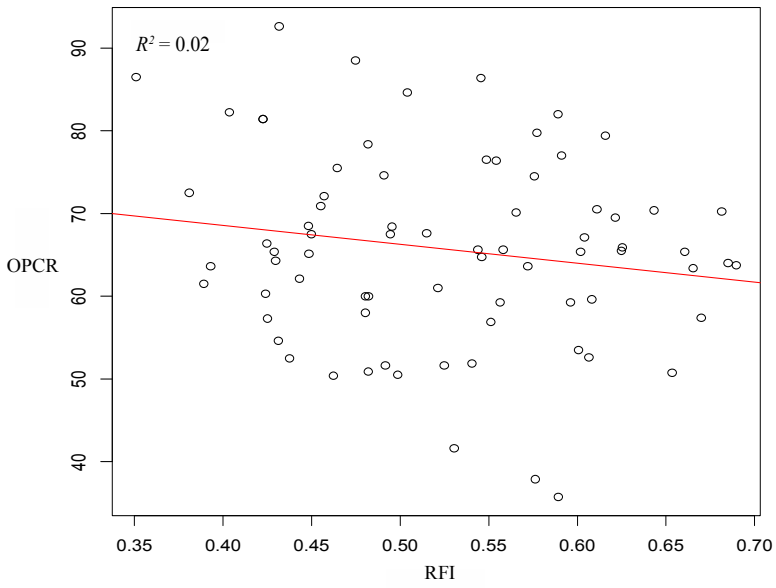

Figure 29: Bivariate plot of OPCR as a function of RFI. Red line represents least squares regression, with associated correlation coefficient presented in upper left-hand corner of plot.

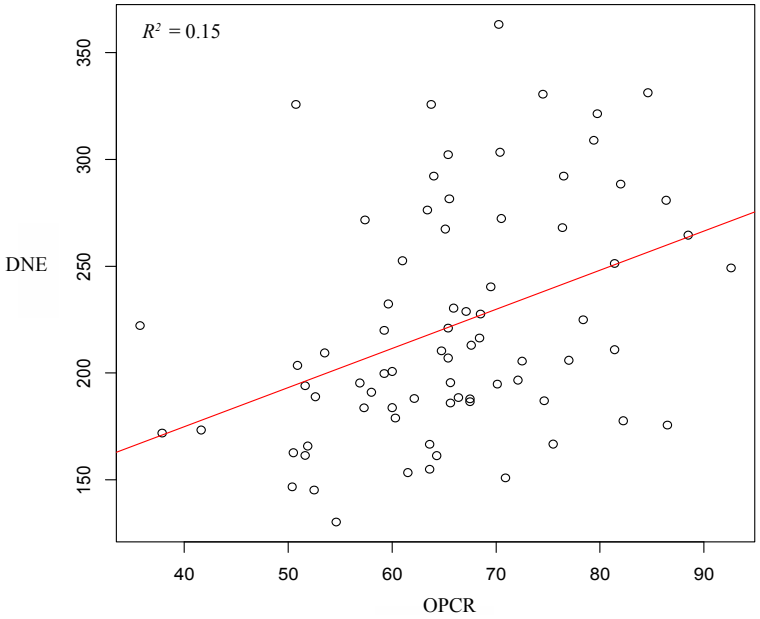

Figure 30: Bivariate plot of DNE as a function of OPCR. Red line represents least squares regression, with associated correlation coefficient presented in upper left-hand corner of plot.

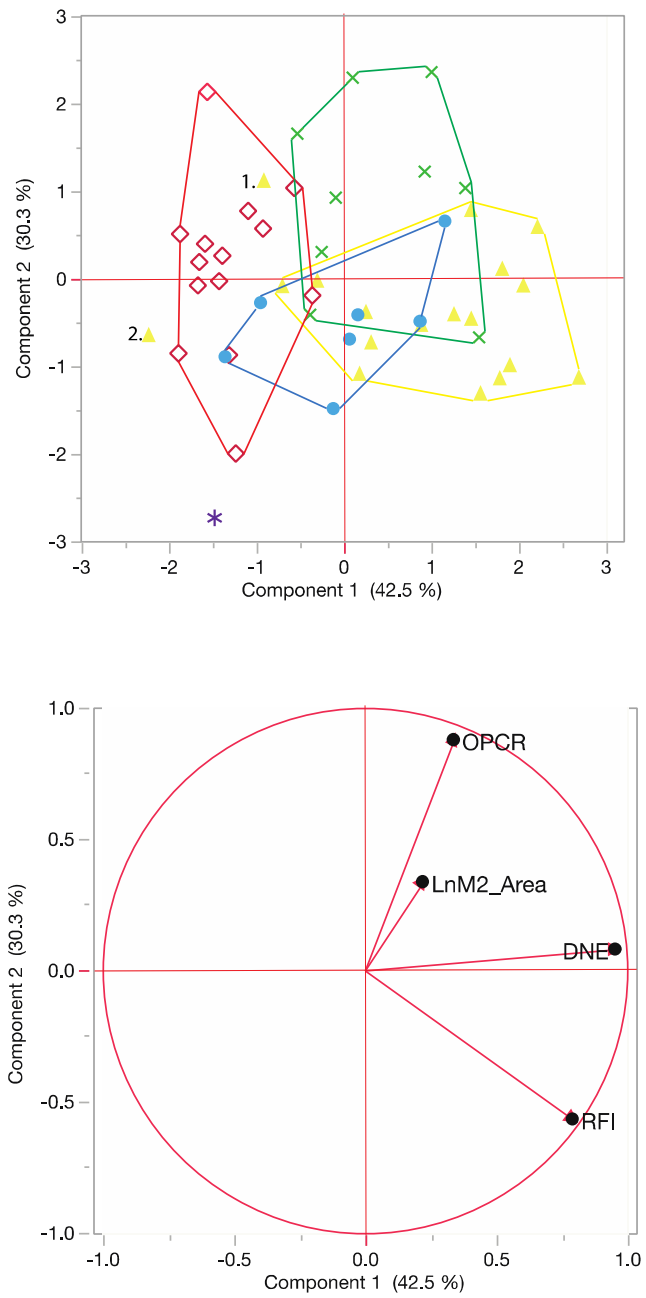

Figure 31: Principal components analysis including the three dental topography metrics and the natural log of M_2 area. The symbol key is as follows: Red diamonds = frugivores; Blue circles = browsers; Green *x*'s = folivores; Yellow triangles

= insectivores; Purple star = faunivore (*Sarcophilus harrisii*). The numbered triangles correspond to 1. *Dactylopsila palpator* and 2. *Dactylopsila trivirigata*.

4.3.1.2 Phylogenetic ANOVAs

Phylogenetically-corrected one-way ANOVA tests were conducted to compare the effect of diet on dental topography metrics. Using a Bonferroni-corrected alpha level of 0.019, I do not find a statistically significant effect of diet on any of the topographic metrics. However, after the two species of *Dactylopsila,* a genus that specializes on soft-skinned insects such as beetle larvae, and the meat-eating carnivores (*Sarcophilus harrisii*) were excluded from the analysis, my results indicate a significant effect of diet on DNE ($F(2,44)=23.498$, $p = 0.009$). A phylogenetically-corrected post-hoc Tukey HSD test indicated that there are significant differences in the means of DNE between frugivores-insectivores, frugivores-folivores/browsers, and insectivores-folivores/browsers. After phylogenetic correction and removal of *Dactylopsila* and *Sarcophilus*, I do not find a statistically significant dietary signal in either RFI or OPCR, though the *p*-value for RFI is very close to significance ($p = 0.036$). Data for these tests are presented in Tables 13-15.

In general, insectivores and folivores/browsers have higher values of DNE and RFI than do frugivores and faunivores. This is illustrated both in the box plots of Figure 32 and in the PCA plot (Fig. 31). The PCA plot in particular shows a distinct clustering of frugivores apart from the other dietary groups, with much of this variance being due to DNE and RFI. The exceptions to this are the two *Dactylopsila* species (yellow triangles

labeled 1. *D. palpator* and 2. *D. trivirigata*), which cluster in amongst the other frugivores. The PCA plot also demonstrates the similar amounts of variance in OPCR that exists in each dietary category, and the especially low value of OPCR associated with the meat-eating faunivore, *Sarcophilus harrisii.*

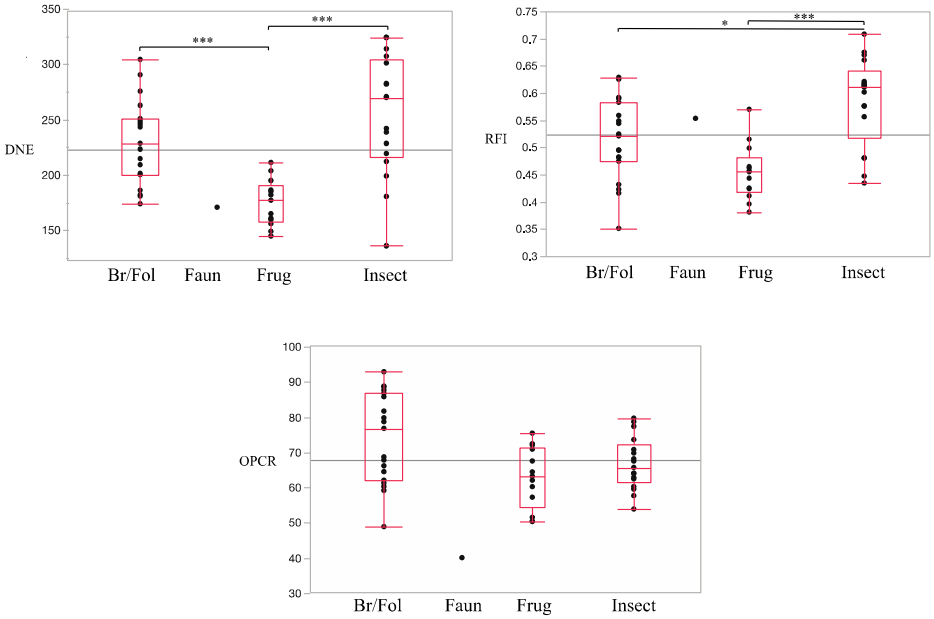

Figure 32: Quantile plots of species means for each of the three dental topography metrics. Bars and asterisks indicate significantly different relationships as recognized by a post-hoc Tukey's HSD test (* indicates a *p*-value < 0.05, * indicates a *p*-value < 0.001).**

Table 13: Phylogenetically-corrected ANOVA table for dietary group means of DNE. A. results from an ANOVA performed on the entire dataset; B. results from an ANOVA performed after removing the two *Dactylopsila* species as well as *Sarcophilus harrisii* and *Chironectes minimus*.

A.	**df**	**Sum-Sq**	**Mean-Sq**	**F-value**	**Pr (>F)**	**Pr (>F) given phylogeny**
Diet	3	50674	16891.2	9.925	3.673e-05	0.039
Residuals	46	78284	1701.8			

B.	**df**	**Sum-Sq**	**Mean-Sq**	**F-value**	**Pr (>F)**	**Pr (>F) given phylogeny**
Diet	2	60000	30000.2	23.498	1.141e-07	**0.009**
Residuals	44	56174	1276.7			

Table 14: Phylogenetically-corrected ANOVA table for dietary group means of RFI. A. results from an ANOVA performed on the entire dataset; B. results from an ANOVA performed after removing the two *Dactylopsila* species as well as *Sarcophilus harrisii* and *Chironectes minimus*.

A.	**df**	**Sum-Sq**	**Mean-Sq**	**F-value**	**Pr (>F)**	**Pr (>F) given phylogeny**
Diet	3	0.129	0.043	8.201	1.771e-03	0.099
Residuals	46	0.241	0.005			

B.	df	Sum-Sq	Mean-Sq	F-value	Pr (>F)	Pr (>F) given phylogeny
Diet	2	0.162	0.081	18.498	1.478e-06	0.036
Residuals	44	0.193	0.004			

Table 15: Phylogenetically-corrected ANOVA table for dietary group means of OPCR. A. results from an ANOVA performed on the entire dataset; B. results from an ANOVA performed after removing the two *Dactylopsila* species as well as *Sarcophilus harrisii* and *Chironectes minimus*.

A.	df	Sum-Sq	Mean-Sq	F-value	Pr (>F)	Pr (>F) given phylogeny
Diet	3	1782.5	594.18	5.756	0.002	0.139
Residuals	46	4748.4	103.23			
B.	**df**	**Sum-Sq**	**Mean-Sq**	**F-value**	**Pr (>F)**	**Pr (>F) given phylogeny**
Diet	2	970.7	485.34	4.809	0.013	0.277
Residuals	44	4440.2	100.91			

4.3.1.3 Discriminant Function Analysis

Results from a DFA performed on the data suggest that dental topography metrics, in combination with the natural log of M_2 area, perform moderately well in categorizing marsupials (as a clade) by diet. Overall, species were accurately categorized

74.6% of the time. Taking a closer look at the results, I find that browsers/folivores and insectivores are categorized at much higher rates (83.8% and 72.7%, respectively) when compared to frugivores, for which the DFA is performing at a rate nearly equivalent to random chance (62.5%).

Experimenting with pairs of topographic measures (each model including the natural log of molar area), I do not find any significant differences between models. DFAs performed on individual topographic variables—in conjunction with molar area—reveal that DNE has slightly more discriminatory power (76.1%) than either RFI (70.1%) or OPCR (62.7%). This pattern holds for all dietary categories. RFI was more successful at discriminating frugivores than OPCR (37.5% and 6.3%, respectively), though both had equivalent rates of discrimination for browsers/folivores and insectivores.

Performing a DFA on species belonging to Diprotodontia alone slightly improve accuracy, with species correctly allocated at an overall rate of 77.8%. Frugivores in this sample were classified correctly 100% of the time, and the accuracy of classifying browsers and folivores was also increased to 89%. Non-diprotodont marsupials, taken alone, show a much lower accuracy in classification at 61%, with only insectivores being correctly identified at all (84.6%).

4.3.2 Dental Topography and Environmental Reconstruction

See Table 16 for the complete distribution of all three statistics for the ecometrics at each Australian and New Guinean locality. My results (shown in Table 17) show that

the mean of DNE at each locality has a significant negative correlation ($p < 0.006$) with MAP and canopy height (R^2, and significant positive correlation with temperature seasonality ($p = 0.0096$). The coefficient of variation (CoV) and the skewness of DNE distributions at localities do not show any significant correlations with any of the six bioclimatic variables (Tables 18 and 19).

Table 16: Distribution statistics of DNE, OPCR, and RFI for 17 localities across Australia and Papua New Guinea.

Locality	DNE mean	DNE range	DNE SD	OPCR mean	OPCR range	OPCR SD	RFI mean	RFI range	RFI SD
Crater Lakes National Park	17.77	62.24	0.04	8.75	8.12	0.49	0.52	0.19	0.07
Croajingolong National Park	29.14	79.08	3.56	9.38	7.00	1.84	0.52	0.33	0.08
Dunggir National Park	23.45	62.24	8.20	6.97	7.00	1.33	0.51	0.25	0.07
Fitzgerald National Park	29.31	39.81	6.07	3.56	.50	2.47	0.55	0.27	0.11
Girraween National Park	29.64	62.24	0.47	0.28	5.12	11.25	0.50	0.23	0.08
Grampians National Park	33.04	79.08	0.68	8.40	7.00	11.71	0.52	0.33	0.09
Kakadu National Park	54.94	37.69	0.68	7.40	9.40	8.32	0.56	0.27	0.10
Kosciuszko National Park	19.13	62.24	3.51	6.98	5.12	10.86	0.51	0.23	0.07
Lamington National Park	24.39	62.24	4.60	8.07	2.24	13.35	0.51	0.25	0.08
Lavinia Nature Reserve	35.28	20.84	5.55	8.72	8.45	10.66	0.54	0.19	0.07
Prince Regent Nature Reserve	16.64	16.59	4.46	9.12	6.50	11.89	0.49	0.23	0.09
Shoalwater and Corio Bays Area	07.09	59.36	0.13	5.89	2.24	14.66	0.48	0.15	0.05
Uluru-Kata Tjuta National Park	58.49	39.81	1.04	3.68	.50	1.98	0.60	0.27	0.11

Yathong Nature Reserve	87.14	37.69	6.51	7.25	7.30	8.14	0.62	0.27	0.13
Kaijende Highlands	11.97	77.93	2.82	6.30	8.10	13.08	0.49	0.23	0.08
Kaironk Valley	15.88	77.93	4.03	5.81	9.00	7.77	0.51	0.23	0.08
South Karius	03.50	77.93	5.50	6.94	8.10	12.24	0.47	0.22	0.06

The mean of RFI (Table 16) shows a significant ($p < 0.01$) positive correlation ($R^2 = 0.40$) with temperature seasonality, and a significant ($p < 0.006$) negative correlation with MAP ($R^2 = 0.49$), NPP ($R^2 = 0.44$), and canopy height ($R^2 = 0.50$). The CoV of RFI (Table 18) shows a statistically significant ($p < 0.005$) negative correlation with both NPP ($R^2 = 0.44$) and canopy height ($R^2 = 0.44$), and a correlation that nears significance with MAP ($p = 0.017$; $R^2 = 0.34$). These three relationships are illustrated in bivariate plots in Figure 33. The skewness of RFI distributions (Table 19) are not statistically significant with any of the bioclimatic variables after a Bonferroni correction, though the correlation between RFI skew and NPP—as well as canopy height—near significance ($p = 0.011$ and 0.015, respectively.

Finally, neither the mean, nor the CoV, nor the skew, of OPCR distributions at Australian localities show any significant correlations with any of the bioclimatic variables (Tables 17-19). An ecological interpretation of the results from the distributions of all three metrics and their relationship to environment is given in the discussion below.

Table 17: ANOVA statistics from the test of effect of bioclimatic variables on the mean of DNE, OPCR, and RFI at each Australian and New Guinean locality.

	DNE			
Bioclimatic Variable	***F*-ratio**	***p*-value**	R^2	**Slope**
MAT	0.1779	0.6796	0.0125	+
Temp. Seasonality	8.972	**0.0096**	0.3906	+
MAP	13.5709	**0.0025**	0.4922	-
Precip. Seasonality	0.0194	0.8911	0.0014	-
NPP	6.4725	0.0234	0.3162	-
Canopy Height	10.5408	**0.0059**	0.4295	-
	OPCR			
MAT	0.0757	0.7873	0.0054	-
Temp. Seasonality	0.0669	0.7996	0.0048	-
MAP	0.0015	0.9699	0.0001	+
Precip. Seasonality	0.466	0.506	0.0322	+
NPP	2.2102	0.1593	0.1363	+
Canopy Height	1.3166	0.2704	0.086	+
	RFI			
MAT	0.085	0.7749	0.006	+
Temp. Seasonality	9.2598	**0.0088**	0.3981	+
MAP	13.6902	**0.0024**	0.4944	-
Precip. Seasonality	0.008	0.93	0.0006	-
NPP	11.136	**0.005**	0.443	-
Canopy Height	13.7909	**0.0023**	0.4962	-

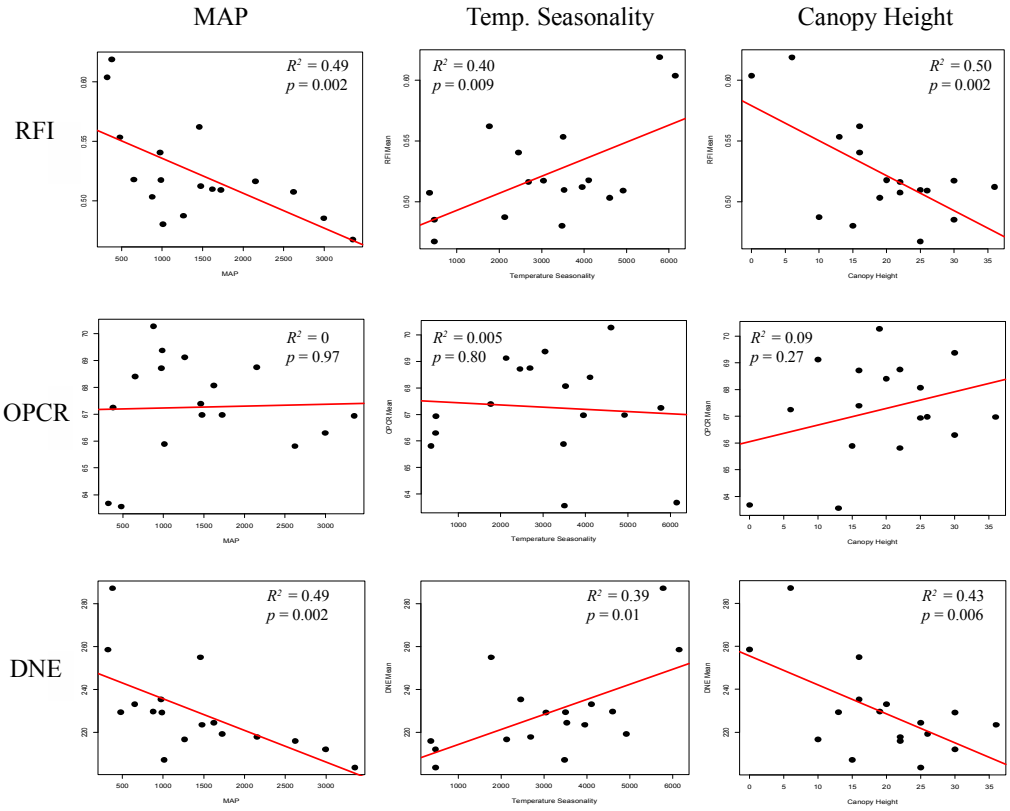

Figure 33: Bivariate plots of means of RFI, OPCR, and DNE against MAP, temperature seasonality, and canopy height. RFI and DNE show statistically significant results whereas OPCR does not.

Table 18: ANOVA statistics from the test of effect of bioclimatic variables on the coefficients of variation of DNE, OPCR, and RFI distributions.

	DNE			
Bioclimatic Variable	***F*-ratio**	***p*-value**	***R*²**	**Slope**
MAT	0.129	0.725	0.009	-
Temp. Seasonality	0.766	0.395	0.049	+
MAP	0.513	0.477	0.034	-
Precip. Seasonality	0.871	0.365	0.055	-
NPP	1.370	0.260	0.084	-

Canopy Height	0.806	0.384	0.051	-
	OPCR			
MAT	0.034	0.857	0.002	-
Temp. Seasonality	1.882	0.190	0.111	-
MAP	3.329	0.088	0.182	+
Precip. Seasonality	0.001	0.980	0	-
NPP	6.008	0.027	0.286	+
Canopy Height	8.120	0.012	0.351	+
	RFI			
MAT	1.3557	0.2638	0.088	+
Temp. Seasonality	2.122	0.1673	0.132	+
MAP	7.2643	0.0174	0.342	-
Precip. Seasonality	0.0752	0.788	0.005	-
NPP	11.1356	**0.0049**	0.443	-
Canopy Height	11.1255	**0.0049**	0.443	-

Table 19: ANOVA statistics for the test of effect of climatic variables on the skew of DNE, OPCR, and RFI distributions. The two asterisks next to NPP under RFI denote that this was a polynomial fit. Variables with significant values are illustrated in Figure 40.

	DNE			
Bioclimatic Variable	***F*-ratio**	***p*-value**	R^2	**Slope**
MAT	0.119	0.735	0.008	+
Temp. Seasonality	3.987	0.064	0.210	-
MAP	2.280	0.152	0.132	+
Precip. Seasonality	0.715	0.411	0.046	+
NPP	1.614	0.223	0.097	+

Canopy Height	1.503	0.239	0.091	+
	OPCR			
MAT	0.012	0.916	0.001	+
Temp. Seasonality	3.700	0.078	0.236	-
MAP	2.740	0.124	0.186	+
Precip. Seasonality	1.355	0.267	0.101	-
NPP	2.749	0.123	0.186	+
Canopy Height	0.556	0.470	0.044	+
	RFI			
MAT	0.3935	0.5406	0.0273	-
Temp. Seasonality	5.7933	0.0305	0.2927	-
MAP	7.5646	0.0156	0.3508	+
Precip. Seasonality	1.9796	0.1812	0.1239	-
NPP**	6.4927	0.0111	0.4997	n/a
Canopy Height	7.7215	0.0148	0.3555	+

4.4 Discussion

Using a broad sample, I seek here to establish the efficacy of DNE, RFI, and OPCR—as well as the three in combination with the natural log of molar area—to distinguish general dietary groups in marsupial taxa based on dental topography. To date, studies incorporating dental topography metrics have been limited to a handful of mammalian clades. Marsupials represent a diverse taxon, both ecologically and geographically, that have been underrepresented in broad-scale morphological studies. This also represents a valuable test of these topography metrics in a clade that is: 1)

phylogenetically distinct from any other in previous topographic studies; and 2) phylogenetically and ecologically diverse, giving us the chance to test the limits of these metrics as to how broad a sample they can be applied.

My results provide positive evidence in marsupials for the trends that have been observed in DNE in primates (Boyer, 2008; Ledogar et al., 2013; Winchester et al., 2014). DNE exhibits significant differences among dietary groups and in several significant pairwise comparisons. Results from OPCR and RFI suggest less discriminatory power, which is consistent with other studies incorporating similar techniques (Winchester et al., 2014; Pineda-Munoz et al., 2016).

4.4.1 Issues of Defining Dietary Categories

As with any ecomorphological study, the *a priori* placement of species into ecological categories presents some philosophical and functional issues. Specifically, in relation to diet, these issues tend to focus around the summary of a species' entire diet into a convenient umbrella term (e.g. frugivore, folivore, insectivore, etc.). The obvious problem with this practice is that mammalian species rarely have diets that can be so succinctly summarized, though this is as detailed as one can frequently expect to be in the fossil record. By categorizing diets in broad terms, we are likely going to encounter noise in the data that could be explained with greater resolution of species' diets.

Another issue that specifically arises when discussing dietary categories in the context of dental morphology is that these categories are often constructed because of

the supposed similar material properties of the foods that compose any given category. Bearing in mind that tooth morphologies have been demonstrated to reflect dietary preference, this results in studies of dental morphology and dietary ecology that begin with *a priori* groupings that may bias the construction of the analysis and interpretation of the results.

4.4.1.1 Excluding *Dactylopsila* and *Sarcophilus*

The rationale to exclude the genera *Dactylopsila* and *Sarcophilus* from the discriminant function analyses was generally motivated by their status as evolutionary outliers in this data set. *Sarcophilus harrisii* is the only meat-eating hypercarnivore in my dataset—all others include large amounts of insects amongst their prey—and as such was difficult for the model to classify. Additionally, given the distinctive morphology of the carnassial molar, it is unlikely that any knowledgeable morphologist would have difficulty ascertaining the diet of a species with such a tooth. *Dactylopsila* represents a unique ecological niche in my dataset, one that includes tree gouging and the extraction of soft-bodied insects, such as grubs. This is not unlike the strepsirrhine primate *Daubentonia* (Cartmill, 1974)—the aye-aye—which was also excluded from the dental topographic analysis of primates by Winchester et al. (2014). This specialization on soft-bodied insects is reflected in the dentition of *Dactylopsila*—and indeed *Daubentonia*—as both these genera have very low crowned, bunodont molars that resemble those of frugivores.

4.4.2 Correlations Among DNE, RFI, and OPCR

My results show that of the three measures, only DNE and RFI seem to show a significant correlation ($p < 0.019$, $R^2 \cong 0.38$). This should not come as a surprise, as both metrics have been shown to have a close relationship with shearing (Boyer, 2008; Winchester et al., 2014). The discrepancy between the two metrics is likely due to the very fact that one metric, DNE, is more directly affected by the length and sharpness of these features—as mentioned in the introduction, the sharper the feature, the more it contributes to the total DNE of a surface. RFI on the other hand, because it is a simple ratio of the 3D surface area of the tooth to the 2D footprint area, is not likely to be affected by such small-scale differences like sharpness. The effects that these differences have in the discernment of dietary groups in marsupials is discussed in detail further below.

DNE and OPCR—as well as RFI and OPCR—do not have colinear relationships in my marsupial sample, despite these measures all having been proposed as proxies of dental shearing efficiency (cf., Bunn et al., 2011; Evans and Janis, 2014; Evans et al., 2007; Winchester et al., 2014). This incongruent behavior among measurements purported to be signals of dietary behavior was also noted by Pampush et al. (2016b). I interpret this as a reflection of the enhanced ability of DNE, relative to RFI or OPCR, to capture the parts of the marsupial tooth that have the most mechanical efficiency during mastication—including cusps and crests—and, importantly, is sensitive to both the edge

length and relative "sharpness" of these features. OPCR on the other hand, does not directly account for either of these mechanically important features. This is not to say that OPCR is without merit, as recent studies have indicated that it can differentiate dietary groups in other mammalian clades, such as rodents (Evans et al., 2007), bats (Santana et al., 2011), and equids (Evans and Janis, 2014). However, studies of primate teeth incorporating OPCR (e.g., Bunn et al., 2011; Winchester et al., 2014; Ledogar et al., 2013) have found that OPCR does a generally poor job in consistently discerning dietary groups, whereas DNE consistently performs well. Given the gross similarity of the marsupial dentition to that of primates, it is then not surprising that I find similarly poor discernment of OPCR as a means of discriminating diets.

4.4.3 Differences Among Dietary Groups

As mentioned above, my results in marsupials generally indicate similar trends in dental topography as seen in the dietary groups of primates (Ledogar et al., 2013; Winchester et al., 2014). Namely, the teeth of species that have diets that are associated with tougher or more fibrous foods (e.g., leaves, browse, insects, etc.), have more prominent dental shearing features. Figure 34 illustrates the differences between dietary categories using 3D representations of tooth surfaces generated in R with the package "molaR." This serves as a useful illustration of the differences between dental topographies as they are measured here.

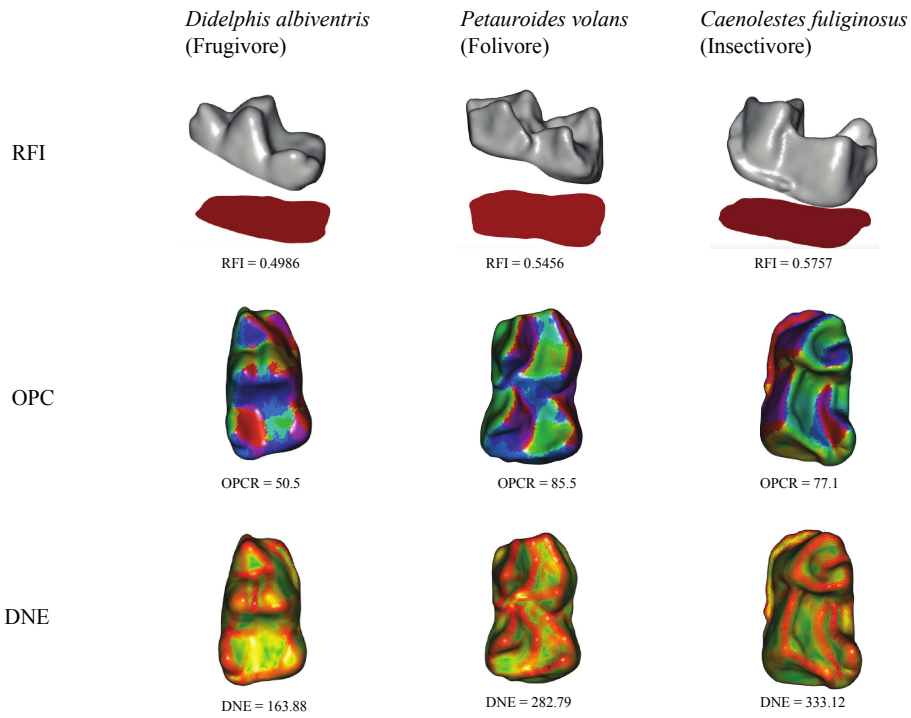

Figure 34: 3D surfaces of the M_2s of three species from three different dietary categoires. Images were produced using the *R* package "molaR". Images are not to scale.

4.4.3.1 OPCR

Overall, my results from OPCR indicate that it does not differ significantly amongst most of the dietary groups included in this study. In fact, only meat-eating carnivores differ significantly from any other dietary group in having consistently lower OPCR values (see Fig. 32), though the limited number of vertebrate-prey faunivores in this study (N=2) makes this result tentative. Nevertheless, this finding is consistent with the results of Evans et al. (2007), who found that in a sample of carnivorans and rodents, the more carnivorous the species, the more likely it was to have lower OPCR values.

Evans et al. (2007) interpreted this result as a reflection of the relatively high digestability of vertebrate tissue when compared to plant material or even chitinous insect exoskeletons, an argument that mirrors the study of Kay and Hylander (1978) which looked specifically at the shearing crests of primates and phalangeriform marsupials. Evans et al. (2007) reason that if the complexity of the tooth surface—as measured by the number of differently oriented patches—is seen as an adaptation to the mechanical stresses of the ingested food, then the greater the complexity, the greater the ability to break down fibrous materials. That my results show meat-eating carnivores have the least complex tooth surfaces is consistent with this observation.

Nevertheless, the similarity in OPCR scores of folivores and frugivores is a surprising result that is not in line with the supposed aim of the metric, nor with previous studies that have considered differences in tooth morphology between these dietary groups (e.g., Kay, 1975; Rosenberger, 1982; Kay and Covert, 1984; Anthony and Kay, 1993). Generally, fruit-bearing trees that are adapted for the consumption of their fruit as a means of seed dispersal through the consumer's feces, have soft pericarps with relatively few physical properties to hinder its processing and consumption, a fact that has been demonstrated many times in studies of food mechanical properties (Lucas and Luke, 1984; Kinsey and Norconk, 1990; Kunzek et al., 1999; Vogel et al., 2008; Berthaume, 2016). This in contrast to leaves, which serve as a plant's principal sites of photosynthesis and transpiration, and are vital to the plant's homeostasis. Thus, in order

to discourage predation, leaves typically have defense mechanisms that make their consumption difficult, or even dangerous, to the consumer. While over the course of evolution these defenses have taken a myriad of forms, of particular interest to studies of dental morphology is the toughness of leaves (e.g., Kay, 1975; Lucas and Pereira, 1990; Coley and Barone, 1996; Berthaume, 2016). This toughness is associated with more complicated occlusal surfaces in general (e.g., M'Kirera and Ungar, 2003; Lucas, 2004; Bunn and Ungar, 2009; Evans et al., 2007; Boyer, 2008; Winchester et al., 2014), and specifically with higher cusps and more prominent shearing crests (Kay and Hiiemae, 1974; Rosenberger and Kinzey, 1976; Kay, 1977; Teaford and Ungar, 2006; Winchester et al., 2014). Nevertheless, my results from marsupials—in combination with results from primates (Ledogar et al., 2013; Winchester et al., 2014)—make it clear that OPCR is unable to consistently pick up these visually obvious differences in tooth shape. It is possible that my use of dietary categories based on food types rather than food mechanical properties is at fault for this lack of correlation, as undoubtedly there is overlap between the material properties of certain kinds of fruits and leaves (Strait, 1997; Berthaume, 2016). Unfortunately, the testing of food material properties for such a broad taxonomic sample is beyond the scope of this paper.

4.4.3.2 RFI

Similar to OPCR, my results indicate that diet (as I categorize it) does not have a statistically significant relationship with RFI in a non-phylogenetically-corrected

analysis. However, the results from my phylogenetically-corrected ANOVA indicate that this effect approaches significance ($p = 0.0495$, compared to the Bonferroni-corrected alpha value of 0.019), and suggests that RFI and diet are related in my broad taxonomic sample. This is consistent with other studies incorporating RFI that have used broad taxonomic samples (Boyer, 2008; Winchester et al., 2014).

RFI is a particularly valuable metric for understanding differences in dental topography for two reasons: 1) given that it is a simple ratio of the 3D surface area to the 2D planometric area, it is easy to visualize and comprehend; and 2) due to its coarse nature of measurement, it is relatively insensitive to the minor defects on a surface that can affect the measurement of OPCR or DNE (Boyer, 2008; Evans et al., 2007; Spradley et al., 2017). These defects can be caused by taphonomic processes (Boyer, 2008), tooth wear (Boyer, 2008; Pampush et al., 2016b), or noise introduced by the scanning process (Spradley et al., 2017). However, for these same reasons, RFI may be have less utility in detecting finer-scale differences in tooth surface morphology that are more likely captured by metrics such as OPCR or DNE. This problem can manifest in a sample such as this one, where many of the species could very well be described as generally 'omnivorous' (though with specific dietary tendencies). The topographic features that may separate teeth by these preferences, such as sharpness or complexity, will likely not be captured by RFI.

The coarse nature of RFI likely explains the significant but weak relationship RFI has with diet in my results. While my frugivore and insectivore categories were significantly different from one another, no other pair was significantly different when incorporating Bonferonni correction for the alpha level. Unlike DNE (discussed below), there is considerable overlap between the frugivores and folivores in my sample, which is likely indicative of the fact that many marsupial frugivores consume leaves and vice versa (Kay and Hylander, 1978), and that the differences in dental topography are more likely to be captured in the qualities of the features rather than by their presence or absence.

Visual inspection of some of the tooth surfaces in my sample (Fig. 35) show the similarity of tooth surfaces within a specific marsupial clade, Didelphidae. The American didelphids show very similar gross tooth morphology despite diversity in dietary preference. This similarity confounds the signal within RFI, but these surfaces can be differentiated by DNE.

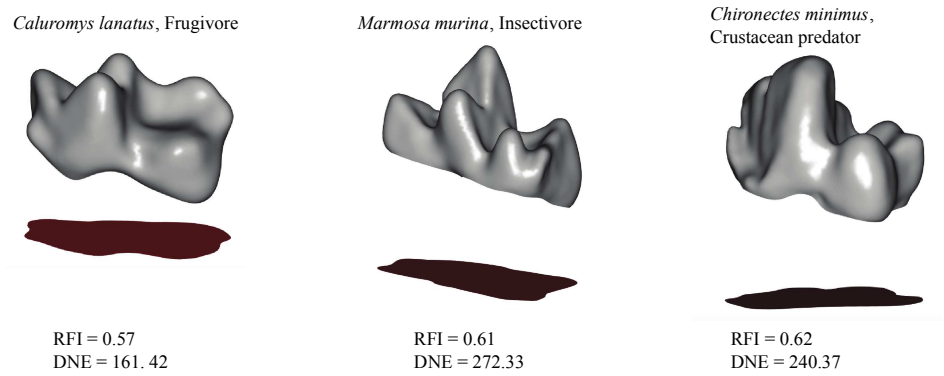

Figure 35: 3D surfaces of three didelphid marsupials with corresponding RFI and DNE values. Note that the RFI values are roughly equivalent while the DNE values show differentiation.

Finally, the combined browser/folivore category may be masking an RFI signal that exists between arboreal and terrestrial browsers. A Student's t-test between the means of RFI for arboreal folivores and terrestrial browsers (Figure 36) suggest that the difference between these two groups is likely present, though I fail to find a statistically significant difference ($p = 0.069$). This result is similar to Williams and Kay (2001), which found that hypsodonty index (Van Valen, 1960; Janis, 1988)—a measure inherently related to RFI (Boyer, 2008)—was higher in terrestrial rodent species relative to arboreal species when controlling for diet. This is likely related to the fact that terrestrial species are more likely to encounter exogenous grit in the form of dust silica (Janis, 1988; Fortelius, 1985; Hummel et al., 2011), though other studies have shown that arboreal species are not immune to the effects of dust in the trees (Ungar et al., 1995; Spradley et al., 2016). This siliceous grit wears down teeth (Janis, 1988) and higher relief can be

viewed as an adaptation to prolong the functional life of the tooth in the presence of such high rates of wear (Williams and Kay, 2011). Though I do not find an especially strong signal, this would likely explain the difference I do see between arboreal folivores and terrestrial browsers.

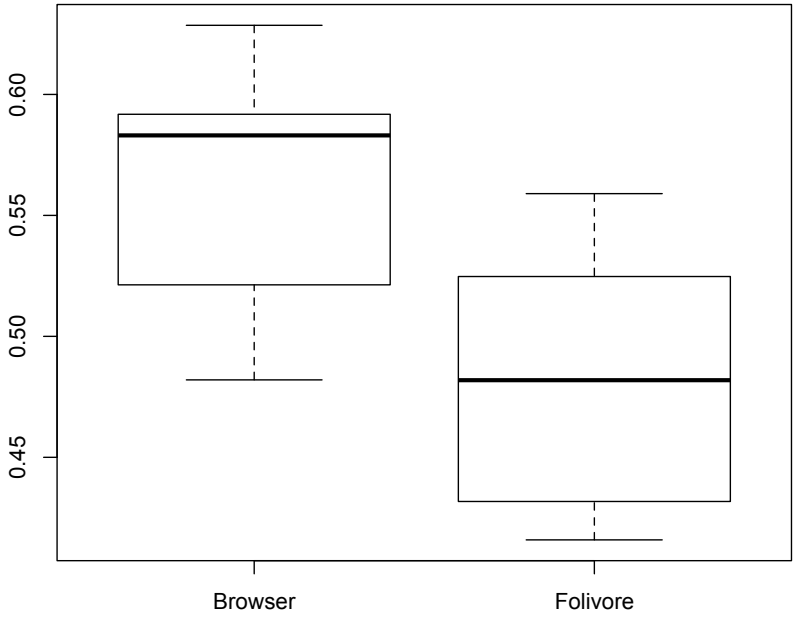

Figure 36: Quantile plots representing the RFI values of the arboreal folivores and terrestrial browsers in my sample, demonstrating the difference between the two groups (p = 0.069).

4.4.3.3 DNE

In my results, DNE stands out as the most effective discriminator of dietary categories using molars. This mirrors the results of similar studies that have incorporated all three dental topography metrics in primate clades (Ledogar et al., 2013;

Winchester et al., 2014), which also found DNE to be the most effective. The importance of shearing (or sharp) features on the marsupial dentition in discriminating dietary categories was also noted by Kay and Hylander (1978), who focused on a sample of phalangeroid marsupials as well as examples from various primate clades. Using multivariate analysis, they found that folivorous primate species were more distinctly differentiated from frugivorous species based on shearing and cusp height than were phalangeroid marsupials. They noted that that many phalangeroid marsupials also had a greater amount of shearing in the premolars—often manifested as a serrated blade-like lower premolar—that may amount to lesser shearing demand placed on the molars. Nevertheless, the shearing of their phalangeroid sample had a clear relationship with dietary preference.

Expanding this analysis to include a much broader array of marsupial species and diets, as I have here, we see that this pattern largely holds. Insectivorous species, like South American *Caenolestes fuliginosus* or Australian *Sminthopsis crassicaudata*, have some of the highest DNE values in my sample, likely reflecting the tough chitinous exoskeletons of the insects they consume. The high degree of overlap between insectivorous and browsing/folivorous species is in agreement with other studies that have shown that shearing/sharpness is generally equivalent between folivorous and insectivorous primates (e.g. Kay, 1975; Winchester et al., 2014).

4.4.3.4 Dental Topography Metrics as Predictors of Diet

Ultimately, a major goal of this study is to demonstrate whether dental topography metrics can be used reliably as proxies for dietary ecology and then applied to the study of extinct species and faunas. A discriminant function analyses (DFAs) were used to examine this premise. Several different models were created using different combinations of metrics. A DFA model using all three topographic measurements, and the natural log of molar area, resulted in individual specimens being successfully categorized by diet 74.6% of the time. Molar area is a useful way of distinguishing high-crowned sharp-crested insectivores and folivores, as Kay (1975) demonstrated a lower limit for folivore body size (circa 500g).

This result is less accurate than a similar model used by Winchester et al. (2014), which reported a success rate of 93% when combining DNE, RFI, OPCR, and M_2 area in a sample of platyrrhines. However, when they ran the same model for their total data set, including both platyrrhine and strepsirrhine primates—a more taxonomically diverse sample that approaches what I present here—this accuracy drops to 77%, much more in line my results.

4.4.4 Ecometric Distributions

4.4.4.1 Ecometric Means

The mean value of an ecomorphological feature across a community of taxa has been shown to be a useful proxy of community ecology. This is particularly true when

the relationship between the morphology and ecology is known, allowing for an interpretation between the average value of the ecomorphological measurement and the preponderance of any given ecology within a community. A classic example of this is the average value of hypsodonty with a community of ungulate or rodent mammals. Higher tooth crowns have been demonstrated to be positively correlated with increased amounts of grazing in these mammalian clades (Janis, 1988; Williams and Kay, 2001). In the context of an ecometric distribution, a higher mean hypsodonty value in a community of mammals would suggest a higher relative proportion of grazing mammals in that community. Indeed, the mean hypsodonty has been demonstrated to correlate with drier, more seasonal environments (Williams and Kay, 2001; Madden, 2014).

Interestingly, only the means of DNE and RFI have significant relationships with any of the bioclimatic variables, and both metrics correlate significantly with the same three variables—MAP, temperature seasonality, and canopy height (Tables 17; Figure 33). Both DNE and RFI have positive relationships with temperature seasonality and negative relationships with MAP and canopy height. In this context, and in light of my results from Chapter 2, this would suggest a greater number of frugivores—lower RFI and DNE (Figure 32)—in wetter, less seasonal environments with taller canopies. This is not only consistent with the results from Chapter 2, but also with results of other qualitative analyses of mammalian faunas (Andrews et al., 1979; Kay and Cartmill, 1997;

Kay et al., 1997; Kay et al., 2012). Given the weak discriminatory power of OPCR amongst my dietary categories (Figure 32), it is not surprising that I find no significant results of OPCR means and climate/habitat.

4.4.4.2 Ecometric Coefficients of Variation

While the means of RFI and DNE may suggest a preponderance of one ecological niche relative to another, they do not give us a sense of the total distribution of ecologies present in a locality. To this end, the coefficients of variation (CoV)—which give us a sense of the spread and shape of the distribution that is independent of the mean—are more appropriate. In an ecological context, a greater CoV would suggest a greater ecological disparity amongst the species present, i.e. a greater number of specialists relative to generalists. Following the logic of previously published ecological studies, since the evolution of specialist adaptations is thought to be more likely in stable environmental conditions (Potts, 1996; Genin and Perret, 2003; Kassen, 2002; Colles et al., 2009), we would expect that less variable environments should have more specialists, which would increase disparity, and thus result in higher CoV.

The CoV for RFI has a significant negative correlation ($p < 0.019$) with MAP and canopy height, and a positive correlation with temperature seasonality (Table 18, Figure 37). In other words, as the precipitation and canopy height of a locality increase, the disparity of RFI values decrease (Figure 38). Likewise, as temperature seasonality increases, the disparity of RFI increases. This could presumably be due to increasing

species richness, with a greater absolute number of species causing the distribution to become tighter. However, as can be seen in a plot of RFI CoV and species richness (Figure 39), this is not the case.

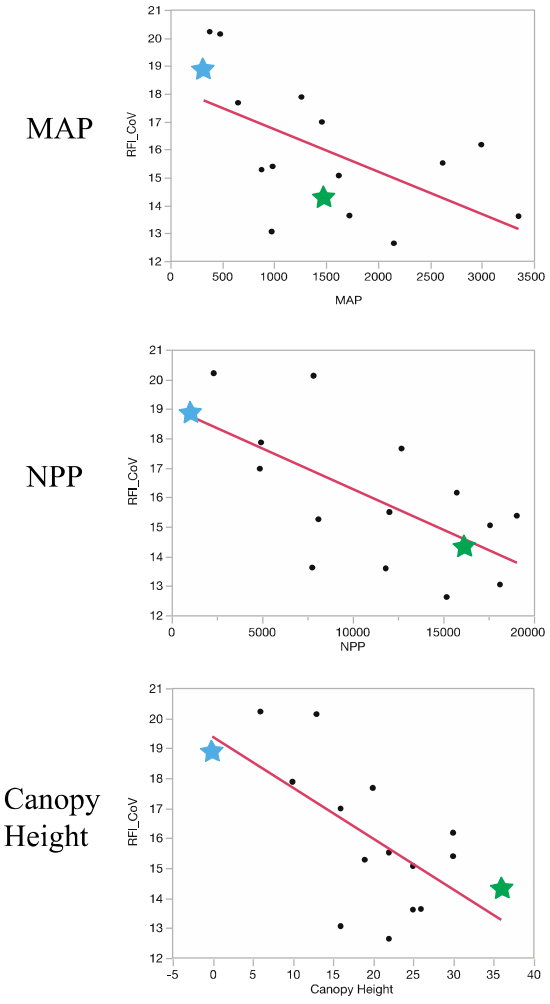

Figure 37: Bivariate plots of the coefficient of variations of distributions of RFI against MAP, NPP, and canopy height. R^2 and p values of the linear fits are presented in each plot. The distributions of the localities represented by the green and blue stars in the RFI plot (bottom) are illustrated in Figure 38.

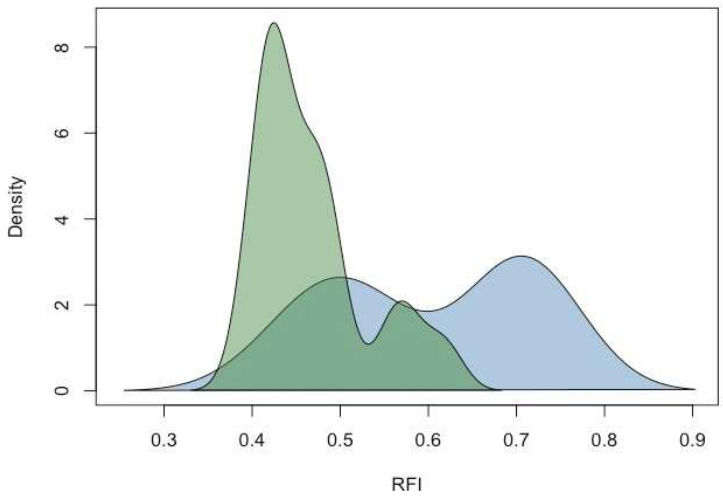

Figure 38: Densities plots of RFI in two localities. The green curve represents the South Karius field site in Papua New Guinea, the blue curve represents the Uluru-Kata Tjuta National Park. The standard deviation of the green curve is less than that of the blue curve (see Figure 37).

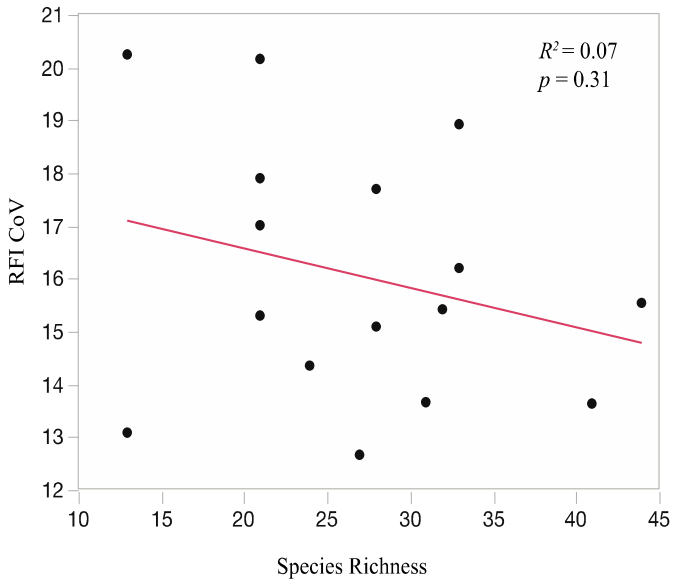

Figure 39: Bivariate plot of RFI CoV and species richness. The R^2 and p-value demonstrate the weakness of this relationship, suggesting that species richness is not driving disparity in RFI across localities.

Instead this suggests that the relative number of species with values of RFI typical for folivores/frugivores (~0.4 - 0.5) is greater in wetter, more arboreal environments. Once again, this conforms to previously published results of qualitative community-level analyses (Kay and Cartmill, 1979; Kay et al., 2012). On the other hand, it directly contradicts my prediction regarding the relative number of specialists versus generalists in relation to environmental variation. There are two possibilities as to why this might be the case. First, dietary specialization (or generalization) is a complex idea, and is not necessarily defined by the presence or absence of highly derived quantifiable attributes (Futuyma and Moreno, 1988). A specialist may not be associated with an atypical morphology, it may simply have a narrow niche (Futuyma and Moreno, 1988; Colles et al., 2009). In this light, by using RFI (or any other ecometric), I am not actually capturing any meaningful signal as to the true number of specialists. The second possibility is that the number of specialists is not actually dependent on stable environments. While this contradicts much of the previously published research, there is evidence of specialist behaviors associated with the scarce season in hypervariable habitats, including gumnivory in cheriogaleid primates (Genin et al., 2010), tool use in primates (Yamakoshi, 1998; Spagnoletti et al., 2012), and prey choice in frogs (Toft, 1980) and birds (Karr, 1976). While these are typically referred to as "fallback" behaviors (Marshall and Wrangham, 2007) because they are only used in times of resource scarcity,

they may nonetheless produce unusual morphologies, driving the disparity of my distributions and increasing the CoV.

Interestingly, I do not find significant results in the context of DNE. This is surprising given that in my ecomorphological analyses above, DNE demonstrates the strongest correlation with diet (Table 13). However, the CoV of DNE does not have a significant correlation with any of my bioclimatic variables, and in fact does not even have correlation that might be described as "approaching" significance ($p < 0.10$).

Finally, the CoV of OPCR does not have a significant correlation with climate/habitat. Considering that OPCR does not have a clear relationship with diet in my marsupial sample, I would expect the that the distributions of OPCR would not elucidate any particularly informative content related to the relative proportions of ecologies in a fauna. Instead, what I find is a fairly consistent pattern of roughly equivalent CoVs across different habitats, confirming my expectations.

4.4.4.3 Ecometric Skew

Related to CoV, I can also look at the skewness of my distributions across localities. In its most general definition, skewness is a measure of the asymmetry of a distribution, i.e. the length of the "tail" of a distribution. In an ecological context skewness can intuitively be thought of as the presence of specialists, i.e. species with a narrow niche breadth when compared to other species (Colles et al., 2009). While the skew of a distribution (of DNE, RFI, OPCR, etc.) is unlikely to give us a complete picture

of the total number of specialists in an environment—after all, median values of RFI and DNE do not necessarily exclude the possibility that the species is a specialist (e.g. the koala, a specialist of eucalyptus leaves)—it nevertheless may be informative as an indicator of relative numbers of distinct dietary specializations. In the context of my dietary ecology study, I would expect that more seasonal, less productive environments should have a negative skew—that is, a higher mean value of both RFI and DNE with a longer tail to the left of the distribution, suggesting fewer low-crowned, rounded cusped molars—than wetter, more productive, aseasonal environments.

Results for RFI match these predictions (Table 19). Positive skew (i.e. a longer tail to the right) is associated with wetter and more arboreal habitats, while negative skew is associated with drier, more seasonal environments. RFI skew appears to have a non-linear relationship with NPP (Figure 40), with the skew approaching zero at the localities with the highest NPP in my sample. Similar to the results from CoV, DNE skew fails to show significant correlations with any climatic/habitat variables (Table 19). Likewise, OPCR skew fails to show any statistically significant correlations with environmental variables.

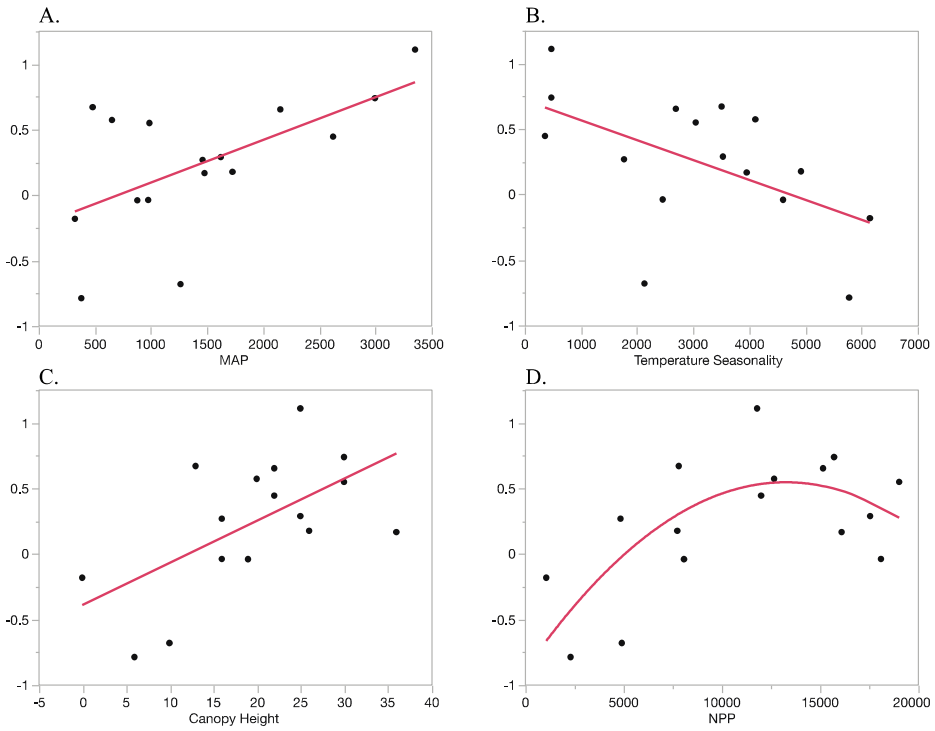

Figure 40: Bivariate plots of RFI skew (y-axis) and four climatic/habitat variables. The variables are as follows: A) MAP; B) Temperature seasonality; C) Canopy height; D) NPP.

4.4.4.4 Using Marsupial Ecometric Distributions as Environmental Proxies

After correlating the distribution statistics, I find distributions of RFI to have the most consistent association with my climatic/habitat variables (Table 17-19). This is not surprising, given the demonstrated relationship of RFI to dietary ecology (see above, as well as Boyer, 2008; Ledogar et al., 2013; Winchester et al., 2014), and my results from Chapter 2 showing that dietary ecologies do have significant correlations with climate and habitat in Australia/New Guinea. It also lends credibility to the potential of ecometric distributions to be used as climatic proxies in the fossil record. Removing the need to reconstruct the ecology of each species/genus has the potential to make

community-level paleoecological analyses more broadly applicable and quicker to perform. The mean, CoV, and skew work best for predicting climatic/habitat variables, whereas the range does not correlate well with any of these variables.

The lack of significant correlations amongst the summary statistics of DNE distribution is surprising. DNE apparently has a significant relationship with dietary ecology in marsupials (see above), but unlike RFI this does not seem to translate into distributions that reflect the results from Chapter 2. Looking at three DNE and RFI density plots from localities of differing amounts of rainfall (Figure 41), we see that the differences in the shape of these distributions, while present, is more subtle than what we see in RFI. This slight tendency towards similarity in DNE distributions is likely the reason I do not find significant correlations. It is possible that more complete sampling of the marsupial faunas at these localities may make these correlations significant.

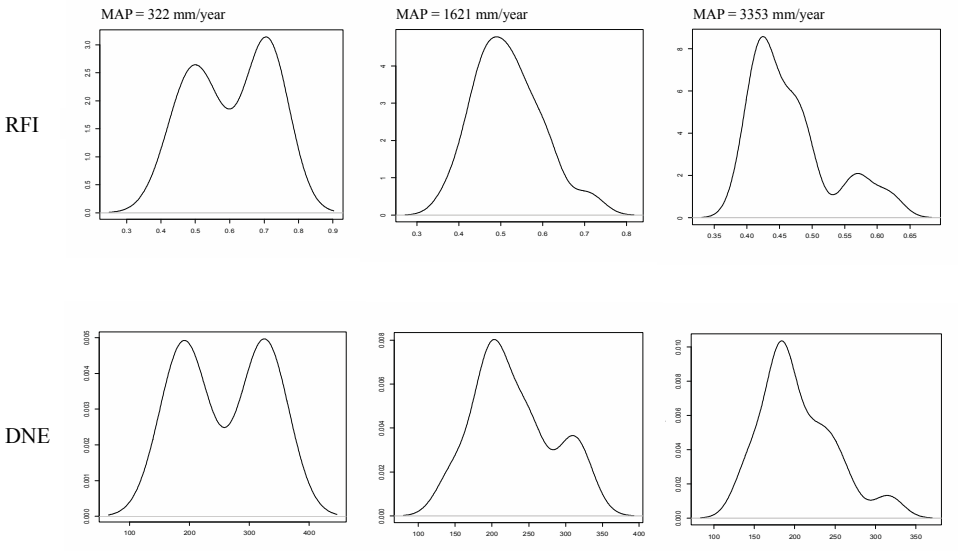

Figure 41: Density plots of RFI and DNE from three different localities, with associated MAP values for each. The localities are as follows: left – Ulura-Kata Tjuta; middle – Croajingolong; right – South Karius.

4.5 Conclusions

Beginning with a sample of both (South?) American and Australian/New Guinean marsupials, I demonstrate here using phylogenetically-corrected ANOVA tests that dental topography metrics can be used to reliably predict or reconstruct general dietary ecology in this clade. These results can be summarized in the following:

1. DNE, a measure of surface sharpness, demonstrates the strongest dietary signal in my data, with frugivores having consistently lower DNE values than either browsers/folivores or insectivores.

2. RFI, or surface relief, also shows a statistically significant relationship with diet. Lower relief is associated with frugivores, while browsers/folivores and insectivores have higher relief.
3. OPCR, a measurement of surface complexity, does not correlate well with diet, and amongst the dietary categories included in my study only significantly differentiates faunivores specializing in vertebrate prey from other dietary groups.

A discriminant function analysis performed using all three metrics, in combination with the natural log of molar area, resulted in individual specimens being correctly segregated by dietary group at a rate significantly better than random chance (~75%).

Having demonstrated the utility of these metrics in reconstructing individual species' dietary ecologies, I also explored the utility of the distributions of these metrics within a locality as a proxy for a number of climatic and habitat variables at that locality. Four summary statistic of distributions were used: mean, range, coefficient of variation, and skew. Climatic and habitat variables included precipitation, temperature, seasonality, productivity, and canopy height. My results from theses correlation analyses are summarized as follows:

1. The means of RFI and DNE both have statistically significant correlations with precipitation (negative correlation), temperature seasonality (positive),

and canopy height (negative). The mean of OPCR does not have a significant correlation with any variable.

2. The range of RFI, DNE, and OPCR does not correlate well with any climatic/habitat variable.
3. The coefficient of variation for RFI has significant correlation with precipitation, temperature seasonality, and canopy height. The same is not true for the coefficient of variation for DNE or OPCR.
4. Positive skew in RFI was associated with wetter, more productive habitats with greater canopy height, and negative skew was associated with drier, more seasonal climates.

In conclusion, dental topography metrics demonstrate potential to not only distinguish diet in disparate taxa, but their distributions may have some utility as proxies for climate and habitat in paleoecological reconstructions. This may eliminate the need to make often problematic assumptions about diet in fossil taxa.

5. Dental Topography in South American Rodents: Proxies for Dietary Ecology and Environmental Reconstruction

5.1 Introduction

Living rodents represent the most speciose order of mammals on the planet, with 2277 recognized species—over 40% of all recognized mammal species (Wilson and Reeder, 2005)—and can be found on every continent except Antarctica. They occupy every terrestrial habitat (Kay and Hoekstra, 2008) and span a wide range of ecological niches. The largest living rodent, the South American capybara (*Hydrochoerus* spp.) can weigh up to 65kg—the largest fossil rodent, *Josephoartigasia monesi* from Uruguay weighed approximately 1000kg—while the smallest, the pygmy mouse (*Mus minutoides*) is a mere 7g (Hautier and Cox, 2015; Kay and Hoekstra, 2008). So successful were the early rodents, that after their initial appearance in the fossil record of Laurasia at the end of the Paleocene (55-60mya) (Meng et al., 1994; Kay and Hoekstra, 2008), they could already be found on every continent except Australia and Antarctica by the mid-Eocene (Antoine et al., 2011). They would later be one of the few terrestrial mammalian clades to cross "Wallace's Line" into Australia without the aid of introduction by human colonists, at approximately 10 Mya (Rowe et al., 2008).

This rapid radiation and diversification has since led to their near ubiquity in terrestrial mammalian fossil localities from the Cenozoic (Kay and Hoekstra, 2008). This has fostered intense interest in rodents as a potential source of evidence for the reconstruction of past climates and environments (Montuire et al., 1997; Aguilar et al.,

1999; Legendre et al., 2005; Montuire et al., 2006). These efforts have primarily focused on species richness within specific living rodent families with known climatic distributions. Clade-specific species richness can be estimated for fossil sites and climate reconstructions are done using a regressive model derived from modern clade distributions. While such an approach has proven effective in reconstructing Quarternary period climates (Montuire et al., 2006), they are limited in their scope for two reasons. First, sympatric species identification in the fossil record is inherently difficult, especially for a diverse small mammal clade like the rodents (Gingerich, 1974), making estimates species richness circumspect. Second, such studies are limited both spatially and temporally by the families that are chosen for the analyses. In this study, I seek to broaden the applicability of these types of analyses by using the distribution of ecomorphology in rodent dentitions from a continent-wide sample of rodent communities.

5.1.1 Rodent Dental Ecomorphology

Prior to analyzing the rodent ecometric distributions in relation to environments—as I did for marsupials in Chapter 4—it first must be demonstrated that the metrics of interest are functionally related to the species' ecologies. Since the rodent fossil record is largely represented by jaws and isolated teeth, the dentition (feeding ecology) will once again be my study focus. Rodent molar morphology is highly derived and unlike that of the primitive therian tribosphenic molar pattern. Further, the clade

spans a wide range in dietary ecologies (Hillson, 1986). Many taxa have complicated series of cusps, lophs, and ridges aligned buccolingually, so that when the jaw is moved back and forth these ridges of enamel cut against one another (Hillson, 1986). Due to the wide diversity of rodent molars, broad-scale analyses of dental ecomorphology in rodents has been limited to just a few studies (Williams and Kay, 2001; Evans et al., 2007; Samuels, 2009; Croft et al., 2011), and two of these studied focused solely on linear measurements of the incisors (Samuels, 2009; Croft et al., 2011)—though Samuels (2009) also included a broader analysis of skull morphology as it relates to dietary ecology. Most taxonomically-broad studies of rodent molar morphology have instead focused on the distinguishing characteristics of molars in determining taxonomic placement or phylogenetic relationships (Tullberg 1899; Simpson, 1945; Schaub, 1958; Wood, 1965; Lazzari et al., 2008a; Lazzari et al., 2008b; Vucetich et al., 2015). In this study, I will instead try to correlate dietary ecology with molar morphology by using the same dental topography metrics from Chapter 4; DNE, RFI, and OPCR. The methodological descriptions of these metrics have been presented in detail in previous chapters (number them here).

Some previously published literature suggests that these dental topographic metrics may be informative for rodent occlusal surfaces. The utility of OPC, a measure of dental complexity, was originally demonstrated with an analysis of rodents (as well as carnivorans) (Evans et al., 2007; Evans and Jernvall, 2009). In their results, Evans et al.

(2007) demonstrated that complexity values increase for entire cheek-tooth rows with increasing herbivory. This was interpreted as an increased ability of the tooth row to break down high-fiber plant materials. Having also demonstrated the same pattern within carnivorans, Evans et al. (2007) claim that these disparate morphologies are subject to the same functional constraints. By expanding on their analysis with more dental topography metrics as well as a broader taxonomic sample of rodents (Evans et al. used only muroids, the rats and mice), I seek to explore whether such functional constraints apply to individual teeth within the tooth row, and if there are other functional constraints beyond just surface complexity.

Surface relief has also been studied in rodents, at least to the extent that relative surface relief can be equated with relative hypsodonty (Boyer, 2008). Hypsodonty, or high-crowned teeth, has been hypothesized as an adaptation to prolong the functional life of the tooth when the physical properties of the food ingested (Fortelius, 1985; Janis 1988) or exogenous grit in the environment (Ungar et al., 1995; Fortelius and Solounias, 2000; Lucas et al., 2013) subjects the organism to intense tooth wear. Williams and Kay (2001) present correlations between hypsodonty, diet, and substrate preference in a taxonomically-broad sample of South American rodents (not unlike the sample I use in this study). Their results suggest that hyposdonty and diet are significantly correlated, specifically that hypsodonty was positively correlated with abrasive diets. This pattern

has also been observed in ungulates (Janis, 1988; Williams and Kay, 2001; Lucas et al., 2013).

Studies of molar sharpness (analogous to DNE) in rodents have been limited. Black (1963) differentiated North American squirrels on the basis of sharpness of their molar lophs—as well as their relative hypsodonty—and concluded that tree squirrels generally have more rounded features than do ground squirrels. This was interpreted by Black (1963) to reflect the high amounts of grass that is consumed by ground squirrels relative to arboreal and scansorial sciurids. Prufrock et al. (2016) also included some extinct taxa of rodents—ischyromyids, which presumably resembled modern squirrels (Korth, 1994)—and measured DNE on the M^2. In these ischyromyid species, DNE values were relatively low, approximately the same as frugivorous platyrrhine primates from the dataset of Winchester et al. (2014). However, Prufrock et al. (2016) did not include any comparative dataset of living squirrels with known ecologies, so the precise relationship between DNE and diet in sciurids remains speculative.

Combining the above information into a coherent set of predictions for my own data set, I lean towards the hypothesis of Evans and Sanson (2003), namely that functional constraints on the mammalian dentition result in shape similarities that are ideal for the processing of certain food materials, despite differences in historical or developmental constraints (Gould, 1989). In this context, I would expect my results from the rodent sample to mirror those from the marsupial sample in Chapter 4; more

abrasive, tougher (high fiber) diets such as grass, leaves, or insects should correlate with higher values of complexity, relief, and sharpness. Likewise, I expect that frugivorous species, such as some of the South American pacas (Myoprocta), should have the lowest values of all three metrics, since frugivory is associated with less exaggerated surface features (Kay, 1975; Winchester et al., 2014; Chapter 4 of this dissertation). There are also a large number of rodent species that can be described as "seed-predators." The difficulty of this category in the context of predicting dental morphology is that the mechanical properties of seeds are variable, ranging from hard and brittle (Agrawal et al. 1997; Lucas, 2004) to tough and crush resistant (Ayres, 1989; Kinzey and Norconk, 1993; Norconk and Veres, 2011). In other words, while bite force is likely high regardless of the type of seed, the amount of chewing effort will differ significantly between those seeds that are more likely to propagate a crack versus those that resist cracking (Lucas, 2004). This difference in chewing effort is likely to be reflected in the dental morphology, though without proper data as to what rodents are eating what types of seeds, it is impossible to differentiate amongst them. Therefore, I include the seed predators in amongst the "plant-dominated omnivores" in my sample.

I limit this analysis to South American rodents, as the diversity and morphological disparity of rodents is higher in South America than it is on any other continent, and rodents have made up an important constituent of South American mammalian faunas since the Oligocene (Vucetich et al., 2015). Living South American

rodents comprise three clades; the caviomorphs, the sigmodontines, and the sciurids. Of these three groups, the molecular (Poux et al., 2006) and fossil evidence (Vucetich et al., 2015) suggest that only the caviomorphs reached South America before the joining of North and South America via the Panamanian isthmus—though genetic data indicate that the ancestors of at least one genus of Amazonian squirrel, *Sciurillus*, may have made it to the continent before this event (Mercer and Roth, 2003). The sciurids and the sigmodontines on the other hand made it to South America only (relatively) recently, with the latter group subsequently radiating into almost 400 species in the course of approximately 5 million years (Engel et al., 1998; Smith and Patton, 1999). Comparing this to the caviomorphs, of which there are *only* 240 species found in South America today (Upham and Patterson, 2015), it is clear that evolutionary history may have played an important role in the morphological disparity of different clades of rodents. To account for these potential differences, I make phylogenetic corrections in my analyses as well as perform separate analyses on both caviomorphs and the non-caviomorphs (sciurids and sigmodontines).

5.1.1 Rodent Ecometric Distributions as an Environmental Proxy

As mentioned above, a major objective of this study is to explore the potential of rodent ecometrics as proxies for climate and habitat in the fossil record. Given their ubiquity after their appearance in the Eocene, rodents have tremendous potential in this respect. Beyond the studies discussed above, Kay et al. (1999) also observed that the

percentage of sigmodontine rodents that could be classified as hypsodont increased with temperature seasonality and decreased with rainfall and higher average temperatures. While the mechanisms that drive these distributions will not necessarily be addressed directly in this paper, I seek to test, refine, and expand on the brief analysis of Kay et al. (1999) to include more ecometrics, more climatic variables, and more detailed statistics of distributions. I predict that ecometrics that reflect more abrasive diets in the first part of this paper (if such results are found) should have a greater impact on the distributions in more arid, more seasonal, and less productive habitats. Much like in Chapter 4, summary statistics of distributions—mean, range, skew, and coefficient of variation—will be regressed against climatic and habitat variables across the South American localities. The utility and possible ecological interpretations of results are discussed in Chapter 4 as well as in the discussion of this paper.

In addition, I seek to include the same regression techniques in Chapter 2, including multivariate linear regression and the machine-learning algorithms; regression trees, random forests, and Gaussian process regression. Rather than the using the ecological indices as my predictor variables, I will include the aforementioned distribution statistics as predictors (with the bioclimatic variables being the response variables which I am trying to estimate). This last section will thus represent multiple parts of this dissertation in a single analysis, and will give us some notion of how well

the use of modern techniques in both data collection and model production can improve the accuracy of paleoenvironmental reconstruction.

5.2 Materials and Methods

5.2.1 Topography and Dietary Ecology

To investigate the relationship between dental topography and dietary ecology in South American rodents, I scanned and segmented the lower M_2s of 80 individual specimens representing 59 different South American rodent species (35 genera) (Table 20), including both caviomorph and sigmodontine species. Specimens were obtained from the National Museum of Natural History (NMNH), the Louisiana State University Museum of Natural History (LSUMZ), and the University of Florida Museum of Natural History (FLMNH), and include both skeletal material and epoxy casts poured from molds taken from skulls. A subset of dentitions were both directly scanned, and casted to assess the accuracy of surface reconstructions from casts. The complete sample of species, along with a phylogenetic tree topology, is presented in Figure 42. Primary dietary categories were assigned to each species according to MammalDIET, an online archive of dietary information (Kissling et al., 2014), and supplemented with primary sources (Patton et al., 2015). These sources are summarized along with those from the marsupial sample in Appendix C. These dietary categories are necessarily low resolution, and the consequences of this low resolution is further elaborated upon in the discussion. In this study I recognize five different dietary categories: frugivore, folivore,

grazers, plant dominated omnivores—including putative fungivorous and gramnivorous species—and animal dominated omnivores, including insectivores (Evans et al., 2007). Species classified in the latter two categories inhabit very broad dietary niches, but can be distinguished by the relative amounts of insects in the diets (Evans et al., 2007). An ANOVA test separating the identified seed-predators in my sample from the other species considered "plant-dominted omnivores" (PDO) suggests that the differences between the means of these two groups is not significant for DNE ($p = 0.77$), RFI ($p = 0.51$), or OPCR ($p = 0.60$). Therefore, seed-predators were left in the PDO category for further analyses.

Table 20: Means of DNE, RFI, OPCR, and M_2 area for every species included in this study.

Family	Species	N	Diet	DNE	RFI	OPCR	M_2 Area
Cricetidae	*Abrothrix jelskii*	1	PDO	148.55	0.54	119.00	3.01
Cricetidae	*Akodon aerosus*	2	PDO	134.84	0.39	87.00	0.82
Cricetidae	*Akodon mollis*	1	PDO	195.28	0.61	78.38	2.29
Cricetidae	*Akodon orophilus*	1	PDO	139.46	0.41	96.88	2.55
Cricetidae	*Akodon subfuscus*	1	PDO	153.14	0.52	79.00	1.92
Cricetidae	*Akodon torques*	1	PDO	192.54	0.57	112.38	2.68
Caviidae	*Cavia tschudii*	2	Grass	477.99	0.69	160.19	11.42
Echimyidae	*Clyomys laticeps*	1	PDO	307.13	0.58	151.62	13.66
Erethizontidae	*Coendou prehensilis*	2	Folivore	284.94	0.41	274.75	35.34
Erethizontidae	*Coendou rothschildi*	1	Folivore	311.02	0.54	120.12	32.73
Cuniculidae	*Cuniculus paca*	1	Frugivore	270.74	0.59	202.88	54.81
Echimyidae	*Dactylomys dactylinus*	2	Folivore	567.73	0.43	175.31	31.68
Dasyproctidae	*Dasyprocta fuliginosa*	2	Frugivore	377.23	0.61	215.00	25.50
Dasyproctidae	*Dasyprocta punctata*	2	Frugivore	305.90	0.57	202.75	41.50
Echimyidae	*Diplomys labilis*	1	Frugivore	517.14	0.54	165.75	12.84
Caviidae	*Dolichotis salinicola*	1	Grass	252.55	0.71	113.50	12.04
Caviidae	*Galea musteloides*	2	Grass	303.83	0.64	174.38	12.28

Caviidae	*Galea spixii*	2	Grass	303.03	0.67	108.56	12.52
Heteromyidae	*Heteromys anomalus*	2	PDO	284.58	0.64	191.56	2.78
Cricetidae	*Holochilus brasiliensis*	1	PDO	255.11	0.43	133.25	4.69
Echimyidae	*Hoplomys gymnurus*	2	Frugivore	322.27	0.51	213.57	13.11
Cricetidae	*Ichthyomys hydrobates*	1	ADO	138.00	0.49	66.00	1.62
Cricetidae	*Kunsia tomentosus*	1	ADO	330.09	0.60	171.25	6.74
Chinchillidae	*Lagidium peruanum*	1	Grass	455.96	0.73	163.38	32.90
Echimyidae	*Makalata didelphoides*	2	Frugivore	310.06	0.70	188.38	7.89
Echimyidae	*Mesomys hispidus*	1	PDO	245.22	0.51	247.62	8.08
Sciuridae	*Microsciurus flaviventer*	1	ADO	108.16	0.44	72.50	2.87
Dasyproctidae	*Myoprocta acouchy*	1	PDO	234.42	0.55	157.12	22.75
Cricetidae	*Neacomys spinosus*	2	PDO	179.97	0.45	95.38	1.58
Cricetidae	*Nectomys squamipes*	1	ADO	278.42	0.50	155.25	4.26
Cricetidae	*Oecomys superans*	1	PDO	203.81	0.44	135.00	2.01
Cricetidae	*Oligoryzomys arenalis*	1	ADO	108.15	0.40	91.25	2.43
Cricetidae	*Oligoryzomys chacoensis*	1	ADO	146.21	0.43	137.50	1.05
Cricetidae	*Oligoryzomys destructor*	1	ADO	119.66	0.46	77.62	1.10
Cricetidae	*Oligoryzomys fulvescens*	2	ADO	180.94	0.50	109.32	1.80
Cricetidae	*Oligoryzomys microtis*	1	ADO	125.14	0.58	79.25	1.52
Cricetidae	*Oryzomys albigularis*	1	ADO	228.90	0.42	159.75	2.59
Cricetidae	*Oryzomys auriventer*	1	PDO	181.86	0.45	208.50	6.33
Cricetidae	*Oryzomys keaysi*	1	ADO	241.87	0.43	201.38	4.80
Cricetidae	*Oryzomys nitidus*	1	PDO	120.05	0.53	80.12	2.18
Cricetidae	*Oryzomys xanthaeolus*	1	PDO	255.71	0.57	143.38	3.77
Cricetidae	*Phyllotis xanthopygus*	2	PDO	232.93	0.64	103.25	4.09
Echimyidae	*Proechimys brevicauda*	1	PDO	337.80	0.66	184.75	7.33
Echimyidae	*Proechimys cuvieri*	2	PDO	275.01	0.55	187.00	8.39
Echimyidae	*Proechimys guairae*	2	PDO	360.10	0.67	185.56	9.32
Echimyidae	*Proechimys semispinosus*	1	PDO	184.49	0.46	134.88	1.11
Echimyidae	*Proechimys simonsi*	1	PDO	250.52	0.56	186.19	4.08
Sciuridae	*Sciurus granatensis*	1	PDO	134.41	0.47	71.00	9.27
Sciuridae	*Sciurus ignitus*	1	PDO	129.47	0.43	77.88	11.59
Sciuridae	*Sciurus igniventris*	1	PDO	157.49	0.44	82.62	7.65
Sciuridae	*Sciurus spadiceus*	3	PDO	148.07	0.41	93.66	15.41
Sciuridae	*Sciurus stramineus*	1	PDO	133.98	0.44	70.38	7.25

Cricetidae	*Thomasomys aureus*	1	ADO	271.28	0.52	112.25	3.30
Cricetidae	*Thomasomys cinereus*	1	ADO	208.90	0.35	141.88	3.95
Echimyidae	*Thrichomys apereoides*	2	PDO	260.37	0.51	119.69	8.19
Cricetidae	*Zygodontomys brevicauda*	3	PDO	208.29	0.69	104.94	1.66

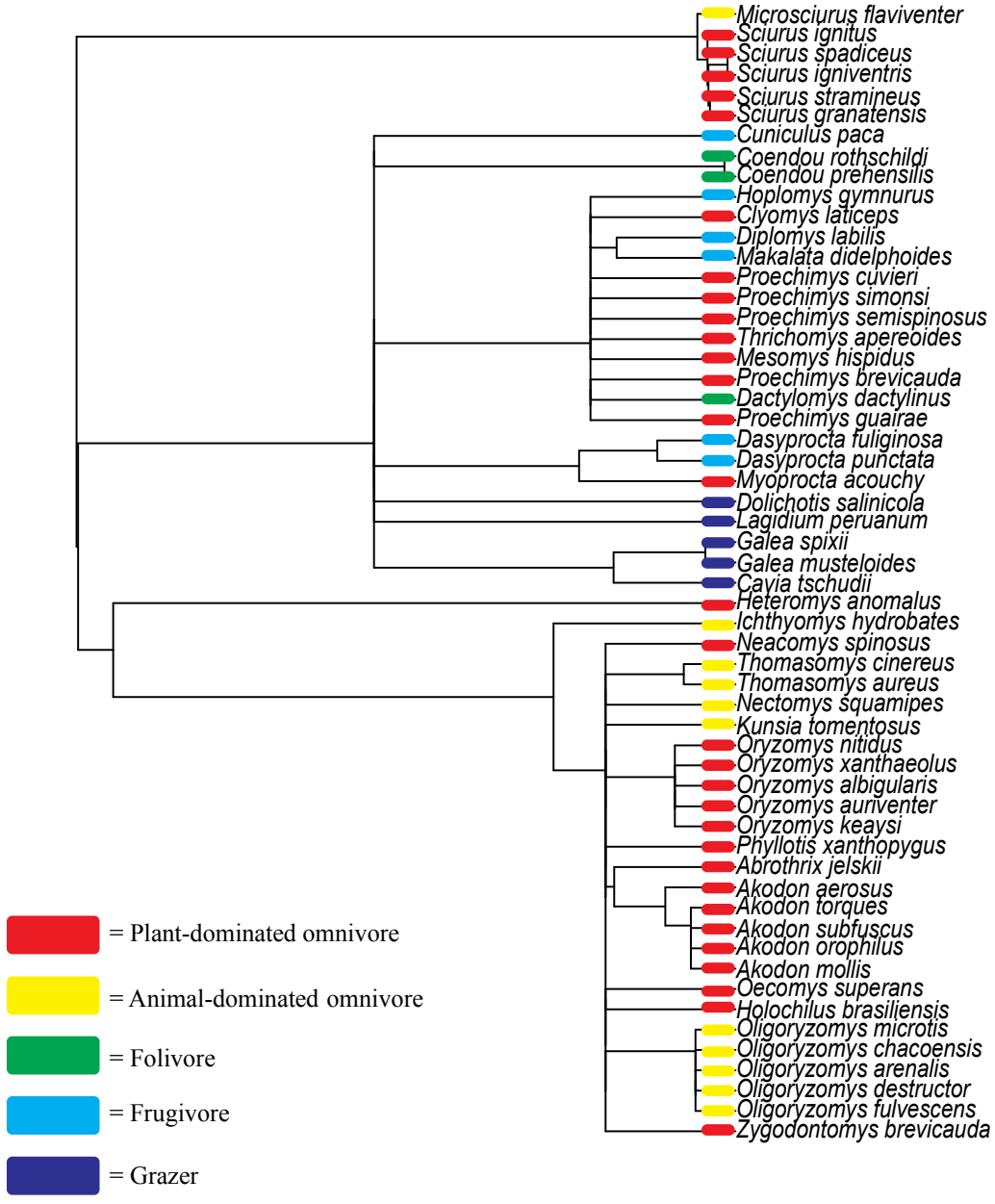

Figure 42: Phylogenetic tree of all rodent species included in this study. Tree topology derived from Bininda-Emmons et al. (2008).

After scanning and segmentation, it is necessary to perform retriangulation on surfaces in order to eliminate any possible artifacts that may influence the measurement

of dental topography. This was done in accordance with Spradley et al. (2017), which outlines proper decision making with regards to retriangulation. Ultimately, I chose to downsample all PLY files to 10,000 faces and smooth the 3D mesh via 25 smoothing iterations performed in Avizo (FEI Visualization Sciences Group, Berlin, Germany). Once again, artifacts were produced on a limited number of surfaces in my sample, and to fix these they were deleted and the resultant hole was filled using Geomagic.

After all PLY files were retriangulated, the resultant files uploaded to R via the package "molaR." DNE, RFI, and OPCR were recorded for each tooth surface. A data limit problem was encountered in relation to the measurement of OPCR on many of the surfaces. This problem was identified as being related to the high walls of the molars that many rodents possess. In brief, these walls are recorded as especially large patches in OPCR, and such large patches create memory issues as the computer attempts to handle large amounts of information at once while running the analysis. In order to overcome this obstacle, I cropped the tooth surfaces in Avizo for the DNE and OPCR analyses. Given the wide disparity of rodent molar morphology, it is difficult to standardize a cropping procedure using precise terminology. Howerver, surfaces were cropped in such a way that preserved all potentially functionally relevant features on the occlusal surface, while eliminating as much of the presumably non-functioning walls as possible. Cropping was done at the same level as the deepest point on the occlusal surface; which is similar to previous cropping procedures (Winchester et al., 2014;

Prufrock et al., 2017). It has been demonstrated that cropping teeth does not significantly affect the measurement of DNE and OPCR, as it does for RFI (Prufrock et al., 2017). This is because the walls of the tooth do not contribute significantly to the measurement of either DNE or OPCR, as the flat walls are not overly sharp or complex.

Correlations between topopgraphy metrics were performed using linear regression. A Shapiro-Wilks test performed for each metric failed to reject the hypothesis that RFI and OPCR are normally distributed in my sample ($p > 0.017$), but a test performed for DNE did reject the null hypothesis ($p < 0.01$), suggesting non-normality for DNE in my sample. In order to test for the effect of diet on dental topography, mean species values were compiled and a phylogenetic ANOVA—which is robust to skewness and small sample sizes (Khan and Rayner, 2003)—was performed on these means. A phylogenetically-corrected post-hoc Tukey's Honestly Significant Differences (HSD) test was then used to test for differences between pairs of dietary categories. In order to understand how diet and the topography metrics interact, a principal components analysis was performed on the three metrics and analyzed visually. Finally, a discriminant function analysis (DFA) was performed to test the ability of the dental topography metrics to successfully bin taxa by diet category. All analyses were performed in the open-source statistical software R.

5.2.2 Ecometric Distributions

Distributions of DNE, RFI, and OPCR were compiled for rodent species occupying 85 South American localities listed in Chapter 2. For genera in which I have multiple species sample in the first part of my study—and the values of topography metrics are relatively close to one another—the average was taken between two or more species in that genus, and this average was used as a stand-in value for non-sampled species. From these distributions, four statistics of distributions were calculated: mean, range, coefficient of variation, and skew. These statistics were then correlated with the six climatic/habitat variables from Chapters 2 and 4. Included in this analysis are the machine-learning regression algorithms introduced in Chapter 2; regression trees, random forests, and Gaussian process regression.

5.3 Results

5.3.1 Dental Topography and Dietary Ecology

5.3.1.1 Correlations between Dental Topography Metrics

Table 21: Results from correlation analyses between dental topography metrics.

Comparison	F-ratio	*p*-value	R^2	Slope
DNE-RFI	17.917	**<.001**	0.249	+
DNE-OPCR	67.012	**<.001**	0.554	+
RFI-OPCR	2.8518	0.097	0.050	+

Results from correlation analyses between the three dental topography metrics are presented in Table 21, and illustrated in Figure 43. A modified Bonferonni correction

was used for the alpha level, resulting in an alpha level of 0.019. My results indicate that DNE has a significant positive correlation with both RFI and OPCR, while RFI and OPCR do not demonstrate a significant correlation with one another. There are two notable outliers for DNE values that are far above the expected values for my regressions, *Dactylomys dactylinus* and *Diplomys labilis*. The significance of these outliers is discussed in detail below.

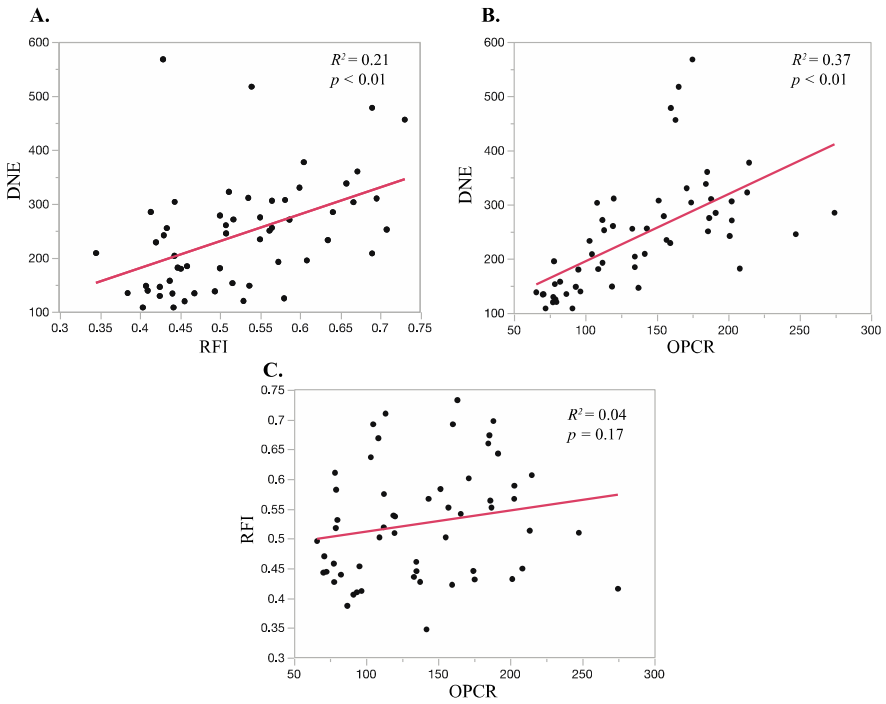

Figure 43: Linear regressions of dental topography metrics against one another. A. DNE-RFI; B. DNE-OPCR; C. RFI-OPCR.

5.3.1.2 Phylogenetically-corrected ANOVAs

Results from phylogenetically-corrected ANOVA tests are presented in Tables 22-24. My results indicate no significant correlations between diet and any of the dental

topography metrics after phylogeny is taken into account. However, post-hoc Tukey's HSD tests indicated that, after a Bonferroni corrected alpha-level of .005, there are several significantly different pairs included in the distributions of DNE (Table 25), particularly between the omnivorous categories (PDO and ADO) and other dietary categories. My results also indicate a significant difference between grazers and other dietary groups in RFI, as well as between folivores and frugivores. I find no significantly different pairs in OPCR.

The box plots in Figure 44 illustrate the general patterns in my results. In brief, the more highly herbivorous species tend to have higher values of both DNE and RFI—and grazers having especially high values of RFI relative to the total sample—while the generalist categories tend to have slightly lower values, albeit with wide ranges. Average OPCR values for all dietary groups tend to fall near a total sample average of 148, with considerable overlap between all groups. This is reflected in the results from the ANOVA test ($p = 0.525$, Table 24).

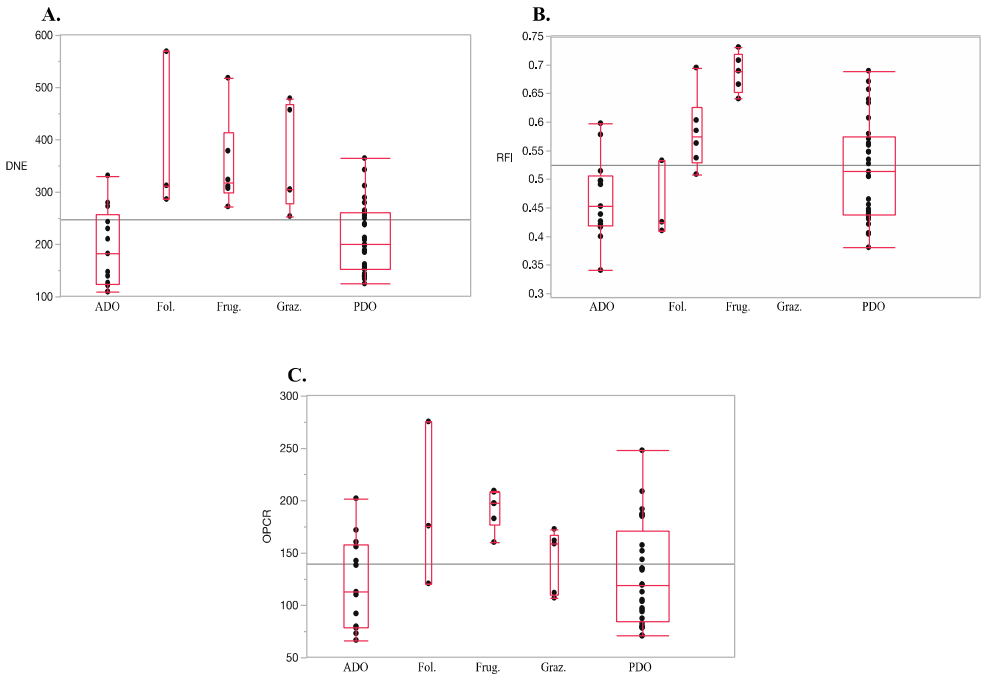

Figure 44: Oneway bivariate plots of A) DNE; B) RFI; and C) OPCR by diet. Grey line represents mean values of each metric. Summary statistics for phylogenetically-corrected ANOVAs are presented in Tables 22-24. Results from post-hoc Tukey HSD tests of all pairs are presented in Table 25.

Table 22: Phylogenetically-corrected ANOVA for test of effect of diet on DNE in South American rodents.

	df	Sum-Sq	Mean-Sq	F-value	Pr(>F)	Pr(>F) given phylogeny
Diet	4	268808	69263	10.814	2.004e-06	0.40
Residuals	51	316920	6291			

Table 23: Phylogenetically-corrected ANOVA for test of effect of diet on RFI in South American rodents.

	df	Sum-Sq	Mean-Sq	F-value	Pr(>F)	Pr(>F) given

						phylogeny
Diet	4	0.205	0.051	8.4695	2.553e-05	0.198
Residuals	51	0.308	0.006			

Table 24: Phylogenetically-corrected ANOVA for test of effect of diet on OPCR in South American rodents.

	df	Sum-Sq	Mean-Sq	F-value	Pr(>F)	Pr(>F) given phylogeny
Diet	4	36380	9095	4.421	0.004	0.525
Residuals	51	104930	2057.5			

Table 25: Summary statistics from phylogenetically-corrected post-hoc Tukey's Honest Significant Differences tests. Bolded numbers indicate statistical significance (alpha level = 0.005). Dietary abbreviations: Fol = folivore; Frug = frugivore; Grass = grazing; ADO = animal dominated omnivore; PDO = plant dominated omnivore.

	DNE			RFI			OPCR		
	Diff.	Std. Err Diff.	p-value	Diff.	Std. Err Diff.	p-value	Diff.	Std.Err Diff.	p-value
Fol-ADO	196.69	50.49	**0.001**	0.011	0.054	0.262	68.89	29.05	0.256
Fol-PDO	179.46	46.81	**0.033**	0.061	0.051	0.064	61.85	27.05	0.146
Grass-ADO	167.46	41.48	**0.044**	0.177	0.044	**<.001**	22.83	23.87	0.287
Frug-ADO	159.35	38.91	**0.044**	0.113	0.041	0.070	76.89	22.39	0.330
Grass-PDO	150.24	38.17	**0.002**	0.127	0.041	**<.001**	15.79	21.96	0.328
Frug-PDO	142.12	35.35	**<.001**	0.063	0.038	0.451	69.85	20.34	0.134
Fol-Frug	37.34	55.74	**0.049**	0.124	0.059	**0.017**	7.99	32.07	0.659
Fol-Grass	29.22	57.57	0.449	0.188	0.061	**0.002**	46.06	33.13	0.056
PDO-ADO	17.23	26.31	0.947	0.011	0.028	0.212	7.037	15.14	0.688
Grass-Frug	8.12	47.73	0.396	0.064	0.051	**0.035**	54.05	27.47	0.066

5.3.1.3 Discriminant Function Analysis

Several discriminant function analyses (DFAs) were performed on the dataset to test the predictive capabilities of these metrics in categorizing species by diet (Table 26). Results from a DFA performed on the data suggest that dental topography metrics, in combination with the natural log of M_2 area, perform moderately well in characterizing rodent tooth surfaces by dietary category. Individual specimens were correctly categorized at a rate of ~59%, and a chi-squared test indicated that the predicted diets were *not* independent of the actual dietary categories ($p < 0.001$). In other words, the DFA did not perform at random chance, which would be a rate of 20% accuracy (100% divided by 5 groups = 20%). Different combinations of topography metrics in the model—i.e., subtracting one or more metrics from the DFA model—results in lower accuracy rates. Results also suggest that those species belonging to certain dietary groups—including PDO (82.5%), grazers (62.5%), and frugivores (60%)—were more consistently placed the correct dietary category by the DFA than folivores (40%) or ADO (6.7%).

I also segregated the data by taxonomy, performing separate DFAs for caviomorph rodents and non-caviomorph rodents. The DFA for caviomorph rodents performed approximately as well (~58%) as that from the complete rodent dataset. The DFA from the non-caviomorph—comprised of both sigmodontine and sciurid rodents—performed slightly better (~66%) than either of these other models, though the non-

caviomorph sample comprises only two dietary categories, plant-dominated omnivore (PDO) and animal-dominated omnivore (ADO).

Table 26: Results from discriminant function analysis (DFA) performed using dental topography metrics in combination with M_2 area, for the complete rodent dataset.

	All Rodents							
	ADO	**Folivore**	**Frugivore**	**Grazer**	**PDO**	**TOTAL**	χ^2	p
% Correctly Identified	6.7	40.0	60.0	50.0	82.5	59.0	59.84	**<0.001**

Finally, a visual analysis of a principal components analysis (PCA) plot (Figure 45) illustrates that the frugivorous, folivorous, and grazing species tend towards higher values of RFI, DNE, OPCR, and log molar area than omnivorous species. There is further separation between the grazers and the folivores/frugivorous by RFI, as grazers tend to have higher relief. As for the two omnivorous dietary categories, plant-dominated omnivores tend towards higher values of all metrics relative to animal-dominated omnivores.

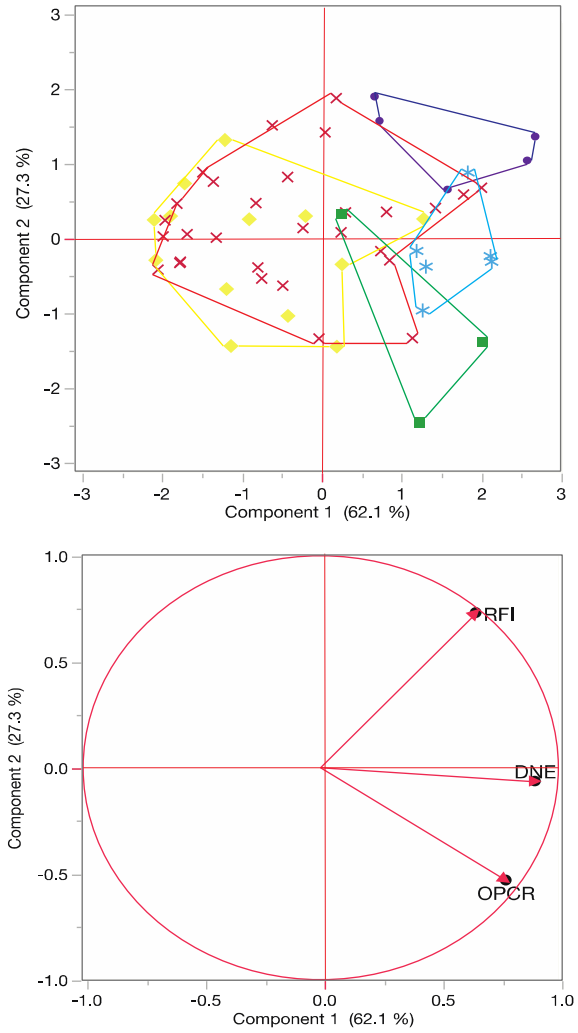

Figure 45: Principal components analysis of DNE, RFI, and OPCR demonstrating separation of dietary categories in morphospace. Symbol key: Yellow diamonds = PDO; Red Xs = ADO; Green squares = Folivore; Blue stars = Frugivore; Purple circles = Grazer.

5.3.2 Ecometric Distributions and Climate

5.3.2.1 Ecometric Means

Table 27: Summary statistics of correlation analyses between means of distributions of DNE, RFI, and OPCR across South American localities and six variables of climate and habitat.

			DNE	
	***F*-ratio**	***p*-value**	**R^2**	**Slope**
MAT	0.044	0.835	0.001	+
Temp. Seasonality	6.727	0.011	0.078	-
MAP	0.024	0.878	0.000	+
Precip. Seasonality	9.703	**0.002**	0.109	+
NPP	0.375	0.542	0.005	-
Canopy Height	1.185	0.280	0.015	-
			RFI	
MAT	67.085	**<0.0001**	0.462	-
Temp. Seasonality	2.171	0.004	0.103	+
MAP	23.3163	**<0.0001**	0.230	-
Precip. Seasonality	6.535	0.013	0.077	+
NPP	23.040	**<0.0001**	0.226	-
Canopy Height	11.403	**0.001**	0.128	-
			OPCR	

MAT	38.773	**<0.0001**	0.329	+
Temp. Seasonality	41.136	**<0.0001**	0.342	-
MAP	32.145	**<0.0001**	0.289	+
Precip. Seasonality	0.008	0.928	0.000	-
NPP	5.635	0.020	0.067	+
Canopy Height	8.146	0.006	0.093	+

The means of the distributions of rodent dental ecometrics were compiled for each South American locality presented in Chapter 2. These means were then correlated with the six bioclimatic variables from Chapter 2. Localities that had less than 5 rodent species were excluded from the analysis. The results from these correlation analyses are presented in Table 27.

Amongst these six variables, my results show that, after a Bonferroni correction of 0.003 reflective of the 18 separate tests performed in this analysis, the mean of DNE at a given locality is only weakly positively correlated ($R^2 = 0.11$) with precipitation seasonality, suggesting higher average DNE values with more seasonality in rainfall. Otherwise, I find no other statistically significant correlations with the mean of DNE. Only the correlation with temperature seasonality approaches significance ($p = 0.01$).

My results demonstrate statistically significant negative correlations of the mean of RFI with MAT, MAP, and NPP, suggesting that RFI decreases with warmer, wetter,

and more productive environments. Of these three correlations, the mean of RFI has the strongest relationship with MAT ($R^2 = 0.42$).

The mean of OPCR has statistically significant positive correlations with both MAT and MAP, and a significant negative correlation with temperature seasonality. In other words, the average rodent OPCR value increases with warmer and wetter environments, and decreases significantly in more seasonal environments.

5.3.2.2 Ecometric Ranges

Results from correlation analyses of the ranges of my three dental topography metrics and climate are presented in Table 28. Statistical significance is once again based on a Bonferroni corrected alpha value of 0.003. My results indicate that the range of DNE has a statistically significant positive correlation with both NPP and canopy height. The range of RFI only shows a statistically significant negative association with temperature seasonality.

My results suggest that the range of OPCR is the most informative of the three metrics. The range of OPCR has a significant positive relationship with MAT, MAP, NPP, and canopy height, and a negative correlation with temperature seasonality (Table 28).

Table 28: Summary statistics of correlation analyses between ranges of distributions of DNE, RFI, and OPCR across South American localities and six variables of climate and habitat.

	DNE

	F-ratio	*p*-value	R^2	Slope
MAT	4.954	0.029	0.060	-
Temp. Seasonality	0.012	0.918	0.000	-
MAP	0.556	0.458	0.007	+
Precip. Seasonality	0.184	0.669	0.002	-
NPP	2.025	0.159	0.025	+
Canopy Height	3.988	0.049	0.049	+
			RFI	
MAT	0.636	0.428	0.008	+
Temp. Seasonality	2.1636	0.145	0.021	-
MAP	0.117	0.733	0.002	-
Precip. Seasonality	9.029	0.004	0.105	+
NPP	2.803	0.098	0.035	-
Canopy Height	0.059	0.808	0.001	-
			OPCR	
MAT	41.115	**<0.0001**	0.345	+
Temp. Seasonality	15.031	**0.0002**	0.162	-
MAP	20.800	**<0.0001**	0.211	+
Precip. Seasonality	0.507	0.479	0.006	+
NPP	10.036	**0.002**	0.114	+

Canopy Height	18.482	**<0.0001**	0.192	+

5.3.2.3 Ecometric Coefficients of Variation

My results (summarized in Table 29) for the coefficients of variation (CoV) of DNE distributions suggest no statistically significant relationships between DNE CoV and climate/habitat variables. RFI CoV results indicate a single noteworthy association, a positive correlation of RFI CoV and precipitation seasonality that is extremely close to my threshold of statistical significance ($p = 0.0037$). Results from OPCR once again show the most statistical significance. OPCR CoV has a statistically significant correlation with all variables except precipitation seasonality. This includes positive correlations with MAT, MAP, NPP, and canopy height, and a negative correlation with temperature seasonality. In the context of environment, this would suggest a greater disparity of OPCR values in more tropical-like habitats, and a lower disparity in drier, more seasonal habitats.

Table 29: Summary statistics of correlation analyses between coefficients of variation (CoV) of distributions of DNE, RFI, and OPCR across South American localities and six variables of climate and habitat.

	DNE			
	F-ratio	*p*-value	R^2	Slope
MAT	4.954	0.029	0.060	-
Temp. Seasonality	0.012	0.918	0.000	-

MAP	0.556	0.458	0.007	+
Precip. Seasonality	0.184	0.669	0.002	-
NPP	2.025	0.159	0.025	+
Canopy Height	3.988	0.049	0.049	+
			RFI	
MAT	0.636	0.428	0.008	+
Temp. Seasonality	2.1636	0.145	0.021	-
MAP	0.117	0.733	0.002	-
Precip. Seasonality	9.029	0.004	0.105	+
NPP	2.803	0.098	0.035	-
Canopy Height	0.059	0.808	0.001	-
			OPCR	
MAT	41.115	**<0.0001**	0.345	+
Temp. Seasonality	15.031	**0.0002**	0.162	-
MAP	20.800	**<0.0001**	0.211	+
Precip. Seasonality	0.507	0.479	0.006	+
NPP	10.036	**0.002**	0.114	+
Canopy Height	18.482	**<0.0001**	0.192	+

5.3.2.3 Ecometric Skewness

I find no statistically significant relationships between the skewness of the distributions of my dental topography metrics and the bioclimatic variables included in this study.

5.3.3 Machine-learning Regression Techniques

Mean absolute error (MAE) and root mean squared error (RMSE)—error metrics that demonstrated the average difference between predicted and actual observations—for the six bioclimatic variables across the different regression techniques are presented in Table 30. MAE and RMSE differ for each bioclimatic variable because they are presented in the same units as those variables. The three machine-learning regression methods—regression tree (RTA), random forests (RF), and Gaussian process regression (GPR)—generally have lower error metrics than multivariate linear regression. Bivariate plots of the estimated bioclimatic variables versus the actual values of these variables are presented in Figure 46-50. R^2 values in these plots give a measurement of the fit between estimations and observations. The highest R^2 values are found in the estimations of MAP, including regression tree ($R^2 = 0.90$), Gaussian process regression ($R^2 = 0.74$), and random forests ($R^2 = 0.89$).

Table 30: Mean Absolute Error (MAE) and Root Mean Squared Error (RMSE) for the estimations of bioclimatic variables using different regression techniques.

	Mean Annual Temperature	
Method	**MAE**	**RMSE**
Baseline Average	50.03	60.61

Linear Regression	38.89	53.16
Regression Tree (RTA)	36.16	54.04
Random Forests (RF)	26.9	44.05
Gaussian Process Regression (GPR)	28.89	43.23
	Temperature Seasonality	
Baseline Average	1440.48	1736.38
Linear Regression	1053.24	1420.42
Regression Tree (RTA)	587.28	771.33
Random Forests (RF)	639.02	899.14
Gaussian Process Regression (GPR)	875.12	1192.65
	Mean Annual Precipitation	
Baseline Average	731.3	963.79
Linear Regression	637.4	830.54
Regression Tree (RTA)	705.85	838.53
Random Forests (RF)	551.01	683.51
Gaussian Process Regression (GPR)	575.91	730.12
	Canopy Height	
Baseline Average	9.33	10.04
Linear Regression	8.5	9.01
Regression Tree (RTA)	7.14	8.83
Random Forests (RF)	6.45	7.31
Gaussian Process Regression (GPR)	7.15	7.9
	Net Primary Productivity	
Baseline Average	4938.95	5954.46
Linear Regression	4713.63	5588.82
Regression Tree (RTA)	3326.44	4318.86
Random Forests (RF)	3809.63	4734.92
Gaussian Process Regression (GPR)	4528.59	5849.59

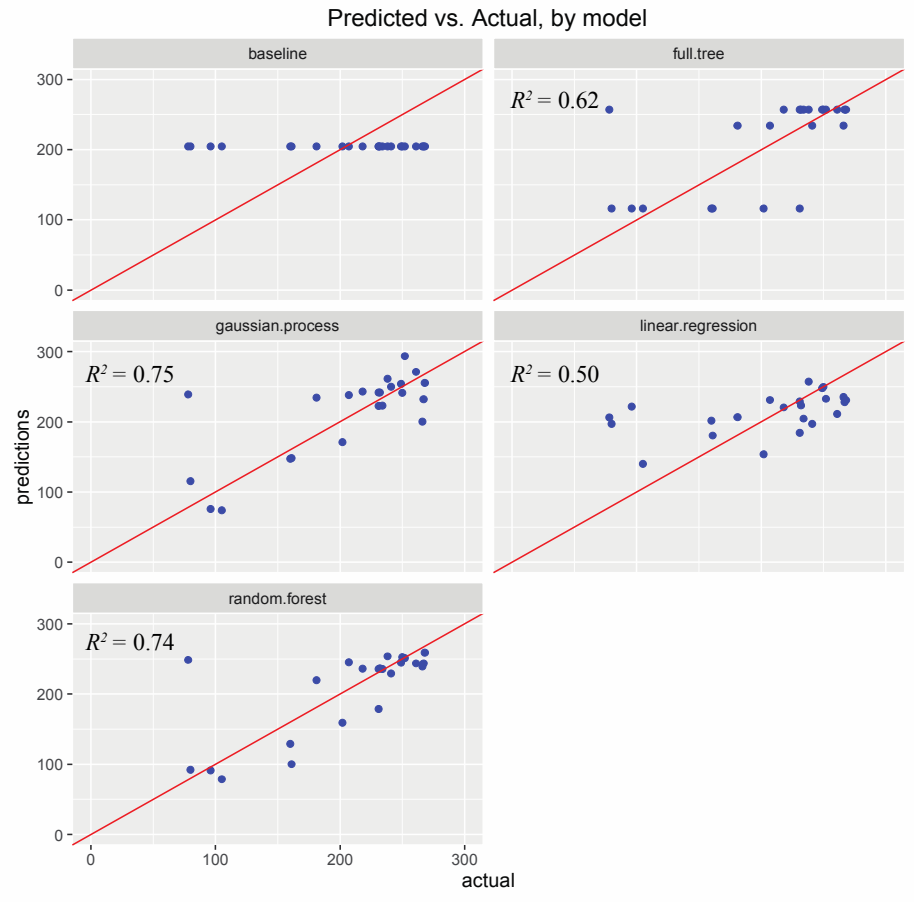

Figure 46: Actual mean annual temperature (MAT) (x-axis) and predicted MAT (y-axis) values for the test dataset using rodent dental topography metric distributions as the predictor variables. MAT values are presented as °C x 10. The plots represent the five different regression techniques—and a baseline mean (top left corner) that represents the average value for MAT across all localities included in this study. The red line represents a hypothetical 1:1 relationship between predicted and actual values, and would suggest a perfect fit for the values predicted by the models and the observed values.

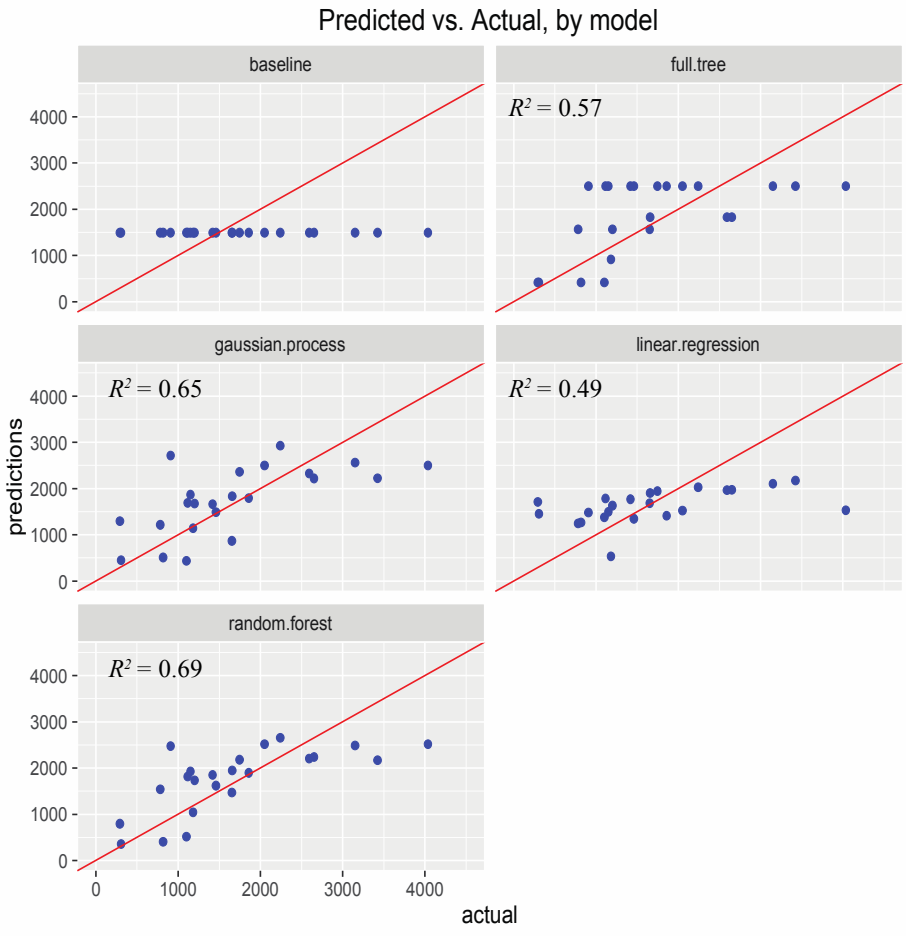

Figure 47: Actual temperature seasonality (x-axis) and predicted temperature seasonality (y-axis) values for the test dataset.

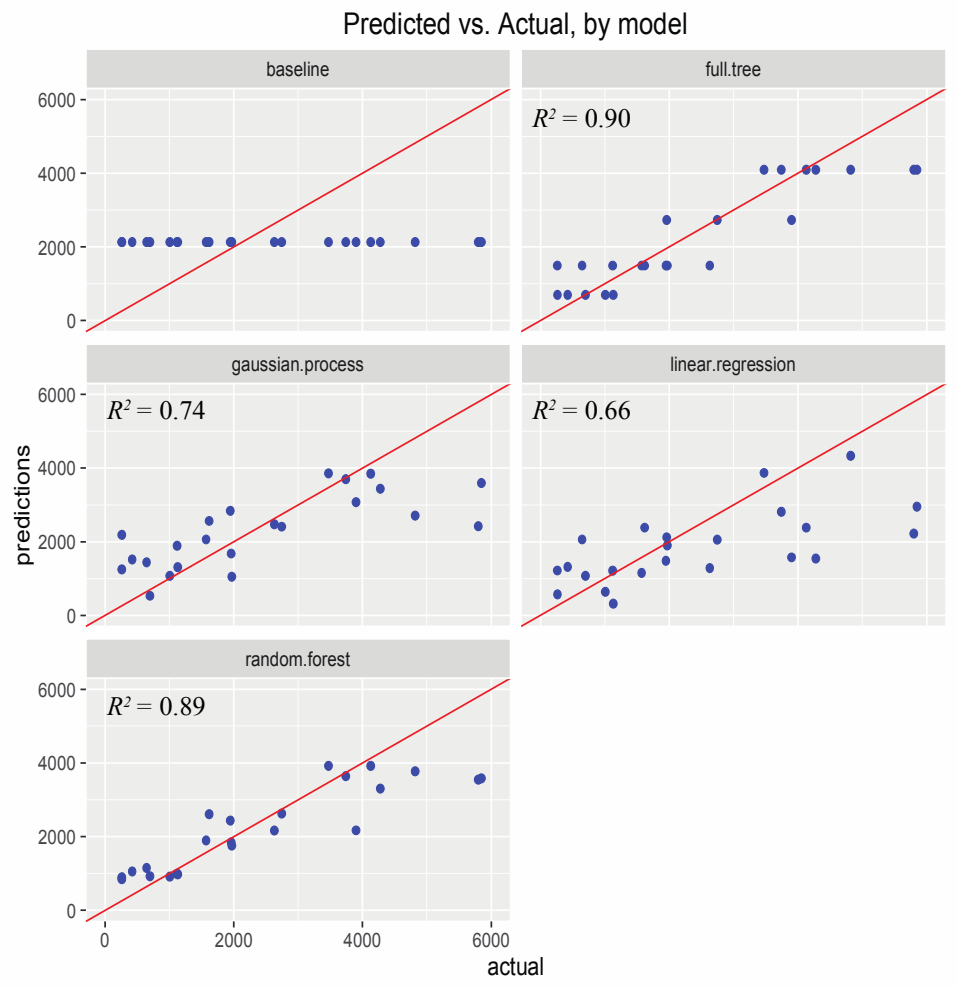

Figure 48: Actual mean annual precipitation (MAP) in millimeters per year (x-axis) and predicted MAP (y-axis) values for the test dataset.

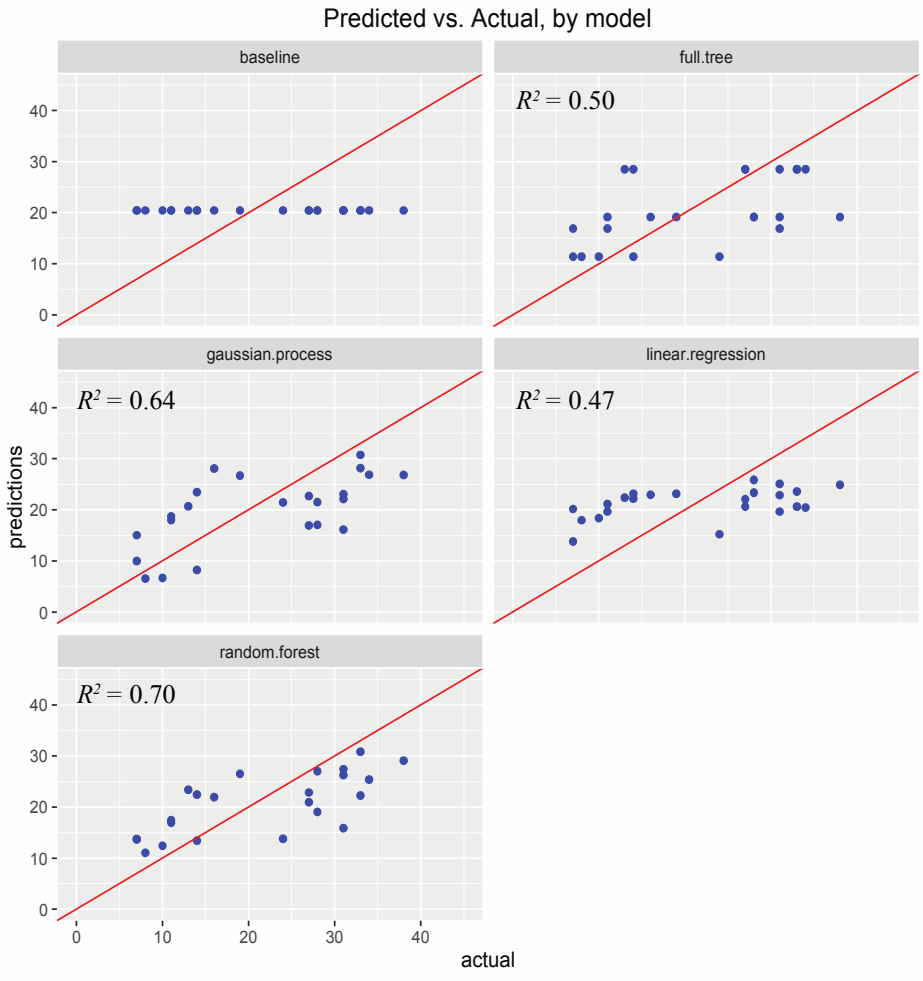

Figure 49: Actual canopy height in meters (x-axis) and predicted canopy height (y-axis) values for the test dataset.

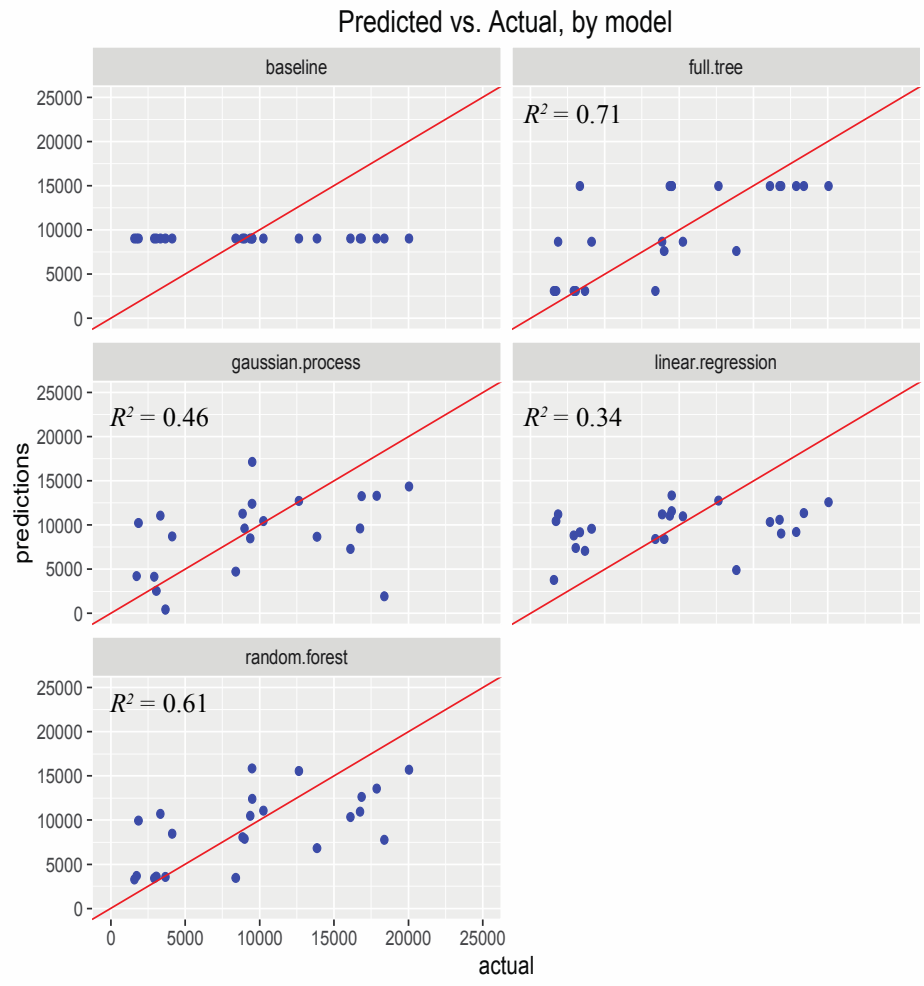

Figure 50: Actual net primary productivity (NPP) (x-axis) and predicted NPP (y-axis) values for the test dataset.

5.4 Discussion

In my results I provide correlations of lower M_2 dental topography—specifically sharpness (DNE), relief (RFI), and complexity (OPCR)—with diet categories in a broad taxonomic sample of South American caviomorph, sigmodontine, and sciurid rodents.

In the introduction I stated that I expected rodent molars, despite their vastly different gross morphology compared to primates or marsupials, to nevertheless abide by the same functional constraints of the teeth of these clades. This expectation was built on the hypothesis of Evans and Sanson (2003) that there exists ideal tooth shapes and configurations for the breaking down of specific categories of food materials. Though Evans and Sanson (2003) discussed this hypothesis primarily in the context of the tribosphenic molar, Evans et al. (2007) demonstrated that similar constraints were acting on the tooth rows of both rodents and carnivorans. Thus, the null hypothesis is that rodent molar topography shows similar patterns to what see in primates (Boyer, 2008; Winchester et al., 2014) and marsupials (Chapter 4), namely that an increase in sharpness, relief, and complexity should be associated with diets consisting of tougher food materials.

5.4.1 Dental Topography and Dietary Ecology

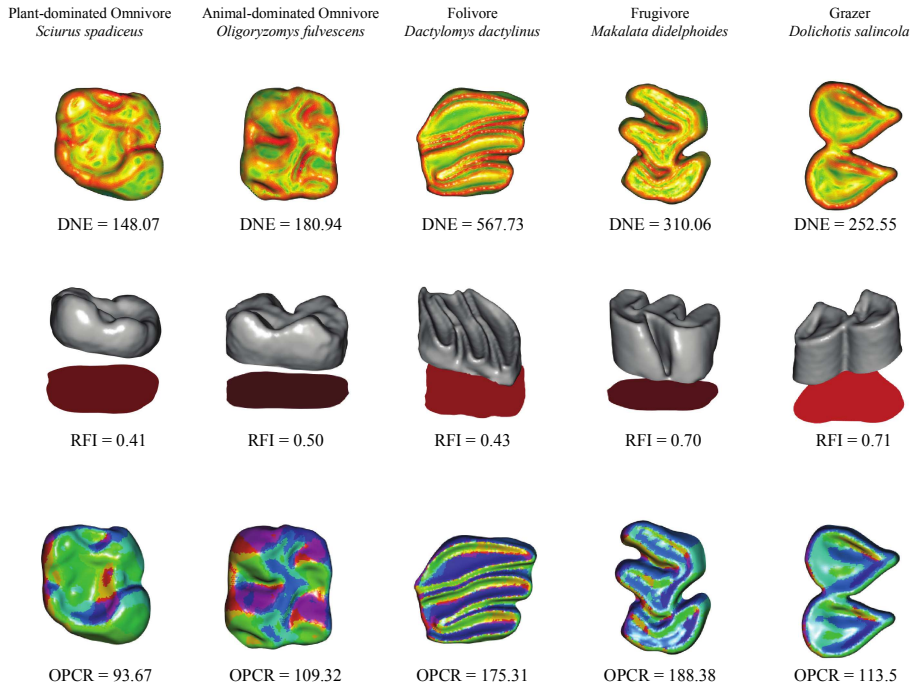

Figure 51: 3D reconstructions of rodent lower M_2s illustrating the measurement of DNE, RFI, and OPCR. This figure demonstrates a representative species of each dietary category included in my study. From left to right, these species are *Sciurus spadiceus* (PDO), *Oligoryzomys fulvescens* (ADO), *Dactylomys dacytlinus* (Folivore), *Makalata didelphoides* (Frugivore), and *Dolichotis salincola* (Grazer).

5.4.1.1 Dirichlet Normal Energy (DNE)

My results suggest that topographic sharpness also likely increases with tougher foods, though my evidence for this pattern is based largely on trends rather than statistical significance. In general, rodents have higher DNE values than any of the other mammalian orders in which DNE has been measured (Winchester et al., 2014; Chapter 4). However, this could very well be due to differences in processing protocols of 3D meshes, and should not serve as a necessarily meaningful conclusion without proper

testing. Visual analysis of the surfaces suggests that the highest DNE values are being recorded on rodent molars that have more elaborate patterns of enamel ridges and folds (Fig. 51). The species that have these more elaborate molars also tend to be the dietary "specialists" in my sample, i.e. those species that are described as frugivorous, folivorous, or grazing rather than placed into one of the two omnivorous categories. This would suggest that DNE in rodents has a relationship with dietary ecology like that found in primates and marsupials (Ledogar et al., 2013; Winchester et al., 2014; Chapter 4), insofar as sharper occlusal surfaces may be associated with tougher, high fiber foods such as leaves or grass. This sharpness, correlated with the tooth's ability for shearing (Kay, 1975; Winchester et al., 2014), allows the tooth to more efficiently slice through the tough cell walls of plants. My results are the first to demonstrate that sharpness on the rodent molar morphology is similarly correlated with these food material properties.

On the other hand, that the frugivorous rodent species in my sample also have high DNE values would suggest that this relationship is more complicated in rodents than it is in other mammalian taxa. One potential explanation for this is that the dietary signal from DNE may be confounded by body size. As can be seen in the rodent sample in Figure 52, DNE is positively correlated with the natural log of molar area. While DNE is typically independent of size (Winchester et al., 2014), it would appear that larger rodent molars are more likely to have more sharp enamel ridges and folds, a feature that was also noted by Hillson (1986) in his review of rodent tooth morphologies. The species

with the highest DNE in my sample include *Cavia tschudii* (637g, Patton et al., 2015), *Dactylomys dactylinus* (~650g, Patton et al., 2015), *Diplomys labilis* (~228g, Patton et al., 2015), and *Lagidium peruanum* (~1.25kg, Patton et al., 2015). Interestingly, these are not the largest species in my sample, indicating that molar size does not explain all of the variance of DNE. It is beyond the scope of this study to discern whether or not larger rodent species are more likely to be specialized in their diets relative to small rodent species, or if larger rodent species are just easier to study in the wild and thus have better dietary data. Regardless, I do find that there is a tendency for herbivorous rodent species to have higher DNE than rodents that consume considerable amounts of insects (Fig. 44).

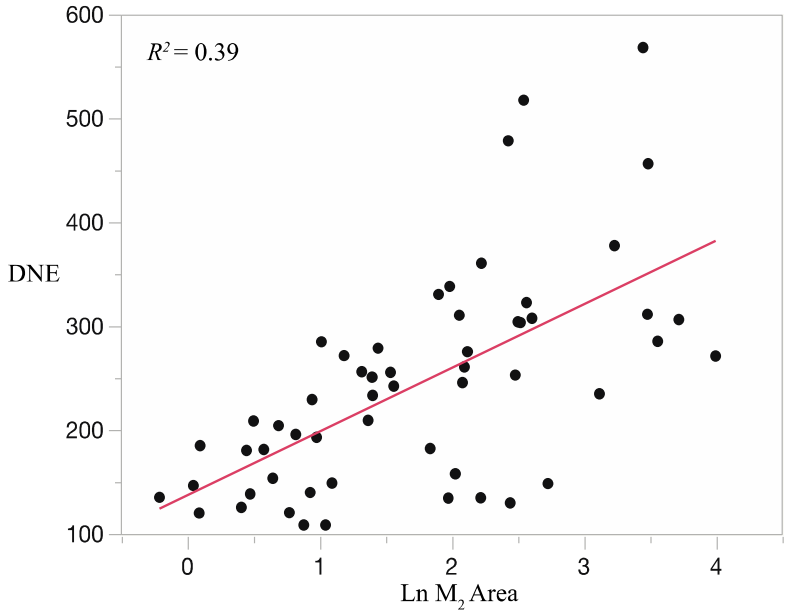

Figure 52: Linear regression of the natural log of M_2 area and DNE.

5.4.1.2 Relief Index (RFI)

Of the three dental topography metrics, RFI demonstrates the best correlation with diet after correcting for phylogeny (p = 0.198). My results from RFI suggest a similar trend as DNE of herbivorous rodents having higher values. The exception to this is that frugivorous rodents have RFI values that are more in line with animal-dominated omnivores and in the lower end of plant-dominated omnivores. This matches my expectation based on previous results from previously published studies of rodents (Williams and Kay, 2001), as well as other mammalian taxa (Janis, 1988; Williams and Kay, 2001; Ungar and M'Kirera, 2003; Boyer 2008; Winchester et al., 2014; Chapter 4). Based on the interpretations of these previous studies, this would suggest that frugivorous rodents likely do not experience the same levels of wear as folivores and grazers.

Williams and Kay (2001) found that grazing South American rodents had considerably higher hypsodont indices—a measure analogous to RFI—than either folivorous or frugivorous species. My results are generally in agreement with those of Williams and Kay (2001), with grazing species having the highest mean RFI (0.688) of any dietary group in my study. Williams and Kay (2001) interpreted their result as an adaptation to rapid tooth wear due to either the abrasive nature of phytoliths in grass,

the exogenous grit commonly associated with consuming fine particles of dirt adhering to grass, or a combination of the two.

Beyond the distinguishing of grazing rodents from other species, RFI is generally poor at discriminating diet, as there is considerable overlap in RFI between the other dietary groups (Figure 44). However, Williams and Kay (2001) also found that terrestriality was a significant factor in the evolution of rodent hypsodonty, suggesting that exogenous grit may be a primary driver of hypsodonty in rodents and other mammals. In order to test this possibility in my dataset, I first classified every rodent species as either terrestrial or arboreal/semi-arboreal (including scansorial). Following Williams and Kay (2001), the grazers were dropped from the dataset, as they may confound any signal because of their already abrasive diet. After removing grazers and controlling for phylogeny, I do not find a significant correlation between terrestriality and RFI ($p = 0.27$). This is surprising, given that Williams and Kay (2001) found a significant correlation in their sample of South American rodents, which is very similar to my own. A potential explanation for this discrepancy is that RFI is not precisely equivalent to a measure like hypsodonty index. Hypsodonty index is typically measured as the ratio of tooth crown height over tooth width or length (Van Valen, 1960; Janis, 1980). RFI more completely captures the relief of the whole surface by measuring the 3D surface area (Boyer, 2008). Thus, the hypsodonty signal distinguishing terrestrial and

arboreal rodents detected by Williams and Kay (2001) may be getting lost in the contributions from other occlusal features that compose the RFI metric.

5.4.1.3 Orientation Patch Count Rotated (OPCR)

Dental complexity, or OPCR, is also not significantly correlated with diet in my sample. This is particularly surprising as previously published studies have found that complexity in the rodent tooth row (Evans et al., 2007) and complexity in individual lower teeth (Evans and Jernvall 2009) are significantly correlated with diet. They use dietary categories that are very similar to my own—including animal-dominated omnivore (ADO), plant-dominated omnivore (PDO), and herbivore. Here I separate 'herbivore' into folivore, frugivore, and grazer.

There are a couple likely explanations for results relative to those of the other two studies; 1) my separation of their "herbivore" category into multiple different categories made the dietary signal of OPCR weaker; or 2) my inclusion of a phylogenetic correction. In order to test whether our separation of the herbivorous "specialists" into different categories affected my results, I combined these specialists—i.e., frugivores, folivores, and grazers—into a single herbivore group. A phylogenetically-corrected ANOVA performed on this dataset did not indicate a significant effect of diet on OPCR ($p = 0.41$). The other potential explanation for my lack of a significant correlation is that rodent occlusal morphology carries with it a strong phylogenetic signal. As a brief test of whether the distributions of rodent topographies are equivalent within dietary

categories but across different families, I performed a Mann-Whitney U-test on the two most well-sampled families in my dataset, Cricetidae (Rodentia: Sigmodontia) and Echimyidae (Rodentia: Caviomorpha), specifically those species categorized with the diet plant-dominated omnivore (PDO). A Mann-Whitney U-test is a nonparametric comparison of the averages of two independent groups of samples (equivalent to the Student's *t*-test for non-normal distributions). The results of this test (Table 31) indicate that the distributions of DNE and OPCR within the same dietary category—PDO—are not equivalent ($p < 0.01$), but could be considered equivalent in RFI ($p = 0.27$). This provides further evidence that the phylogenetic signal may be strong within different rodent families.

Table 31: Results of Mann-Whitney U-test for comparisons between cricetid and echimyid plant-dominated omnivores. *p*-values in bold represent statistical significance at an alpha level of 0.017.

Variable	*p*-value
DNE	**0.001**
OPCR	**0.002**
RFI	0.267

Given that the unique occlusal morphology of many rodent taxa is used to identify them at the family level (Simpson, 1945; Hillson, 1986), and that these features are the primary contributors to DNE and OPCR especially, and to RFI to a lesser extent, it should come as no surprise then that phylogeny would be an important variable in determining the measurement of dental topography.

5.4.1.4 Dental Topography as a Discriminator of Rodent Dietary Ecologies

In short, my results discussed above suggest that dental topography is generally a poor discriminator of dietary ecology in South American rodents. A discriminant function analysis (DFA) performed with all three metrics and the natural log of molar area results in individual specimens being correctly categorized by diet 59% of the time. While this is significantly better than random chance (20%), this is nevertheless a low percentage, particularly when compared to similar tests on primates (Winchester et al., 2014) and marsupials (Chapter 4). This begs the question as to why rodent occlusal morphology does not demonstrate the same patterns as primates and marsupials. The most obvious answer to this question would be to look towards the defining characteristic of all rodents, the ever-growing, hypselodont incisors in both the upper and lower jaw. These incisors serve as remarkably efficient and flexible tools for rodents across a broad array of ecological niches (Van Valen, 2004). Croft et al. (2011) demonstrated that upper incisor morphology in herbivorous caviomorph rodents could be used as an effective discriminator of dietary ecology. In combination with my results from the molars, this might suggest that the incisor toolkit provided to the rodents may have released their molars from the functional constraints that have maintained the general tribosphenic molar shape in other mammalian clades that nevertheless occupy similar niches as modern rodents. The other potential explanation is that the molars are

suited for processing the material they masticate after the incisors have processed the food. That is, the cheek-teeth are adapted to handle incisor-processed materials.

On the other hand, there is a strong possibility that the lack of dietary signal in my results is not due to a true biological phenomenon, but rather is due to the particularly coarse resolution of the dietary data available for the majority of rodent species in my sample. Unlike Croft et al. (2011), I included species for which wild diet data is not extensive. These poorly studied species—primarily the various species of rats and mice that are near ubiquitous in South American ecosystems—largely make up my omnivorous categories; both of which demonstrate considerable overlap with other dietary categories, especially in DNE and OPCR (Fig. 44). There is potential that more discrete classification of diet in these rodents in these categories may elucidate a relationship between molar topography and diet. Of course, this potential is dependent on the acquisition of behavioral data of notoriously difficult-to-study mammals, many of which are found in remote, inaccessible forests.

5.4.2 Rodent Dental Topography Distributions as Environmental Proxies

I proceed to the distributions of these topography metrics as potential proxies of climate and habitat. Tables 28-30 summarize the results from correlation analyses of bioclimatic variables and the means, ranges, and coefficients of variation of the dental topography metrics. I do not present results from analyses of skewness as I did not find any significant correlations.

5.4.2.1 DNE

Of the three metrics, my results suggest that the distributions of DNE are the least informative for estimating climate and habitat. The handful of significant relationships between DNE distribution statistics and environment are illustrated in Figure 53. Of the four climatic variables (MAT, MAP, temperature seasonality, precipitation seasonality) and the two habitat variables (NPP and canopy height), the mean of DNE only shows one significant correlation, a positive correlation with precipitation seasonality (Table 28). Based on the trends that are illustrated in Fig. 44, this would suggest a greater number of folivores, frugivores, and/or grazers with precipitation seasonality. Considering the nature of seasonal environments, this would likely reflect an increase in the number of grazing rodents. However, given the uncertainty of my results in linking molar DNE to diet, as well as the difficulty in estimating precipitation seasonality (see Chapter 2), I cannot rule out the possibility that this is a spurious result. That the mean of DNE has no other statistically significant association with any other variable only contributes further to the dubiousness of this result.

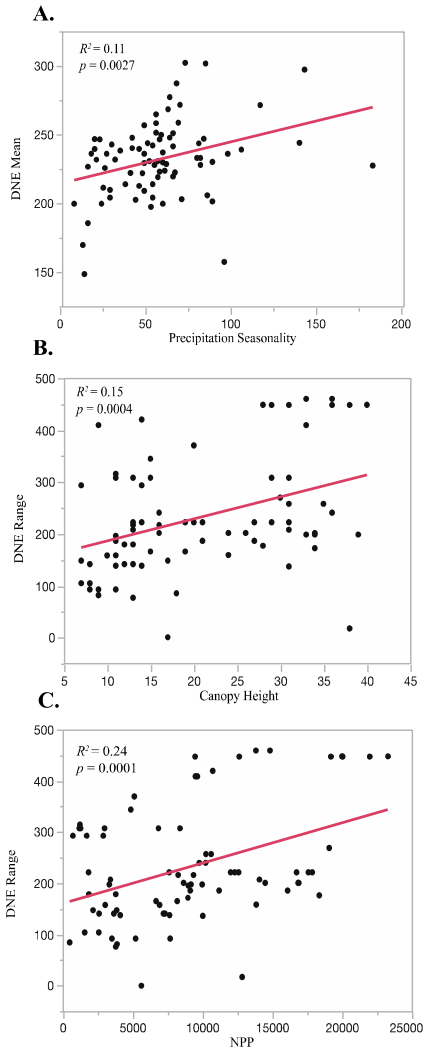

Figure 53: Bivariate plots of statistically significant relationships between DNE distribution statistics and environmental variables. A) DNE mean vs. Precipitation Seasonality; B) DNE Range vs. Canopy Height; C) DNE Range vs. NPP.

The range of DNE, however, demonstrates a positive correlation with both NPP and canopy height ($p < 0.001$). A greater range would suggest a larger total "spread" of the distribution. In the context of my data, the most likely implication is that there is mix of both omnivores and herbivorous "specialists" in more productive environments with

greater canopy height. Since grazers are unlikely to be affected by canopy height, we can assume that this reflects a greater number of frugivores and/or folivores, both of which have generally higher average DNE values in my sample. The correlation of DNE range and MAP is also very close to statistical significance ($p = 0.004$, compared to a Bonferroni-corrected alpha value of 0.003), suggesting that DNE range is associated with the presence of tropical forests, and the weakness of these correlations—none of the correlation coefficients (R^2) for these significant correlations rise above 0.163—is likely due to the fact that grazing rodents, indicative of grasslands (Kay et al., 1999), also have high DNE values. This in turn is creating high ranges in open, highly seasonal environments.

Finally, my results indicate that the coefficient of variation (CoV) of DNE distributions has no significant correlation with any of six variables of climate and habitat. As discussed in Chapter 4, CoV in the context of my study, can be interpreted as a measure of the average disparity (Gould, 1991) in dental topography at a given locality. More so than range and mean, CoV is robust to the presence of just one species with a high DNE value. For this reason, my finding that DNE CoV is not significantly correlated with any of the climate or habitat variables indicates that the distribution of DNE is not a useful proxy of environment. This is ultimately unsurprising given that DNE was a poor predictor of dietary ecology in my results, as well.

5.4.2.2 RFI

My results from the distributions of RFI, when viewed through the lens of my ecomorphological study, suggest that the presence or absence of grazing rodents is largely driving the significant correlations that I find. Grazers have significantly higher RFI values than do any other dietary category, and I find that the mean of RFI has a significantly negative correlation with MAT, MAP, NPP, and canopy height (Table 28). Additionally, the mean of RFI nears significance for a positive correlation with temperature seasonality ($p = 0.004$). Further, RFI range has a significant positive correlation with temperature seasonality (Table 29). All of these results are indicative of a trend towards higher RFI values in drier, seasonal grasslands that dominate the southern third of South America. These results agree with those of Kay et al. (1999), who found a correlation between the percentage of hypsodont rodent species and MAP, MAT, seasonal temperature amplitude (similar to my use of temperature seasonality), and mean temperature of coldest month. Kay et al. (1999) also found negative correlations with MAP and MAT, and a positive correlation with seasonal temperature amplitude. The discrepancy between RFI and the hypsodonty index is discussed in further detail above, but my results would suggest that hypsodonty index may serve as the better proxy for environment, as it is not affected by occlusal features that are heavily influenced by phylogeny.

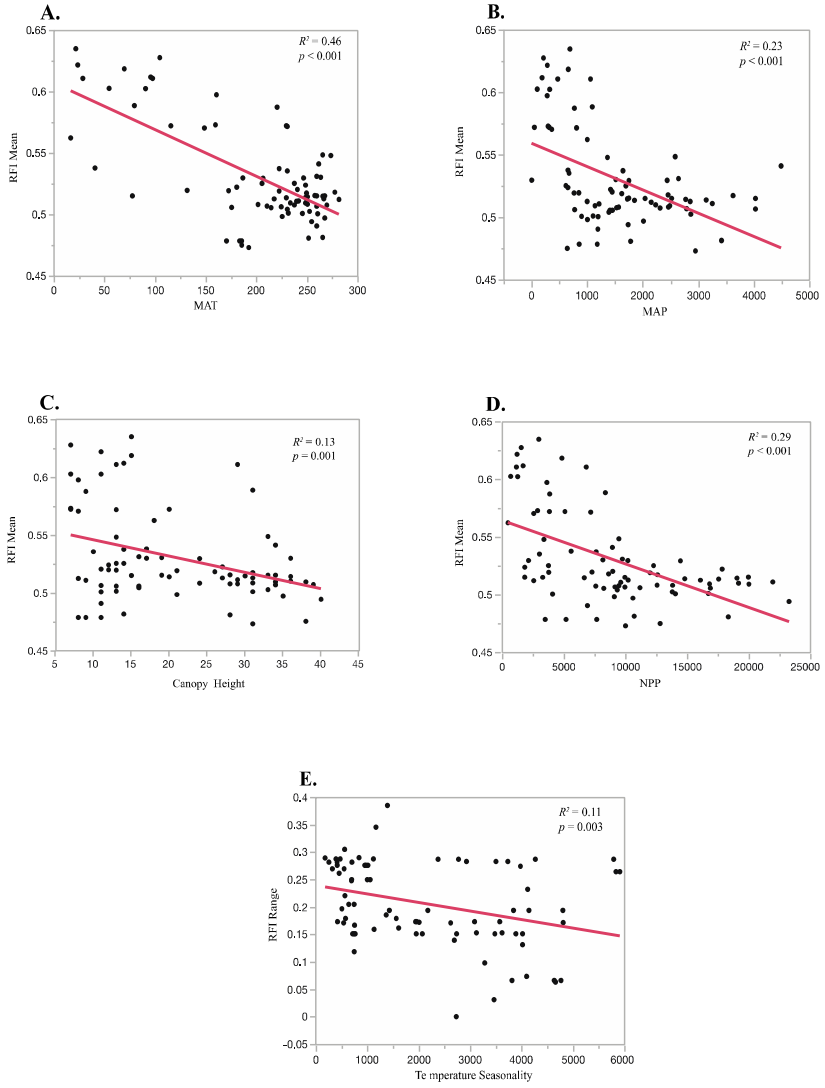

Figure 54: Bivariate plots of statistically significant relationships between RFI distribution statistics and environmental variables. A) RFI mean vs. MAT; B) RFI mean vs. MAP; C) RFI mean vs. Canopy Height; D) RFI mean vs. NPP; E) RFI range vs. Temperature Seasonality.

The CoV of RFI does not show any significant correlations with any of the environmental variables, pointing to RFI being more informative in identifying the presence of grazing species, which in turn can lead one to assume a more open, seasonal

environment (or not). Similar studies have shown how the presence of other mammalian orders, for which living representatives have known environmental tolerances or preferences, can be used as environmental proxies (Kay et al., 1997; Vizcaíno et al., 2006). In conclusion, much like DNE, the dearth of significant correlations with environmental variables is reflective of my failure to find strong evidence of RFI's ecomorphological relationship to diet in rodents.

5.4.2.3 OPCR

Whereas the distributions of RFI and DNE do not show much potential as proxies for environment, my results from the analyses of OPCR suggest that this may not be the case for tooth complexity. Quite surprisingly, given the generally poor performance of OPCR as an ecomorphological discriminator in primates and marsupials—see above, as well as Chapter 4 and Winchester et al. (2014)—I find that the distributions of OPCR have significant correlations with environment regardless of which distribution statistic is used. I will discuss my results in the context of each statistic below.

The mean of OPCR shows a significant increase with MAT and MAP, and a decrease with temperature seasonality. Additionally, the positive correlations for both NPP and canopy height are also close to my alpha value ($p = 0.02$ and $p = 0.006$, respectively). The only variable that it does not correlate well with is precipitation seasonality, which I demonstrated in Chapter 2 to be generally difficult to model. Based

on my ecomorphological results in the first section of this paper, it is clear that an ecological interpretation of these analyses is complicated. I found no significantly different dietary pairs in my post-hoc tests in regards to OPCR—though the frugivores in my sample appear to have a mean that is slightly higher than other dietary groups (Fig. 44)—which makes it difficult to assume which dietary niches are driving these correlations. However, viewing my results in combination with those of the OPC/OPCR studies of Evans et al. (2007) and Evans and Jernvall (2009), this would suggest a greater number of highly herbivorous species in more tropical-like environments. The strongest correlation in my results is that with temperature seasonality and MAT (R^2 = 0.34 and 0.32, respectively), suggesting a strong latitudinal gradient in our data. In fact, a correlation of the mean of OPCR and latitude shows a significant positive correlation (p < 0.001), though the lower correlation coefficient indicates that latitude does not explain all the variation in my data (Fig. 56, R^2 = 0.27).

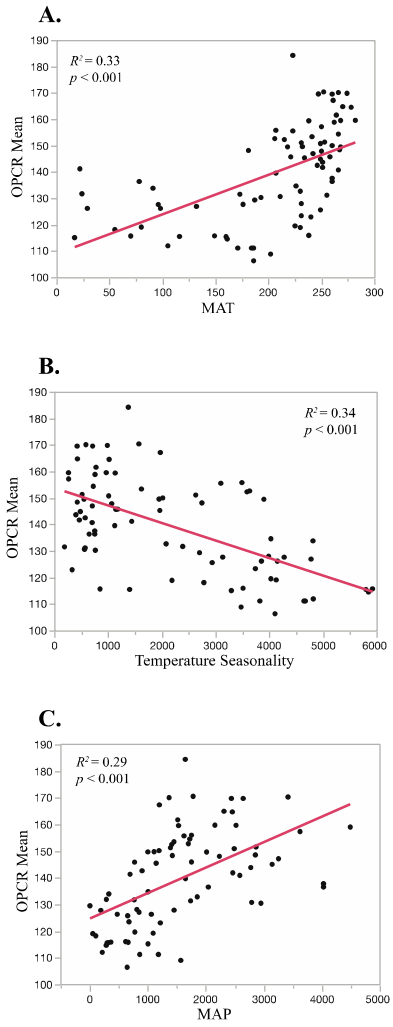

Figure 55: Bivariate plots of statistically significant relationships between OPCR mean and A) MAT; B) Temperature seasonality; and C) MAP.

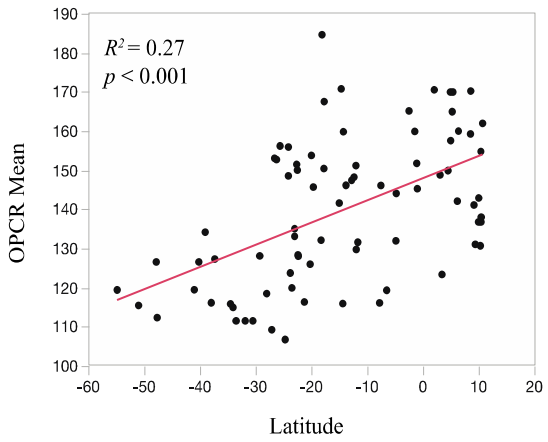

Figure 56: Linear regression of latitude and the mean of OPCR.

The range and CoV of a distribution are best discussed together, as both give different perspectives of the relative morphological disparity of a rodent community. This is because range is a proxy of the *maximum* disparity while CoV is a proxy of the *average* disparity. In this context, range and CoV of OPCR show us that the disparity of rodent occlusal complexity increases with MAT, MAP, NPP, and canopy height, and decreases with temperature seasonality (Tables 28, 29; Figures 57, 58). The only variable that OPCR disparity apparently does not correlate well with is precipitation seasonality.

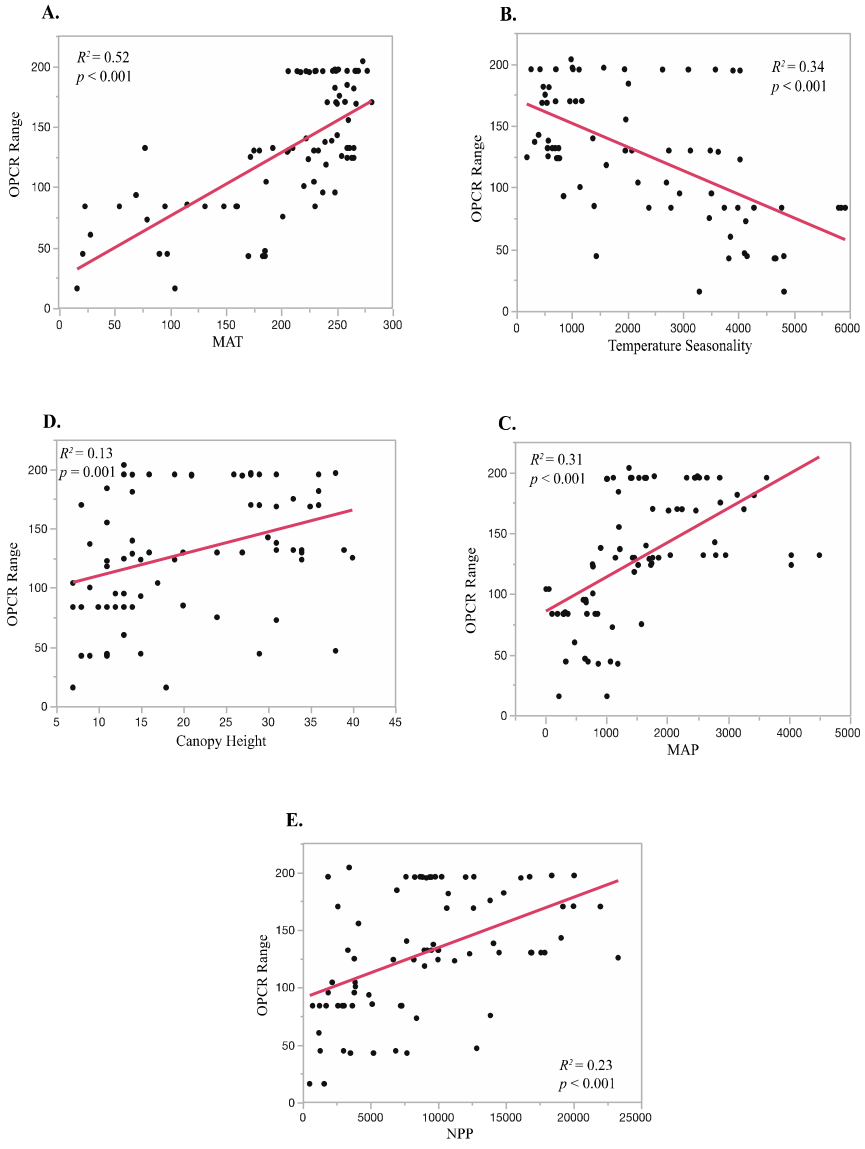

Figure 57: Bivariate plots of statistically significant relationships between OPCR mean and A) MAT; B) Temperature seasonality; C) MAP; D) Canopy height; and E) NPP.

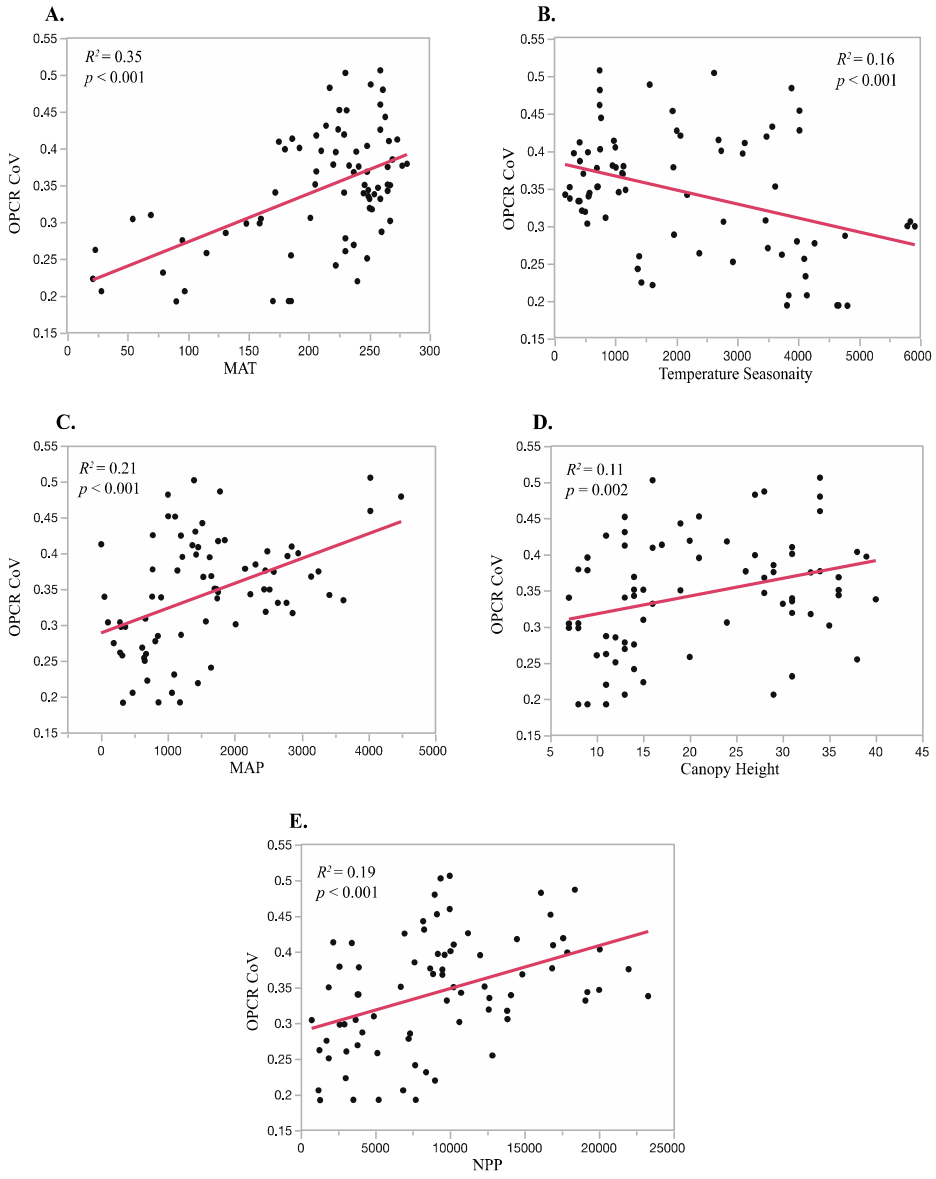

Figure 58: Bivariate plots of statistically significant relationships between OPCR coefficient of variation and A) MAT; B) Temperature seasonality; C) MAP; D) Canopy height; and E) NPP.

That I would find significant correlations in the context of OPCR distributions and climate but *not* in my dietary ecology analysis is likely indicative of one of two possibilities: 1) the results from the OPCR distributions are spurious; or 2) I failed to

detect a dietary signal in OPCR due to coarse data on diet in rodents. I introduced the first possibility in the discussion of DNE above, pointing to the fact that the small number of significant correlations associated with the distributions of DNE could be due to chance. However, the large number of significant correlations in association with OPCR, and the fact these correlations are consistent regardless of the type of distributions statistic analyzed, suggests that this is almost certainly not the case for OPCR. The more likely explanation is that OPCR does in fact have a relationship with diet that I was unable to pick up in my ecomorphological analysis. This latter explanation would seemingly provide support to the conclusions of Evans et al. (2007) and Evans and Jernvall (2009), but it is nevertheless intriguing that I was unable to find significant correlations despite using very similar dietary categories as these two studies. One reason for this may be that I have a much broader taxonomic sample than Evans et al. (2007), who sampled rodents only from the superfamily Muroidea, whereas I have representatives from three different suborders; Hystricomorpha (the caviomorphs in my sample), Sciuromorpha (the sciurids), and Myomorpha (the sigmodontine rats and mice). As discussed above, it may be that occlusal topography carries with it a strong phylogenetic signal. On the other hand, many of these rodent families are sympatric, and likely avoid competition through niche separation. This introduces the possibility that the phylogenetic signal and the ecological signal may be intertwined, as specific

families general adopt one niche over another (Wiens and Graham, 2005; Blomberg and Garland, 2002).

Regardless of what the ultimate mechanism may be, it is obvious that such studies as these would benefit greatly from more precise data on the diets of rodents. The plausibility of complete data on such small, typically nocturnal mammals is low, but even enough data to more precisely define appropriate dietary categories within rodents would give researchers the ability to study ecomorphology in a much more definitive way. The opportunistic nature of so many rodent species (Kay and Hoekstra, 2008) defies the broad dietary categories that are used in most dietary ecomorphological studies (including my own). Based on these distribution analyses, of the three dental topography metrics I present in this paper, OPCR seems the most likely candidate for a good discriminator of the dietary ecologies of rodents (however those might be defined). This would suggest that the enamel ridges and folds that distinguish rodent molars (Hillson, 1986) are adding complexity to the surface rather than sharpness (as measured by DNE). The lack of distinct differences in sharpness may be explained by the fact that tough food materials are being processed by the incisors (Croft et al., 2011).

Finally, a principal components analysis (PCA) of the 85 South American localities using the ranges, mean, and CoVs of DNE, RFI, and OPCR (Figure 59) illustrates the distribution statistics of OPCR (PC2) explain approximately 28.7% of the variance, while the distribution statistics of DNE and RFI together explain

approximately 30% of the variance. The distributions of OPCR are particularly effective at segregating the tropical localities (green diamonds)—i.e., localities within 23.43°N and 23.43°S latitude—and subtropical localities (red *x*'s). In fact, on the second component axis, those subtropical localities that cluster with the majority of the tropical localities are the five subtropical sites that have the highest mean annual precipitation and net primary productivity.

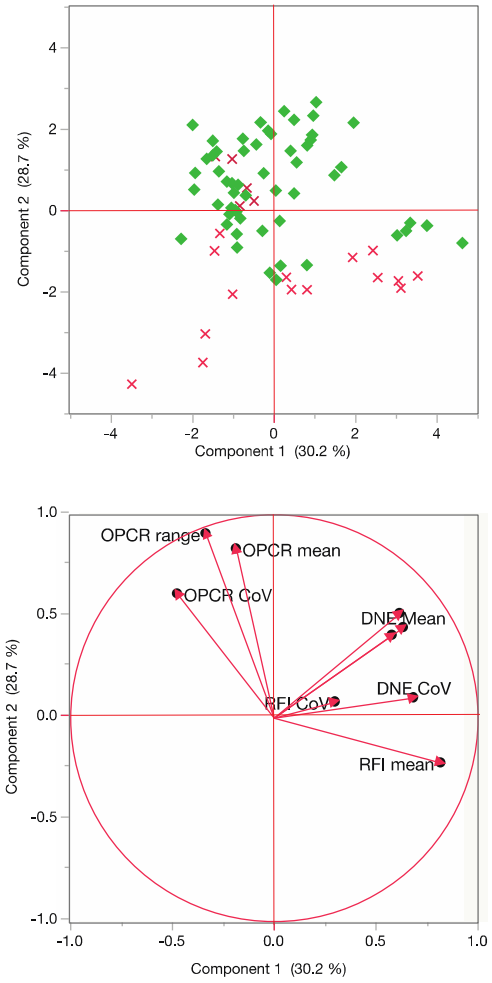

Figure 59: Principal components analysis (PCA) plot of the 85 South American localities segregated by the distribution statistics of DNE, RFI, and OPCR. Green diamonds represent localities located within the tropics (±23.43° latitude), and red *x*'s represent localities outside of the tropics.

5.4.2.4 Tropical Mammal Distributions

Finally, this rodent dataset allows us to segregate the localities in a way that I am unable to do with the marsupial data (Chapter 4). That is, there are enough localities in

this dataset to do analyses that are wholly confined to the tropics. After running analyses equivalent to those above in the wholly tropical dataset (and excluding sites of elevation >1500m), I find no significant correlations between distributions of any of the ecometrics and environment. This once again speaks to the generalist nature of rodents, suggesting that dietary niche is a much harder notion to define in rodents.

5.4.3 Combining Ecometrics and Regression Techniques

Rodents are near ubiquitous in mammalian fossil records for much of the Cenozoic after their appearance in the early Eocene (Antoine et al., 2011)—and there is particularly great potential in their use as environmental and climatic proxies (Montuire et al., 1997; Kay et al., 1999; Aguilar et al., 1999; Montuire et al., 2006). Another analysis that is made possible by the size of this rodent dataset is a revisit of the regression methods used in Chapter 2. For this purpose I include the means, ranges, and CoVs of DNE, RFI, and OPCR to estimate five bioclimate variables (all of the variables included in Chapter 2 except precipitation seasonality, which from my results clearly does not model well). The error metrics—mean absolute error (MAE) and root mean squared error (RMSE)—of these analyses are presented in Table 30 and the correlations of estimated values and actual observed values are illustrated in Figures 46-50.

In general, my results (Table 30) from using these distributions of dental topography are comparable to the results from Chapter 2 in which I use ecological indices of entire mammalian faunas, though the error terms are slightly higher for the

rodent distributions. Much like my findings in Chapter 2, the non-parametric regression methods—including regression tree analysis (RTA), random forests (RF), and Gaussian process regression (GPR)—show lower MAE and RMSE than the multivariate linear regression. This is reflected in the correlation coefficients of estimated vs. observed values. The two exceptions to the comparability of the results from rodent dental topography distributions and ecological indices are the high error terms for GPR for temperature seasonality and NPP. Because the output of GPR is not readily illustrated, it is difficult to explain these results, particularly because the other regression techniques do not show such high error.

That the use of rodent dental topography distributions performs approximately as well as a large number of ecological indices associated with entire mammalian faunas is remarkable. In the context of paleoenvironment reconstruction (the ultimate focus of this dissertation), using distributions of quantitative measurements taken directly from teeth would allow researchers to bypass the assumptions that have to be made in using ecological indices; namely that behavioral reconstructions of extinct species are accurate (e.g. Kay and Madden, 1997; Croft, 2001; Kay et al., 2012). This is not to say that such behavioral reconstructions are misguided or poorly done, but they do nevertheless introduce a possible source of error, as well as delay paleoenvironmental reconstructions until every species has been studied.

5.5 Conclusions

Using three dental topography metrics of occlusal sharpness (Dirichlet normal energy; DNE), relief (relief index; RFI), and complexity (orientation patch count rotated; OPCR), and the natural log of molar area, I attempt to correlate dental topography of lower M_2s and dietary ecology in a broad taxonomic sample of South American rodents. My results from these analyses suggest that rodent dental topography is not generally a good discriminator of rodent diets, as phylogenetically-corrected ANOVAs reveal no statistically significant relationships. However, post-hoc tests reveal some noteworthy trends in my sample when corrected for the effects of phylogeny:

1. Grazing rodents tend to have much higher dental relief (mean RFI = 0.69) relative to rodents inhabiting other ecological niches ($p < 0.001$).
2. Herbivorous rodent species—frugivores, folivores, and grazers—tend towards higher DNE values than more omnivorous species. Visual inspection of these molars suggests that this increase in sharpness is being driven by the presence of long ridges of enamel on the occlusal surface relative to the more omnivorous species in my sample.

A discriminant function analysis also reveals that using all three metrics in conjunction with the natural log of molar area results in a predictive model that performs significantly better than chance.

I also include a correlative analysis of the distributions of these metrics across a large number of localities in South America, specifically with regard to a number of variables associated with climate and habitat. This analysis reveals that the distribution of OPCR has the strongest association with environment. I postulate that this signifies a potential ecological signal of OPCR that I was unable to detect in the ecomorphological analyses, though more precise dietary data is likely the only avenue to confirm this hypothesis. My results also indicate that disparity in rodent dental topography increases with wetter, warmer, more productive conditions. Finally, I also use the distribution statistics from this analysis in conjunction with sophisticated regression techniques—including machine-learning algorithms—to demonstrate that such distributions can be used in place of qualitative ecological indices, such as I use in Chapter 2.

6. Summary

Several important outcomes of this dissertation are:

1) I find that dental topography metrics are correlated with dietary ecology in small South American and Australian marsupial and rodent species, extending previous published findings for primates; and

2) When the distributions of the dental ecomorphology metrics are compiled for extant South American and Australian communities of rodents they provide a powerful proxy for climate and habitat.

The first finding is important because these orders were important contributors to mammalian faunal diversity in the Miocene of South America and therefore open a window for the study of extinct species. The value of the second finding is that the utilization of distributions of quantitative measurements obviates the need for precise reconstruction of behavior in extinct species, a potential source of error in any paleoecological analysis. As long as a measurement is demonstrated to be ecologically relevant, then the distribution of that measurement within a community of species can potentially be used as a summary of the ecological niches filled within a given ecosystem.

6.1 Summary of Results

In Chapter 2, I begin with a review of community-level paleoenvironment reconstruction using mammals and the various statistical approaches that have been employed to do so. Using data compiled from long-term field studies of extant small

South American and Australian/New Guinean marsupials and South American rodents, I compile a complete species-level dataset of non-volant mammals from 85 localities from across South America. Long-term field sites of relatively small size were preferred in this list for two reasons; 1) faunal lists compiled from overlapping species distribution maps were deemed to be too unreliable, particularly in the tropics of South America where regional species richness is extraordinarily high and demarcation of species ranges is poorly documented; and 2) short-term field studies may fail to observe rare species that are nonetheless important to the ecosystem. Both of these points are particularly problematic for small mammal species, which can be difficult to observe and study in the wild.

The ecologies of each species each faunal list were compiled and expressed as ecological indices to quantitatively describe the niche space of the community, i.e. the types and relative number of niches filled within any given community. Different niche measurements that may be related to the environment at that locality, include, for example, the relative number of arboreal species, frugivorous species, and grazing species, and the ratio of predators to prey species. Using these indices as my predictor variables and six bioclimatic variables—precipitation (MAP), temperature (MAT), temperature seasonality, precipitation seasonality, net primary productivity (NPP), canopy height—as my response variables, I produced a number of regression models from the South American communities. The regression techniques include machine-

learning algorithms—regression trees, random forests, and Gaussian process regression—that can allow non-linear relationships to be modeled more accurately. The models were based on the South American faunas. To test the general applicability of models derived from South American localities, I estimate climate variables in Australian and New Guinean localities. Australia/New Guinea was chosen as a test region because it represents a geographically and phylogenetically distinct region from South America that spans a similar range of latitude and a similarly broad ecological spectrum. My results indicate that ecological indices from the South American model can be used to estimate climate variables, and that the machine-learning algorithms are particularly powerful tools of analysis.

I conclude this chapter by applying the findings from the extant communities to the reconstruction of the bioclimatic variables in two particularly well known Miocene fossil communities in South America; the Middle Miocene 'Monkey Beds Fauna' of La Venta, Colombia and the Early Miocene Faunal Levels 1-7 in the Santa Cruz Formation of Argentina. My estimations are generally in line with previous paleoecological analyses of these two deposits. This represents the first time that such algorithms have been used for this purpose.

In Chapter 3, I lay a methodological foundation for the type of data collection and analysis I use in Chapters 4 and 5. This is because in Chapters 4 and 5, I examine the correlation between dental topography and dietary ecology utilizing three specific

metrics of dental topography; Dirichlet normal energy (DNE), orientation patch count rotated (OPCR), and relief index (RFI), each of which is taken from 3D meshes representing the occlusal surfaces of teeth. These 3D meshes are produced from microCT scans taken of skulls, mandibles, and/or epoxy dental casts, and the digitial preparation of these meshes—namely downsampling the number of faces that represent the surface and smoothing that surface—can have a significant impact on the values of these metrics. These effects have been previously studied in regards to both OPCR and RFI, but not as well in regards to DNE. Therefore, Chapter 3 presents a brief analysis of the effect of downsampling and smoothing—together termed "retriangulation"—on the measurement of DNE. As DNE is essentially a measure of the sharpness of a surface, smoothing in particular has the potential to drastically alter this measurement. Starting with a simple hemisphere, the easiest geometric shape on which to measure DNE, I test how retriangulation affects DNE values. My results indicate that the degree of smoothing is inversely related to the values of DNE, and that the inclusion of more 'aggressive' smoothing algorithms—as has been done in some previously published studies incorporating DNE—exacerbates this effect. Downsampling—i.e. decreasing the number of triangular faces used to represent the surface, a necessary step for computation—has a less dramatic effect, and my results suggest that a surface with 10,000 faces will have approximately the same DNE value as one with 20,000 or 30,000 faces. Given that current software programs are not typically able to handle surfaces of

20,000 or more faces, I propose that using 10,000 faces is a reasonable standard going forward as it represents a sufficient compromise between faithfulness of surface representation and computational speed. These conclusions guide my protocol decisions for the next two chapters.

In Chapter 4, I explore the relationship between the above-mentioned dental topography and the dietary ecology in South American and Australian/New Guinean marsupials. This chapter anticipates the application of my results to the pre-Interchange Miocene faunas of South America when marsupials were especially diverse and filled many niches now occupied by Carnivora. I employ a phylogenetically-corrected one-way ANOVA to test for the effect of diet on the mean values of DNE, OPCR, and RFI. Results from this test suggest that, after controlling for phylogeny, diet has a significant effect on DNE ($p < 0.01$). RFI has a correlation that is trending towards significance ($p = 0.036$, with a Bonferroni-corrected alpha level of 0.019). OPCR does not have a significant relationship with diet in my marsupial sample. Post-hoc tests suggest that frugivores have significantly lower values in DNE and RFI relative to other dietary categories. A discriminant function analysis correctly identified dietary groups at a rate of ~75%, and a principal components analysis suggests that M^2s with higher RFI and higher DNE are related to dietary ecologies associated with tougher food materials (particularly folivores and insectivores). Having demonstrated that dental topography is informative in marsupials' dietary ecology, I move on to compile the distributions of

dental topography metrics in faunas from across Australia and New Guinea. I calculate the mean, range, coefficient of variation, and skewness of the distribution of each metric in 17 marsupial faunas and correlate these statistics with the same six bioclimatic variables in Chapter 2. ANOVAs performed on these correlations revealed that the distributions of RFI had the most significant correlations with environment, including MAP, NPP, and canopy height. The mean and coefficient of variation of RFI together suggest that these results are associated with a greater number of arboreal frugivores in wetter, more productive habitats with taller canopies. This suggest that the distribution of a topographic measurement alone can give similar information as ecological indices.

In Chapter 5, I perform an equivalent analysis to Chapter 4, except with a taxonomically-broad sample of South American rodents, including caviomorphs (Rodentia: Hystricognathi: Caviomorpha), sciurids (Rodentia: Sciuromorpha: Sciuridae), and sigmodontines (Rodentia: Muroidea: Cricetidae). Rodents are especially specious on the South American continent—both in the Miocene and today—and the sample I present in Chapter 5 samples most of this diversity. For rodents, unlike for marsupials, DNE does not seem to correspond as well to dietary ecology in rodents. RFI is especially high in grazing species, but otherwise does not differentiate will between diets. Similar to the results in marsupials, OPCR does not seem to correlate well with diet. However, analyzing the distributions of these metrics across the South American localities presented in Chapter 2, we see that the distribution of OPCR has a surprisingly

significant association with environment. I believe that this likely reflects a dietary signal in OPCR that is lost in the necessarily coarse dietary categories (on account of the poor quality of dietary information) used in the rodent analyses. The large number of localities in this chapter also allowed me to use the machine-learning regression techniques I present in Chapter 2, and the error metrics associated with using rodent dental ecometrics in place of whole-fauna ecological indices are reasonably close to what I found with the ecological indices. I conclude this chapter by discussing the significance of using rodent dental topography distributions to reconstruct climate and habitat.

6.1.1 Conclusions

Viewing these results in concert, it is clear that community structure is at least in part driven by environment, and as such, the structure can be used to estimate specific aspects of the environment, now and in the past. This has been demonstrated in previous studies, though I demonstrate the power of machine-learning algorithms, which can minimize the error in these estimations. Random forests and Gaussian process regression models seem especially effective at minimizing error relative to other techniques. I also demonstrate that by utilizing ecologically relevant morphology—in this case dental topography—we can construct distributions that serve as useful proxies for the abundance and disparity of niches filled within a faunal system. The dental topography metrics that I utilize here—OPCR, DNE, and RFI—are particularly useful as they do not rely on the identification of homologous landmarks, and instead can

quantify whole tooth surfaces. This can allow paleoecologists to collect large amounts of useful data in extinct species that are frequently only represented by isolated teeth or jaws. While the scanning of surfaces can be time-consuming and costly, online archives of 3D surfaces are making data more readily available. This increases the feasibility of this kind of community-level analysis.

6.1.2 Species Sampling

As with any study, even a brief retrospective can elucidate the way my study design could be improved. An obvious place to begin would be with the sampling protocol of living faunas and dental specimens, as it would be ideal to 1) increase the number of specimens per species, to ensure that species averages are accurate representations of the true species mean; and 2) obtain a more complete sample of Australian/New Guinean marsupials and South American rodents. Though given the restrictions on time and resources the sample is fairly exhaustive, where are several major holes in the data set. For instance, I was unable to obtain any usable specimens of the rodent family Octodontidae, which is restricted to the southwest of the South American continent. This is in large part due to the difficulty in obtaining access to specimens of particularly rare species, as well as time and financial constraints related to CT scanning.

6.2 Future Directions

The obvious next step for this line of research is the application to the fossil record, namely the fossil localities that are mentioned explicitly throughout my chapters; La Venta and the Santa Cruz. This requires the scanning of the marsupial and rodent fossil teeth from these localities. While obtaining fossil specimens is frequently a difficult task, original specimens from these two localities are housed in several museums in the United States and readily accessible collections in Argentina, and there are a number of casts housed at Duke University. Given the results of Chapter 5, I would expect that the regressions using ecometric distributions as predictor variables should mirror those of regressions using ecological indices, and in turn mirror the conclusions of previous paleoecological analyses at these sites. However, this would serve as a valuable first application for this method beyond the proof-of-concept approach of this dissertation.

Related to this is the inclusion of other types of morphological data in the models for better representation of niche structure at a locality. One obvious approach is to measure morphologies associated with locomotion. A commonly preserved postcranial element in the fossil record is the calcaneus, and research has suggested that locomotion in mammals can be reconstructed using simple ratios of linear measurements in the calcaneus (Polly, 2010). Likewise, articular facets on the other ankle bone, the astragalus, can be used to represent body size more accurately than molar size (Yapuncich et al.,

2015). Ultimately, direct measurements of fossils can potential replace ecological indices entirely for the purposes of paleoenvironmental reconstruction.

Additionally, the inclusion of a similar analysis of primate distributions might provide the ability to discern finer scale differences in tropical habitats, as primates have their greatest species richness in the topics. Based on previously published data on the dental topography of primates, the easiest datasets to complete would be that for the platyrrhines—only the callitrichines have not been broadly sampled and I have already have geographic/climatic data for a good deal of faunas that include primates in South America—and/or the strepsirrhines of Madagascar.

Appendix A

Table 32: DNE values for hemispheres simplified to various face counts, and smoothed to different levels in Avizo, as well as calculated with different boundary exclusion criteria. Mesh face count is in bold in the left column. The "Leg" boundary exclusion criterion excludes all faces that have two vertices and an edge connecting them on the mesh boundary. The "Vertex" exclusion criterion excludes all faces that have even a single vertex on the mesh boundary (it is more exclusive, reflected in lower DNE values).

Smoothing Iterations	1		25		100	
Boundary Exclusion	Leg	Vertex	Leg	Vertex	Leg	Vertex
500	10.2462	9.3459	10.7988	9.9720	11.5960	10.6911
1000	11.6354	11.1188	12.5868	12.1064	13.5977	12.8162
5000	11.9546	11.6225	12.9009	12.5256	13.3549	12.9423
10000	12.2270	11.9913	13.0097	12.7128	13.6772	13.2050
20000	12.4059	12.2439	13.0528	12.8744	13.5266	13.2442
30000	12.4275	12.2930	12.9532	12.8017	13.4076	13.1022
40000	12.4404	12.3264	12.8617	12.7073	13.5870	12.9898
50000	12.5123	12.4144	13.6044	12.9423	15.5489	13.3314
62500	12.5528	12.4555	13.7332	13.1921	15.3250	13.7265
75000	12.5349	12.4401	13.4700	13.1583	14.6243	13.6457
87500	12.5989	12.5099	13.8544	13.4370	15.0107	13.9673

Appendix B

Gaussian process regression (GPR) is a non-linear, non-parametric, Bayesian regression technique. Originally developed as "kriging" in the field of geostatistics, GPR has not seen wide application in ecology or paleoecology (Golding, 2016), but is nonetheless useful in these applications because of its expressiveness and flexibility.

GPR can be viewed as an extension of simple linear regression.

Equation 2

$$f(x) = x^{\intercal}w, \;\; y = f(x) + \varepsilon$$

Here, $x^{T}w$ is a dot product between a transposed vector of dependent variables, x^{T}, and their associated weights, w. The error term ε is modeled as a Gaussian distribution. Thus, the likelihood function (i.e., fit of model to the data given the weights) is given as:

Equation 3

$$p(y|X, w) = \prod_{i=1}^{n} p(y_i|x_i, w), \;\; y_i \sim N(x_i^{\intercal}w, \sigma_{\varepsilon})$$

where σ_{ε} is the variance of the error term.

Further, the distribution of the linear regression coefficients or weights (**w**) is given a multivariate Gaussian distribution:

Equation 4

$$w \sim N(0, \Sigma_Q)$$

where $\mathbf{\Sigma}_Q$ is the covariance matrix of the weights. This prior distribution over the weights also leads to an interpretation of Gaussian processes as specifying a distribution over functions. Each function represents a Gaussian distribution centered at the input point—in this case at zero because the distribution is z-transformed—with all of these functions having a joint Gaussian distribution. Due to the tractability of computing integrals of the Gaussian distribution, the posterior and predictive distributions have closed-form solutions (i.e., solvable real numbers), as shown in Rasmussen (2006).

This Bayesian linear regression model is the basis for Gaussian process regression, but is limited by the inflexibility of the linear model. To overcome this limitation, the predictors are projected into "feature space" using a non-linear function (denoted by $\phi(x)$) $\phi(x)$). A simple example is the polynomial expansion, which projects a 1D vector x into a 3D vector:

$$\phi(x) = [x, x^2, x^3]$$

In the case of Gaussian processes, the projection functions are always used in the context of dot-products (known formally as inner-products). For example, the following expression, which is derived in Rasmussen (2006), is a dot product of a projection function $\phi(x)$ and a covariance matrix $\mathbf{\Sigma}_Q$:

Equation 5

$$\phi(x)^{\intercal}\Sigma_p\phi(x)$$

The use of projection functions in dot products allows the use of the "kernel trick" to replace the projection function. This common operation in machine learning models, stemming from Mercer's theorem (Mercer, 1909), allows projection functions in inner products to be represented by a covariance function. Thus, the complex projection function into feature space does not have to be explicitly calculated. Instead one can operate only on a function that represents the covariance between two points projected into the feature space. This allows significantly more complex, non-linear interactions between predictors to be represented in the model, using only a computationally simple covariance function.

The Gaussian radial basis function is a commonly used kernel (Chang, 2010) that is derived from the Gaussian distribution. It has a single parameter *sigma* that controls the smoothness of the resulting regression function. Additionally, the ANOVA kernel was tested. This kernel was selected based on results from Stitson et al. (1999) showing good performance on a similar multivariate regression problem. The ANOVA kernel has two parameters that can be tuned, *sigma* and *degree*. While harder to interpret than the single *sigma* parameter of the Gaussian radial basis function, these parameters roughly control the smoothness and magnitude of the regression function, respectively.

Appendix C

Table 33: Ecological information for marsupial and rodent species included in Chapters 4 and 5, respectively. References for information are also included. Body size categories correspond as follows: I= 10-100g; II=100g-1kg; III=1-10kg; IV= 10-100kg.

Species	Diet	Locomotion	Body Size Category	Reference
Abrothrix jelskii	PDO	Arboreal	I	Alhajeri, 2014
Akodon aerosus	PDO	Small Terrestrial	I	Alhajeri, 2014
Akodon mollis	PDO	Small Terrestrial	I	Myers & Patton, 1989
Akodon orophilus	PDO	Small Terrestrial	I	As for genus
Akodon subfuscus	PDO	Small Terrestrial	I	Solari, 2007
Akodon torques	PDO	Small Terrestrial	I	Solari, 2007
Cavia tschudii	Grass	Small terrestrial	II	Redford & Eisenberg, 1992; as for genus
Clyomys laticeps	PDO	Semi-fossorial	II	Nowak, 1991; Redford & Eisenberg; 1992; Kay & Madden, 1997
Coendou prehensilis	Folivore	Arboreal	III	Emmons & Feer, 1997
Coendou rothschildi	Folivore	Arboreal	III	Eisenberg, 1989
Cuniculus paca	Frugivore	Large Terrestrial	III	Emmons & Feer, 1997
Dactylomys dactylinus	Folivore	Arboreal	II	Emmons & Feer, 1997; Emmons, 1981
Dasyprocta	Frugivore	Large	III	Emmons & Feer,

fuliginosa		Terrestrial		1997
Dasyprocta punctata	Frugivore	Large Terrestrial	III	Emmons & Feer, 1997
Diplomys labilis	Frugivore	Arboreal	II	Eisenberg & Redford, 1999
Dolichotis salinicola	Grass	Large Terrestrial	III	Redford & Eisenberg, 1992; Ojeda & Mares, 1989
Galea musteloides	Grass	Small Terrestrial	II	Nowak, 1991; Redford & Eisenberg, 1992; Ojeda & Mares, 1989
Galea spixii	Grass	Small Terrestrial	II	Mares et al., 1981
Heteromys anomalus	PDO	Small Terrestrial	I	Emmons & Feer, 1997; Eisenberg et al., 1979
Holochilus brasiliensis	PDO	Semi-aquatic	II	Redford & Eisenberg, 1992; Ojeda & Mares, 1989
Hoplomys gymnurus	Frugivore	Small Terrestrial	II	Eisenberg & Redford, 1999
Ichthyomys hydrobates	ADO	Semi-aquatic	II	Voss, 1988; as for genus
Kunsia tomentosus	ADO	Small Terrestrial	II	Alhajeri, 2014
Lagidium peruanum	Grass	Large Terrestrial	III	Eisenberg & Redford, 1999
Makalata didelphoides	Frugivore	Scansorial	II	Nowak, 1991; as for genus
Mesomys hispidus	PDO	Arboreal	II	Emmons & Feer, 1997
Microsciurus flaviventer	ADO	Arboreal	I	Emmons & Feer, 1997
Myoprocta acouchy	PDO	Large Terrestrial	III	Emmons & Feer, 1997

Neacomys spinosus	PDO	Small Terrestrial	I	Emmons & Feer, 1997; Alho, 1982
Nectomys squamipes	ADO	Semi-aquatic	II	Redford & Eisenberg, 1992
Oecomys superans	PDO	Scansorial	I	Janson & Emmons, 1990
Oligoryzomys arenalis	ADO	Small Terrestrial	I	Patton et al., 2015
Oligoryzomys chacoensis	ADO	Scansorial	I	Patton et al., 2015
Oligoryzomys destructor	ADO	Scansorial	I	As for genus
Oligoryzomys fulvescens	ADO	Scansorial	I	As for genus
Oligoryzomys microtis	ADO	Scansorial	I	Redford & Eisenberg, 1992
Oryzomys albigularis	ADO	Small Terrestrial	I	Patton et al., 2015
Oryzomys auriventer	PDO	Small Terrestrial	I	As for genus
Oryzomys keaysi	ADO	Small Terrestrial	I	Alhajeri, 2014
Oryzomys nitidus	PDO	Small Terrestrial	II	Galetti et al., 2016
Oryzomys xanthaeolus	PDO	Small Terrestrial	I	Alhajeri, 2014
Phyllotis xanthopygus	PDO	Small Terrestrial	I	Alhajeri, 2014
Proechimys brevicauda	PDO	Small Terrestrial	II	Janson & Emmons, 1990
Proechimys cuvieri	PDO	Small Terrestrial	II	Eisenberg & Redford, 1999
Proechimys guairae	PDO	Small Terrestrial	II	As for genus
Proechimys semispinosus	PDO	Small Terrestrial	II	Eisenberg & Redford, 1999
Proechimys simonsi	PDO	Small Terrestrial	II	Janson & Emmons, 1990
Sciurus granatensis	PDO	Scansorial	II	Emmons & Feer, 1997

Sciurus ignitus	PDO	Scansorial	II	Emmons & Feer, 1997
Sciurus igniventris	PDO	Scansorial	II	Emmons & Feer, 1997
Sciurus spadiceus	PDO	Scansorial	II	Emmons & Feer, 1997
Sciurus stramineus	PDO	Arboreal	II	Merrick et al., 2012
Thomasomys aureus	ADO	Scansorial	I	Alhajeri, 2014
Thomasomys cinereus	ADO	Scansorial	I	Eisenberg & Redford, 1999
Thrichomys apereoides	PDO	Scansorial	II	Nowak, 1991
Zygodontomys brevicauda	PDO	Small Terrestrial	I	Eisenberg, 1989; Fleming, 1970
Acrobates pygmaeus	Frugivore	Gliding	I	Strahan, 1995
Aepyprymnus rufescens	Browsing	Large Terrestrial	III	Strahan, 1995
Antechinus minimus	Insectivore	Small Terrestrial	II	Strahan, 1995
Bettongia gaimardi	Browsing	Large Terrestrial	III	Strahan, 1995
Caenolestes fuliginosus	Insectivore	Small Terrestrial	I	Eisenberg, 1989
Caluromys derbianus	Frugivore	Arboreal	II	Eisenberg, 1989
Caluromys lanatus	Frugivore	Arboreal	II	Emmons & Feer, 1990
Cercartetus caudatus	Frugivore	Arboreal	I	Strahan, 1995
Chironectes minimus	Faunivore	Semi-Aquatic	II	Redford & Eisenberg, 1992
Dactylopsila palpator	Insectivore	Arboreal	II	Strahan, 1995
Dactylopsila trivirgata	Insectivore	Arboreal	II	Strahan, 1995

Dasykaluta rosamondae	Insectivore	Small Terrestrial	I	Flannery, 1995
Dasyurus hallucatus	Insectivore	Scansorial	II	Strahan, 1995
Dendrolagus lumholtzi	Folivore	Scansorial	III	Strahan, 1995
Didelphis albiventris	Frugivore	Scansorial	III	Emmons & Feer, 1997; Ojeda & Mares, 1989
Dorcopsis hageni	Browsing	Large Terrestrial	III	Flannery, 1995
Dorcopsis luctuosa	Browsing	Large Terrestrial	III	Flannery, 1995
Dorcopsulus macleayi	Browsing	Large Terrestrial	III	Flannery, 1995
Dromiciops gliroides	Insectivore	Arboreal	I	Fonturbel et al., 2012
Hemibelideus lemuroides	Folivore	Arboreal	II	Strahan, 1995
Hypsiprymnodon moschatus	Frugivore	Small Terrestrial	II	Strahan, 1995
Isoodon obesulus	Insectivore	Small Terrestrial	II	Strahan, 1995
Macrotis lagotis	Omnivore	Semi-Fossorial	III	Strahan, 1995
Marmosa mexicana	Insectivore	Scansorial	I	Emmons & Feer, 1997
Marmosa murina	Insectivore	Arboreal	I	Emmons & Feer, 1997
Metachirus nudicaudatus	Insectivore	Small Terrestrial	II	Emmons & Feer, 1997; Redford & Eisenberg, 1992
Monodelphis domestica	Insectivore	Small Terrestrial	I	Emmons & Feer, 1997; Redford & Eisenberg, 1992; Streilein, 1982
Peroryctes raffrayana	Insectivore	Small Terrestrial	II	Flannery, 1995
Petauroides	Folivore		III	Strahan, 1995

volans		Gliding		
Petaurus australis	Frugivore	Gliding	II	Strahan, 1995
Petaurus breviceps	Frugivore	Gliding	II	Strahan, 1995
Petropseudes dahli	Folivore	Large Terrestrial	III	Strahan, 1995
Phalanger gymnotis	Frugivore	Scansorial	III	Flannery, 1995
Phalanger mimicus	Frugivore	Arboreal	III	Flannery, 1995
Phalanger orientalis	Frugivore	Arboreal	III	Flannery, 1995
Phascolarctos cinereus	Folivore	Arboreal	III	Strahan, 1995
Potorous tridactylus	Folivore	Large Terrestrial	III	Strahan, 1995
Pseudocheirus peregrinus	Folivore	Arboreal	II	Strahan, 1995
Pseudochirops archeri	Folivore	Arboreal	III	Strahan, 1995
Pseudochirulus larvatus	Folivore	Arboreal	II	Flannery, 1995
Sarcophilus harrisii	Faunivore	Large Terrestrial	III	Strahan, 1995
Setonix brachyurus	Browsing	Large Terrestrial	III	Strahan, 1995
Sminthopsis crassicaudata	Insectivore	Small Terrestrial	I	Strahan, 1995
Spilocuscus maculatus	Frugivore	Scansorial	III	Flannery, 1995
Strigocuscus pelengensis	Frugivore	Scansorial	III	Flannery, 1995
Thylamys elegans	Insectivore	Arboreal	I	Ojeda & Mares, 1989
Thylogale stigmatica	Folivore	Large Terrestrial	III	Strahan, 1995
Trichosurus vulpecula	Frugivore	Scansorial	III	Strahan, 1995

Vombatus ursinus	Browsing	Large Terrestrial	IV	Strahan, 1995
Wallabia bicolor	Browsing	Large Terrestrial	IV	Strahan, 1995
Wyulda squamicaudata	Folivore	Scansorial	III	Strahan, 1995

References

Aguilar J-P, Escarguel G, and Michaux J. 1999. A succession of Miocene rodent assemblages from fissure fillings in southern France: palaeoenvironmental interpretation and comparison with Spain. Palaeogeography, Palaeoclimatology, Palaeoecology 145: 215-230.

Aizen MA and Ezcurra C. 1998. High incidence of plant-animal mutualisms in the woody flora of the temperate forest of southern South America: biogeographical origin and present ecological significance. Ecologica Austral 8: 217-236.

Alhajeri B. 2014. Adaptation, Diversification, and Desert Ecology of the Most Diverse Order of Mammals (Mammalia, Rodentia). *Electronic Theses, Treatises and Dissertations*. Paper 8930.

Alho CJR. 1982. Brazilian rodents: their habitats and habits. Pymatuning Laboratory of Ecology, University of Pittsburgh Special Publication Series 6: 143-166.

Allen KL, Cooke SB, Gonzales LA, and Kay, RF. 2015. Dietary inference from upper and lower molar morphology in platyrrhine primates. PloS ONE 10(3): e0118732.

Andrews P, Lord JM, and Nesbit-Evans EM. 1979. Patterns of ecological diversity in fossil and modern mammalian faunas. Biological Journal of the Linnean Society 11:177-205.

Andrews P and Hixson H. 2014. Taxon-free methods of palaeoecology. Annales Zoologici Fennici: 269-284.

Andrews P and O'Brien EM. 2000. Climate, vegetation, and predictable gradients in mammal species richness in southern Africa. Journal of Zoology 251:205-231.

Andrews P and Van Couvering JAH. 1975. Palaeoenvironments in the East African Miocene. Approaches to Primate Paleobiology 5: 62-103.

Anthony MRL, and Kay RF. 1993. Tooth form and diet in ateline and alouattine primates: reflections on the comparative method. American Journal of Science 283A:356-382.

Antoine PO, Marivaux L, Croft DA, Billet G, Ganerød M, Jaramillo C, Martin T, Orliac MJ, Tejada J, Altamirano AJ, and Duranthon F. 2011. Middle Eocene rodents from Peruvian Amazonia reveal the pattern and timing of caviomorph origins and biogeography. Proceedings of the Royal Society: Biological Sciences: 279(1732): 1319-1326.

Ashby M. 1992. *Materials selection in mechanical design*. Oxford: Pregamon Press.

Ashton KG, Tracy MC, and de Queiroz A. 2000. Is Bergmann's rule valid for mammals?. The American Naturalist 156(4): 390-415.

Barke R and Lamb S. 2006. Late Cenozoic uplift of the Eastern Cordillera, Bolivian Andes. Earth and Planetary Science Letters 249: 350-367.

Beard KC, Tong Y, Dawson MR, Wang J, and Huang X. 1996. Earliest complete dentition of an anthropoid primate from the Late Middle Eocene of Shanxi Province, China. Science 272: 82-85.

Behrensmeyer AK. 1982. Time resolution in fluvial vertebrate assemblages. Paleobiology 8(3): 211-227.

Behrensmeyer AK and Dechant-Boaz DE. The recent bones of Amboseli Park, Kenya, in relation to East African paleoecology. *Fossils in the making: vertebrate taphonomy and paleoecology*, pp. 72-92. University of Chicago Press, Chicago.

Behrensmeyer AK, Hook RW, Badgley CE, Boy JA, Chapman RE, Dodson P, Gastaldo RA, Graham RW, Martin LD, Olsen PE, and Spicer RA. 1992. Paleoenvironmental contexts and taphonomic nodes. In *Terrestrial ecosystems through time: evolutionary paleoecology of terrestrial plants and animals*, pp. 15-136. University of Chicago Press.

Berthaume MA. 2016. Food mechanical properties and dietary ecology. American Journal of Physical Anthropology 159: S79-S104.

Black CC. 1963. A review of the North American Tertiary Sciuridae. Museum of Comparative Zoology, Harvard Univesity Bulletin 130(3): 305-322.

Blackburn TM, Gaston KJ, and Loder N. 1999. Geographic gradients in body size: a clarification of Bergmann's rule. Diversity and Distributions 5(4): 165-174.

Blomberg SP and Garland T. 2002. Tempo and mode in evolution: phylogenetic inertia, adaptation and comparative methods. Journal of Evolutionary Biology 15(6): 899-910.

Borcard D, Gillet F, and Legendre P. 2011. *Numerical Ecology With R*, pp. 232-236.

Boyer DM. 2008. Relief Index of second mandibular molars is a correlate of diet among prosimian primates and other euarchontan mammals. Journal of Human Evolution 55:1118-1137.

Boyer DM, Seiffert ER, Gladman JT, and Bloch JI. 2013. Evolution and allometry of calcaneal elongation in living and extinct primates. PloS one 8(7):e67792.

Brieman L. 2001. Random forests. Machine Learning 45(1): 5-32.

Bunn JM, Boyer DM, Lipman Y, St. Clair EM, Jernvall J, and Daubechies I. 2011. Comparing Dirichlet normal surface energy of tooth crowns, a new technique of moalr shape quantification for dietary inference, with previous methods in isolation and in combination. American Journal of Physical Anthropology 145: 247-261.

Bunn JM, Ungar PS. 2009. Dental topography and diets of four old world monkey species. American Journal of Primatology 71:466–477.

Cartelle C and Hartwig WC. 1996. A new extinct primate among the Pleistocene megafauna of Bahia, Brazil. Proceedings of the National Academy of Sciences USA 93: 6405-6409.

Cartmill M. 1974. *Daubentonia, Dactylopsila,* woodpeckers and klinorhynchy. In *Prosimian Biology* (Martin RD, Doyle GA, Walker AC, eds.). Gerald Duckworth and Co. Ltd., London, pp. 655-670.

Cerling TE, Wynn JG, Andanje SA, Bird MI, Korir DK, Levin NE, Mace W, Macharia AN, Quade J, and Remien CH. 2011. Woody cover and hominin environments in the past 6 million years. Nature 476: 51-56.

Chai T and Draxler RR. 2014. Root mean squared error (RMSE) or mean absolute error (MAE)?—Arguments against avoiding RMSE in the literature. Geoscientific Model Development 7: 1247-1250.

Chang YW, Hsieh CJ, Chang KW, Ringgaard M, and Lin CJ. 2010. Training and testing low-degree Polynomial Data Mappings via Linear SVM. Journal of Machine Learning Research 1471-1490.

Cheverud JM. 2001. A simple correction for multiple comparisons in interval mapping genome scans. Heredity 87: 52-58.

Chew AE. 2009. Paleoecology of the early Eocene Willwood mammal fauna from the central Bighorn Basin, Wyoming. Paleobiology 35(1): 13-31.

Chornogubsky L, Goin FJ, and Reguero M. 2009. A reassessment of Antarctic polydolopid marsupials (middle Eocene, La Meseta Formation). Antarctic Science 21(3): 285-297.

Churchfield S. 1990. *The natural history of shrews*. Cornell University Press.

Coley PD and Barone JA. 1996. Herbivory and plant defenses in tropical forests. Annual Review of Ecology and Systematics 27: 305-335.

Colles A, Liow LH, and Prinzing A. 2009. Are specialists at risk under environmental change? Neoecological, paleoecological and phylogenetic approaches. Ecology Letters 12: 849-863.

Copes LE, Lucas LM, Thostenson JO, Hoekstra HE, and Boyer DM. 2016. A collection of non-human primate computed tomography scans housed in MorphoSource, a repository for 3D data. *Scientific Data* 3.

Conroy GC. 1987. Problems of body-weight estimation in fossil primates. International Journal of Primatology 8(2): 115-137.

Croft DA. 2001. Cenozoic environmental change in South America as indicated by mammalian body size distributions (cenograms). Diversity and Distributions 7: 271-287.

Croft DA. 2013. What constitutes a fossil mammal community in the early Miocene Santa Cruz Formation?. Journal of Vertebrate Paleontology 33(2): 401-409.

Croft DA, Niemi K, and Franco A. 2011. Incisor morphology reflects diet in caviomorph rodents. Journal of Mammalogy 92(4): 871-879.

Crompton AW. 1971. The origin of the tribosphenic molar. Early Mammals 50: 65-87.

Crompton AW, and Lumsden AGS. 1970. Functional significance of the therian molar pattern. Nature 227:197-199.

Cutler DR, Edwards TC, Beard KH, Cutler A, Hess KT, Gibson J, and Lawler JJ. 2007. Random forests for classification in ecology. Ecology 88(11): 2783-2792.

Dagosto M and Terranova CJ. 1992. Estimating the body size of Eocene primates: a comparison of results from dental postcranial variables. International Journal of Primatology 13(3): 307-344.

Damuth J. 1982. Analysis of the preservation of community structure in assemblages of fossil mammals. Paleobiology 8(4): 434-446.

Damuth JD, Jablonski D, Harris JA, Potts R, Stucky RK, Sues HD, and Weishampel DB. 1992. Taxon-free characterization of animal communities. In *Terrestrial ecosystems through time: evolutionary paleoecology of terrestrial plants and animals*, pp. 183-203.

Damuth JD and Janis CM. 2011. On the relationship between hypsodonty and feeding ecology in ungulate mammals, and its utility in palaeoecology. Biological Reviews 86(3): 733-758.

Danell K, Lundberg P, and Niemela P. 1996. Species richness in mammalian herbivores: patterns in the boreal zone. Ecography 19:404-409.

Darwin C. 1859. The Origin of Species, Sixth Edition (1872). London: reprinted by D. Appleton and Company.

De'ath G. 2002. Multivariate regression trees: a new technique for modeling species-environment relationships. Ecology 83(4): 1105-1117.

De'ath G and Fabricius KE. 2000. Classification and regression trees: a powerful yet simple technique for ecological data analysis. Ecology 81(11): 3178-3192.

Desbrun M, Meyer M, Schröder P, and Burr AH. 1999. Implicit fairing of irregular meshes using diffusion and curvature flow. SIGGRAPH 99 (Conf. Proc.): 317-324.

Dennis JC, Ungar PS, Teaford MF, and Glander KE. 2004. Dental topography and molar wear in *Alouatta palliata* from Costa Rica. American Journal of Physical Anthropology 125: 152-161.

Dunning J, Stewart D, Danielson B, Noon B, Root T, Lamberson R, and Stevens E. 1995. Spatially explicit population models: current forms and future uses. Ecological Applications 5: 3-11.

Duque-Caro H. 1990. Neogene stratigraphy, paleoceanography and paleobiogeography in northwest South America and the evolution of the Panama Seaway. Palaeogeography, Palaeoclimatology, Palaeoecology 77: 203-234.

Eisenberg JF. 1989. *Mammals of the Neotropics, vol. 1. The northern neotropics: Panama, Colombia, Venezuela, Guyana, Suriname, French Guiana.* The University of Chicago Press: London.

Eisenberg JF, O'Connell MA, and August PV. 1979. Density, productivity, and distribution of mammals in two Venezuelan habitats. In *Vertebrate ecology in the northern Neotropics* (JF Eisenberg, ed.), Smithsonian Institute Press: Washington, D.C. pp. 187-207.

Eisenberg JF and Redford KH. 1999. *Mammals of the Neotropics, vol. 2. The central Neotropics: Ecuador, Peru, Bolivia, Brazil.* The University of Chicago Press: London.

Elton CS. 2001. *Animal Ecology*. University of Chicago Press: Chicago, IL.

Emmons LH. 1981. Morphological, ecological, and behavioral adaptations for arboreal browsing in *Dactylomys dactylinus* (Rodentia, Echimyidae). Journal of Mammalogy 62(1): 183-189.

Emmons LH and Feer F. 1997. Neotropical rainforest mammals. *A field guide, 2.*

Engel SR, Hogan KM, Taylor JF, and Davis SK. 1998. Molecular systematics and paleobiogeography of the South American sigmodontine rodents. Molecular Biology and Evolution 15(1): 35-49.

Eronen JT, Polly PD, Fred M, Damuth J, Frank DC, Mosbrugger V, Scheidegger C, Stenseth NC, and Fortelius M. 2010a. Ecometrics: the traits that bind the past and present together. Integrative zoology 5(2): 88-101.

Eronen JT, Puolamäki K, Liu L, Lintulaakso K, Damuth J, Janis CM, and Fortelius M. 2010b. Precipitation and large herbivorous mammals II: application to fossil data. Evolutionary Ecology Research 12(2): 235-248.

Evans AR and Janis CM. 2014. The evolution of high dental complexity in the horse lineage. Annales Zoologici Fennici 51: 73-79.

Evans AR and Jernvall J. 2009. Patterns and constraints in carnivorans and rodent dental complexity and tooth size. Journal of Vertebrate Paleontology 29: 92.

Evans AR and Sanson GD. 2003. The tooth of perfection: functional and spatial constraints on mammalian tooth shape. Biological Journal of the Linnean Society 78: 173-191.

Evans AR, Wilson GP, Fortelius M, and Jernvall J. 2007. High-level similarity of dentitions in carnivorans and rodents. Nature 445: 78-81.

Feldkamp LA, Davis LC, and Kress JW. 1984. Practical cone-beam algorithm. Journal of the Optical Society of America A 1(6): 612-619.

Flannery TF. 1995. *Mammals of New Guinea*. Reed, 1995.

Fleming TH. 1970. Notes on the rodent faunas of two Panamanian forests. Journal of Mammalogy 51(3): 473-490.

Fleming TH. 1973. Numbers of mammalian species in north and central american forest communities. Ecology 54:555-563.

Flessa KW, Cutler AH, and Meldahl KH. 1993. Time and taphonomy: quantitative estimates of time-averaging and stratigraphic disorder in a shallow marine habitat. Paleobiology 19(2): 266-286.

Flynn JJ, Guerrero J, and Swisher CC. 1996. Geochronology of the Honda Group. In *Vertebrate Paleontology in the Neotropics: The Miocene Fauna of La Venta, Colombia* (Kay RF, Madden RH, Cifelli RL, and Flynn JJ, eds.). Smithsonian Institution Press: Washington, D.C.

Foote M. 1992. Rarefaction analysis of morphological and taxonomic diversity. Paleobiology 18(1): 1-16.

Fonturbel FE, Franco M, Rodriguez-Cabal MA, Rivarola MD, and Amico GC. 2012. Ecological consistency across space: a synthesis of the ecological aspects of *Dromiciops gliroides* in Argentina and Chile. Naturwissenschaften 99(11): 873-881.

Fortelius M. 1985. Ungulate cheek teeth: Developmental, functional, and evolutionary interrelations. Acta Zoologica Fennica 180: 1-76.

Fortelius M, Eronen J, Jernvall J, Liu L, Pushkina D, Rinne J, Tesakov A, Vislobokova I, Zhang Z, and Zhou L. 2002. Fossil mammals resolve regional patterns of Eurasian climate change over 20 million years. Evolutionary Ecology Research 4(7): 1005-1016.

Fortelius M and Solounias N. 2000. Functional characterization of ungulate molars using the abrasion-attrition wear gradient: a new method for reconstructing paleodiets. American Museum Novitates: 1-36.

Fox RC. 1975. Molar structure and function in the early Cretaceous mammal *Pappotherium*: evolutionary implications for Mesozoic Theria. Canadian Journal of Earth Sciences 12: 412-442.

Futuyma DJ and Moreno G. 1988. The evolution of ecological specialization. *Annual Review of Ecological Systems* 19207-19233.

Galetti M, Rodarte RR, Neves CL, Moreira M, and Costa-Pereira R. 2016. Trophic niche differentiation in rodents and marsupials revealed by stable isotopes. PloS one 11(4): e0152494.

Gardner AL, ed. 2008. *Mammals of South America, volume 1: marsupials, xenarthrans, shrews, and bats.* Chicago: University of Chicago Press.

Genin FGS, Masters JC, and Ganzhorn JU. 2010. Gummivory in cheirogaleids: primitive retention or adaptation to hypervariable environments?. In *The Evolution of Exudativory in Primates*, Springer: New York. pp. 123-140.3.

Gingerich PD. 1974. Size variability of the teeth in living mammals and the diagnosis of closely related sympatric fossil species. Journal of Paleontology 48(5): 895-903.

Gingerich PD. 1977. Correlation of tooth size and body size in living hominoid primates, with a note on the relative brain size in *Aegyptopithecus* and *Proconsul*. American Journal of Physical Anthropology 47: 395-398.

Gingerich PD. 1989. *New earliest Wasatchian mammalian fauna from the Eocene of northwestern Wyoming: composition and diversity in a rarely sampled high-floodplain assemblage.* No. 56 GIN.

Gingerich PD, Smith BH, and Rosenberg K. 1982. Allometric scaling in the dentition of primates and prediction of body weight from tooth size in fossils. American Journal of Physical Anthropology 58: 81-100.

Golding N and Purse BV. 2016. Fast and flexible Bayesian species distribution modelling using Gaussian processes. Methods Ecol Evol, 7: 598–608.

Gould SJ. 1982. The Stinkstones of Oeningen. Natural History 91(6): 6-13.

Gould SJ. 1989. A developmental constraint in *Cerion*, with comments on the definition and interpretation of constraint in evolution. *Evolution* 43: 516-539.

Gould SJ. 1991. The disparity of Burgess Shale arthropod fauna and the limits of cladistic analysis: why we must strive to quantify morphospace. Paleobiology17(4): 411-423.

Gould SJ, and Lewontin RC. 1979. The spandrels of San Marco and the Panglossian paradigm: a critique of the adaptationist programme. Proceedings of the Royal Society of London B: Biological Sciences 205(1161):581-598.

Guerrero J. 1996. Stratigraphy, sedimentary environments, and the Miocene uplift of the Colombian Andes. In *Vertebrate Paleontology in the Neotropics: The Miocene Fauna of La Venta, Colombia* (Kay RF, Madden RH, Cifelli RL, and Flynn JJ, eds.). Smithsonian Institution Press: Washington, D.C.

Harrison JL. 1962. The distribution of feeding habits among animals in a tropical rain forest. Journal of Animal Ecology 34:53-64.

Hautier L and Cox PG. 2015. Rodentia: a model order?. In *Evolution of the Rodents Advances in Phylogeny, Functional Morphology and Development* (Cox PG and Hautier L, eds.). Cambridge University Press: Cambridge.

Hawkins BA, Field R, Cornell HV, Currie DJ, Guegan JF, Kaufman DM, Kerr JT, Mittelbach GG, Oberdorff T, O'Brien EM, Porter EE. Energy, water, and broad-scale geographic patterns of species richness. Ecology 84(12): 3105-3117.

Hayes JM, Freeman KH, Popp BN, and Hoham CH. 1990. Compound-specific isotopic analyses: a novel tool for reconstruction of ancient biogeochemical processes. *Organic Geochemistry* 16(4): 1115-1128.

Heck KL, van Belle G, and Simberloff D. 1975. Explicit calculation of the rarefaction diversity measurement and the determination of sufficient sample size. Ecology 56(6): 1459-1461.

Helgen KM. 2007. The mammal fauna of the Kaijende Highlands, Enga Province, Papua New Guinea. In *A Rapid Biodiversity Assessment of the Kaijende Highlands, Enga Province, Papua New Guinea*, pp. 52-68. Conservation International.

Hillson S. 1986. *Teeth*. Cambridge University Press: Cambridge.

Hoffman T, Schölkopf B, and Smola AJ. 2008. Kernel methods in machine learning. The Annals of Statistics: 1171-1220.

Hoorn C, Guerrero J, Sarmiento GA, and Lorente MA. 1995. Andean tectonics as a cause for changing drainage patterns in Miocene northern South America. Geology 23(5): 237-240.

Horton BK, Parra M, Saylor JE, Nie J, Mora A, Torres V, Stockli DF, and Strecker MR. 2010. Resolving uplift of the northern Andes using detrital zircon age signatures. GSA Today 20(7): 4-10.

Hummel J, Findeisen E, Sudekum K-H, Ruf I, Kaiser TM, Bucher M, Clauss M, and Codron D. 2011. Biological Sciences 278(1712): 1742-1747.

Hurlbert SH. 1971. The nonconcept of species diversity: a critique and alternative parameters. Ecology 52(4): 577-586.

Huston MA. 1994. *Biological diversity: the coexistence of species*. Cambridge University Press.

Hutchinson GE. 1965. *The ecological theater and the evolutionary play.* Yale University Press.

Iverson L and Prasad A. 1998. Estimating regional plant biodiversity with GIS modelling. Diversity and Distributions 4(2): 49-61.

Janis CM. 1988. An estimation of tooth volume and hypsodonty indices in ungulate mammals, and the correlation of these factors with dietary preference. In *Teeth Revisited: Proceedings of the VIIth International Symposium on Dental Morphology, Memoires du Museum national d'histoire Naturelle* (*Serie C*) *53* (Russell DE, Santoro JP, and Signogneau-Russell D, eds.). pp. 367-387. Editions du Museum: Paris.

Janis CM. 1993. Tertiary mammal evolution in the context of changing climates, vegetation, and tectonic events. Annual Review of Ecology and Systematics: 467-500.

Janis CM and Fortelius M. 1988. On the means whereby mammals achieve increased functional durability of their dentitions, with special reference to limiting factors. Biological Reviews 63(2): 197-230.

Janson CH and Emmons LH. 1990. Ecological structure of the nonflying mammal community at Cocha Cashu biological station, Manu National Park, Peru. *Four neotropical rainforests*: 314-338.

Jernvall J and Fortelius M. 2002. Common mammls drive the evolutionary increase of hypsodonty in the Neogene. Nature 417(6888): 538-540.

Jernvall J and Selanne L. 1999. Laser confocal microscopy and geographic information systems in the study of dental morphology. Palaeontologia Electronica 2: 1-18.

Karatzoglou A, Smola A, Hornik K, Zeileis Achim 2004. kernlab - An S4 Package for Kernel Methods in R. Journal of Statistical Software 11(9): 1-20.

Kassen R. 2002. The experimental evolution of specialists, generalists, and the maintenance of diversity. Evolutionary Biology 15(2): 173-190.

Kay EH and Hoekstra HE. 2008. Rodents. Current Biology 18(10): R406-R410.

Kay RF. 1975. The functional adaptations of primate molar teeth. American Journal of Physical Anthropology 43: 195-216.

Kay RF. 1977. The evolution of molar occlusion in the Cercopithecidae and early

early catarrhines. American Journal of Physical Anthropology 46: 327-352.

Kay RF and Cartmill M. 1977. Cranial morphology and adaptations of *Palaechthon nacimienti* and other Paromomyidae (Plesiadapoidea, ? Primates), with a description of a new genus and species. Journal of Human Evolution 6(1):19IN533-3253.

Kay RF and Covert HH. 1984. Anatomy and behaviour of extinct primates. In *Food acquisition and processing in primates*, pp. 467-508. Springer US.

Kay RF and Hiiemae KM. 1974. Jaw movement and tooth use in recent and fossil primates. American Journal of Physical Anthropology 40: 227-256.

Kay RF and Madden RH. 1996. Paleogeography and paleoecology. In *Vertebrate Paleontology in the Neotropics: The Miocene Fauna of La Venta, Colombia* (Kay RF, Madden RH, Cifelli RL, and Flynn JJ, eds.). Smithsonian Institution Press: Washington, D.C.

Kay RF and Madden RH. 1997. Mammals and rainfall: paleoecology of the middle Miocene at La Venta (Colombia, South America). Journal of Human Evolution 32:161-199.

Kay RF, Madden RH, Vucetich MG, Carlini AA, Mazzoni MM, Ré GH, Heizler M, and Sandeman H. 1999. Revised age of the Casamayoran South American Land Mammals "Age"—climatic and biotic implications. Proceedings of the National Academy of the USA 96: 13236-13240.

Kay RF and Simons EL. 1980. The ecology of oligocene African anthropoidea. International Journal of Primatology 1(1): 21-37.

Kay RF, Madden RH, Van Schaik C, and Higdon D. 1997. Primate species richness is determined by plant productivity: implications for conservation. Proceedings of the National Academy of Sciences of the United States of America 94: 13023-13027.

Kay RF, Schmitt D, Vinyard CJ, Perry JM, Shigehara N, Takai M, and Egi N. 2004. The paleobiology of Amphipithecidae, south Asian late Eocene primates. Journal of Human Evolution 46(1): 3-25.

Kay RF, Vizcaíno SF, and Bargo MS. 2012a. The paleoenviroinment and paleoecology of the coastal Miocene Santa Cruz Formation (late Early Miocene, Argentina). Journal of Vertebrate Paleontology 32(6):119.

Kay RF, Vizcaíno SF, and Bargo MS. 2012b. A review of the paleoenvironment and paleoecology of the Miocene Santa Cruz Formation. In: Vizcaíno SF, Kay RF, and Bargo MS, editors. Early Miocene Paleobiology in Patagonia: High-Latitude Paleocommunities of the Santa Cruz Formation. Cambridge, UK: Cambridge University Press. p 331-364.

Keast A. 1977. Historical biogeography of the marsupials. In *The biology of marsupials*, pp. 69-95. Macmillan Education UK.

Khan A and Rayner GD. 2003. Robustness to non-normality of common tests for the many-sample location problem. Journal of Applied Mathematics and Decision Sciences 7(4): 187-206.

Kidwell SM and Behrensmeyer AK, eds. 1993. *Taphonomic approaches to time resolution in fossil assemblages: Short courses in Paleontology 6*, 302 pp.

Kidwell SM and Flessa KW. 1996. The quality of the fossil record: populations, species, and communities 1. Annual Review of Earth and Planetary Sciences 24(1): 433-464.

Kinzey WG and Norconk MA. 1990. Hardness as a basis of fruit choice in two sympatric primates. American Journal of Physical Anthropology 81: 5-15.

Kissling WD, Dalby L, Fløjgaard C, Lenoir J, Sandel B, Sandom C, Trøjelsgaard K, and Svenning JC. 2014. Establishing macroecological trait datasets: digitalization, extrapolation, and validation of diet preferences in terrestrial mammals world-wide. Ecology and Evolution 4(14): 2913-2930.

Kohn MJ. 2010. Carbon isotope compositions of terrestrial C3 plants as indicators of (paleo) ecology and (paleo) climate. *Proceedings of the National Academy of Sciences* 107(46): 19691-19695.

Korth WW. 1994. *The Tertiary Record of Rodents in North America*. Plenum Press: New York.

Kowaleski M. 1996. Time-averaging, overcompleteness, and the geological record. The Journal of Geology: 317-326.

Kunzek H, Kabbert R, Gloyna D. 1999. Aspects of material science in food processing: changes in plant cell walls of fruits and vegetables. Zeitschrift Fur Leb und – Forsch a 208: 233-250.

Lazzari V, Charles C, Tafforeau P, Vianey-Liaud M, Aguilar J-P, Jaeger J, Michaux J, and Viriot L. 2008a. Mosaic convergence of rodent dentitions. PLoS ONE 3(10): e3607.

Lazzari V, Tafforeau P, Aguilar JP, and Michaux J. 2008b. Topographic maps applied to comparative molar morphology: the case of murine and cricetine dental plans (Rodentia, Muroidea). Paleobiology 34(1): 46-64.

Ledogar JA, Winchester JM, St. Clair EM, and Boyer DM. 2013. Diet and dental topography in pitheciine seed predators. American Journal of Physical Anthropology 150: 107-121.

Legendre S, Montuire S, Maridet O, and Escarguel G. 2005. Rodents and climate: a new model for estimating past temperatures. Earth and Planetary Science Letters 234: 408-420.

Lenfant C. 1973. High altitude adaptation in mammals. American Zoologist 13(2): 447-456.

Liaw A and Wiener M. 2002. Classification and regresion by randomForest. R news 2(3): 18-22.

Liu L, Puolamäki K, Eronen JT, Ataabadi MM, Hernesniemi E, and Fortelius M. 2012. Dental functional traits of mammals resolve productivity in terrestrial ecosystems past and present. Proceedings of the Royal Society of London B: Biological Sciences: rspb20120211.

Louys J, Meloro C, Elton S, Ditchfield P, and Bishop LC. 2011. Mammal community structure correlates with arboreal heterogeneity in faunally and geographically diverse habitats: implications for community convergence. Global Ecology and Biogeography 20: 717-729.

Louys J, Meloro C, Elton S, Ditchfield P, and Bishop LC. 2015. Analytical framework for reconstructing environmental variables from mammal community structure. Journal of Human Evoltion 78:1-11.

Lowe JJ and Walker MJ. 1984. *Reconstructing Quarternary Environments*. Longmans, London, 389 pp.

Lucas PW. 2004. *Dental functional morphology: how teeth work*. New York: Cambridge University Press. 371pp.

Lucas PW, Constantino P, Wood B, and Lawn B. 2008. Dental enamel as a dietary indicator in mammals. BioEssays 30(4): 374-385.

Lucas PW and Luke DA. 1984. Chewing it over: basic principles of food breakdown. Eds. Chivers DA, Wood BA, Bilsborough A. New York, NY: Plenum Press. p. 283-301.

Lucas PW, Omar R, Al-Fadhalah K, Almusllam AS, Henry AG, Michael S, Arockia Thai L, Watzke J, Strait DS, and Atkins AG. 2013. Mechanisms and causes of wear in tooth enamel: implications for hominin diets. Journal of the Royal Society Interface 10(80): 20120923.

Lucas PW and Pereira B. 1990. Estimation of the fracture toughness of leaves. Functional Ecology 4: 819.

Luo Z-X, Cifelli RL, and Kielan-Jaworowska Z. 2001. Dual origin of tribosphenic mammals. Nature 409(6816): 53.

MacFadden BJ. 2000. Cenozoic mammalian herbivores from the Americas: reconstructing ancient diets and terrestrial communities. Annual Review of Ecology and Systematics: 33-59.

Madden RH, Guerrero J, Kay RF, Flynn JJ, Swisher CC, and Walton AH. 1996. The Laventan Stage and Age. In *Vertebrate Paleontology in the Neotropics: The Miocene Fauna of La Venta, Colombia* (Kay RF, Madden RH, Cifelli RL, and Flynn JJ, eds.). Smithsonian Institution Press: Washington, D.C.

Mamu T. 2008. Environmental impact study of terrestrial mammals for the PNG LNG Project, Papua New Guinea. In *Terrestrial biodiversity analysis of the upstream project area*, Annex 03: 1-57. Papua New Guinea Liquefied Natural Gas Project.

Mares MA, Ojeda RA, and Kosco MP. 1981. Observations on the distribution and ecology of the mammals of Salta Province, Argentina. Carnegie Museum of Natural History.

Marshall AJ and Wrangham RW. 2007. Evolutionary consequences of fallback foods. International Journal of Primatology 28: 1219-1235.

Martin RA. 1981. On extinct hominid population densities. Journal of Human Evolution 10(5): 427-428.

Mercer, J. (1909), "Functions of positive and negative type and their connection with the theory of integral equations", Philosophical Transactions of the Royal Society A, 209 (441–458): 415–446.

Mercer JM and Roth VL. 2003. The effects of Cenozoic global change on squirrel phylogeny. Science 299: 1568.

Meng J, Wyss AR, Dawson MR, and Zhai R. 1994. Primitive fossil rodent from Inner Mongolia and its implications for mammalian phylogeny. Nature 370: 134-136.

Merrick MJ, Koprowski JL, and Gwinn RN. 2012. *Sciurus stramineus* (Rodentia: Sciuridae). Mammalian Species: 44-50.

M'Kirera F and Ungar PS. 2003. Occlusal relief changes with molar wear in *Pan troglodytes troglodytes* and *Gorilla gorilla gorilla.* American Journal of Primatology 60: 31-41.

Monestiez P, Dubroca L, Bonnin E, Durbec JP, and Guinet C. 2005. Comparison of model based geostatistical methods in ecology: application to fin whale spatial distribution in northwestern Mediterranean Sea. In *Geostatistics Banff 2004*, pp. 777-786. Springer Netherlands.

Monge C and Leon-Velarde F. 1991. Physiological adaptation to high altitude: oxygen transport in mammals and birds. Physiology Review 71(4): 1135-1172.

Montuire S, Maridet O, and Legendre S. 2006. Late Miocene-Early Pliocene temperature estimates in Europe using rodents. Palaeogeogrpahy, Palaeoclimatology, Palaeoecology 238(1): 247-262.

Montuire S, Michaux J, Legendre S, Aguilar J-P. 1997. Rodents and climate: 1. A model for estimating past temperatures using arvicolids (Mammalia: Rodentia). Palaeogeography, Palaeoclimatology, Palaeoecology 128: 187-206.

Moore DE, Lees BG, and Davey SM. 1991. A new method for predicting vegetation distributions using decision tree analysis in a geographic information system. Journal of Environmental Management 15:59-71.

Myers P and Patton JL. 1989. A new species of *Akodon* from the cloud forests of eastern Cochabamba Department, Bolivia (Rodentia: Sigmodontinae). Occasional Papers of the Museum of Zoology, The University of Michigan, No. 720.

Newbrun E and Pigman W. 1960. The hardness of enamel and dentine. Australian Dental Journal 5(4): 210-217.

Nowak RM. 1991. *Walker's Mammals of the World, 5th Edition.* Johns Hopkins University Press: Baltimore.

Ojeda RA and Mares MA. 1989. A biogeographic analysis of the mammals of Salta Province, Argentina: patterns of species assemblage in the Neotropics. No. 27. Texas Tech University Press.

Okubo A and Levin SA. 1980. *Diffusion and ecological problems.* New York: Springer.

Owen R. 1871. Monograph of the fossil Mammalia of the Mesozoic formations. Palaeontographical Society of London, vol. for 1871.

Pampush JD, Winchester JM, Morse PE, Vining AQ, Boyer DM, and Kay RF. 2016a. Introducing molaR: a new R package for quantitative topographic analysis of teeth (and other topographic surfaces). Journal of Mammalian Evolution doi: 10.1007/s10914-016-9326-0.

Pampush JD, Spradley JP, Morse PE, Harrington AR, Allen KL, Boyer DM, and Kay RF. 2016b. Wear and its effects on dental topography measures in howling monkeys (*Alouatta palliata*). American Journal of Physical Anthropology 161(4): 705-721.

Patterson B and Pascual R. 1968. The fossil mammal fauna of South America. The Quarterly Review of Biology 43(4): 409-451.

Patton JL, Pardiñas UFJ, and D'Elía, eds. 2015. *Mammals of South America: Volume 2 Rodents*. The University of Chicago Press: Chicago.

Pausas JG and Austin MP. 2001. Patterns of plant species richness in relation to different environments: an appraisal. Journal of Vegetatation Science 12(2): 153-166.

Pearson OP. 1947. The rate of metabolism of some small mammals. Ecology 28(2): 127-145.

Pineda-Munoz S, Lazagabaster IA, Alroy J, and Evans AR. 2016. Inferring diet from dental morphology in terrestrial mammals. Methods in Ecology and Evolution. doi: 10.1111/2041-210X.12691.

Polly PD. 2010. Tiptoeing through the trophics: geographic variation in carnivoran locomotor ecomorphology in relation to environment. Carnivoran evolution: new views on phylogeny, form, and function: 374-401.

Poux C, Chebret P, Huchon D, de Jong WW, and Douzery EJ. 2006. Arrival and diversification of caviomorph rodents and platyrrhine primates in South America. Systematic Biology 55(2): 228-244.

Potts R. 1996. Evolution and climate variability. Science 273: 922-923.

Prasad AM, Iverson LR, and Liaw A. 2006. Newer classification and regression tree techniques: bagging and random forests for ecological prediction. Ecosystems 9: 181-199.

Prufrock KA, Boyer DM, and Silcox MT. 2016. The first major primate extinction: an evaluation of paleoecological dynamics of North American stem primates using a homology free measure of tooth shape. American Journal of Physical Anthropology.

Rasmussen CE and Williams CKI. 2006. *Gaussian Processes for Machine Learning*.

Read DW. 1975. Hominid teeth and hominid phylogeny. American Journal of Physical Anthropology 42(1); 105-125.

Redford KH and Eisenberg JF. 1992. Mammals of the Neotropics, Vol. 2. *The Southern Cone: Chile, Argentina, Uruguay, Paraguay*. University of Chicago Press: Chicago.

Reed DNO. 1997. Contour mapping as a new method for interpreting diet from tooth morphology. American Journal of Physical Anthropology 102(s24): 194.

Reed KE. 2013. Mutliproxy paleoecology: reconstructing evolutionary context in paleoanthropology. In *A companion to paleoanthropology* (DR Begun, ed.), pp. 204-225. Wiley-Blackwell, Oxford.

Ricklefs RE. 2004. A comprehensive framework for global patterns in biodiversity. Ecology Letters 7(1): 1-15.

Rigby P, Pizarro O, and Williams SB. 2010. Towards adaptive benthic habitat mapping using gaussian process classification. Journal of Field Robotics 27(6): 741-758.

Rosenberger AL. 1992. Evolution of feeding niches in New World monkeys. American Journal of Physical Anthropology 88(4): 525-562.

Rosenberger AL and Kinzey WG. 1976. Functional patterns of molar occlusion in platyrrhine primates. American Journal of Physical Anthropology 45: 281-297.

Ross CF and Kirk EC. 2007. Evolution of eye size and shape in primates. Journal of Human Evolution 52(3): 294-313.

Rowe KC, Reno ML, Richmond DM, Adkins RM, and Steppan SJ. 2008. Pliocene colonization and adaptive radiations in Australia and New Guinea (Sahul): Multilocus systematics of the old endemic rodents (Muroidea: Murinae). Molecular Phylogenetics and Evolution 47: 84-101.

Samuels JX. 2009. Cranial morphology and dietary habits of rodents. Zoological Journal of the Linnean Society 156: 864-888.

Santana SE, Strait S, and Dumont ER. 2011. The better to eat you with: functional correlates of tooth structure in bats. Functional Ecology 25(4): 839-847.

Schaub S. 1958. Simplicidentata. In *Traite de Paleontologie* (Piveteau J, ed.) 6(2): 659-818. Masson et Cie.: Paris.

Schlager S. 2015. Morpho: Calculations and visualisations related to geometric morphometrics. https://cran.r.project.org/web/packages/Morpho/index.html Version=2.3.1.1.

Secord R, Bloch JI, Chester SGB, Boyer DM, Wood AR, Wing SL, Kraus MJ, McInerney FA, and Krigbaum J. 2012. Evolution of the earliest horses driven by climate change in the Paleocene-Eocene Thermal Maximum. Science 335(6071): 959-962.

Seiffert ER, Perry JM, Simons EL, and Boyer DM. 2009. Convergent evolution of anthropoid-like adaptations in Eocene adapiform primates. Nature 461(7267): 1118-1121.

Sepkoski D and Ruse M (Eds.). 2009. *The paleobiological revolution: essays on the growth of modern paleontology*. University of Chicago Press.

Sept JM. 1994. Bone distribution in a semi-arid riverine habitat in eastern Zaire: Implications for the interpretation of faunal assemblages at early archaeological sites. Journal of Archaeological Science 21(2): 217-235.

Simpson GG. 1933. The 'Plagiaulacoid' Type of Mammalian Dentition, A Study of Convergence. Journal of Mammalogy 14(2): 97-107.

Simpson GG. 1945. The principles of classification and a classification of mammals. Bulletin of the American Museum of Natural History 85.

Simpson GG. 1950. History of the fauna of Latin America. American Scientist 38(3): 361-389.

Simpson GG. 1961. Historical zoogeography of Australian mammals. Evolution: 431-446.

Smith MF and Patton JL. 1999. Phylogenetic relationships and the radiation of sigmodontine rodents in South America: evidence from cytochrome b. Journal of Mammalian Evolution 6(2): 89-128.

Smith RJ. 2002. Estimation of body mass in paleontology. Journal of Human Evolution 43(2): 271-287.

Solari S. 2007. Trophic relationships within a highland rodent assemblage from Manu National Park, Cusco, Peru. The Quintessential Naturalist: Honoring the Life and Legacy of Oliver P. Pearson 134: 225.

Spradley JP, Glander KE, and Kay RF. 2016. Dust in the wind: How climate variables and volcanic dust affect rates of tooth wear in Central American howling monkeys. American Journal of Physical Anthroplogy 159(2): 201-222.

Spradley JP and Kay RF. 2016. Homology-free dental topography measures can distinguish dietary categories in marsupials. Society of Vertebrate Paleontology, Annual Meeting: 230.

Spradley JP, Pampush JD, Morse PE, and Kay RF. 2017. Smooth operator: The effects of different 3D mesh retriangulation protocols on the computation of Dirichlet normal energy. American Journal of Physical Anthropology.

Spradley JP, Williams BA, and Kay RF. 2015. Environmental variables affecting primate richness in the Neotropics. American Journal of Physical Anthropology 156(S60): 294.

Steudel K. 1980. New estimates of early hominid body size. American Journal of Physical Anthropology 52: 63-70.

Stitson M, Gammerman A, Vapnik V, Vovk V, Watkins C, and Wetson J. 1999. Support vector regression with ANOVA decomposition kernels. In *Advances in kernel methods—Support vector learning*, pp. 285-292.

Strahan R. 1995. *Mammals of Australia*. Smithsonian Institute Press.

Strait SG. 1997. Tooth use and the physical properties of food. Evolutionary Anthropology: Issues, News, and Reviews 5(6): 199-211.

Streilein KE. 1982. Behavior, ecology, and distribution of South American marsupials. Special Publication of the Pymatuning Laboratory of Ecology 6: 231-250.

Stucky R. 1990. Evolution of land mammal diversity in North America during the Cenozoic. Current Mammalogy: 375-432.

Szalay FS. 2006. *Evolutionary history of the marsupials and an analysis of osteological characters.* Cambridge University Press, Cambridge.

Taubin G. 1995. Estimating the tensor of curvature from a surface of polyhedral approximation. In Proc. 5th International Conference on Computer Vision: 902-907.

Teaford MF and Ungar PS. 2006. Dental adaptations of African apes. In *Handbook of Paleoanthropology, Volume 1: principles, methods, and approaches* (Henke W, Rothe W, Tattersal I, eds.). Heidelberg: Springer. pp. 1107-1132.

Therneau T, Atkinson B, and Ripley B. 2015. Package 'rpart'. 3-1.

Toft CA. 1980. Feeding ecology of thirteen syntopic species of anurans in a seasonal tropical environment. Oecologia 45: 131-141.

Ungar PS. 2004. Dental topography and diets of *Australopithecus afarensis* and early *Homo*. Journal of Human Evolution 46: 605-622.

Ungar PS. 2010. Monotremata and Marsupalia. In *Mammal teeth: origin, evolution, and diversity*, pp. 129-143. JHU Press.

Ungar PS, Bunn JM. 2008. Primate dental topographic analysis and functional morphology. In: Irish JD, Nelson GC, editors. *Technique and Application in Dental Anthropology*. New York: Cambridge University Press. p 253–265.

Ungar PS and M'Kirera F. 2003. A solution to the worn tooth conundrum in primate functional anatomy. Proceedings of the National Academy of Sciences of the United States of America 100: 3874-3877.

Ungar PS, Teaford MF, Glander KE, and Pastor RF. 1995. Dust accumulation in the canopy: a potential cause of dental microwear in primates. American Journal of Physical Anthropology 97(2): 93-99.

Ungar PS, Williamson MD. 2000. Exploring the effects of tooth wear on functional morphology: a preliminary study using dental topographic analysis. Palaeontologica Electronica 3(1): 1-18.

van Dam JA. 2006. Geographic and temporal patterns in the late Neogene (12-3 Ma) aridification of Europe: the use of small mammals as paleoprecipitation proxies. Palaeogeography, Palaeoclimatology, Palaeoecology 238(1): 190-218.

Van Valen L. 1960. A functional index of hypsodonty. Evolution: 531-532.

Van Valen L. 2004. Adaptation and the origin of rodents. Bulletin of the American Museum of Natural History 285: 110-119.

Verrelst J, Alonso L, Camps-Valls G, Delegido J, and Moreno J. 2012. Retrieval of vegetation biophysical parameters using Gaussian process techniques. IEEE Transactions on Geoscience and Remote Sensing 50(5): 1832-1843.

Vizcaíno SF, Bargo MS, Kay RF, Fariña RA, Di Giacomo M, Perry JM, Prevosti FJ, Toledo N, Cassini GH, and Fernicola JC. 2010. A baseline paleoecological study for the Santa Cruz Formation (late-early Miocene) at the Atlantic coast of Patagonia, Argentina. Palaeogeography, Palaeoclimatology, Palaeoecology 292(3): 507-519.

Vizcaíno SF, Bargo MS, Kay RF, and Milne N. 2006. The armadillos (Mammalia, Xenarthra, Dasypodidae) of the Santa Cruz Formation (early-middle Miocene): An approach to their paleobiology. Palaeogeography, Palaeoclimatology, Palaeoecology 237: 255-269.

Vizcaíno SF, Kay RF, and Bargo MS, eds. 2012. *Early Miocene Paleobiology in Patagonia: High-Latitude Paleocommunities of the Santa Cruz Formation.* Cambridge University Press.

Vogel ER, van Woerden JT, Lucas PW, Utami Atmoko SS, van Schaik CP, Dominy NJ. 2008. Functional ecology and evolution of hominoid molar enamel thickness: *Pan troglodytes schweinfurthii* and *Pongo pygmaeus wurmbii*. Journal of Human Evolution 55: 60-74.

Voss RS. 1988. Systematics and ecology of *Ichthyomys* rodents (Muroidea): patterns of morphological evolution in a small adaptive radiation. Bulletin of the American Museum of Natural History 188: 260-463.

Vrba ES. 1992. Mammals as a key to evolutionary theory. Journal of Mammalogy 73(1): 1-28.

Vucetich M, Arnal M, Deschamps C, Pérez M, and Vieytes E. 2015. A brief history of caviomorph rodents as told by the fossil record. *Biology of caviomorph rodents: diversity and evolution. Buenos Aires: SAREM Series A*.

Walker A, Hoeck HN, and Perez L. 1978. Microwear of mammalian teeth as an indicator of diet. Science 201(4359): 908-910.

Walker KR and Bambach RK. 1971. The significance of fossil assemblages from fine-grained sediments: Time-averaged communities. Geological Society of America Abstracts with Programs 3: 783-784.

Wasserman L. 2005. *All of Statistics*, pp. 363-364.

Welling SH, Refsgaard HH, Brockhoff PB, and Clemmensen LH. 2016. Forest Floor Visualizations of Random Forests. *arXiv preprint arXiv:1605.09196.*

Whitmore FC and Stewart RH. 1965. Miocene mammals and Central American seaways. Science 148: 180-185.

Whittaker RH. 1972. Evolution and measurement of species diversity. Taxon: 213-251.

Wiens JJ and Graham CH. 2005. Niche conservatism: integrating evolution, ecology, and conservation biology. Annual Review of Ecology, Evolution, and Systematics 36: 519-539.

Williams CK. 1998. Prediction with Gaussian processes: From linear regression to linear prediction and beyond. In *Learning in graphical models*, pp. 599-621. Springer Netherlands.

Williams SH and Kay RF. 2001. A comparative test of adaptive explanations for hypsodonty in ungulates and rodents. Journal of Mammalian Evolution 8(3): 207-229.

Williams SH, Wright BW, Truong VD, Daubert CR, and Vinyard CJ. 2005. Mechanical properties of foods used in experimental studies of primate masticatory function. American Journal of Primatology 67: 329-346.

Wilson JL. 1974. Characteristics of carbonate platform margins. American Association of Petroleum Geologists Bulletin 58: 810-824.

Wilson DE and Reeder DM, eds. 2005. *Mammal species of the world: a taxonomic and Geographic reference*. JHU Press.

Winchester JM. (2016) MorphoTester: An open source application for morphological topographic analysis. PLoS ONE vol 11(2): e0147649.doi:10.1371/journal.pone.0147649.

Winchester JM, Boyer DM, St. Clair EM, Gosselin-Ildari AD, Cooke SB, and Ledogar JA. 2014. Dental topography of platyrrhines and prosimians: convergence and contrasts. American Journal of Physical Anthropology 153: 29-44.

Wood AE. 1965. Grades and clades among rodents. Evolution: 115-130.

Woodburne MO, Rich TH, and Springer MS. 2003. The evolution of tribospheny and the antiquity of mammalian clades. Molecular Phylogenetics and Evolution 28(2): 360-385.

Yapuncich GS, Gladman JT, and Boyer DM. 2015. Predicting euarchontan body mass: a comparison of tarsal and dental variables. American Journal of Physical Anthropology 157(3): 472-506.

Zuccotti LF, Williamson MD, Limp WF, and Ungar PS. 1998. Modeling primate occlusal topography using geographic information systems technology. American Journal Physical Anthropology 107:137-142.

Biography

Jackson Spradley was born in Little Rock, Arkansas on February 15th, 1990 to Patricia and Ples Spradley. Having spent his entire childhood growing up on a farm in central Arkansas, he attended the University of Arkansas in Fayetteville beginning in August 2008. In May 2012 he graduated summa cum laude with a Bachelor of Arts degree in Anthropology and a minor in Arabic language. He also wrote a honors thesis with Dr. Peter Ungar entitled "Intra-tooth variation in dental microwear in *Macropus rufus*".

He then moved on to begin his Ph.D. with Dr. Richard Kay in August 2012. Whilst working on his Ph.D., Jackson published two first author papers including: "Dust in the Wind: How climate variables and volcanic ash affect molar wear rates in Central American howling monkeys" in the American Journal of Physical Anthropology in 2016; and "Smooth Operator: The effects of different 3D mesh retriangulation protocols on the computation of Dirichlet normal energy" also in the American Journal of Physical Anthropology in 2017. He has won several awards from Duke University Graduate School, including the Summer Research Fellowship and the International Travel Award.

He will be joining the faculty of the Department of Biology and Marine Biology at the University of North Carolina-Wilmington in August 2017.